December 2020

Development of Extracellular Vesicle Isolation and Model Systems Toward Early Ovarian Cancer Diagnostics

Tyler Slonecki
Clemson University, sloneckity@gmail.com

DEVELOPMENT OF EXTRACELLULAR VESICLE ISOLATION AND MODEL SYSTEMS TOWARD EARLY OVARIAN CANCER DIAGNOSTICS

A Dissertation
Presented to
the Graduate School of
Clemson University

In Partial Fulfillment
of the Requirements for the Degree
Doctor of Philosophy
Bioengineering

---

by
Tyler Jordan Slonecki
December 2020

Accepted by:
Dr. Terri Bruce, Committee Chair
Dr. R. Kenneth Marcus
Dr. Jeoung Soo Lee
Dr. Brian W. Booth

ABSTRACT

Ovarian cancer (OC) is characterized by late stage discovery and low survivability. However, when diagnosed early (Stages I or II) the 5-year survival rate is 92% up from 29%.[5] The extreme dichotomy in survivability is what makes OC a prime candidate for early diagnosis techniques. Exosomes, a subtype of extracellular vesicles, may bridge the gap between early and late diagnosis, but are lacking consistent isolation and detection technologies. Here poly(ethylene terephthalate) (PET) capillary channeled polymer (C-CP) fibers employing an HIC protocol are investigated as a novel exosome isolation method and a quick, inexpensive, and easy-to-use platform for OC diagnosis. The cell model system, immunoaffinity protocols, and biomarker identification tools developed here will aid in the refinement of a selective PET C-CP exosome isolation. The exosome isolation and diagnostic technique developed as a result of these investigations will allow for earlier and routine diagnosis of OC and save many women from one of the deadliest cancers.

DEDICATION

I would like to dedicate this dissertation to my parents, sister, family, and friends who kept me motivated along this journey. In particular, this dissertation is dedicated to the memory of my aunt Doris Logan who was impassioned by biology and taken from us too soon by ovarian cancer.

ACKNOWLEDGMENTS

First and foremost, I would like to thank my advisor, Dr. Terri Bruce, for guiding me through this project, pushing me to produce high quality material, and providing motivation and emotional support along the way. Your brilliant mind and crazy ideas are what pushed this project forward and are what got me to where I am now.

I would like to thank my committee members, Dr. R Kenneth Marcus, Dr. Jeoung Soo Lee, and Dr. Brian W. Booth for allowing me the privilege to present this research and for guiding me during this project.

Thank you, Rhonda Powell, for being my unofficial second advisor. I would not have survived graduate school without your guidance and expertise in the lab. You deserve more credit than you're officially given and I appreciate the hard work, dedication, and many laughs you bring to the lab every day. Additional thanks to all the interns at the Clemson Light Imaging Facility for helping me in the lab and always bringing a positive attitude to our group.

Thank you, Dr. Larry Puls, Lorie Allen, and Tina Pettry of Prisma Health, for providing guidance and supplying patient samples in the continued partnership with Clemson University. Additional thanks to Dr. Brian Dean and Dr. Billy Bridges for providing analysis guidance on this research project.

Thank you to all my colleagues, Clay Morton, Sisi Huang, Lei Wang, Kaylan Kelsey, and Paritra Mandal, that have worked alongside me on this project. I appreciate every one of you and realize I could not have completed this journey without all of you.

Thank you to my parents, sister, and family who have supported me along this journey. Thank you for giving me the confidence to complete this project and the constant support during the process.

I would also like to thank Alissa Williams for her continual guidance and support. You are a truly amazing friend that has been willing help me at a moment's notice. A special thanks to Justin Whitaker for being true to Atlanta, reviving and motivating me during this project, and for always listening to Alissa and me, even if you didn't understand what we were talking about.

And last, but not least, I would like to thank the Gibbs Foundation for Cancer Research, The Eppley Foundation for Research, the National Science Foundation and Prisma health for continued funding and partnerships.

TABLE OF CONTENTS

Page

Table of Contents (Continued) Page

Table of Contents (Continued) Page

LIST OF TABLES

Table Page

LIST OF FIGURES

List of Figures (Continued)

Figure Page

List of Figures (Continued)

Figure Page

List of Figures (Continued)

Figure Page

LIST OF ABBREVIATIONS

OC	ovarian cancer
EV	extracellular vesicle
sEV	small extracellular vesicle
lEV	larger extracellular vesicle
PET	poly(ethylene terephthalate)
C-CP	capillary-channeled polymer
HIC	hydrophobic interaction chromatography
DNA	deoxyribonucleic acid
RNA	ribonucleic acid
GFP	green fluorescence protein
tGFP	turbo green fluorescence protein
copGFP	copepoda green fluorescence protein
RFP	red fluorescence protein
miRNA	micro ribonucleic acid
siRNA	small interfering ribonucleic acid
mRNA	messenger ribonucleic acid
MVB	multivesicular body

List of Abbreviations (Continued)

MVE	multivesicular endosome
ILV	intraluminal vesicle
ESCRT	endosomal sorting protein complexes required for transport
TSG101	tumor susceptibility gene 101
ALIX	programmed cell death 6-interacting protein
MHC	major histocompatibility complex
MSC	mesenchymal stem cell
ADSC	adipose tissue-derived stem cell
EpCAM	epithelial cell adhesion molecule
L1CAM	L1 cell adhesion molecule
EGFR	epidermal growth factor receptor
HER2	human epidermal growth factor receptor 2
CA-125	cancer antigen 125
CD	cluster of differentiation
DDS	drug delivery system
RVG	rabies-virus glycoprotein
IPSC	induced pluripotent stem cell

List of Abbreviations (Continued)

EMT	epithelial-mesenchymal transition
MSA	multiple system atrophy
ALS	amyotrophic lateral sclerosis
MS	multiple sclerosis
ISEV	international society of extracellular vesicles
NTA	nanoparticle tracking analysis
DLS	dynamic light scattering
TEM	transmission electron microscopy
SEM	scanning electron microscopy
AFM	atomic force microscopy
STED	stimulated emission depletion
PALM	photoactivated localization microscopy
ELISA	enzyme-linked immunosorbent assay
FACS	flow cytometry
UC	ultracentrifugation
UF	ultrafiltration
SEC	size exclusion chromatography

List of Abbreviations (Continued)

PEG	polyethylene glycol
EXPLORS	exosomes for protein loading via optically reversible protein-protein interaction
LC	liquid chromatography
HPLC	high performance liquid chromatography
VEGF	vascular endothelial growth factor
PARP	poly(adenosine diphosphate ribose) polymerase
ECM	extracellular matrix
IHOE	immortalized human ovarian epithelial
BSA	bovine serum albumin
Chimo	α-chymotrypsinogen A
CRM	certified reference material
DC	differential centrifugation
HMDS	hexamethyldisilazane
IMAC	immobilized metal affinity chromatography
RP	reversed-phase
LYSO	lysozyme

List of Abbreviations (Continued)

Myo	myoglobin
Ribo	ribonuclease A
SPE	solid phase extraction
SPR	surface plasmon resonance
PBS	phosphate buffered saline
UV	ultraviolet
MALS	multi-angle light scatter
CLDN3	claudin 3
CLDN4	claudin 4
PCNA	proliferating cell nuclear antigen
TGF-β1	transforming growth factor - β1
MAGE3/6	melanoma antigen gene 3/6
FASN	fatty acid synthase
ERBB2	receptor tyrosine-protein kinase
APOE	apolipoprotein E
DI	deionized
RIPA	radioimmunoprecipitation assay

List of Abbreviations (Continued)

PVDF	polyvinylidene difluoride
TBS	tris buffered saline
PEEK	polyether ether ketone
FE-SEM	field emission scanning electron microscopy
DAPI	4',6-Diamidino-2-Phenylindole, Dihydrochloride
DIC	differential interference contrast
CL	cell lysate
MOI	multiplicity of infection
CM	cervical mucus
THP	Tamm–Horsfall protein
EDTA	ethylenediaminetetraacetic acid
ACN	acetonitrile
STD EXO	standard exosome
PCA	principal component analysis
TMM	trimmed mean of M-values
CPM	counts per million
FC	fold change

List of Abbreviations (Continued)

GMP	good manufacturing practices
BRCA	breast cancer gene

CHAPTER 1
LITERATURE REVIEW

Introduction

Cell signaling is an encompassing term that covers a variety of complex processes in which biological systems, collections of cells, and individual cells communicate information, directives, and functions. Most methods of cellular communication involve transmission of soluble molecules, neurotransmitters, hormones, or ligands followed by signal reception, signal transduction, and cellular response. However, more recently, exosomes have emerged as an accompanying and complex means of cell signaling.[6] Exosomes are a class of lipid bilayer membrane vesicles, approximately 30-150 nm in diameter, that play a variety of roles in autocrine and paracrine signaling. Prior to investigation into exosomes' role in cellular communication, the vesicles were assumed to play a role in dissemination and disposal of intracellular waste.[1, 7]

Over the last several years, exosomes have generated immense excitement within the biotech and scientific communities. As such, there has been an explosion of research, with exponential growth in the number of articles published over the last 10 years. Remarkably, exosomes may be involved in a variety of processes including stem cell renewal, cancer metastasis, inflammation, coagulation, and chemotaxis.[6-12] As more information about the complex role of exosomes is discovered, further potential medical and research applications are being examined. Exosome applications may include

biomarker disease diagnostics, drug delivery, gene therapy, cancer therapy, and tissue regeneration.[1, 7, 10, 13-15]

Exosomes contain transmembrane, cytosolic, intracellular proteins, and several types of RNA that may be used as biomarkers for cancers and various disease states.[13, 16-18] Furthermore, since exosomes are derived directly from cells, there is little immune response associated with inserting autologous exosomes back into the same human system.[19-22] Remarkably, Alvarez et al.[23] have been able to manipulate the lipid bilayer membrane content of exosomes to include a peptide that specifically targets neurons, microglia, and oligodendrocytes in the brain. The versatility and applications of exosomes seem endless and will surely impact the field of medicine in the future. Their potential for disease diagnostics could alone eliminate the need for biopsies and more invasive procedures. Simply put, with exosome biomarkers, a urine, blood, or cerebrospinal sample may be used for early detection of diseases.

Despite the emerging popularity of exosome research, very little is known about what happens to an exosome once it reaches and enters a target cell. There is an extensive understanding of how an exosome is manufactured and released in the original cell, but the mechanisms of transport in the target cell still remain in the dark.[24] In the original cell, exosomes do not simply bud off from the plasma membrane. In the 1980s, Harding et al.[25] and Pan et al.[26] revealed a slightly more complex mechanism of exosome formation and secretion. They showed that exosomes are formed by inward budding of intracellular endosomes. The intracellular endosomes containing the exosomes then fuse with the plasma membrane, thus releasing the exosomes outside of the cell. There are a

number of theorized mechanisms for exosome uptake, transport, and dissemination into the target cell, none of which have gained widespread backing. In particular, understanding of these mechanisms is crucial for developing the proper drugs for exosome loading, determining how to manipulate exosome drug vector targeting properly, and increasing the efficacy of loaded drugs. For instance, if the exosomes were to follow the endocytic pathway and eventually come in contact with a lysosome, the loaded drug could become deactivated or degraded. Greater understanding of the biochemical makeup, biogenesis, transport, uptake, and dissemination mechanisms will enhance our ability to capitalize on the natural properties of exosomes.

One of the largest problems preventing exosome technology from advancing into the clinical setting is the lack of a quick, efficient, and reliable exosome isolation method. Current exosome isolation techniques can be crude, often producing small yields and damaging the exosomes. Before any potential applications of exosomes can be realized, we need to learn how to better isolate exosomes. Furthermore, current methods of studying exosomes can be expensive due to the cost of mammalian cells lines, cell media, and equipment. The burgeoning amount of research being conducted on exosomes and related vesicles calls for the development of new exosome isolation techniques that may result in clinical translation. Our research group has proposed using hydrophobic interaction chromatography and Polyethylene terephthalate (PET) Capillary-Channeled Polymer (C-CP) fibers in order to achieve a lower cost, faster, and more effective exosome isolation and ultimately develop an all-in-one exosome isolation and disease diagnostic test for ovarian cancer. However, the testing of such a diagnostic technique

will require expensive and time consuming marker detection. In this study, we detail the development of two new cell lines, one cancerous and one normal, which express fluorescent tags on exosome and extracellular vesicle-enriched proteins and demonstrate the ability to differentiate between these two populations of vesicles using antibody capture.

Our research has resulted in three primary outcomes. First, we have developed and tested a poly(ethylene terephthalate) (PET) capillary-channeled polymer (C-CP) fiber EV isolation method employing a hydrophobic interaction chromatography (HIC) protocol. This new method will allow for faster, cheaper, and easier EV isolation for diagnostic and therapeutic applications. Second we have developed and tested a model system of cell lines, one normal ovarian cell line with green fluorescent protein (GFP)-tagged CD81 and one ovarian cancer cell line with red fluorescent protein (RFP)-tagged CD9. This model system will be used to investigate and refine a selective PET C-CP EV isolation method. We have demonstrated that EV populations from these two cell lines can be differentiated using antibody capture on nitrocellulose membranes and fluorescence microscopy. The ability to differentiate cancerous and non-cancerous vesicle populations is an important step in the development of a selective diagnostic test. Third, we have shown the importance of sample selection for downstream analysis of EVs through comparison of urine and cervical mucus and demonstrated the diagnostic potential of miRNA expression patterns to compare ovarian cancer and non-cancerous clinical samples. Continued analysis of the miRNA expression data and ongoing proteomics will reveal biological pathways and connections that will identify novel

biomarkers for OC. These biomarkers can be applied to a PET C-CP EV isolation method for further refinement of EV selective capture. The achievements of these investigations will ultimately aid in the development of a tool for earlier, routine OC diagnosis that will save the lives of many women.

The following review covers the different topics investigated by this research including the current understanding of exosome and extracellular vesicle mechanisms, physiological responsibilities, techniques, and medical applications, the potential of liquid chromatography to separate and isolate extracellular vesicles, an overview of ovarian cancer and exosome involvement in tumorigenesis, and the use of antibody capture to identify extracellular vesicles.

Exosome Biogenesis, Sorting, and Release

Exosome are a class of extracellular vesicles (EVs), approximately 30-150 nm in diameter.[8] Typically, the varying categories of extracellular vesicles are classified based on size and method of biogenesis. Exosomes are formed by inward budding of multivesicular bodies (MVBs, or multivesicular endosomes; MVEs) followed by extracellular release by MVB fusion with the cell membrane (see Figure 1.1).[2] The membrane contents and interior contents are determined by a number of factors unique to individual cell types and the function of the exosome being produced.

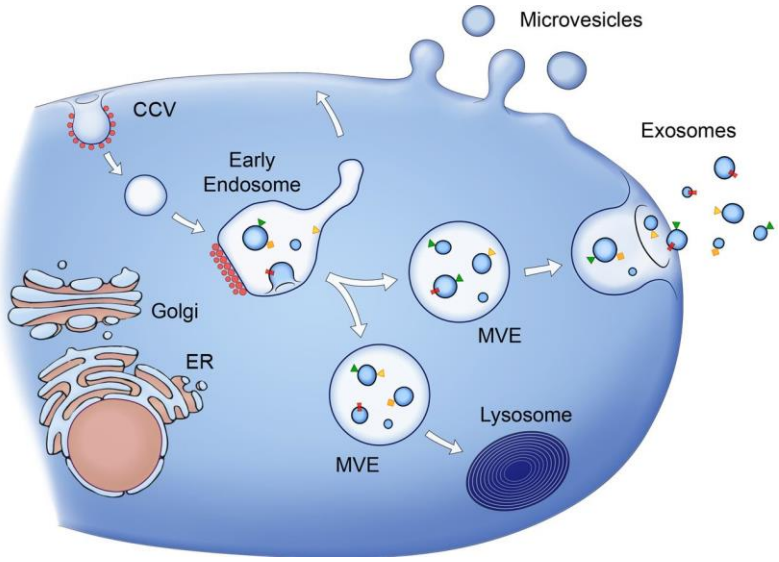

Figure 1.1. Diagram of exosome and microvesicle biogenesis. Adapted from Raposo et al.[2]

Initially, intraluminal vesicles (ILVs) are formed by inward budding of the endosomal membrane into MVBs. After maturing from late stage endosomes, MVBs then either fuse with a lysosome to degrade any internal contents or fuse with the cell membrane to release any contents into the extracellular environment. ILVs are referred to as exosomes only after extracellular release. During the formation process, specific proteins and RNAs are sorted into the cytosol and membranes of the ILVs.[27] The very complex protein sorting process, although still not fully understood, is thought to be primarily guided by the endosomal sorting protein complexes required for transport (ESCRTs).[28] As such, most ILV sorting mechanisms are categorized as ESCRT-dependent or ESCRT-independent mechanisms. During the sorting process, ILVs are typically enriched in specific proteins including tetraspanins CD63, CD81, and CD9,

cytosolic protein tumor susceptibility gene 101 (TSG101) and programmed cell death 6-interacting protein (ALIX).[28-33] Although not nearly as well understood as the protein sorting mechanisms, RNA sorting mechanisms are now being discovered. RNA sorting is often thought to be associated with special 4 nucleotide motifs. Specifically, the nucleotide sequence GGAG may be involved in the sorting and management of miRNA.[32, 33] The proteins and RNAs enriched in exosomes are distinctive from the original cell membrane and cytosolic RNAs, suggesting an advanced preferential means of determining exosome content exists.[34] However, despite the knowledge surrounding the mechanisms, proteins, and RNAs involved in ILV formation and sorting, the means of determining vesicle content and production are still shrouded in mystery.

Exosome release into the extracellular environment is mediated by fusion of MVBs with the plasma membrane of the cell. However, depending on the cell type and physiological state of the cell, the mechanisms by which the MVB fuses with the plasma membrane can vary. Much like other endosomal and endocytic vesicles, the mechanisms of MVB plasma membrane fusion are facilitated by a variety of membrane-trafficking Rab GTPase or SNARE proteins including RAB7, RAB11, RAB27a, RAB31, RAB35, YKT6, and VAMP7.[1, 11, 28, 35-37] Often, each mechanism of MVB plasma membrane fusion is associated with enrichment of certain proteins in the exosomes.

Exosome Uptake and Dissemination

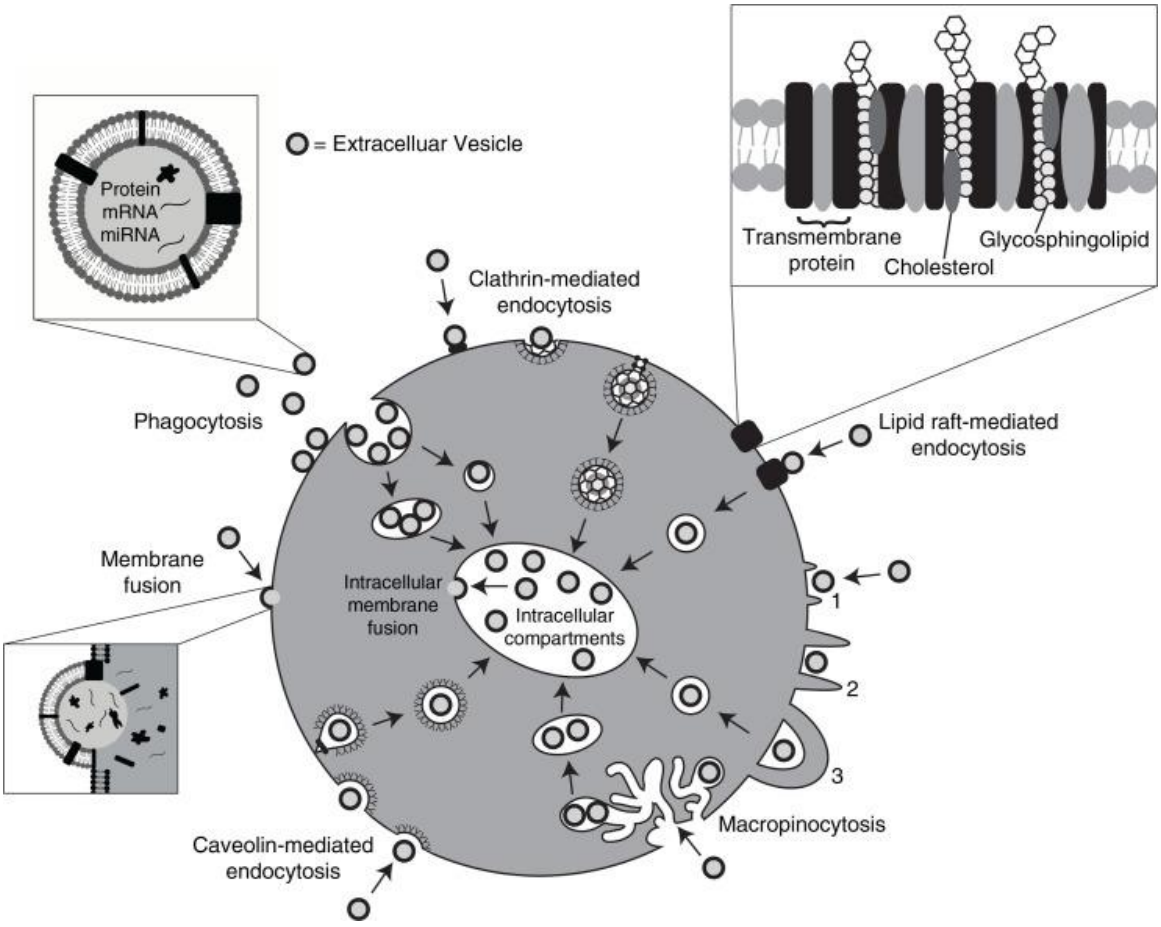

Figure 1.2. Possible mechanisms of extracellular vesicle uptake in the recipient cell. Adapted from Mulcahy et al.[3]

There are several known mechanisms that are likely involved in exosome target cell uptake including clathrin-mediated endocytosis, caveolin-dependent endocytosis, micropinocytosis, phagocytosis, lipid rafts, and cell surface membrane fusion.[3, 38, 39] Mulcahy et al.[3] describe the range of possibilities for each of these uptake mechanisms

and suggest that certain mechanisms have greater involvement in extracellular vesicle uptake than others depending on the cell type.

Exosomes are initially taken into the target cell by either plasma membrane fusion or endocytosis. If the exosome fuses directly with the plasma membrane of the target cell, then its contents are presumably delivered directly into the cytoplasm, but very little is known of the whereabouts of the contents after entry into the cell. If the exosome is taken up by endocytosis, the exosome would likely fuse with the endosomal plasma membrane and release its contents into the cytoplasm (see Figure 1.2). However, it is unknown where along the endocytic pathway the exosomes may fuse with the endosome. As the endocytic pathway is designed to digest incoming material, there is the potential that incoming exosomes will be destroyed by lysosome fusion as well. As exosomes are, by nature, vehicles of transportation, it is important to understand the mode of transport and location of delivery. Knowledge of the uptake and dissemination mechanisms of exosomes could have large impacts on the development of many medical applications.

Division of Extracellular Vesicles

Exosomes

Exosomes are one of several types of EVs. There is some debate regarding the actual divisions of EVs based on size, but by defining the vesicles based on size, function, content, and mode of biogenesis, general divisions can be created.[40, 41] However, when the vesicles cannot be identified as a specific division of extracellular

vesicle, it is more appropriate to label samples as small EVs (sEVs), large EVs (lEVs), or, more generally, EVs, based on the isolation method. Exosomes are generally accepted to be approximately 30-150 nm in diameter, with wide ranging functions within cell signaling including inflammation mediation, antigen presentation, coagulation, and angiogenesis among others.[14, 18, 42, 43] Furthermore, exosomes are formed through inward budding of the endosomal membrane of MVBs and released into the extracellular environment (see Figure 1.1).[27]

Microvesicles

Perhaps most often confused for exosomes, microvesicles are a distinct class of EVs with vastly different size, function, content, and biogenesis than exosomes. With a size range of 100-1000 nm [24, 34], microvesicles can be easily confused as exosomes when solely looking at vesicle diameter, especially if larger microvesicles have been eliminated. When defining and characterizing vesicles after EV isolation, it is important to distinguish between these two EVs. Furthermore, when microvesicle roles are compared to exosome roles, the functions look very similar. Microvesicles are involved in a variety of processes including inflammation, coagulation, and stem cell renewal, but are capable of carrying much larger cargo like circular DNA and loaded reporter molecules.[34, 44] The biogenesis of microvesicles involves outward budding and fission from the plasma membrane of the cell (see Figure 1.1). Therefore, the membrane and internal content composition tends to be very different than exosomes.

Apoptotic Bodies

Lastly, apoptotic bodies, EVs approximately 500-4000 nm in diameter, only appear when a cell begins undergoing apoptosis.[24] Apoptotic bodies are not usually confused with exosomes or microvesicles since their diameter, functions, content, and biogenesis are distinct from smaller EVs. The formation of apoptotic bodies is likely a means for dividing cell components for easier digestion by phagocytes. Characteristically, apoptotic bodies will contain organelles, large cell components, and genetic information. Most findings suggest that apoptotic bodies are used for cell disposal, but some studies have found that they may be able to pass genetic information upon uptake.[45, 46]

Physiological Roles of Exosomes

Exosomes are released by many cells *in vivo* and *in vitro* and have been found in every biological fluid tested thus far, including urine, blood, saliva, breast milk, cervical mucus, amniotic fluid, cerebrospinal fluid, and ascitic fluid.[13, 27, 47] With such a large presence in biological fluids, it makes sense that exosomes would have a variety of important physiological roles. As carriers for cell communication, exosomes may play a diverse regulatory role depending on the vesicle contents including, but not limited to, immunomodulation and antigen presentation, wound healing and angiogenesis, inflammation, drug resistance, disease propagation, regulation of the central nervous system, synaptic plasticity, reproduction and embryonic development, and homeostasis.[1, 7, 8, 14, 43, 48]

Several aspects of exosomes have been extensively studied, but perhaps the most well-characterized is their role in immunomodulation and antigen presentation. The

adaptive immune response is an incredibly complex system in which exosomes may play a regulatory role. In particular, exosomes derived from immune cells have demonstrated antitumor effects and have been found to display class I and II major histocompatibility complex (MHC) molecules involved in antigen presentation.[49] However, tumor cells have benefited from the same immunomodulatory properties of exosomes. Tumor cell-derived exosomes have been shown to promote tumor development through a variety of mechanisms.[43, 50] These contradictory functions further demonstrate the versatility of exosome communication and function under both normal and pathological physiological conditions.

Immunomodulation and Antigen Presentation

Exosomes that contain MHC class I and II molecules play an important antigen presentation role in the adaptive immune system.[51] Dendritic cells and macrophages, two types of antigen presenting cells, release exosomes with these MHC-peptide complexes, which can have both stimulatory and suppressive effects on the immune system.[52-54] Exosomes released by these cells can form an antigen-MHC complex which can be used to directly present the antigen to T-cells, thereby leading to T-cell activation. Additionally, exosomes containing this antigen-MHC complex can present the antigen to other antigen presenting cells resulting in processing of the antigen and cross-presentation to T-cells.[43, 54, 55] Pregnancy immune regulation presents a unique immunomodulatory situation in which the fetus must be protected from the allogenic immune response of the mother. The immunomodulatory effects of exosomes released by

the placenta may play a role in this regulation.[11, 56] In fact, exosome concentration in the amniotic fluid increases over each pregnancy trimester.[56]

Wound Healing and Angiogenesis

Wound healing is a remarkable process that is regulated and controlled by a complex network and cascade of growth factors, cytokines, and proteins. Through homeostasis, inflammation, proliferation, and remodeling, damaged tissue is repaired and reconstructed to restore tissue function.[57-59] Exosomes may play a significant role in regulating the intricate interactions of chronic and acute would healing developments. By carrying gene influencing material, exosomes can initiate wound healing pathways (PI3K/Akt, ERK, STAT3)[57, 60], promote expression of growth factors (hepatocyte growth factor, insulin-like growth factor-1, nerve growth factor, stromal-derived growth factor-1), heat shock proteins, and other signaling molecules.[57, 61, 62] Specifically, mesenchymal stem cells (MSCs) and adipose tissue-derived stem cells (ADSCs) play an important role in modifying and controlling wound healing. Likewise, exosomes derived from MSCs and ADSCs play a significant role in communicating to fibroblasts, promoting cell migration and proliferation, and promoting angiogenesis.[60, 61] Exosomes may allow for further paracrine signaling to aid in faster wound healing and angiogenesis. Furthermore, several cell types have been revealed to release pro-angiogenic exosomes, including endothelial cells, tumor-derived cells, hematopoietic stem cells, mesenchymal stem cells, and cardiomyocyte- and myocardial progenitor cells.[14, 63-67]

Inflammation

Inflammation is a normal physiological process that is used to defend against generic foreign material and infection and to remove damaged tissue. It is characterized by a large increase in inflammatory cell migration to the injury site.[68] Although the inflammatory process is closely tied to the adaptive and innate immune response, the control mechanisms and processes are quite different. Depending on the type of injury or reaction, inflammation is typically mediated by neutrophils, basophils, eosinophils, macrophages, lymphocytes, and monocytes.[69, 70] Exosomes, as mediators of communication, are particularly involved in controlling the inflammatory response through the use of miRNA and protein genetic modulatory molecules.[18] Specifically, exosomes released by lipopolysaccharide-injected macrophages have demonstrated inflammatory modulating abilities, including NF-kappaB activation.[53] Furthermore, dendritic cell-derived exosomes have been shown to suppress inflammation in murine collagen-induced arthritis.[71, 72] However, other dendritic cell-derived exosomes have shown the ability to induce inflammation in the spleen.[73] Such vast and varying responsibilities within inflammation alone suggest that exosome-mediated responses depend heavily on the exosome content and the type and physiological state of the target cell. As such, exosome makeup and content are determined by the original cell type and its current physiological state.

Drug Resistance

Drug resistance is a major combatant of many newly developed cancer drug therapies and chemotherapies. Cancer cells, either by acquired or de novo mutations, can obtain means to defend against drugs and promote cancer growth. Mutations in the genome and epigenome ultimately result in a series of changes that may confer drug resistance by drug metabolism, inactivation, efflux, or DNA damage repair.[74, 75] Much like other pathogens or microbes, cancer cells mutate quickly and thus may develop these genetic and epigenetic changes quickly. As exosomes are mediators of genetic expression, it makes sense that they may be involved in the complex network of changes required to develop drug resistance. Specifically, exosomes may play a role in multiple myeloma development of bortezomib resistance.[74, 76] Exosomes may be able to aid in the expulsion of drugs, counteract immunotherapy drugs, and aid in the spread of resistance.[77] Drug resistance is a developing problem for current and future cancer therapies and requires further investigation. Although exosomes may only play a small role in development of drug resistance, understanding the mechanisms behind exosome dissemination, transport, and loading may prove useful in the effort to develop effective cancer therapies and combat against drug resistance.

Exosome Medical Applications

More and more frequently, studies are revealing the ever expansive roles that exosomes may play in cell communication. Since cell communication is a universal necessity for development of complex multicellular life, there is much speculation that exosomes are involved in many more processes than currently known. Consequently, exosomes have been given a great deal of contemplation with regards to potential medical applications and functional biological understanding. As of now, many exosome applications are being investigated including disease diagnostics, drug delivery, immune system modulation, and other therapeutics. The theranostic potential for exosomes is seemingly boundless, with patient-specific and personalized medicine at the core of these applications.

Disease Diagnostics

Exosomes appear to be packaged in a very uniform and controlled manner so as to preserve the accuracy and precision of the message to be delivered. However, the exosome contents can actually vary greatly depending on the cell of origin and the physiological state of the cell of origin. Fortunately, the consistency among identical cell types and the variation of exosome components between distinct cell types may allow for tracing of the cellular origins of exosomes. In other words, the lipid, protein, and RNA signature of an exosome may provide enough clues to determine what type of cell released the exosome. This unique feature of exosomes may allow for downstream identification of abnormal cell types using only a body fluid sample. Specifically, several types of cancer exosome markers, including ovarian, breast, prostate, pancreatic,

glioblastoma, and colorectal, have been identified and may potentially be used for early cancer diagnosis.[78] Furthermore, exosome markers have been found for other pathologies, including acute kidney injury, renal ischemia reperfusion, alcoholic liver disease, and nephrotic syndrome.[79] Cancer exosome marker identification is occurring at a rapid pace and markers are quickly being translated into multiplexed marker diagnosis protocols. For example, Zhao et al.[80] have developed a microfluidics device that captures and identifies ovarian cancer exosomes using the multiplexed ovarian cancer exosome markers, epithelium cell adhesion molecule (EpCAM) and cancer antigen 125 (CA-125). Although most other types of cancers are awaiting exosome marker identification and cataloging, circulating exosomes have been identified in lung, ovary, and gastric cancer patients, which bodes well for potential marker identification.[37] New biochemical exosome RNA, protein, and lipid information is being discovered and amassed, on such online databases as ExoCarta, EVpedia, Vesiclepedia, and exoRBase, so as to aid in the creation of diagnostic profiles and the advancement of exosome knowledge. Furthermore, several groups are working on developing devices that will simultaneously isolate exosomes and provide a diagnosis.[80] For these reasons, exosome biomarker disease diagnosis is perhaps the most promising and likely first attainable application of exosomes.

Drug Delivery

When developing any pharmaceutical drug, it is important to keep in mind the pathway that the designed drug will follow. The four processes of pharmacokinetics (absorption, distribution, metabolism, and elimination) are critical to understand when

developing any drug. Particularly, the drug must be able to reach the intended target in the correct formation and concentration and must be capable of being eliminated or excreted after achieving its intended function. One strategy to combat potential drug degradation is to develop a drug delivery system (DDS) to deliver the drug to a location where it can function appropriately. Many DDSs have been developed and implemented in modern pharmaceuticals, including polymeric dendrimers and micelles, stimuli-responsive carriers, nanoparticles, and biological materials.[81] Exosomes are being investigated as a potential DDS due to their size, histocompatibility, natural targeting ability, and ability to cross unique barriers, such as the placenta or blood brain barrier.[82-84] Although exosomes contain major histocompatibility complex (MHC) molecules, there is very little immune reaction to the vesicles.[54, 85, 86] However, to date, any exosome clinical trials have been performed using autologous exosomes to avoid greater immune reaction.[87] Additionally, exosomes are very similar in basic composition to liposomes, which have been used in various DDS applications. Liposomes and exosomes are made up of a lipid bilayer enclosing internal media, however, exosomes are much smaller and have a much more complex makeup of proteins, lipids, and RNAs.[88] Several investigators have explored different possibilities for loading drugs into exosomes, including exogenous and endogenous techniques with varying success.[33, 83, 89-91] Another important factor in drug delivery, besides protecting the drug, is targeting the drug to a particular location to increase drug bioavailability to a subset of cells. Natural exosomes, depending on the source, may already target specific cell types, but may also be engineered to target a number of desired cell types. For instance, Alvarez et al.[23] have loaded exosomes with

siRNA and inserted a rabies-virus glycoprotein (RVG) peptide into the surface membrane of the exosomes that successfully targeted the exosomes to the central nervous system in mice. In order to further engineer and manipulate exosomes for drug delivery purposes and other applications, several groups are now working on developing synthetic and semi-synthetic exosomes.[91, 92] Given the unique exosome features, exosome drug delivery is a real possibility that may provide a useful DDS for treatment or therapies for cardiovascular diseases, neurodegenerative diseases, cancers, and countless ailments.

Immunotherapy

As discussed previously, exosomes are heavily involved in immune system modulation, antigen presentation, and T-cell activation. Their involvement within the immune system offers extensive opportunities and advantages for immunotherapy applications. Engineering and manipulation of exosome contents and membranes may allow for consistent activation or suppression of the immune system.[93] In particular, exosome cancer immunotherapy is being investigated as an alternative therapy for cancer treatment. By artificially activating or suppressing the immune system, immune cells may be specifically activated to target and destroy cancer cells. Similar to drug delivery applications, liposomes, artificial lipid-membrane nanocarriers, have already been used in cancer immunotherapy applications.[88, 91] However, as immunotherapy nanocarriers, exosomes may provide many advantages over liposomes including natural histocompatibility, biocompatibility, targeting, and ability to cross biological barriers.[23, 55, 94, 95] Among the most promising exosome-based immunotherapy applications is their use in the generation of vaccines against diseased cells through immunization and antigen

presentation and immune system stimulation.[19, 86, 96] However, the natural exosome immune system suppressive properties may be particularly useful for avoiding transplant rejection and treating autoimmune disorders such as rheumatoid arthritis, inflammatory bowel disease, and multiple sclerosis.[93, 97, 98] Exosome immunotherapy is an exciting prospect, offering a strong alternative to artificial drug delivery for disease treatment. Although in the early stages of research, exosome immunotherapy treatments may be able to take advantage of the body's natural defense system to combat internal disease.

Regenerative Medicine and Other Therapeutics

Given the extensive number of biological processes that may involve exosome communication, therapeutics may be developed through manipulation of exosome presence and content. In recent years, regenerative medicine has focused on development of stem cell therapies to help regenerate or reform tissue. Stem cells are capable of reproducing indefinitely and differentiating into other cell types, which makes them ideal candidates for aiding in regeneration of tissues. Furthermore, in recent years, stem cell research has overcome many controversial hurdles through development of induced pluripotent stem cells (IPSCs) and use of adult stem cells like mesenchymal stem cells (MSCs) and adipose tissue-derived stem cells (ADSCs). However, cell-based therapies are often expensive and run into biocompatibility, histocompatibility, teratoma, and ectopic tissue formation issues when introducing allogeneic or autologous cells as therapeutic agents.[97, 99] Exosomes derived from stem cells may offer an alternative therapy to direct stem cell therapy, but without many of the concerns associated with stem cell therapy. As much of the cellular changes that occur during tissue regeneration

and reformation are enacted by stem cell-derived exosomes, standalone stem cell-derived exosomes may be used to induce tissue regeneration instead.[99] Thus far, exosome driven tissue regeneration has been investigated in many tissues including, neural, myocardial, hepatic, renal, cutaneous, skeletal, chondral, and muscular.[99] However, despite the recent advances in exosome understanding, particularly within tissue regeneration, it is still uncertain whether exosomes will ultimately evolve into a reliable therapy for regenerative medicine.

Several maladies, including cancers and neurodegenerative diseases, have been found to be associated with an increased release of exosomes or exosome involvement in disease progression.[100-105] Therefore, several groups have theorized that inhibition of exosome formation, release, or uptake or removal of particular exosomes or miRNAs found in exosomes may help prevent or slow disease progression.[1] Specifically, exosomes have been found to aid in environmental preparation for cancer metastasis and acquisition of cancer cell chemoresistance.[77, 103] Filtration or elimination of cancer exosomes may potentially slow progression of epithelial-mesenchymal transition (EMT) in tumor cells and aid in chemotherapy of tumors.[100, 102, 106, 107] Furthermore, exosomes have been implicated in the prion-like propagation of neurodegenerative diseases including Alzheimer's disease, Parkinson's disease, multiple system atrophy (MSA), amyotrophic lateral sclerosis (ALS), Huntington's disease, and multiple sclerosis (MS) through transfer of toxic proteins or miRNA.[108] Similarly, filtration or elimination of exosomes involved in the spread of neurodegenerative diseases may slow the progression of their pathology. To this end, further understanding of pathology and the role of

exosomes in cancer metastasis, cancer cell acquisition of chemoresistance, and propagation of neurodegenerative diseases may ultimately aid in the development of treatments for these maladies.

Exosome Characterization and Biochemical Profile

As exosomes are approximately 30-150 nm, it is often difficult to characterize their defining properties. Furthermore, being derived from cellular components, exosomes can be difficult to differentiate from other cellular debris and nanoparticles. Therefore, the International Society for Extracellular Vesicles (ISEV) has defined several basic requirements for defining and differentiating types of EVs.[40, 41] The requirements for EV definition primarily focus on two categories of characterization: Physical and Chemical.

Physical Characterization

Physical characterization is used to evaluate individual vesicles based on size, diameter, concentration, and morphology. ISEV recommends that at least two single-vesicle technologies be used to characterize EVs. Nanoparticle tracking analysis (NTA) and dynamic light scattering (DLS) can be used to obtain vesicle size distributions and vesicle concentrations. However, both NTA and DLS can be unreliable as no distinction is made between vesicles and other particulate nanoparticles present in the sample. Likewise, the limit of resolution of NTA and DLS (approximately 30 nm)[109] may hinder the ability to identify smaller vesicles and may lead to misidentification of other non-vesicle particles. Thus, sample purity can affect the dependability of both NTA and DLS.

Transmission electron microscopy (TEM) and scanning electron microscopy (SEM) can be used to characterize size, diameter, and morphology of vesicles in solution or on a surface. Both TEM and SEM have been used extensively to study biologics, materials, and processes at a nanoscale level. However, the sample preparation process can be very harsh and damaging, particularly toward biological samples and EVs. Despite these challenges the morphology and structure of EVs viewed under TEM and SEM are credible when consistently prepared, but the sample preparation methods employed should be taken into account when making conclusions. Finally, several other techniques, including atomic force microscopy (AFM) and super-resolution microscopy techniques, such as stimulated emission depletion (STED) or photoactivated localization microscopy (PALM), have been used to generate EV size distributions and morphology characterizations.[110-112] Although no single-vesicle technique can perfectly qualitatively or quantitatively characterize EVs, when used in tandem, they can provide useful and reliable information to study EVs.

Chemical Characterization and Profile

Chemical characterization of EVs involves identification of protein, RNA, and lipid markers that are typically enriched in EVs. ISEV has laid out particular guidelines for identification of EVs using typical EV-enriched proteins.[40, 41] Membrane associated, cytosolic, intracellular, and extracellular proteins have all been used to identify and differentiate subtypes of EVs. Accordingly, ISEV recommends using at least 3 protein markers to identify and characterize EVs. Proteins typically used to identify and differentiate EVs include CD9, CD81, CD63, ALIX, TSG101, Grp94, Calnexin, and

many disease specific markers (See Table 1.1).[16, 18, 113-116] Protein analysis can be completed using Western blot analysis, enzyme-linked immunosorbent assay (ELISA), flow cytometry (FACS), or mass spectrometry. As with any method of chemical profiling, positive and negative controls of cell lysate and culture medium should be compared to the EV samples. Extensive sequencing and compilation of data has identified different types of RNAs within EVs, including miRNA, mRNA, tRNA, rRNA, piRNA, snRNA, snoRNA, and scaRNA.[13] However, miRNA is perhaps the most commonly used RNA for EV identification and study due to its function in gene regulation.[32] There is likely no single exosome marker that will provide an outright positive or negative diagnosis for any disease. Therefore, many groups have focused on developing a multiplexed diagnostic approach using miRNA or protein identification (see Tables 1.1). Specifically, for ovarian cancer, Yokoi et al.[117] developed an early stage diagnosis technique using expression levels of 8 different miRNAs with an area under the curve of 0.97. Furthermore, Zhao et al.[80] have used 3 exosome ovarian cancer markers, EpCAM, CA-125, and CD24, in conjunction to capture and identify ovarian cancer-specific exosomes. Lipids, which have been less frequently used to identify and differentiate EVs, offer an alternative method to EV biomarker detection. In particular, exosomes have been found to be enriched in particular lipids as compared to the parent cell.[118] For example, Skotland et al.[118, 119] have identified 9 different lipids that were differentially expressed in exosome membranes of prostate cancer patients. Chemical characterization of EVs may reveal important data about the composition and origins of

vesicles. Ultimately, a combination of exosome miRNA, protein, and lipid composition may provide a characterizing profile to identify many maladies.

Table 1.1. Potential exosome miRNA and protein markers for different types of ovarian, lung, and breast cancer.

Ovarian Cancer	miR-16, -21, -26a-5p, -93, -100, -126, -130b-3p -141, -142-3p, -200a-3p, -200b, -200c, -203, -205, -214, -223 -320, -328-3p, -374a-5p, -766-3p[117, 120, 121]	EpCAM, CA-125, CD24, L1CAM, ADAM10, EMMPRIN, TGFβ1, MAGE3/6, Claudin-4[12, 80, 101, 122]
Lung Cancer	miR-17, -3p, -21, -20b, -223, -301, -486, -181-5p, -30a-5p, -30e-3p, -361-5p, -10b-5p, -15b-5p, -320b, let-7d-5p, let-7f[123-125]	CD91, CD317, EGFR, LRG1, NY-ESO-1[30, 126-128]
Breast Cancer	miR-338-3p, -340-5p, and -124-3p, -29b-3p, -20b-5p, -17-5p, -130a-3p, -18a-5p, -195-5p, -486-5p, -93-5p, -1246, -373[129-131]	PKG1, RALGAPA2, NFX1, TJP2, Glypican-1, Her2[9, 132, 133]

Exosome Isolation Techniques

In order to take advantage of any of the potential benefits of exosomes, they must first be isolated from cell growth media or bodily fluids. Given that exosomes are approximately 30 to 150 nanometers in size, this is no easy task. Current techniques for isolating exosomes often involve a number of sequential centrifugation steps to eliminate larger materials from the media. Many isolation strategies follow the protocol laid out by Thery et al. that involves sequentially increasing ultracentrifugation of the media containing the exosomes.[134] Others elect to use filters to eliminate larger materials and

then pellet the exosomes using ultracentrifugation. Both of these current techniques for exosome isolation and other variations require the use of ultracentrifugation, which may not always be available in medical settings. There are a number of exosome isolation kits available commercially that have produced varying results. Importantly, the type of exosome isolation can impact protein and RNA downstream analysis. As it stands now, given the difficulty and varying effectiveness of these isolation techniques, it seems unlikely that any of them will perform effectively, efficiently, and consistently in a clinical setting. For these reasons, there is a need to refine or develop new techniques of exosome isolation that may be more suitable for medical environments.

Differential Centrifugation

Differential Centrifugation exosome isolation takes advantage of the ability of a centrifuge to separate out materials in solution based on the density and size of the material. Higher weight objects will move faster through the solvent and will thus sediment quicker from solution at lower centrifugation speeds. Lower weight objects will begin to sediment faster from solution at much higher centrifugation speeds.[135] Therefore, the heavier objects in the cell growth media (e.g. cells, apoptotic bodies, and debris) will sediment from solution and be removed in a primary centrifugation. A faster secondary centrifugation will pull down lighter objects, including larger EVs and microvesicles, to be removed, and finally a third and fastest centrifugation will sediment the desired exosomes.[136] Typical ultracentrifugation exosome isolations often require a final centrifugation speed greater than 100,000Xg. The ultracentrifugation process requires

upwards of 3 hours to complete depending on the number of centrifugation steps included and experience level of the personnel performing the isolation. Furthermore, the centrifuges and ultracentrifuges required for this method can very expensive (low speed centrifuges – several thousand dollars; high speed centrifuges - $15,000-$100,000) and may not be suitable for smaller labs and organizations. This exosome isolation method is crude, results in highly variant samples, and can potentially damage the exosomes due to the high speeds of centrifugation and the resuspension of the vesicles.[136] By nature of centrifugation, the final isolated exosome sample will contain anything from the original cell growth media of similar or lighter weight than an exosome (for example, lipoproteins and proteins)[137] and may contain aggregate vesicles and proteins. Furthermore, any larger particles that were not eliminated from the solvent may sediment along with the exosomes. Differential centrifugation is relatively easy to perform with the proper equipment and training, but often results in low purity samples with fairly low efficiency. However, due to the relative ease with which this method can be performed, it is one of the most common exosome isolation techniques used today.

Density Gradient Centrifugation

Density gradient centrifugation is very similar to differential centrifugation but includes an extra medium that increases the viscosity of the solution. There are two types of gradients, isopycnic and rate zonal, that have been used to isolate exosomes.[137] During isopycnic gradient centrifugation, samples are dispersed within the gradient medium and separate components based on density, whereas during zonal gradient centrifugation samples are layered as a narrow band at the top of the gradient medium and separate

components based on size (Figure 1.3).[135] Exosome density gradient centrifugation typically uses a sucrose or iodixanol solution that is compatible with the lipid bilayer of the exosomes and vesicles. By increasing the viscosity of the solution, objects of very similar density can be differentiated and separated more easily. Therefore, this method of exosome isolation can result in purer exosome samples with less debris. However, even though the final sample can be purer than differential centrifugation, the range of centrifugation speeds and range of centrifuge times must be more accurate to be in the proper density range for exosomes. Monitoring the centrifugation times and speeds makes this method more difficult than differential centrifugation alone due to the increased density sensitivity of the solution. Variations of density gradient centrifugation have been used to develop exosomes samples for use in clinical trials.[21, 22, 138]

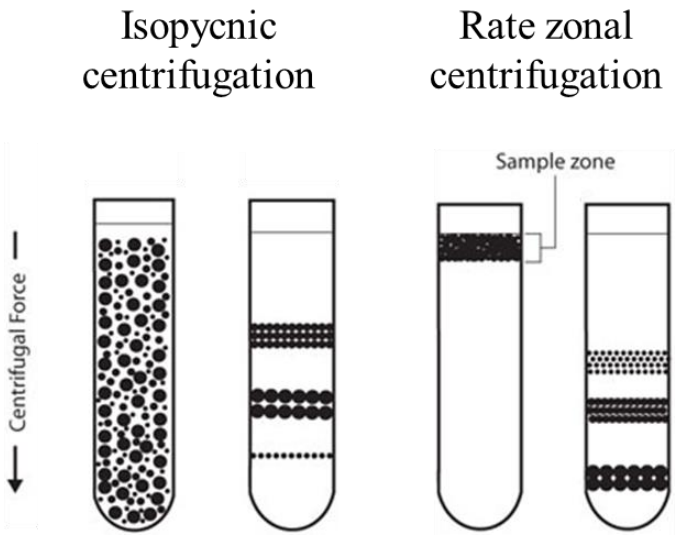

Figure 1.3. Diagram of Isopycnic and Rate zonal density centrifugation. Adapted from Sigma-Aldrich (St, Louis, MO).

Size Exclusion Chromatography

Size exclusion chromatography (SEC) is used to separate molecules within a solution based on the size of the molecule rather than the density or weight of the molecule. The solution flows through a size exclusion column containing small stationary phase beads with nanometer–sized pores. Smaller molecules in the solution will enter and adsorb in the pores, thus slowing their rate of flow through the column and delaying the time of elution. Larger molecules will flow through the column without entering the adsorbent material pores and elute quicker. The same principle can be applied to isolate exosomes from other components of the solution. Böing et al.[139] use sepharose CL-2B beads with 75 nm pores to separate out exosomes from solution. Furthermore, several groups have used SEC in conjunction with other exosome purification or enrichment techniques, such as ultrafiltration or ultracentrifugation, to achieve higher purity samples.[140-142] Size exclusion chromatography can very accurately separate exosomes from solution based on size, but the final exosome eluate may also contain other materials of similar size. Additionally, size exclusion chromatography limits any shear force damage to the exosomes and prevents protein and vesicle aggregation. Despite its efficiency and accuracy, size exclusion chromatography may be severely limited by the amount of eluate obtained and the time it takes to flow through the column.[140, 143, 144] However, recent improvements in this technique have led to faster and cheaper separation of molecules. Böing et al.[139] demonstrate that this technique can be used to isolate a sample of exosomes in as little as 20 minutes.

Ultrafiltration

Much like SEC, ultrafiltration isolates exosomes based on size or molecular weight using pore sizes ranging from 0.8 to 0.1μm.[145] Ultrafiltration is much faster and cheaper than ultracentrifugation, and does not require large, specialized machinery.[146] Similar to SEC, ultrafiltration has been used in tandem with ultracentrifugation or SEC to isolate exosomes.[147, 148] Fluorescent imaging has revealed that ultrafiltration results in a higher RNA yield compared to ultracentrifugation.[149] Unfortunately, by the nature of filtration, any molecules that are smaller than the pore size will pass through into the final sample, resulting in particle contamination.[145] In order to alleviate protein contamination and remove molecules smaller than exosomes, a sequential ultrafiltration has been used to purify the exosomes further. Sequential ultrafiltration of exosomes consists of an initial "dead-end" filtration to remove cells and debris. A secondary tangential flow filtration is used to remove proteins and molecules with a 500kDa filter. Finally, a filter with a pore size of 100 nm is used to isolate the exosomes.[137] Ultrafiltration has been used to isolate exosomes from a variety of cell types and biological fluids, and has been used to isolate exosomes from as little as 0.5 mL of urine.[137, 145, 147, 150]

Polymer-based Precipitation

Exosomes can be precipitated out of solution by manipulating the content of the solvent. In phosphate buffered saline, exosomes will remain in solution, but altering the solvent can change the solubility of the exosomes. By adding a polymer, such as polyethylene glycol (PEG), exosomes will precipitate out of solution at low speed centrifugation.[146] This method requires either pre-centrifugation or pre-filtration to remove cells and larger debris from solution. Polymer-based precipitation can be

performed easily, inexpensively, effectively, and can be completed on a large scale. However, the precipitate may contain polymers and other undesired molecules of similar solubility.[137, 151, 152] Further steps must be taken to fully purify the exosome sample including pre-isolation of lipoproteins and post-isolation of polymeric materials.[137] Several commercially available polymer-based precipitation EV isolation kits that operate with minimal sample exist, including Total Exosome Isolation (Invitrogen, Carlsbad, CA)), ExoQuick exosome precipitation solution (System Biosciences, Palo Alto, CA).[151] The availability and ease of use of polymer-based precipitation kits makes them promising and convenient techniques for research and clinical purposes.

Immunological Separation

Immunoaffinity capture of exosomes is a promising exosome isolation technique with high specificity.[153] Since exosome lipid membranes are composed of proteins, receptors, and transmembrane proteins, antibodies can be developed to specifically target, capture, and isolate exosomes. Immunological separation requires understanding the membrane content of exosomes from all sources and requires discovering a protein or receptor that is common to all exosomes. However, a protein or receptor common to all exosomes must not be common to other biological components of the cellular media. Due to the high specificity of antibodies in immunological separation, exosomes can be isolated at similar efficiency to ultracentrifugation, but with much smaller samples.[113, 137, 154] Several variations of immunoaffinity capture, including modified ELISA exosome isolation and magneto-immunocapture, have had success isolating exosomes with high efficiency.[29, 155-157] Despite the efficiency, effectiveness, quality, and speed of

immunological separation of exosomes, there is still an incomplete understanding of exosome membrane content. It is difficult to differentiate proteins specific to exosomes when much of the content of the exosomal membrane is derived from the cellular membrane. Currently, a common protein targeted is CD63, a tetraspanin membrane protein common to many human exosomes. However, CD63, and other similar tetraspanin proteins can also be found in apoptotic bodies and other extracellular vesicles.[30, 158, 159] Immunoaffinity-based separations using specific antibodies are excellent techniques for isolating exosomes, especially for high quantity and quality RNA extraction from exosomes. Even with a poor understanding of exosome membrane composition, immunoseparation may produce high yields and generate subpopulations of isolated exosomes and extracellular vesicles.[137]

Microfluidics Isolation techniques

Newer strategies involving microfluidics devices have begun to permeate the realm of exosome isolation, as advancing fabrication processes have allowed for easier manufacturing of microfluidics devices. Many of these new techniques use a device that operate on one or more of the principle isolation strategies discussed above. For instance, Lee et al.[160] have developed an acoustic nanofilter that uses ultrasound to isolate microvesicles based on size and density, while Wang[161] et al. have developed ciliated micropillars for selectively capturing lipid vesicles of 40-100nm in size. According to Yang et al.[162], microfluidic device exosome isolation techniques have the potential to be faster and more effective than the current standard exosome isolation techniques.

However, each individual microfluidics technique has drawbacks and many of the devices are still early in development.

Although there are many strategies for isolating exosomes, there is no clear method that stands above the rest. Each technique has its own benefits and downfalls whether it be isolation efficiency, exosome purity, exosome integrity, RNA extraction, cost, scalability or ease of use (see separation strategies summary in Table 1.2). With the realization of the possibilities of exosome technology, there is clearly a need for a solution to exosome isolation.

Table 1.2. A brief summary of extracellular vesicle separation strategies

EV Isolation Method	*Concept*	*Pros*	*Cons*
Ultracentrifugation	Series of differential centrifugations requiring up to 100,00 X G	• Relatively easy to perform and simple procedure	• Potentially damaging to vesicles • Produces impure samples • Time and cost prohibitive
Gradient ultracentrifugation	Centrifugation of sample through a more viscous medium to separate components by density or size	• Produces purer subpopulation of vesicles	• Must be more accurate with centrifugation times • More difficult than normal ultracentrifugation
Size-exclusion chromatography	Fluid flow through stationary phase beads with nanometer sized pores as a size cutoff	• Produces pure sample • Efficient and accurate separation	• May contain contaminants of similar size to vesicles • Limited sample size
Ultrafiltration	Uses filter sizes of 0.8 – 0.1 µm to separate vesicles under vacuum	• Faster and cheaper than ultracentrifugation • Does not require specialized machinery	• Potentially damaging to vesicles • Potential contamination with similar size particles
Polymer-based precipitation	Addition of a polymer to the sample solution will alter the solubility of the vesicles and cause vesicle precipitation	• Easy to perform • Inexpensive • Can be completed on large scales	• Polymer contaminants can remain in solution • Many pre- and post-purification steps required
Immunological separation	Uses antibodies to EV-specific membrane proteins to capture and separate vesicles	• Highly selective toward vesicle populations • Quick separation • Can be added to other separation methods to increase specificity	• Limited sample size • Incomplete understanding of vesicle membrane proteins • May capture larger vesicles as well
Microfluidics isolation	Frequently pair fluid flow and immunological separation techniques to reduce separation disadvantages	• High specificity • Fast, accurate, and specific isolation • Automatic sample processing	• Limited sample size • Early in development

Exosome Loading Techniques

There are a number of different ways to load exosomes with drugs or other markers including electroporation, sonication, saponin incubation, extrusion, transfection, and drug incubation.[83, 89, 91, 94] In general, these and other exosome loading techniques can be categorized as exogenous loading or endogenous loading. Exogenous loading techniques are methods of loading exosomes after the exosomes have been isolated. Conversely, endogenous loading techniques are methods of loading exosomes before the exosomes have been released from the cell.

Exogenous loading

Separated exosomes can be prone to further damage after isolation that may limit their viability and capability to perform functions. In order to load material into the exosomes, exogenous techniques often employ potentially destructive and damaging stimuli to open temporary holes in the exosomal membranes. These techniques, including electroporation, saponin permeabilization, sonication, extrusion, transfection, and drug incubation, while effective, destroy many vesicles in the process.[23, 83, 89] Electroporation is a method of shocking the plasma membrane with a relatively low voltage. The electric shock temporarily makes the plasma membrane of the exosome more permeable and allows for contents in the surrounding solution to enter the exosome. Alvarez et al.[23] have employed this technique to load siRNA into exosomes for drug delivery and treatment of Alzheimer's disease. Typical applications of electroporation involve transfecting genetic material into cells of various types. Sonication, another potential exosome loading

technique, also disrupts the stability of the plasma membrane, thus making the plasma membrane more permeable to loading. According to Haney et al.[83], saponin is a surfactant that is thought to remove plasma membrane cholesterol, temporarily creating holes in the plasma membrane allowing surrounding solution content to load into the exosome. Much like sonication, extrusion and freeze/thaw methods disrupt the integrity of the lipid bilayer and increase the permeability of the plasma membrane. All of these methods have been shown to enable loading of exosomes, but with varying effectiveness and stability. There are many advantages and disadvantages to these approaches, but Haney et al. and Alvarez et al. have shown that exosomes loaded with these methods are still effective for drug delivery.[23, 83]

Endogenous loading

Endogenous loading techniques are significantly less destructive to exosomes, but can be significantly more difficult to accomplish. Loading of an exosome in this manner could mean either modifying the membrane content of the vesicle or having the exosome-producing cell automatically load the vesicles with the appropriate proteins or nucleic acids for drug delivery. In exosomes, modifying membrane protein content is primarily accomplished using genetically engineered plasmid vectors. The plasmids are encoded with particular targeting proteins or peptides that will then be expressed in the cell and inserted into the plasma membrane. Specifically, Alvarez et al.[23, 163] inserted a modified targeting peptide plasmid for Lamp2b, a known exosome membrane protein. They verified the successful expression of the modified Lamp2b peptide using an exosome protein pulldown assay. The modified Lamp2b exosomes primarily targeted neurons,

microglia, and oligodendrocytes, as planned. Furthermore, the Lamp2b exosomes successfully targeted and knocked down *BACE1* expression in neurons, microglia and oligodendrocytes by 60% and 62% using mRNA and protein respectively. BACE1 is a gene involved in Alzheimer's pathogenesis that could be knocked out for potential therapy. Similarly, Monfared et al.[164] have engineered exosomes to express membrane miR-21 sponges in order to induce apoptosis in tumor cells. The ability to modify exosome plasma membrane content is a vital step in targeted drug delivery and evidence has thus far shown that specific targeting with exosomes is possible and effective. One strategy for loading proteins or nucleic acids into the cytosol of exosomes is to engineer the exosome-releasing cells to overexpress the molecule to be loaded.[165] Alternatively, Yim et al.[165] have developed a more advanced method of selective drug loading during biogenesis using exosomes for protein loading via optically reversible protein-protein interaction (EXPLORs). EXPLORs uses engineered cell lines that express selective membrane docking proteins that are photo-activated using blue light. This technique has demonstrated very high loading efficiency in comparison to other loading techniques. Endogenous engineering of vesicle membrane proteins and protein cargo may be used to create a drug delivery system requiring only exosome isolation and administering to patients.

Liquid Chromatography

Although most liquid chromatography (LC) techniques have been used to separate proteins and other macromolecules, there is potential for LC isolation of more complex bio-molecules, including extracellular vesicles and exosomes. LC is a chemical technique

that allows for separation of molecules from solution. Modern LC, referred to as high performance liquid chromatography (HPLC), can be used to separate, detect, and quantify molecules and can isolate molecules based on hydrophobicity, charge, or size.[166] Choice of solid and liquid phase components can determine which molecules can be separated from solution and often vary depending on the specific application. HPLC has been used to separate a variety of types of molecules including amino acids, carbohydrates, lipids, nucleic acids, proteins, steroids, and biological substances.[144] Depending on the physical properties being used, HPLC can be generally subdivided into several categories including normal-phase, reversed-phase, ion-exchange, and size-exclusion. Normal-phase describes liquid chromatography that uses a polar stationary phase and hydrophobic mobile phase, whereas reversed-phase describes liquid chromatography that uses a hydrophobic stationary phase and polar mobile phase.[166] Furthermore, ion-exchange separates molecules based on charge properties and size-exclusion typically uses columns packed with microbeads that slow down the flow of molecules based on size.[139, 144, 167] Although HPLC has typically been used to isolate small or individual molecules, larger more complex biological components have been separated as well. For example, Kasanović et al.[167] have used ion-exchange chromatography to separate EVs from amniotic fluid and An et al.[142] have used size-exclusion chromatography to separate exosomes from human serum. To this end, a variety of combinations and expansive methods of HPLC exist beyond the standard classification that have a diverse set of applications across chemical, material, and biological fields.

One particular type of LC, known as hydrophobic interaction chromatography (HIC), is a variant of reversed-phase LC. HIC, like reversed-phase, uses a stationary phase that is more hydrophobic than the mobile phase. Reversed-phase LC relies on adjusting the polarity of the mobile phase using an organic solvent until the mobile phase is more hydrophobic than the stationary phase.[144] HIC, on the other hand, relies on adjusting the salt concentration of the mobile phase from high concentration to low concentration to change the polarity (see Figure 1.4).[168, 169] Increased concentrations of chaotropic ions can influence the solubility of hydrophobic molecules and cause hydrophobic molecules to adsorb to the stationary phase. Molecule adherence to the stationary phase can be explained by the "salting-out" phenomena, thermodynamics, and van der Waals forces.[4, 144, 168-171] In order to optimize the HIC separation gradient steepness, salt concentration, volume of sample, pH, type of matrix, and flow rates can be varied.[172] HIC may be less damaging than reversed-phase LC and, thus, is often used to separate more sensitive bio-molecules.[168, 173] Most commonly, HIC is used to separate proteins and large polypeptides, but many groups have used HIC for a variety of applications including the separation and isolation of monoclonal antibodies.[168, 169, 174] With this in mind, HIC may provide a method to isolate more complex and larger bio-molecules under the appropriate conditions. In this case, our research group is investigating whether HIC combined with poly(ethylene terephthalate) Capillary-Channeled fibers may be a suitable isolation method for exosomes and extracellular vesicles.[175]

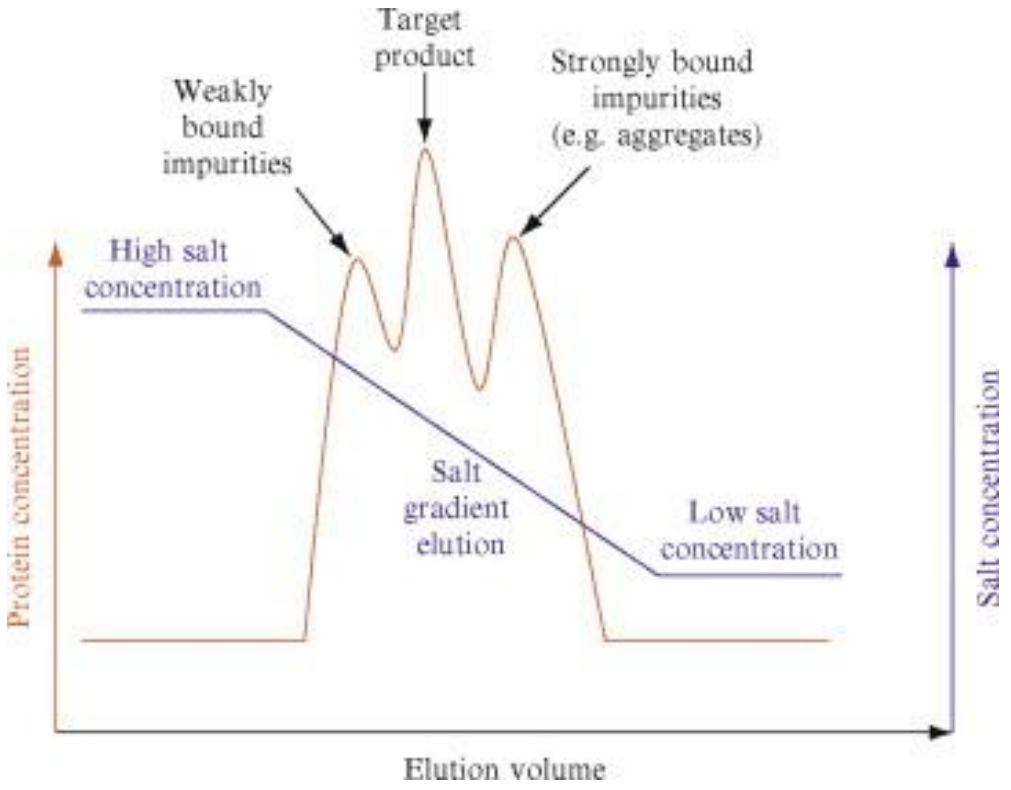

Figure 1.4. Demonstration of hydrophobic interaction chromatography separation theory using a salt concentration gradient. Adapted from McCue et al.[4]

Ovarian Cancer Detection, Diagnosis, and Treatment

Ovarian cancer (OC) is the 7th most diagnosed cancer in women and generally reflects a very poor 5-year prognosis.[5] OC consists of several different histological subtypes that vary in genetic expression, origin, pathogenesis, prognosis, and treatments. Of these subtypes, epithelial ovarian cancer accounts for about 90% of all diagnosed benign and malignant tumors. Malignant epithelial OC can be further subdivided into histotypes including high-grade serous, endometrioid, clear cell, mucinous, and low-grade serous.[5] The pathogenesis and development of OC is still very unclear, but many types may originate from the fallopian tubes or peritoneum.[176, 177] OC is typically detected in late stage, with a 5-year relative survival rate of 29% with early stage 1 detection only occurring about 15% of the time. However, if OC is detected in stage 1, the 5-year relative survival rate is 92%.[5] Early detection of OC is very difficult and effective means for early detection do not currently exist. However, genetic sequencing now allows for detection of particular gene alleles that are correlated with a higher risk of developing OC, including BRCA1/2, MMR, TP53, CHEK2, RAD51, BRIP1, and PALB2 genes.[178] Even with genetic marker testing and screening available, the hallmark of OC remains late stage diagnosis and the corresponding stark prognosis and mortality rates.[179, 180]

The most common methods for OC detection include a transvaginal ultrasound and screening for CA-125 in serum.[181] Combined, these methods are capable of detecting OC and differentiating malignant and benign tumors in low-risk postmenopausal women, but are not highly sensitive in many cases.[182] Once a tumor is detected, biopsy and

histopathological assessment can determine the type, stage, severity, prognosis, and treatment options. New biomarkers in conjunction with CA-125 have been used to increase screening sensitivity and specificity including HE4, CEA, VCAM-1, transthyretin, apolipoprotein A1, β2-microglobulin, and transferrin. However, multiplexed biomarker testing is not prevalent or proven yet.[181] Earlier detection of OC, once achieved, would likely improve prognosis and mortality rates, but current general population screens are not standard.[183]

Regardless of the type and stage, OC, once diagnosed, is typically treated by surgical removal of the tumor often combined with intraperitoneal and intravenous chemotherapy.[184, 185] Interval cytoreduction combined with chemotherapy has remained the standard treatment for late stage treatment of OC, but has only seen a small reduction in mortality over the last 25 years, likely due to preventative measures and accuracy of surgical techniques. More recently, cytoreduction has been paired with neoadjuvant chemotherapy and hyperthermic intraperitoneal chemotherapy, but there is some debate whether or not these techniques are more effective.[185] Indeed, there is a clear need for new strategies and therapies to treat and eradicate OC growth, metastasis, and recurrence.

High-grade serous OC is associated with hypoxic angiogenesis, over-production of vascular endothelial growth factor (VEGF), and the subsequent development of ascites.[186] Therefore, one new therapy strategy is to use anti-angiogenic drugs to combat OC growth and recurrence. Bevacizumab, a VEGF antagonist, has shown promise in reducing recurrence, but its use is controversial due to differences in regulatory approval, varying strategies of use, and lack of improvement over other therapies.[185, 186] Other anti-

angiogenic drugs under investigation include cediranib, pazopanib, nintedanib, and angiopoietin inhibitor.[185] Treatment with Poly(ADP-ribose) Polymerase (PARP) inhibitors are also being investigated as inducers of synthetic lethality in OC and other cancers through disruption of DNA repair.[187] PARP inhibitors, including olaparib, niraparib, rucaparib, have shown promise as primary and post primary treatment, particularly in OC patients with BRCA mutations.[185] Other therapies for OC under investigation include epidermal growth factor receptor tyrosine kinase inhibitors, folate receptor α inhibitors, and immunotherapy.[185] Treatment options for OC are quickly advancing and have demonstrated improvement in survival rates and reduction of recurrence. Even so, OC remains one of the most lethal gynecological maladies, likely due to the asymptomatic nature of early stages leading to late stage detection.[186]

Role of Exosomes in Cancer Metastasis

Tumor invasion, metastasis, and the formation of secondary tumors is the primary reason for high mortality in most cancers.[188] Metastatic tumors are characterized by invasion, intravasation and extravasation into distant tissues, often having very poor outcomes.[189] The stages of tumor epithelial-mesenchymal transition and eventual tumor metastasis are controlled by a number of cascading biological pathways involving many cell types, cytokines, growth factors, chemokines, and small molecule mediators delivered by exosomes.[77, 190, 191] In fact, tumors have been found to release a higher number of exosomes into the microenvironment compared to healthy cells.[192] Typically, exosomes involved in tumor metastasis will influence the microenvironment and surrounding cells to prepare the area for tumor growth and create a pre-metastatic

niche.[193] Such preparations may include promotion of angiogenesis, adaptation to hypoxic environments, immune evasion, and promotion of inflammation (see Figure 1.5).[1, 104, 105, 194-199] Specifically, exosomes can recruit bone-marrow derived cells to mediate vascular permissiveness and inflammation, ultimately leading to pre-metastatic preparation of the extracellular matrix.[50, 77, 200] Additionally, pro-angiogenic factors transmitted by tumor-derived exosomes can boost vascular development which may aid in the development of the pre-metastatic niche and minimize the lethal effects of a hypoxic environment. Furthermore, tumor-derived exosomes may escape immune surveillance by inducing cytotoxic T-cell apoptosis, decreasing natural killer cell activity, and pushing T-helper cells to differentiate into T-regulatory cells that promote inflammation.[1, 197, 198, 201] In short, exosomes are intricately involved in the growth and spread of tumors and new pathways and functions are frequently being unveiled. Greater understanding of the role of exosomes in tumor metastasis and any corresponding pathways will enhance the ability to develop therapies or treatments to prevent or stop tumor proliferation.

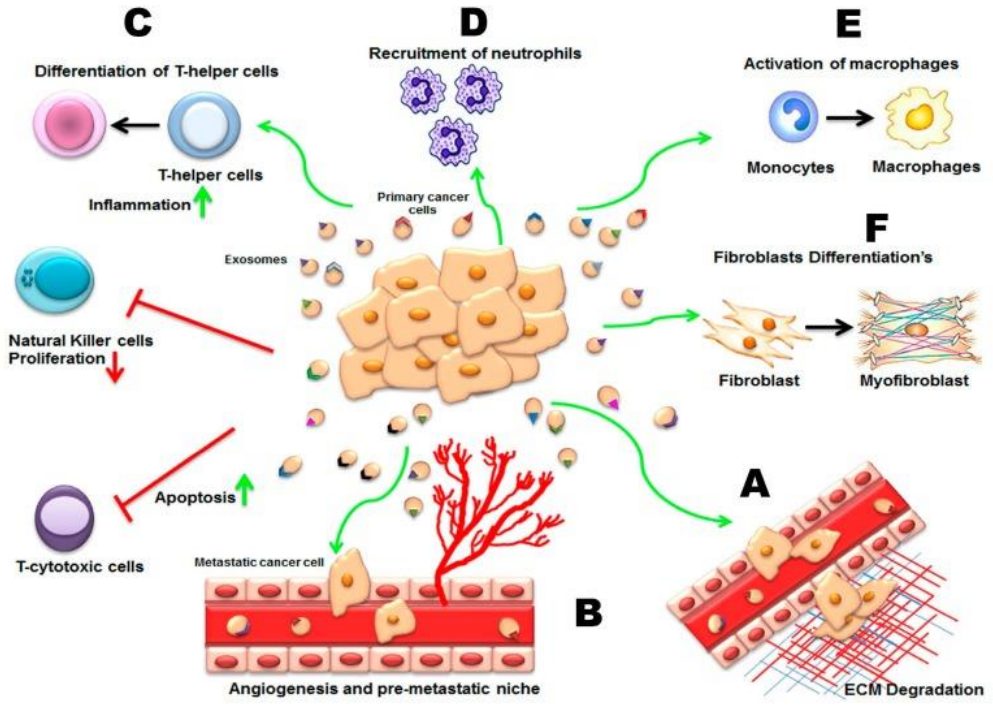

Figure 1.5. Various roles of exosomes released from primary cancer cells. Adapted from Rashed et al.[1]

Role of Exosomes in Ovarian Cancer Diagnosis

As they are carriers of proteins and nucleic acids and are heavily involved in tumor metastasis, exosomes are thought to be potential biomarkers for cancerous cells and tumor progression. By capturing exosomes from circulating fluids, the signal-to-noise ratio of cancer-related molecules can be greatly improved when screening for tumor markers. In recent years, exosome marker identification has yielded an array of common exosome markers that may be useful for capturing and identifying specific types of exosomes and their origins. Identification of an exosome's cell of origin, the molecular cargo carried inside, and potential target cell reveals valuable information about

objectives of the exosomes, the physiological state of the original cell, and potential diagnostic information from diseased cells. Particularly, exosomes are being investigated as potential early stage biomarkers for OC as a remedy for late stage diagnosis. Both protein and miRNA exosome marker profiles are being developed to aid in the diagnosis of OC. Zhao et al.[80] have developed a microfluidics device that captures and identifies OC-specific exosomes using CA-125, EpCAM, and CD24 markers with potential diagnostic ability. Further advances in protein marker profiles for OC will likely enhance diagnostic sensitivity and specificity using multiplexed protein approaches. Similarly, Yokoi et al.[117] have used a combination of 8 different OC-associated exosome miRNA molecules to achieve an area under the curve of 0.97, a sensitivity of 0.92 and a specificity of 0.91 for OC diagnosis. Interestingly, when capturing EpCAM positive exosomes, Taylor et al.[120] found that exosome miRNA profiles had a high correlation with miRNA profiles from the associated biopsy and that miRNA profiles tended to differ between benign and cancerous tumors. This suggests that exosome miRNA profiles may vary enough to differentiate between tumor types and physiological states. Multiplexed exosome biomarker approaches offer promising early diagnostic capabilities for OC and other cancers. In particular, OC stands to benefit greatly from early stage diagnosis as stage 1 detection results in a 92% 5-year relative survival rate.[5]

SKOV-3 and Immortalized Human Ovarian Epithelial Cells

Cell lines are important tools that can be used as models to be able to study biological phenomena. Several cell lines, including SKOV-3, OVCAR-2, OVCAR-3, OVCAR-433, OVCAR-5, IGROV1, and BG-1 have all been used for exosome research

in relation to ovarian cancer.[38, 122, 202, 203] In particular, the SKOV-3 line, a high-grade adenocarcinoma cell line, is among the most popular and commonly used cell lines in publications reporting on OC. It is one of two cell lines that make up 60% of publications relating to OC and one of five cell lines that make up 90% of publications relating to OC.[204] Their popularity and high-grade serous derivations, fast growth rate, and abundant production of extracellular vesicles are some of the main reasons SKOV-3 cells have emerged as popular cells for exosome study. Despite their popularity, many cells lines, including SKOV-3 cells, have come under scrutiny over representative accuracy or how well the cell line genetically and physically represents the original parent carcinoma.[204, 205] Even so, with little in the way of other available options (primary cells are not feasible in most research settings), cell lines remain very popular and widespread and, for the most part, still provide insightful and accurate results.

Most cell lines, by their very nature, are derived from diseased primary cells. Often, the disease is the purveyor of the immortality required to become an endlessly replicating cell line. As with any experiment, it is important to maintain a control, but control cells lines of normal, non-diseased cells, can be difficult to find and maintain. Primary cell lines, which can be used as controls, do not replicate indefinitely *invitro* and are considerably less hardy. Fortunately, immortalized primary cells have emerged as viable alternatives to normal primary cells.[206-208] Through genetic modification of tumor suppressor and cell cycle controller genes, more genetic variance is introduced into the cell environment. Although these are major changes to the cell cycle, immortalized cells are considered more genetically and physically similar to primary cells than carcinoma-

derived cell lines and thus have been used as control cell lines in research.[209] In the case of OC, Immortalized Human Ovarian Epithelial cells, created through simian virus transduction, can be used as a viable control cell line in extracellular vesicle and exosome research

Summary

The mechanisms and roles of exosomes are incredibly complex and evidence thus far has demonstrated the intricate involvement of exosomes in a number of processes, including cell-cell communication and tumorigenesis.[8, 104, 210] Increased understanding of exosomes and their roles in the body will undoubtedly result in fundamental insights that may lead to breakthroughs in such areas as liquid biopsy-based diagnostics, understanding of disease progression and development of new medical treatments. However, to date, exosome isolation presents a number of fundamental challenges that must be overcome before academic research can progress to the point of translational medical applications. An exosome isolation methodology that is practical for use in a clinical setting is greatly needed.

In the following research, we have a developed an EV isolation method and model systems that will support earlier and routine OC diagnosis. The three specific aims of this project are:

1. To develop and investigate a novel poly(ethylene terephthalate)(PET) capillary-channeled polymer (C-CP) fiber-based extracellular vesicle isolation method using *Dictyostelium discoideum* as a model organism.

2. To create fluorescent Immortalized Human Ovarian Epithelial (IHOE)-CD81-GFP (non-cancerous) and SKOV-3-CD9-RFP (cancerous) cell lines to produce green and red small extracellular vesicles, respectively, for use as model sEVs to investigate PET C-CP fiber-based selective EV capture.

3. To investigate urine and cervical mucus as EV sample sources and explore EV miRNA expression data as a tool for distinguishing between ovarian cancer and non-cancer patient samples and discovering novel ovarian cancer biomarkers for use in diagnostics.

References

1. Rashed M, Bayraktar E, Helal G, et al. Exosomes: From Garbage Bins to Promising Therapeutic Targets. Review. *International Journal of Molecular Sciences*. MAR 2017 2017;18(3)ARTN 538. doi:10.3390/ijms18030538

2. Raposo G, Stoorvogel W. Extracellular vesicles: exosomes, microvesicles, and friends. *J Cell Biol*. Feb 2013;200(4):373-83. doi:10.1083/jcb.201211138

3. Mulcahy LA, Pink RC, Carter DR. Routes and mechanisms of extracellular vesicle uptake. *J Extracell Vesicles*. 2014;3doi:10.3402/jev.v3.24641

4. McCue JT. Theory and use of hydrophobic interaction chromatography in protein purification applications. *Methods Enzymol*. 2009;463:405-14. doi:10.1016/S0076-6879(09)63025-1

5. Reid BM, Permuth JB, Sellers TA. Epidemiology of ovarian cancer: a review. *Cancer Biol Med*. Feb 2017;14(1):9-32. doi:10.20892/j.issn.2095-3941.2016.0084

6. Urbanelli L, Magini A, Buratta S, et al. Signaling pathways in exosomes biogenesis, secretion and fate. *Genes (Basel)*. Mar 2013;4(2):152-70. doi:10.3390/genes4020152

7. Vlassov AV, Magdaleno S, Setterquist R, Conrad R. Exosomes: current knowledge of their composition, biological functions, and diagnostic and therapeutic potentials. *Biochim Biophys Acta*. Jul 2012;1820(7):940-8. doi:10.1016/j.bbagen.2012.03.017

8. Yáñez-Mó M, Siljander PR, Andreu Z, et al. Biological properties of extracellular vesicles and their physiological functions. *J Extracell Vesicles*. 2015;4:27066.

9. Fang S, Tian H, Li X, et al. Clinical application of a microfluidic chip for immunocapture and quantification of circulating exosomes to assist breast cancer diagnosis and molecular classification. *PLoS One*. 2017;12(4):e0175050. doi:10.1371/journal.pone.0175050

10. Cheng L, Wu S, Zhang K, Qing Y, Xu T. A comprehensive overview of exosomes in ovarian cancer: emerging biomarkers and therapeutic strategies. *J Ovarian Res*. Nov 2017;10(1):73. doi:10.1186/s13048-017-0368-6

11. Beach A, Zhang H, Ratajczak M, Kakar S. Exosomes: an overview of biogenesis, composition and role in ovarian cancer. Review. *Journal of Ovarian Research*. JAN 25 2014 2014;7ARTN 14. doi:10.1186/1757-2215-7-14

12. Li W, Li C, Zhou T, Liu X, Li X, Chen D. Role of exosomal proteins in cancer diagnosis. *Mol Cancer*. 08 2017;16(1):145. doi:10.1186/s12943-017-0706-8

13. Li M, Zeringer E, Barta T, Schageman J, Cheng A, Vlassov AV. Analysis of the RNA content of the exosomes derived from blood serum and urine and its potential as biomarkers. *Philos Trans R Soc Lond B Biol Sci*. Sep 2014;369(1652)doi:10.1098/rstb.2013.0502

14. Su S, Xie Y, Fu Z, Wang Y, Wang J, Xiang M. Emerging role of exosome-mediated intercellular communication in vascular remodeling. Review. *Oncotarget*. APR 11 2017 2017;8(15):25700-25712. doi:10.18632/oncotarget.14878

15. Lu M, Xing H, Xun Z, et al. Exosome-based small RNA delivery: Progress and prospects. Review. *Asian Journal of Pharmaceutical Sciences*. JAN 2018 2018;13(1):1-11. doi:10.1016/j.ajps.2017.07.008

16. Li A, Zhang T, Zheng M, Liu Y, Chen Z. Exosomal proteins as potential markers of tumor diagnosis. *J Hematol Oncol*. 12 2017;10(1):175. doi:10.1186/s13045-017-0542-8

17. Boukouris S, Mathivanan S. Exosomes in bodily fluids are a highly stable resource of disease biomarkers. *Proteomics Clin Appl*. Apr 2015;9(3-4):358-67. doi:10.1002/prca.201400114

18. Console L, Scalise M, Indiveri C. Exosomes in inflammation and role as biomarkers. *Clin Chim Acta*. Jan 2019;488:165-171. doi:10.1016/j.cca.2018.11.009

19. Li Y, Liu M, Yang ST. Dendritic cells derived from pluripotent stem cells: Potential of large scale production. *World J Stem Cells*. Jan 2014;6(1):1-10. doi:10.4252/wjsc.v6.i1.1

20. Dai S, Wei D, Wu Z, et al. Phase I clinical trial of autologous ascites-derived exosomes combined with GM-CSF for colorectal cancer. *Mol Ther*. Apr 2008;16(4):782-90. doi:10.1038/mt.2008.1

21. Morse MA, Garst J, Osada T, et al. A phase I study of dexosome immunotherapy in patients with advanced non-small cell lung cancer. *J Transl Med*. Feb 2005;3(1):9. doi:10.1186/1479-5876-3-9

22. Escudier B, Dorval T, Chaput N, et al. Vaccination of metastatic melanoma patients with autologous dendritic cell (DC) derived-exosomes: results of thefirst phase I clinical trial. *J Transl Med*. Mar 2005;3(1):10. doi:10.1186/1479-5876-3-10

23. Alvarez-Erviti L, Seow Y, Yin H, Betts C, Lakhal S, Wood MJ. Delivery of siRNA to the mouse brain by systemic injection of targeted exosomes. *Nat Biotechnol*. Apr 2011;29(4):341-5. doi:10.1038/nbt.1807

24. Akers JC, Gonda D, Kim R, Carter BS, Chen CC. Biogenesis of extracellular vesicles (EV): exosomes, microvesicles, retrovirus-like vesicles, and apoptotic bodies. *J Neurooncol*. May 2013;113(1):1-11. doi:10.1007/s11060-013-1084-8

25. Harding C, Heuser J, Stahl P. Endocytosis and intracellular processing of transferrin and colloidal gold-transferrin in rat reticulocytes: demonstration of a pathway for receptor shedding. *Eur J Cell Biol*. Nov 1984;35(2):256-63.

26. Pan BT, Teng K, Wu C, Adam M, Johnstone RM. Electron microscopic evidence for externalization of the transferrin receptor in vesicular form in sheep reticulocytes. *J Cell Biol*. Sep 1985;101(3):942-8.

27. Hessvik NP, Llorente A. Current knowledge on exosome biogenesis and release. *Cell Mol Life Sci*. 01 2018;75(2):193-208. doi:10.1007/s00018-017-2595-9

28. Colombo M, Moita C, van Niel G, et al. Analysis of ESCRT functions in exosome biogenesis, composition and secretion highlights the heterogeneity of extracellular vesicles. *J Cell Sci*. Dec 2013;126(Pt 24):5553-65. doi:10.1242/jcs.128868

29. Oksvold MP, Neurauter A, Pedersen KW. Magnetic bead-based isolation of exosomes. *Methods Mol Biol*. 2015;1218:465-81. doi:10.1007/978-1-4939-1538-5_27

30. Sandfeld-Paulsen B, Aggerholm-Pedersen N, Bæk R, et al. Exosomal proteins as prognostic biomarkers in non-small cell lung cancer. *Mol Oncol*. 12 2016;10(10):1595-1602. doi:10.1016/j.molonc.2016.10.003

31. Street JM, Barran PE, Mackay CL, et al. Identification and proteomic profiling of exosomes in human cerebrospinal fluid. *J Transl Med*. Jan 2012;10:5. doi:10.1186/1479-5876-10-5

32. Zhang J, Li S, Li L, et al. Exosome and exosomal microRNA: trafficking, sorting, and function. *Genomics Proteomics Bioinformatics*. Feb 2015;13(1):17-24. doi:10.1016/j.gpb.2015.02.001

33. Villarroya-Beltri C, Baixauli F, Gutiérrez-Vázquez C, Sánchez-Madrid F, Mittelbrunn M. Sorting it out: regulation of exosome loading. *Semin Cancer Biol*. Oct 2014;28:3-13. doi:10.1016/j.semcancer.2014.04.009

34. Tricarico C, Clancy J, D'Souza-Schorey C. Biology and biogenesis of shed microvesicles. *Small GTPases*. 10 2017;8(4):220-232. doi:10.1080/21541248.2016.1215283

35. Huang T, Deng CX. Current Progresses of Exosomes as Cancer Diagnostic and Prognostic Biomarkers. *Int J Biol Sci*. 2019;15(1):1-11. doi:10.7150/ijbs.27796

36. Abels ER, Breakefield XO. Introduction to Extracellular Vesicles: Biogenesis, RNA Cargo Selection, Content, Release, and Uptake. *Cell Mol Neurobiol*. Apr 2016;36(3):301-12. doi:10.1007/s10571-016-0366-z

37. D'Souza-Schorey C, Clancy JW. Tumor-derived microvesicles: shedding light on novel microenvironment modulators and prospective cancer biomarkers. *Genes Dev*. Jun 2012;26(12):1287-99. doi:10.1101/gad.192351.112

38. Escrevente C, Keller S, Altevogt P, Costa J. Interaction and uptake of exosomes by ovarian cancer cells. *BMC Cancer*. Mar 2011;11:108. doi:10.1186/1471-2407-11-108

39. Andreu Z, Yáñez-Mó M. Tetraspanins in extracellular vesicle formation and function. *Front Immunol*. 2014;5:442. doi:10.3389/fimmu.2014.00442

40. Lötvall J, Hill AF, Hochberg F, et al. Minimal experimental requirements for definition of extracellular vesicles and their functions: a position statement from the International Society for Extracellular Vesicles. *J Extracell Vesicles*. 2014;3:26913.

41. Théry C, Witwer KW, Aikawa E, et al. Minimal information for studies of extracellular vesicles 2018 (MISEV2018): a position statement of the International Society for Extracellular Vesicles and update of the MISEV2014 guidelines. *J Extracell Vesicles*. 2018;7(1):1535750. doi:10.1080/20013078.2018.1535750

42. Zhang W, Ou X, Wu X. Proteomics profiling of plasma exosomes in epithelial ovarian cancer: A potential role in the coagulation cascade, diagnosis and prognosis. *Int J Oncol*. May 2019;54(5):1719-1733. doi:10.3892/ijo.2019.4742

43. Greening DW, Gopal SK, Xu R, Simpson RJ, Chen W. Exosomes and their roles in immune regulation and cancer. *Semin Cell Dev Biol*. Apr 2015;40:72-81. doi:10.1016/j.semcdb.2015.02.009

44. Evans-Osses I, Reichembach LH, Ramirez MI. Exosomes or microvesicles? Two kinds of extracellular vesicles with different routes to modify protozoan-host cell interaction. *Parasitol Res*. Oct 2015;114(10):3567-75. doi:10.1007/s00436-015-4659-9

45. Samos J, García-Olmo DC, Picazo MG, Rubio-Vitaller A, García-Olmo D. Circulating nucleic acids in plasma/serum and tumor progression: are apoptotic bodies involved? An experimental study in a rat cancer model. *Ann N Y Acad Sci*. Sep 2006;1075:165-73. doi:10.1196/annals.1368.022

46. Bergsmedh A, Szeles A, Henriksson M, et al. Horizontal transfer of oncogenes by uptake of apoptotic bodies. *Proc Natl Acad Sci U S A*. May 2001;98(11):6407-11. doi:10.1073/pnas.101129998

47. Flori F, Secciani F, Capone A, et al. Menstrual cycle-related sialidase activity of the female cervical mucus is associated with exosome-like vesicles. *Fertil Steril*. Oct 2007;88(4 Suppl):1212-9. doi:10.1016/j.fertnstert.2007.01.209

48. Iraci N, Leonardi T, Gessler F, Vega B, Pluchino S. Focus on Extracellular Vesicles: Physiological Role and Signalling Properties of Extracellular Membrane Vesicles. *Int J Mol Sci*. Feb 2016;17(2):171. doi:10.3390/ijms17020171

49. Kurywchak P, Tavormina J, Kalluri R. The emerging roles of exosomes in the modulation of immune responses in cancer. *Genome Med*. 03 2018;10(1):23. doi:10.1186/s13073-018-0535-4

50. Milane L, Singh A, Mattheolabakis G, Suresh M, Amiji MM. Exosome mediated communication within the tumor microenvironment. *J Control Release*. Dec 2015;219:278-294. doi:10.1016/j.jconrel.2015.06.029

51. Théry C, Amigorena S. The cell biology of antigen presentation in dendritic cells. *Curr Opin Immunol*. Feb 2001;13(1):45-51.

52. Pitt JM, André F, Amigorena S, et al. Dendritic cell-derived exosomes for cancer therapy. *J Clin Invest*. Apr 2016;126(4):1224-32. doi:10.1172/JCI81137

53. McDonald MK, Tian Y, Qureshi RA, et al. Functional significance of macrophage-derived exosomes in inflammation and pain. *Pain*. Aug 2014;155(8):1527-39. doi:10.1016/j.pain.2014.04.029

54. Robbins PD, Morelli AE. Regulation of immune responses by extracellular vesicles. *Nat Rev Immunol*. Mar 2014;14(3):195-208. doi:10.1038/nri3622

55. Shenoda BB, Ajit SK. Modulation of Immune Responses by Exosomes Derived from Antigen-Presenting Cells. *Clin Med Insights Pathol*. 2016;9(Suppl 1):1-8. doi:10.4137/CPath.S39925

56. Mitchell MD, Peiris HN, Kobayashi M, et al. Placental exosomes in normal and complicated pregnancy. *Am J Obstet Gynecol*. Oct 2015;213(4 Suppl):S173-81. doi:10.1016/j.ajog.2015.07.001

57. Golchin A, Hosseinzadeh S, Ardeshirylajimi A. The exosomes released from different cell types and their effects in wound healing. *J Cell Biochem*. Jul 2018;119(7):5043-5052. doi:10.1002/jcb.26706

58. Han G, Ceilley R. Chronic Wound Healing: A Review of Current Management and Treatments. *Adv Ther*. 03 2017;34(3):599-610. doi:10.1007/s12325-017-0478-y

59. Takeo M, Lee W, Ito M. Wound healing and skin regeneration. *Cold Spring Harb Perspect Med*. Jan 2015;5(1):a023267. doi:10.1101/cshperspect.a023267

60. Zhang W, Bai X, Zhao B, et al. Cell-free therapy based on adipose tissue stem cell-derived exosomes promotes wound healing via the PI3K/Akt signaling pathway. *Exp Cell Res*. Sep 2018;370(2):333-342. doi:10.1016/j.yexcr.2018.06.035

61. Shabbir A, Cox A, Rodriguez-Menocal L, Salgado M, Van Badiavas E. Mesenchymal Stem Cell Exosomes Induce Proliferation and Migration of Normal and Chronic Wound Fibroblasts, and Enhance Angiogenesis In Vitro. *Stem Cells Dev*. Jul 2015;24(14):1635-47. doi:10.1089/scd.2014.0316

62. Atalay M, Oksala N, Lappalainen J, Laaksonen DE, Sen CK, Roy S. Heat shock proteins in diabetes and wound healing. *Curr Protein Pept Sci*. Feb 2009;10(1):85-95.

63. Mineo M, Garfield SH, Taverna S, et al. Exosomes released by K562 chronic myeloid leukemia cells promote angiogenesis in a Src-dependent fashion. *Angiogenesis*. Mar 2012;15(1):33-45. doi:10.1007/s10456-011-9241-1

64. Ribeiro MF, Zhu H, Millard RW, Fan GC. Exosomes Function in Pro- and Anti-Angiogenesis. *Curr Angiogenes*. 2013;2(1):54-59. doi:10.2174/2211552811302002000l

65. Sahoo S, Klychko E, Thorne T, et al. Exosomes from human CD34(+) stem cells mediate their proangiogenic paracrine activity. *Circ Res*. Sep 2011;109(7):724-8. doi:10.1161/CIRCRESAHA.111.253286

66. Sheldon H, Heikamp E, Turley H, et al. New mechanism for Notch signaling to endothelium at a distance by Delta-like 4 incorporation into exosomes. *Blood*. Sep 2010;116(13):2385-94. doi:10.1182/blood-2009-08-239228

67. Taverna S, Flugy A, Saieva L, et al. Role of exosomes released by chronic myelogenous leukemia cells in angiogenesis. *Int J Cancer*. May 2012;130(9):2033-43. doi:10.1002/ijc.26217

68. Medzhitov R. Origin and physiological roles of inflammation. *Nature*. Jul 2008;454(7203):428-35. doi:10.1038/nature07201

69. Geering B, Stoeckle C, Conus S, Simon HU. Living and dying for inflammation: neutrophils, eosinophils, basophils. *Trends Immunol*. Aug 2013;34(8):398-409. doi:10.1016/j.it.2013.04.002

70. Wynn TA, Vannella KM. Macrophages in Tissue Repair, Regeneration, and Fibrosis. *Immunity*. Mar 2016;44(3):450-462. doi:10.1016/j.immuni.2016.02.015

71. Kim SH, Lechman ER, Bianco N, et al. Exosomes derived from IL-10-treated dendritic cells can suppress inflammation and collagen-induced arthritis. *J Immunol*. May 2005;174(10):6440-8.

72. Bianco NR, Kim SH, Ruffner MA, Robbins PD. Therapeutic effect of exosomes from indoleamine 2,3-dioxygenase-positive dendritic cells in collagen-induced arthritis and delayed-type hypersensitivity disease models. *Arthritis Rheum*. Feb 2009;60(2):380-9. doi:10.1002/art.24229

73. Wei G, Jie Y, Haibo L, et al. Dendritic cells derived exosomes migration to spleen and induction of inflammation are regulated by CCR7. *Sci Rep*. 02 2017;7:42996. doi:10.1038/srep42996

74. Di Marzo L, Desantis V, Solimando AG, et al. Microenvironment drug resistance in multiple myeloma: emerging new players. *Oncotarget*. 09 2016;7(37):60698-60711. doi:10.18632/oncotarget.10849

75. Gottesman MM. Mechanisms of cancer drug resistance. *Annu Rev Med*. 2002;53:615-27. doi:10.1146/annurev.med.53.082901.103929

76. Wang J, Hendrix A, Hernot S, et al. Bone marrow stromal cell-derived exosomes as communicators in drug resistance in multiple myeloma cells. *Blood*. Jul 2014;124(4):555-66. doi:10.1182/blood-2014-03-562439

77. Zhang C, Ji Q, Yang Y, Li Q, Wang Z. Exosome: Function and Role in Cancer Metastasis and Drug Resistance. *Technol Cancer Res Treat*. 01 2018;17:1533033818763450. doi:10.1177/1533033818763450

78. Soung YH, Ford S, Zhang V, Chung J. Exosomes in Cancer Diagnostics. *Cancers (Basel)*. Jan 2017;9(1)doi:10.3390/cancers9010008

79. Properzi F, Logozzi M, Fais S. Exosomes: the future of biomarkers in medicine. *Biomark Med*. Oct 2013;7(5):769-78. doi:10.2217/bmm.13.63

80. Zhao Z, Yang Y, Zeng Y, He M. A microfluidic ExoSearch chip for multiplexed exosome detection towards blood-based ovarian cancer diagnosis. *Lab Chip*. Feb 2016;16(3):489-96. doi:10.1039/c5lc01117e

81. Jahangirian H, Lemraski EG, Webster TJ, Rafiee-Moghaddam R, Abdollahi Y. A review of drug delivery systems based on nanotechnology and green chemistry: green nanomedicine. *Int J Nanomedicine*. 2017;12:2957-2978. doi:10.2147/IJN.S127683

82. Yang T, Martin P, Fogarty B, et al. Exosome Delivered Anticancer Drugs Across the Blood-Brain Barrier for Brain Cancer Therapy in Danio Rerio. Article. *Pharmaceutical Research*. JUN 2015 2015;32(6):2003-2014. doi:10.1007/s11095-014-1593-y

83. Haney MJ, Klyachko NL, Zhao Y, et al. Exosomes as drug delivery vehicles for Parkinson's disease therapy. *J Control Release*. Jun 2015;207:18-30. doi:10.1016/j.jconrel.2015.03.033

84. Saadeldin IM, Oh HJ, Lee BC. Embryonic-maternal cross-talk via exosomes: potential implications. *Stem Cells Cloning*. 2015;8:103-7. doi:10.2147/SCCAA.S84991

85. Zhao Z, McGill J, Gamero-Kubota P, He M. Microfluidic on-demand engineering of exosomes towards cancer immunotherapy. *Lab Chip*. 05 2019;19(10):1877-1886. doi:10.1039/c8lc01279b

86. Naseri M, Bozorgmehr M, Zöller M, Ranaei Pirmardan E, Madjd Z. Tumor-derived exosomes: the next generation of promising cell-free vaccines in cancer immunotherapy. *Oncoimmunology*. Jun 2020;9(1):1779991. doi:10.1080/2162402X.2020.1779991

87. Chen YS, Lin EY, Chiou TW, Harn HJ. Exosomes in clinical trial and their production in compliance with good manufacturing practice. *Ci Ji Yi Xue Za Zhi*. 2019 Apr-Jun 2019;32(2):113-120. doi:10.4103/tcmj.tcmj_182_19

88. Sercombe L, Veerati T, Moheimani F, Wu SY, Sood AK, Hua S. Advances and Challenges of Liposome Assisted Drug Delivery. *Front Pharmacol*. 2015;6:286. doi:10.3389/fphar.2015.00286

89. Fuhrmann G, Serio A, Mazo M, Nair R, Stevens MM. Active loading into extracellular vesicles significantly improves the cellular uptake and photodynamic effect of porphyrins. *J Control Release*. May 2015;205:35-44. doi:10.1016/j.jconrel.2014.11.029

90. Kim MS, Haney MJ, Zhao Y, et al. Engineering macrophage-derived exosomes for targeted paclitaxel delivery to pulmonary metastases: in vitro and in vivo evaluations. *Nanomedicine*. Jan 2018;14(1):195-204. doi:10.1016/j.nano.2017.09.011

91. Kim SM, Kim HS. Engineering of extracellular vesicles as drug delivery vehicles. *Stem Cell Investig*. 2017;4:74. doi:10.21037/sci.2017.08.07

92. García-Manrique P, Matos M, Gutiérrez G, Pazos C, Blanco-López MC. Therapeutic biomaterials based on extracellular vesicles: classification of bio-engineering and mimetic preparation routes. *J Extracell Vesicles*. 2018;7(1):1422676. doi:10.1080/20013078.2017.1422676

93. Tran TH, Mattheolabakis G, Aldawsari H, Amiji M. Exosomes as nanocarriers for immunotherapy of cancer and inflammatory diseases. *Clin Immunol*. Sep 2015;160(1):46-58. doi:10.1016/j.clim.2015.03.021

94. Johnsen KB, Gudbergsson JM, Skov MN, Pilgaard L, Moos T, Duroux M. A comprehensive overview of exosomes as drug delivery vehicles - endogenous nanocarriers for targeted cancer therapy. *Biochim Biophys Acta*. Aug 2014;1846(1):75-87. doi:10.1016/j.bbcan.2014.04.005

95. Sancho-Albero M, Navascués N, Mendoza G, et al. Exosome origin determines cell targeting and the transfer of therapeutic nanoparticles towards target cells. *J Nanobiotechnology*. Jan 2019;17(1):16. doi:10.1186/s12951-018-0437-z

96. Besse B, Charrier M, Lapierre V, et al. Dendritic cell-derived exosomes as maintenance immunotherapy after first line chemotherapy in NSCLC. *Oncoimmunology*. Apr 2016;5(4):e1071008. doi:10.1080/2162402X.2015.1071008

97. Urbanelli L, Buratta S, Sagini K, Ferrara G, Lanni M, Emiliani C. Exosome-based strategies for Diagnosis and Therapy. *Recent Pat CNS Drug Discov*. 2015;10(1):10-27.

98. Jiang XC, Gao JQ. Exosomes as novel bio-carriers for gene and drug delivery. *Int J Pharm*. Apr 2017;521(1-2):167-175. doi:10.1016/j.ijpharm.2017.02.038

99. Jing H, He X, Zheng J. Exosomes and regenerative medicine: state of the art and perspectives. *Transl Res*. 06 2018;196:1-16. doi:10.1016/j.trsl.2018.01.005

100. Conigliaro A, Cicchini C. Exosome-Mediated Signaling in Epithelial to Mesenchymal Transition and Tumor Progression. *J Clin Med*. Dec 2018;8(1)doi:10.3390/jcm8010026

101. Szajnik M, Derbis M, Lach M, et al. Exosomes in Plasma of Patients with Ovarian Carcinoma: Potential Biomarkers of Tumor Progression and Response to Therapy. *Gynecol Obstet (Sunnyvale)*. Apr 2013;Suppl 4:3. doi:10.4172/2161-0932.S4-003

102. Mashouri L, Yousefi H, Aref AR, Ahadi AM, Molaei F, Alahari SK. Exosomes: composition, biogenesis, and mechanisms in cancer metastasis and drug resistance. *Mol Cancer*. 04 2019;18(1):75. doi:10.1186/s12943-019-0991-5

103. Qiu J, Yang G, Feng M, et al. Extracellular vesicles as mediators of the progression and chemoresistance of pancreatic cancer and their potential clinical applications. *Mol Cancer*. 01 2018;17(1):2. doi:10.1186/s12943-017-0755-z

104. Quail DF, Joyce JA. Microenvironmental regulation of tumor progression and metastasis. *Nat Med*. Nov 2013;19(11):1423-37. doi:10.1038/nm.3394

105. Filipazzi P, Bürdek M, Villa A, Rivoltini L, Huber V. Recent advances on the role of tumor exosomes in immunosuppression and disease progression. *Semin Cancer Biol*. Aug 2012;22(4):342-9. doi:10.1016/j.semcancer.2012.02.005

106. Zhang HG, Grizzle WE. Exosomes and cancer: a newly described pathway of immune suppression. *Clin Cancer Res*. Mar 2011;17(5):959-64. doi:10.1158/1078-0432.CCR-10-1489

107. Marleau AM, Chen CS, Joyce JA, Tullis RH. Exosome removal as a therapeutic adjuvant in cancer. *J Transl Med*. Jun 2012;10:134. doi:10.1186/1479-5876-10-134

108. Soria FN, Pampliega O, Bourdenx M, Meissner WG, Bezard E, Dehay B. Exosomes, an Unmasked Culprit in Neurodegenerative Diseases. *Front Neurosci*. 2017;11:26. doi:10.3389/fnins.2017.00026

109. Filipe V, Hawe A, Jiskoot W. Critical evaluation of Nanoparticle Tracking Analysis (NTA) by NanoSight for the measurement of nanoparticles and protein aggregates. *Pharm Res*. May 2010;27(5):796-810. doi:10.1007/s11095-010-0073-2

110. Parisse P, Rago I, Ulloa Severino L, et al. Atomic force microscopy analysis of extracellular vesicles. *Eur Biophys J*. Dec 2017;46(8):813-820. doi:10.1007/s00249-017-1252-4

111. Chen C, Zong S, Wang Z, et al. Imaging and Intracellular Tracking of Cancer-Derived Exosomes Using Single-Molecule Localization-Based Super-Resolution Microscope. *ACS Appl Mater Interfaces*. Oct 2016;8(39):25825-25833. doi:10.1021/acsami.6b09442

112. Szatanek R, Baj-Krzyworzeka M, Zimoch J, Lekka M, Siedlar M, Baran J. The Methods of Choice for Extracellular Vesicles (EVs) Characterization. *Int J Mol Sci*. May 2017;18(6)doi:10.3390/ijms18061153

113. de la Torre Gomez C, Goreham RV, Bech Serra JJ, Nann T, Kussmann M. "Exosomics"-A Review of Biophysics, Biology and Biochemistry of Exosomes With a Focus on Human Breast Milk. *Front Genet*. 2018;9:92. doi:10.3389/fgene.2018.00092

114. Li X, Wang X. The emerging roles and therapeutic potential of exosomes in epithelial ovarian cancer. Review. *Molecular Cancer*. MAY 15 2017 2017;16ARTN 92. doi:10.1186/s12943-017-0659-y

115. Merchant ML, Rood IM, Deegens JKJ, Klein JB. Isolation and characterization of urinary extracellular vesicles: implications for biomarker discovery. *Nat Rev Nephrol*. Dec 2017;13(12):731-749. doi:10.1038/nrneph.2017.148

116. Di Meo A, Bartlett J, Cheng Y, Pasic MD, Yousef GM. Liquid biopsy: a step forward towards precision medicine in urologic malignancies. *Mol Cancer*. 04 2017;16(1):80. doi:10.1186/s12943-017-0644-5

117. Yokoi A, Yoshioka Y, Hirakawa A, et al. A combination of circulating miRNAs for the early detection of ovarian cancer. *Oncotarget*. Oct 2017;8(52):89811-89823. doi:10.18632/oncotarget.20688

118. Skotland T, Sandvig K, Llorente A. Lipids in exosomes: Current knowledge and the way forward. *Prog Lipid Res*. 04 2017;66:30-41. doi:10.1016/j.plipres.2017.03.001

119. Skotland T, Ekroos K, Kauhanen D, et al. Molecular lipid species in urinary exosomes as potential prostate cancer biomarkers. *Eur J Cancer*. 01 2017;70:122-132. doi:10.1016/j.ejca.2016.10.011

120. Taylor D, Gercel-Taylor C. MicroRNA signatures of tumor-derived exosomes as diagnostic biomarkers of ovarian cancer. Article. *Gynecologic Oncology*. JUL 2008 2008;110(1):13-21. doi:10.1016/j.ygyno.2008.04.033

121. Pan C, Stevic I, Müller V, et al. Exosomal microRNAs as tumor markers in epithelial ovarian cancer. *Mol Oncol*. Nov 2018;12(11):1935-1948. doi:10.1002/1878-0261.12371

122. Li J, Sherman-Baust CA, Tsai-Turton M, Bristow RE, Roden RB, Morin PJ. Claudin-containing exosomes in the peripheral circulation of women with ovarian cancer. *BMC Cancer*. Jul 2009;9:244. doi:10.1186/1471-2407-9-244

123. Rabinowits G, Gercel-Taylor C, Day J, Taylor D, Kloecker G. Exosomal MicroRNA: A Diagnostic Marker for Lung Cancer. Article. *Clinical Lung Cancer*. JAN 2009 2009;10(1):42-46. doi:10.3816/CLC.2009.n.006

124. Silva J, García V, Zaballos Á, et al. Vesicle-related microRNAs in plasma of nonsmall cell lung cancer patients and correlation with survival. *Eur Respir J*. Mar 2011;37(3):617-23. doi:10.1183/09031936.00029610

125. Jin X, Chen Y, Chen H, et al. Evaluation of Tumor-Derived Exosomal miRNA as Potential Diagnostic Biomarkers for Early-Stage Non-Small Cell Lung Cancer Using Next-Generation Sequencing. *Clin Cancer Res*. Sep 2017;23(17):5311-5319. doi:10.1158/1078-0432.CCR-17-0577

126. Reclusa P, Taverna S, Pucci M, et al. Exosomes as diagnostic and predictive biomarkers in lung cancer. *J Thorac Dis*. Oct 2017;9(Suppl 13):S1373-S1382. doi:10.21037/jtd.2017.10.67

127. Li Y, Zhang Y, Qiu F, Qiu Z. Proteomic identification of exosomal LRG1: a potential urinary biomarker for detecting NSCLC. *Electrophoresis*. Aug 2011;32(15):1976-83. doi:10.1002/elps.201000598

128. Yamashita T, Kamada H, Kanasaki S, et al. Epidermal growth factor receptor localized to exosome membranes as a possible biomarker for lung cancer diagnosis. *Pharmazie*. Dec 2013;68(12):969-73.

129. Hannafon BN, Trigoso YD, Calloway CL, et al. Plasma exosome microRNAs are indicative of breast cancer. *Breast Cancer Res*. 09 2016;18(1):90. doi:10.1186/s13058-016-0753-x

130. Eichelser C, Stückrath I, Müller V, et al. Increased serum levels of circulating exosomal microRNA-373 in receptor-negative breast cancer patients. *Oncotarget*. Oct 2014;5(20):9650-63. doi:10.18632/oncotarget.2520

131. Sueta A, Yamamoto Y, Tomiguchi M, Takeshita T, Yamamoto-Ibusuki M, Iwase H. Differential expression of exosomal miRNAs between breast cancer patients with and without recurrence. *Oncotarget*. Sep 2017;8(41):69934-69944. doi:10.18632/oncotarget.19482

132. Chen IH, Xue L, Hsu CC, et al. Phosphoproteins in extracellular vesicles as candidate markers for breast cancer. *Proc Natl Acad Sci U S A*. 03 2017;114(12):3175-3180. doi:10.1073/pnas.1618088114

133. Melo SA, Luecke LB, Kahlert C, et al. Glypican-1 identifies cancer exosomes and detects early pancreatic cancer. *Nature*. Jul 2015;523(7559):177-82. doi:10.1038/nature14581

134. Théry C, Amigorena S, Raposo G, Clayton A. Isolation and characterization of exosomes from cell culture supernatants and biological fluids. *Curr Protoc Cell Biol*. Apr 2006;Chapter 3:Unit 3.22. doi:10.1002/0471143030.cb0322s30

135. Livshits MA, Livshts MA, Khomyakova E, et al. Isolation of exosomes by differential centrifugation: Theoretical analysis of a commonly used protocol. *Sci Rep*. Nov 2015;5:17319. doi:10.1038/srep17319

136. Jeppesen DK, Hvam ML, Primdahl-Bengtson B, et al. Comparative analysis of discrete exosome fractions obtained by differential centrifugation. *J Extracell Vesicles*. 2014;3:25011.

137. Li P, Kaslan M, Lee SH, Yao J, Gao Z. Progress in Exosome Isolation Techniques. *Theranostics*. 2017;7(3):789-804. doi:10.7150/thno.18133

138. Lamparski HG, Metha-Damani A, Yao JY, et al. Production and characterization of clinical grade exosomes derived from dendritic cells. *J Immunol Methods*. Dec 2002;270(2):211-26.

139. Böing AN, van der Pol E, Grootemaat AE, Coumans FA, Sturk A, Nieuwland R. Single-step isolation of extracellular vesicles by size-exclusion chromatography. *J Extracell Vesicles*. 2014;3doi:10.3402/jev.v3.23430

140. Koh YQ, Almughlliq FB, Vaswani K, Peiris HN, Mitchell MD. Exosome enrichment by ultracentrifugation and size exclusion chromatography. *Front Biosci (Landmark Ed)*. Jan 2018;23:865-874.

141. Benedikter BJ, Bouwman FG, Vajen T, et al. Ultrafiltration combined with size exclusion chromatography efficiently isolates extracellular vesicles from cell culture media for compositional and functional studies. *Sci Rep*. Nov 2017;7(1):15297. doi:10.1038/s41598-017-15717-7

142. An M, Wu J, Zhu J, Lubman DM. Comparison of an Optimized Ultracentrifugation Method versus Size-Exclusion Chromatography for Isolation of Exosomes from Human Serum. *J Proteome Res*. Oct 2018;17(10):3599-3605. doi:10.1021/acs.jproteome.8b00479

143. Baranyai T, Herczeg K, Onódi Z, et al. Isolation of Exosomes from Blood Plasma: Qualitative and Quantitative Comparison of Ultracentrifugation and Size Exclusion Chromatography Methods. *PLoS One*. 2015;10(12):e0145686. doi:10.1371/journal.pone.0145686

144. Coskun O. Separation techniques: Chromatography. *North Clin Istanb*. 2016;3(2):156-160. doi:10.14744/nci.2016.32757

145. Konoshenko MY, Lekchnov EA, Vlassov AV, Laktionov PP. Isolation of Extracellular Vesicles: General Methodologies and Latest Trends. *Biomed Res Int*. 2018;2018:8545347. doi:10.1155/2018/8545347

146. Zeringer E, Barta T, Li M, Vlassov AV. Strategies for isolation of exosomes. *Cold Spring Harb Protoc*. Apr 2015;2015(4):319-23. doi:10.1101/pdb.top074476

147. Xu R, Simpson RJ, Greening DW. A Protocol for Isolation and Proteomic Characterization of Distinct Extracellular Vesicle Subtypes by Sequential Centrifugal Ultrafiltration. *Methods Mol Biol*. 2017;1545:91-116. doi:10.1007/978-1-4939-6728-5_7

148. Nordin JZ, Lee Y, Vader P, et al. Ultrafiltration with size-exclusion liquid chromatography for high yield isolation of extracellular vesicles preserving intact biophysical and functional properties. *Nanomedicine*. May 2015;11(4):879-83. doi:10.1016/j.nano.2015.01.003

149. Channavajjhala SK, Rossato M, Morandini F, et al. Optimizing the purification and analysis of miRNAs from urinary exosomes. *Clin Chem Lab Med*. Mar 2014;52(3):345-54. doi:10.1515/cclm-2013-0562

150. Cheruvanky A, Zhou H, Pisitkun T, et al. Rapid isolation of urinary exosomal biomarkers using a nanomembrane ultrafiltration concentrator. *Am J Physiol Renal Physiol*. May 2007;292(5):F1657-61. doi:10.1152/ajprenal.00434.2006

151. Soares Martins T, Catita J, Martins Rosa I, A B da Cruz E Silva O, Henriques AG. Exosome isolation from distinct biofluids using precipitation and column-based approaches. *PLoS One*. 2018;13(6):e0198820. doi:10.1371/journal.pone.0198820

152. Niu Z, Pang RTK, Liu W, Li Q, Cheng R, Yeung WSB. Polymer-based precipitation preserves biological activities of extracellular vesicles from an endometrial cell line. *PLoS One*. 2017;12(10):e0186534. doi:10.1371/journal.pone.0186534

153. Tauro BJ, Greening DW, Mathias RA, et al. Comparison of ultracentrifugation, density gradient separation, and immunoaffinity capture methods for isolating human colon cancer cell line LIM1863-derived exosomes. *Methods*. Feb 2012;56(2):293-304. doi:10.1016/j.ymeth.2012.01.002

154. Sharma P, Ludwig S, Muller L, et al. Immunoaffinity-based isolation of melanoma cell-derived exosomes from plasma of patients with melanoma. *J Extracell Vesicles*. 2018;7(1):1435138. doi:10.1080/20013078.2018.1435138

155. Ueda K, Ishikawa N, Tatsuguchi A, Saichi N, Fujii R, Nakagawa H. Antibody-coupled monolithic silica microtips for highthroughput molecular profiling of circulating exosomes. *Sci Rep*. Aug 2014;4:6232. doi:10.1038/srep06232

156. Oliveira-Rodríguez M, López-Cobo S, Reyburn HT, et al. Development of a rapid lateral flow immunoassay test for detection of exosomes previously enriched from cell culture medium and body fluids. *J Extracell Vesicles*. 2016;5:31803. doi:10.3402/jev.v5.31803

157. Momen-Heravi F, Balaj L, Alian S, et al. Current methods for the isolation of extracellular vesicles. *Biol Chem*. Oct 2013;394(10):1253-62. doi:10.1515/hsz-2013-0141

158. Kowal J, Arras G, Colombo M, et al. Proteomic comparison defines novel markers to characterize heterogeneous populations of extracellular vesicle subtypes. *Proc Natl Acad Sci U S A*. Feb 2016;113(8):E968-77. doi:10.1073/pnas.1521230113

159. Escola JM, Kleijmeer MJ, Stoorvogel W, Griffith JM, Yoshie O, Geuze HJ. Selective enrichment of tetraspan proteins on the internal vesicles of multivesicular endosomes and on exosomes secreted by human B-lymphocytes. *J Biol Chem*. Aug 1998;273(32):20121-7. doi:10.1074/jbc.273.32.20121

160. Lee K, Shao H, Weissleder R, Lee H. Acoustic purification of extracellular microvesicles. *ACS Nano*. Mar 2015;9(3):2321-7. doi:10.1021/nn506538f

161. Wang Z, Wu HJ, Fine D, et al. Ciliated micropillars for the microfluidic-based isolation of nanoscale lipid vesicles. *Lab Chip*. Aug 2013;13(15):2879-82. doi:10.1039/c3lc41343h

162. Yang F, Liao X, Tian Y, Li G. Exosome separation using microfluidic systems: size-based, immunoaffinity-based and dynamic methodologies. *Biotechnol J*. Apr 2017;12(4)doi:10.1002/biot.201600699

163. El-Andaloussi S, Lee Y, Lakhal-Littleton S, et al. Exosome-mediated delivery of siRNA in vitro and in vivo. Article. *Nature Protocols*. DEC 2012 2012;7(12):2112-2126. doi:10.1038/nprot.2012.131

164. Monfared H, Jahangard Y, Nikkhah M, Mirnajafi-Zadeh J, Mowla SJ. Potential Therapeutic Effects of Exosomes Packed With a miR-21-Sponge Construct in a Rat Model of Glioblastoma. *Front Oncol*. 2019;9:782. doi:10.3389/fonc.2019.00782

165. Yim N, Choi C. Extracellular vesicles as novel carriers for therapeutic molecules. *BMB Rep*. Nov 2016;49(11):585-586.

166. Bird IM. High performance liquid chromatography: principles and clinical applications. *BMJ*. Sep 1989;299(6702):783-7.

167. Kosanović M, Milutinović B, Goč S, Mitić N, Janković M. Ion-exchange chromatography purification of extracellular vesicles. *Biotechniques*. 08 2017;63(2):65-71. doi:10.2144/000114575

168. Fekete S, Veuthey J, Beck A, Guillarme D. Hydrophobic interaction chromatography for the characterization of monoclonal antibodies and related products. Article. *Journal of Pharmaceutical and Biomedical Analysis*. OCT 25 2016 2016;130:3-18. doi:10.1016/j.jpba.2016.04.004

169. O'Connor BF, Cummins PM. Hydrophobic Interaction Chromatography. *Methods Mol Biol*. 2017;1485:355-363. doi:10.1007/978-1-4939-6412-3_18

170. Li JJ, Liu YD, Wang FW, Ma GH, Su ZG. Hydrophobic interaction chromatography correctly refolding proteins assisted by glycerol and urea gradients. *J Chromatogr A*. Dec 2004;1061(2):193-9. doi:10.1016/j.chroma.2004.11.002

171. Fekete S, Veuthey JL, Beck A, Guillarme D. Hydrophobic interaction chromatography for the characterization of monoclonal antibodies and related products. *J Pharm Biomed Anal*. Oct 2016;130:3-18. doi:10.1016/j.jpba.2016.04.004

172. Lienqueo ME, Shene C, Asenjo J. Optimization of hydrophobic interaction chromatography using a mathematical model of elution curves of a protein mixture. *J Mol Recognit*. 2009 Mar-Apr 2009;22(2):110-20. doi:10.1002/jmr.927

173. Stanelle R, Marcus R. Nylon-6 capillary-channeled polymer (C-CP) fibers as a hydrophobic interaction chromatography stationary phase for the separation of proteins. Article. *Analytical and Bioanalytical Chemistry*. JAN 2009 2009;393(1):273-281. doi:10.1007/s00216-008-2457-2

174. Rodriguez-Aller M, Guillarme D, Beck A, Fekete S. Practical method development for the separation of monoclonal antibodies and antibody-drug-conjugate species in hydrophobic interaction chromatography, part 1: optimization of the mobile phase. Article. *Journal of Pharmaceutical and Biomedical Analysis*. JAN 25 2016 2016;118:393-403. doi:10.1016/j.jpba.2015.11.011

175. Bruce TF, Slonecki TJ, Wang L, Huang S, Powell RR, Marcus RK. Exosome isolation and purification via hydrophobic interaction chromatography using a polyester, capillary-channeled polymer fiber phase. *Electrophoresis*. 2018;40(4):571-581.

176. Kindelberger DW, Lee Y, Miron A, et al. Intraepithelial carcinoma of the fimbria and pelvic serous carcinoma: Evidence for a causal relationship. *Am J Surg Pathol*. Feb 2007;31(2):161-9. doi:10.1097/01.pas.0000213335.40358.47

177. Pentheroudakis G, Pavlidis N. Serous papillary peritoneal carcinoma: unknown primary tumour, ovarian cancer counterpart or a distinct entity? A systematic review. *Crit Rev Oncol Hematol*. Jul 2010;75(1):27-42. doi:10.1016/j.critrevonc.2009.10.003

178. Toss A, Tomasello C, Razzaboni E, et al. Hereditary ovarian cancer: not only BRCA 1 and 2 genes. *Biomed Res Int*. 2015;2015:341723. doi:10.1155/2015/341723

179. Jacobs IJ, Menon U, Ryan A, et al. Ovarian cancer screening and mortality in the UK Collaborative Trial of Ovarian Cancer Screening (UKCTOCS): a randomised controlled trial. *Lancet*. Mar 2016;387(10022):945-956. doi:10.1016/S0140-6736(15)01224-6

180. Menon U, Ryan A, Kalsi J, et al. Risk Algorithm Using Serial Biomarker Measurements Doubles the Number of Screen-Detected Cancers Compared With a Single-Threshold Rule in the United Kingdom Collaborative Trial of Ovarian Cancer Screening. *J Clin Oncol*. Jun 2015;33(18):2062-71. doi:10.1200/JCO.2014.59.4945

181. Carter JS, Downs LS. Ovarian Cancer Tests and Treatment. *Female Patient (Parsippany)*. 2011;36(4):30-35.

182. Menon U, Gentry-Maharaj A, Hallett R, et al. Sensitivity and specificity of multimodal and ultrasound screening for ovarian cancer, and stage distribution of detected cancers: results of the prevalence screen of the UK Collaborative Trial of Ovarian Cancer Screening (UKCTOCS). *Lancet Oncol*. Apr 2009;10(4):327-40. doi:10.1016/S1470-2045(09)70026-9

183. Gynecologists ACoOa. ACOG Committee Opinion: number 280, December 2002. The role of the generalist obstetrician-gynecologist in the early detection of ovarian cancer. *Obstet Gynecol*. Dec 2002;100(6):1413-6.

184. Doubeni CA, Doubeni AR, Myers AE. Diagnosis and Management of Ovarian Cancer. *Am Fam Physician*. Jun 2016;93(11):937-44.

185. Cortez AJ, Tudrej P, Kujawa KA, Lisowska KM. Advances in ovarian cancer therapy. *Cancer Chemother Pharmacol*. 01 2018;81(1):17-38. doi:10.1007/s00280-017-3501-8

186. Bookman MA. Optimal primary therapy of ovarian cancer. *Ann Oncol*. 04 2016;27 Suppl 1:i58-i62. doi:10.1093/annonc/mdw088

187. Yap TA, Sandhu SK, Carden CP, de Bono JS. Poly(ADP-ribose) polymerase (PARP) inhibitors: Exploiting a synthetic lethal strategy in the clinic. *CA Cancer J Clin*. 2011 Jan-Feb 2011;61(1):31-49. doi:10.3322/caac.20095

188. Nguyen DX, Bos PD, Massagué J. Metastasis: from dissemination to organ-specific colonization. *Nat Rev Cancer*. Apr 2009;9(4):274-84. doi:10.1038/nrc2622

189. Jiang WG, Sanders AJ, Katoh M, et al. Tissue invasion and metastasis: Molecular, biological and clinical perspectives. *Semin Cancer Biol*. Dec 2015;35 Suppl:S244-S275. doi:10.1016/j.semcancer.2015.03.008

190. Garnier D, Magnus N, Lee TH, et al. Cancer cells induced to express mesenchymal phenotype release exosome-like extracellular vesicles carrying tissue factor. *J Biol Chem*. Dec 2012;287(52):43565-72. doi:10.1074/jbc.M112.401760

191. Weidle UH, Birzele F, Kollmorgen G, Rüger R. The Multiple Roles of Exosomes in Metastasis. *Cancer Genomics Proteomics*. 01 2017;14(1):1-15. doi:10.21873/cgp.20015

192. Sharma S, Zuñiga F, Rice GE, Perrin LC, Hooper JD, Salomon C. Tumor-derived exosomes in ovarian cancer - liquid biopsies for early detection and real-time monitoring of cancer progression. *Oncotarget*. Nov 2017;8(61):104687-104703. doi:10.18632/oncotarget.22191

193. Jung T, Castellana D, Klingbeil P, et al. CD44v6 dependence of premetastatic niche preparation by exosomes. *Neoplasia*. Oct 2009;11(10):1093-105.

194. Hood JL, Pan H, Lanza GM, Wickline SA, (C-TRAIN) CfTRiAIaN. Paracrine induction of endothelium by tumor exosomes. *Lab Invest*. Nov 2009;89(11):1317-28. doi:10.1038/labinvest.2009.94

195. Hegmans JP, Bard MP, Hemmes A, et al. Proteomic analysis of exosomes secreted by human mesothelioma cells. *Am J Pathol*. May 2004;164(5):1807-15. doi:10.1016/S0002-9440(10)63739-X

196. Park JE, Tan HS, Datta A, et al. Hypoxic tumor cell modulates its microenvironment to enhance angiogenic and metastatic potential by secretion of proteins and exosomes. *Mol Cell Proteomics*. Jun 2010;9(6):1085-99. doi:10.1074/mcp.M900381-MCP200

197. Andreola G, Rivoltini L, Castelli C, et al. Induction of lymphocyte apoptosis by tumor cell secretion of FasL-bearing microvesicles. *J Exp Med*. May 2002;195(10):1303-16.

198. Huber V, Fais S, Iero M, et al. Human colorectal cancer cells induce T-cell death through release of proapoptotic microvesicles: role in immune escape. *Gastroenterology*. Jun 2005;128(7):1796-804.

199. Wieckowski EU, Visus C, Szajnik M, Szczepanski MJ, Storkus WJ, Whiteside TL. Tumor-derived microvesicles promote regulatory T cell expansion and induce apoptosis in tumor-reactive activated CD8+ T lymphocytes. *J Immunol*. Sep 2009;183(6):3720-30. doi:10.4049/jimmunol.0900970

200. Peinado H, Alečković M, Lavotshkin S, et al. Melanoma exosomes educate bone marrow progenitor cells toward a pro-metastatic phenotype through MET. *Nat Med*. Jun 2012;18(6):883-91. doi:10.1038/nm.2753

201. Liu C, Yu S, Zinn K, et al. Murine mammary carcinoma exosomes promote tumor growth by suppression of NK cell function. *J Immunol*. Feb 2006;176(3):1375-85.

202. Kobayashi M, Salomon C, Tapia J, Illanes SE, Mitchell MD, Rice GE. Ovarian cancer cell invasiveness is associated with discordant exosomal sequestration of Let-7 miRNA and miR-200. *J Transl Med*. Jan 2014;12:4. doi:10.1186/1479-5876-12-4

203. Sinha A, Ignatchenko V, Ignatchenko A, Mejia-Guerrero S, Kislinger T. In-depth proteomic analyses of ovarian cancer cell line exosomes reveals differential enrichment of functional categories compared to the NCI 60 proteome. *Biochem Biophys Res Commun*. Mar 2014;445(4):694-701. doi:10.1016/j.bbrc.2013.12.070

204. Domcke S, Sinha R, Levine DA, Sander C, Schultz N. Evaluating cell lines as tumour models by comparison of genomic profiles. *Nat Commun*. 2013;4:2126. doi:10.1038/ncomms3126

205. Ince TA, Sousa AD, Jones MA, et al. Characterization of twenty-five ovarian tumour cell lines that phenocopy primary tumours. *Nat Commun*. Jun 2015;6:7419. doi:10.1038/ncomms8419

206. Bouïs D, Hospers GA, Meijer C, Molema G, Mulder NH. Endothelium in vitro: a review of human vascular endothelial cell lines for blood vessel-related research. *Angiogenesis*. 2001;4(2):91-102.

207. Lehman TA, Modali R, Boukamp P, et al. p53 mutations in human immortalized epithelial cell lines. *Carcinogenesis*. May 1993;14(5):833-9. doi:10.1093/carcin/14.5.833

208. Ouellette MM, McDaniel LD, Wright WE, Shay JW, Schultz RA. The establishment of telomerase-immortalized cell lines representing human chromosome instability syndromes. *Hum Mol Genet*. Feb 2000;9(3):403-11. doi:10.1093/hmg/9.3.403

209. Obinata M. The immortalized cell lines with differentiation potentials: their establishment and possible application. *Cancer Sci*. Mar 2007;98(3):275-83. doi:10.1111/j.1349-7006.2007.00399.x

210. Shen J, Zhu X, Fei J, Shi P, Yu S, Zhou J. Advances of exosome in the development of ovarian cancer and its diagnostic and therapeutic prospect. *Onco Targets Ther*. 2018;11:2831-2841. doi:10.2147/OTT.S159829

CHAPTER 2

EXOSOME ISOLATION AND PURIFICATION VIA HYDROPHOBIC INTERACTION CHROMATOGRAPHY USING A POLYESTER, CAPILLARY-CHANNELED POLYMER FIBER PHASE

Abstract

Extracellular vesicles, including microvesicles and exosomes, are lipidic membrane-derived vesicles that are secreted by most cell types. Exosomes, one class of these vesicles that are 30-100 nm in diameter, hold a great deal of promise in disease diagnostics, as they display the same protein biomarkers as their originating cell. For exosomes to become useful in disease diagnostics, and as burgeoning drug delivery platforms, they must be isolated efficiently and effectively without compromising their structure. Most current exosome isolation methods have practical problems including being too time-consuming and labor intensive, destructive to the exosomes, or too costly for use in clinical settings. To this end, this study examines the use of poly(ethylene terephthalate) (PET) capillary-channeled polymer (C-CP) fibers in a hydrophobic interaction chromatography (HIC) protocol to isolate exosomes from diverse matrices of practical concern. Results demonstrate the ability to isolate extracellular vesicles enriched in exosomes with comparable yields and size distributions on a much faster time scale when compared to traditional isolation methods. As a demonstration of the potential analytical utility of the approach, extracellular vesicle recoveries from cell

culture milieu and a mock urine matrix are presented. Scalable separations covering sub-milliliter spin-down columns to the preparative scale are projected.

It should be noted that this is collaborative work that has been published as a peer-reviewed article and was performed with Dr. Ken Marcus of the Clemson University Chemistry Department. Of note, the hydrophobic interaction chromatography work outlined in this chapter was primarily performed by Dr. Lei Wang and Ms. Sisi Huang. This chapter appears here directly as published (with minimal additions) for completeness.

Terri F. Bruce, **Tyler J. Slonecki**, Lei Wang, Sisi Huang, Rhonda P. Powell, R. Kenneth Marcus, Exosome isolation and purification via hydrophobic interaction chromatography using a polyester, capillary-channeled polymer fiber phase. *Electrophoresis* **2019,** 40 (4), 571-581.

Introduction

Exosomes are tiny lipid-bound vesicles, approximately 30-100 nm in diameter, that are secreted by most types of cells, including both normal and disease-state cells. They carry internal "cargo" molecules, such as nucleic acids and proteins, which are derived from their cell of origin. These biomarkers make exosomes a promising means of minimally-invasive early disease diagnosis [1-4]. Once considered cellular debris, research has demonstrated that exosomes have multiple biological roles. Exosomes may be involved in a myriad of normal physiological processes including cross-placental communication between the mother and fetus, fetal development, and bone calcification, as well as disease processes including metastasis, pathogenesis of thrombosis, diabetes, atherosclerosis, tumor growth, arthritis, and progression of neurodegenerative diseases [4, 5]. Exosomes can be found in most body fluids, including urine, saliva, amniotic fluid, semen, breast milk, plasma, and blood, making them a promising basis for the development of liquid biopsies [6, 7]. Exosomes have been shown to have unique microRNA (miRNA) signatures that could soon open the door for clinical and therapeutic applications [8]. Exosomes are being exploited for disease diagnostics [7, 9, 10], including cancer [11, 12], with potential biomarkers identified relative to a number of different types of cancers, including ovarian, lung, breast, prostate, and pancreatic cancer [11-14].

Despite these promising attributes, the analysis of exosomes is currently limited by the processes required to isolate them from body fluids [15-17]. In most cases, exosomes are isolated by differential centrifugation (DC), requiring the use of a high-speed centrifuge over several hours, including the sedimentation of other particulate debris and

potentially impacting the integrity of the lipid bilayer membrane of the exosome. Other emerging exosome isolation techniques include density gradient centrifugation, size exclusion chromatography, ultrafiltration, polymer-based precipitation, immunological separation, and microfluidics techniques [13, 18-23]. Some of these methods are generic with respect to the specific types of exosomes which can be isolated, while others solely capture vesicles originating from specific cell types. Each of these exosome isolation techniques has benefits, but the aforementioned shortcomings are fairly universal [17, 18, 24]. Thus, none are currently sufficient for use in clinical diagnostics or for isolation of larger lots from cell culture media as would be required for drug delivery applications.

Exosome isolation methods are generally based on the size/hydrodynamic radii of the vesicles, i.e, centrifugation, filtration, and sieve-based approaches, or their affinity towards capture surfaces used in spin-down formats. However, methods relying on chemical separation and processing platforms, such as those employed in HPLC, have not been fully explored; yet, they may have many attractive features. Most of the common LC stationary phases used for chemical separations, such as porous silica beads, would not be practical, as exosomes would likely be excluded from the internal pore structures, and clogging would be a major operational problem. This study describes the use of capillary-channeled polymer (C-CP) fibers as stationary phases for the isolation and recovery of exosome-enriched populations of extracellular vesicles (referred to as "exosomes" from here forward) from culture media, buffer, and urine. C-CP fibers have been employed by Marcus and co-workers as stationary phases for protein separations via reversed phase, ion exchange, hydrophobic interaction, and affinity chromatographies [25-

[31]. These fibers are melt-extruded from commodity polymers (nylon 6, polypropylene, and poly(ethylene terephthalate) (polyester,PET)), having a unique cross-sectional profile consisting of eight "legs" on the periphery. When packed in column formats, the fibers inter-digitate to create massive numbers of 1-4 μm-wide channels that provide high permeability to fluid flow. The non-porous nature of the fiber surfaces (at least on the size scale of proteins) means that intra-phase diffusion of solutes is prohibited. This combination of macro and micro characteristics results in the ability to affect protein separations at exceedingly high linear velocities (>50 mm sec^{-1}) without the mass transfer limitations common to porous phases. These hydrodynamic advantages are complemented by a high degree of chemical separation diversity. In addition to the range modalities of separation that can be affected using different base polymers, an extensive tool box of simple surface modification approaches has also been developed. The fiber surfaces may be modified to affect high ligand densities for ion exchange (cationic and anionic) and affinity chromatography [30-32]. Affinity separations include the use of protein A for IgG purification and quantification, biotin-streptavidin interactions, and chelates for immobilized metal affinity chromatography (IMAC) [33-35]. In total, these attributes make the utilization of the C-CP fibers for exosome isolation a promising alternative to traditional isolation methodologies.

This study describes the first successful use of the PET C-CP fibers to isolate and elute exosomes via a hydrophobic interaction chromatography (HIC) protocol. The procedure, first developed for protein separations [27], is readily implemented to isolate exosomes from from host cell proteins and concomitant components present in cell

culture media, phosphate buffer, and urine. The hydrophobic exosome surfaces adhere to the weakly-ionized surfaces of the PET fibers, making HIC a selective method of exosome isolation. Use of an HIC approach, involving an inverse salt gradient for elution, is much preferred over a common reversed-phase (RP) method as organic solvents employed in RP might result in the loss of important species (e.g. proteins) adhered to the exosome surfaces. It is important to note that while hydrophobic substrates have been used in previous exosome assay methods such as the Qiagen exoEasy Kit, use of a truly chromatographic method holds the promise for higher throughput and sampling/analysis of other matrix components such as host cell proteins as retentates can be selectively eluted. Such advantages would be the same as argued in any case of solid phase extraction versus liquid chromatography.

In order to investigate the ability of the C-CP fibers to isolate exosomes, *Dictyostelium discoideum* cells were used to generate generic exosomes. *D.discoideum* is not only simple and inexpensive to culture in the lab, but it is also a model organism used for studying cell signaling, the endocytic pathway, and generation of extracellular vesicles and exosomes [36, 37]. Under normal conditions, it is a common single-cell, soil-dwelling amoeba; however, under environmental stress, such as lack of water and nutrients, its cells can form multi-cellular aggregates, the formation of which require direct cell-to-cell communication [37]. The ease with which *Dictyostelium discoideum* can be cultured, the prominent role of cellular communication in its life cycle, and its use as a model organism for exosome research, make it a useful organism for generating exosomes needed to investigate isolation techniques.

In this demonstration study, the efficacy and efficiency of the new HIC C-CP fiber exosome isolation methodology are compared to two commonly utilized exosome isolation methods, standard differential centrifugation (DC), as it is the most widely used isolation method, and the exoEasy Maxi Kit (QIAGEN), as it is the most similar commercially-available method to the proposed HIC C-CP fiber approach [38]. The kit method uses post-centrifugation, spin-down processing and a membrane-based stationary phase to affect an "affinity" (presumably a hydrophobic interaction) binding step to isolate exosomes and other EVs from serum and plasma, or cell culture supernatants. There is no selectivity with regards to size or cellular origin of the EVs. It relies on generic characterstics of the vesicle surfaces to capture all forms of EVs in the sample. The implementation of a chromatographic (flow through) approach versus the spin-down, solid phase extraction (SPE) approach, would seem to present a number of potential advantages. These attributes are highlighted herein. The utility of the C-CP fiber HPLC separation is further demonstrated by investigation of recovery of exosomes from simulated urine and standard cell culture media.

Materials and methods

Exosome Expression by Dictyostelium discoideum

Dictyostelium discoideum AX2 cells (provided by L. Temesvari, Clemson University) were grown and maintained axenically in HL5 medium supplemented with 100 μg mL^{-1} ampicillin at room temperature in 25 mL culture flasks [39]. Cells were passaged at 70-90% confluency.

For exosome expression, AX2 cells were used to inoculate 50 mL of HL5 media supplemented with 100 μg mL^{-1} ampicillin at a starting cell concentration of 5 – 10 x 10^5 cells mL^{-1} in a 250 mL Erlenmeyer flask. After inoculation, the flask was covered in aluminum foil to block out light and placed on a shaker (150 RPM, 22˚C) for 48 hours [37].

Isolation of exosomes via differential centrifugation and Qiagen exoEasy Kit

Two widely accepted methods of exosome isolation, differential centrifugation and the Qiagen exoEasy Maxi Kit, were chosen as benchmarks for comparison to the proposed PET C-CP HIC isolation method. These specific methods were chosen because differential centrifugation is one of the most widely used methods for exosome isolation and the exoEasy Maxi Kit is most like the PET C-CP HIC isolation method in terms of being an exosome/surface adhesion process. While differential centrifugation is the most utilized method of exosome isolation, it can sediment host cell proteins along with exosomes. The process is also time consuming, and requires expensive equipment [18-20, 24]. The Qiagen exoEasy Maxi kit uses a membrane-based affinity column to separate exosomes and other extracellular vesicles from solutions, in much less time in comparison to differential centrifugation; however, the process still takes up to 30 minutes to complete and costs approximately $32 per sample [40]. Another shortcoming of the exoEasy method is the high carryover of host cell proteins along with the derived exosomes.

All resulting differential centrifugation and exoEasy kit exosome isolations were resuspended in either PBS or Qiagen elution buffer and subsequently divided into two aliquots. One aliquot of each sample was used for nanoparticle tracking analysis (NTA)

for the determination of exosome concentration and size distribution, while the other was used as a concentrated exosome sample during the initial testing of the HIC C-CP fiber isolation method.

Differential centrifugation

Differential centrifugation retrieval of *D. discoideum* derived exosomes was conducted as previously described by Tatischeff et al., with slight modifications [41]. Due to the novelty of *D. discoideum* in exosome research, all centrifugation steps followed previous research completed by Tatischeff et al., rather than standard mammalian cell exosome isolation ultracentrifugation protocols. All centrifugation steps performed below 12,000X*g* were performed using an Eppendorf Centrifuge 5430R (Eppendorf, Hamburg, Germany). Centrifugations of 12,000X*g* or more were performed using a Beckman Coulter Avanti J-26S XPI Centrifuge with a JA-25.50 rotor (Beckman Coulter, Brea, CA). The first centrifugation step was performed at 700X*g* (5 min., 22˚C) in a 50 mL conical centrifuge tube. After centrifugation, 45 mL of the supernatant was transferred to a new 50 mL conical centrifuge tube for further centrifugation, with the remaining 5 mL of supernatant saved for exosome isolation via the C-CP HIC method. The second centrifugation was performed at 2,000X*g* (10 min., 22ºC.) The final centrifugation step was performed at 12,000X*g* (30 min., 4ºC.) The supernatant was carefully removed and the final pellet was re-suspended in 400 µL of PBS and stored at 4ºC.

Qiagen exoEasy Maxi Kit

The QIAGEN exoEasy Maxi kit (QIAGEN, Hilden, Germany) isolations were accomplished per the manufacturer's instructions. All of the centrifugation steps required by the kit were performed using an Eppendorf Centrifuge 5430R. Briefly, 10 mL of the *D. discoideum* cell growth media prepared for exosome isolation were filtered using a 0.8 µm syringe filter. An additional 1 mL of the remaining media was filtered using a 0.8 µm syringe filter and set aside for exosome isolation via the C-CP HIC method. The resulting exosomes were eluted using 400 µL of the Qiagen XE elution buffer and stored at 4^{o}C.

Hydrophobic interaction chromatography (HIC) method

The poly(ethylene terephthalate) (PET) C-CP fibers were produced by the Materials Science and Engineering Department, Clemson University. All solvents were purchased from EMD (EMD Millipore, Billerica, MA). Ammonium sulfate ($(NH_4)_2SO_4$) and all other chemicals and proteins were purchased from Sigma-Aldrich (St. Louis, MO). Deionized water (DI-H_2O) was secured from a Milli-Q water system. The chromatographic exosome separations were performed on a Dionex Ultimate 3000 HPLC system, LPG-3400SD Quaternary pump, and MWD-3000 UV–vis absorbance detector (Thermo Fisher Scientific, Waltham, MA). A Rheodyne model 8125 low dispersion injector with 20 and 60 µL injection loops was used for exosome sample injections.

The PET C-CP fiber microbore columns (column length: 200 mm, i.d., 0.762 mm PEEK, 450 fibers) prepared as described previously [28], were used for the exosome separations. After flushing the column with Buffer C (10 mM potassium phosphate

buffer; pH = 7.4), it was equilibrated with Buffer A (1.8 M $(NH_4)_2SO_4$ solution dissolved in PBS; pH = 7.4). As previously described in research regarding antibody purification using HIC, appropriate amounts of organic additives (such as methanol and acetonitrile) in the elution buffer demonstrate improved protein recovery [42-44]. As such, 30% acetonitrile (v/v) dissolved in PBS was employed as buffer B. A mobile phase flow rate of 0.5 mL min^{-1} and a 20 min gradient from 100% buffer A to 100% buffer B was used for exosome separation. Briefly, exosome samples were injected onto the column during the high-salt (buffer A) mobile phase. Under these conditions, latent HCPs and exosomes are adsorbed to the PET fiber media, with the gradient subsequently eluting species of increasingly greater hydrophobicity. UV absorbance at 216 nm was monitored as a means of detecting the eluting species (proteins and exosomes). Based on the detector response reflecting their elution, purified exosomes were collected post-column.

HIC elution and isolation of exosomes from simulated urine and standard cell culture media

In order to demonstrate the HIC C-CP column isolation of exosomes from body fluids, and to assess the potential quantitative aspects of the exosome isolation method, previously isolated exosomes were spiked into a simulated urine matrix (194 g urea, 6 g $CaCl_2$, 11 g Mg_2SO_4, and 80 g NaCl in 1 L of DI-H_2O), spiked with myoglobin (Myo), α-chymotrypsinogen A (Chymo), ribonuclease A (Ribo), bovine serum albumin (BSA), and lysozyme (Lyso) (0.1 mg mL^{-1} each), as simple representatives of the variety of proteins present in urine. HIC isolation of the vesicles from the simulated urine was followed by quantification based on the integrated peak areas of the eluted exosomes. The gradient

baseline absorbance, obtained by running the gradient with no exosomes injected, was subtracted from the exosome-spiked separation chromatograms.

Exosome characterization via Nanoparticle Tracking Analysis (NTA)

Nanoparticle tracking analysis (NTA) was performed using a Nanosight (Malvern, Worcestershire, UK) NS500 with a 532 nm laser and 565 nm long pass cut off fluorescent filter (Center for Nanotechnology in Drug Delivery, UNC Eshelman School of Pharmacy). Samples were diluted to a concentration between $1x10^8$ and $5x10^8$ particles mL^{-1} with 20 nm filtered PBS. For each sample, particles moving under Brownian motion were recorded on video five times for 40 seconds each. Hydrodynamic diameters were calculated using the Stokes-Einstein equation.

Transmission Electron Microscopy Fixation, Staining, and Imaging

Transmission electron microscopy (TEM) imaging was used to verify the physical size of single vesicles. *D. discoideum* differential centrifugation extracellular vesicles and human urine standard exosomes (Galan Laboratory Supplies, North Haven, CT) were fixed in 4% paraformaldehyde for 1 hour. Immediately following fixation, 5 µl of each sample was applied to 200 mesh formvar carbon coated copper grids (Electron Microscopy Sciences, Hatfield, PA) and allowed to adsorb for 5 minutes. Each sample grid was negatively stained with 5 µl of 2% Uranyl Acetate for 5 minutes. Grids were then washed 3 times in 10 µl of distilled water for 5 minutes each and allowed to dry for imaging. All TEM images were obtained using a Hitachi H-7600 TEM (Hitachi, Tokyo, Japan) in the Clemson Electron Microscopy Lab.

Scanning Electron Microscope Fixation and Imaging

The capture of intact exosomes onto the C-CP fiber surfaces was confirmed by scanning electron microscopy (SEM) imaging. Proprietary PET C-CP fiber-packed tips were produced according to a previously described method [45]. The fiber surfaces were wetted by flushing with 1 mL of H_2O, and then rinsed in 2M $(NH_4)_2SO_4$ in PBS. 100 µL of each sample (DC-derived exosomes, milieu or 2M $(NH_4)_2SO_4$) were mixed with 2M $(NH_4)_2SO_4$, followed by flushing through the tip (300X*g* for 5 min). The prepared fibers were fixed in 1% osmium tetroxide for 1 hour and washed 3 times for 3 minutes each in distilled water to remove any excess osmium tetroxide. Next, each sample was washed in a 6 step gradient of ethanol-distilled water solutions starting at 50% ethanol and ending at 100% ethanol for 3 minutes each. An additional 100% ethanol wash step was performed to ensure that all water had been removed from the sample. Finally, each sample was washed in a 50-50 hexamethyldisilazane (HMDS)-ethanol solution for 3 minutes and dried in 100% HMDS overnight. Samples were sputter-coated with platinum at 70 millitorr argon for 2 minutes using a Hummer 6.2 Sputtering system (Anatech USA, Union City, CA). SEM imaging was performed on a Hitachi S-4800 at 5.0 kV (Hitachi, Tokyo, Japan).

Results and Discussion

HIC isolation of exosomes

In order to determine whether or not exosomes could be isolated via HIC using the PET C-CP fibers, aliquots of the *D. discoideum*-derived exosomes that had been previously isolated using the benchmark techniques were run on the PET C-CP columns with a mobile phase flow rate of 0.5 mL min^{-1} and a 20 minute gradient from 100% buffer A (1.8 M $(NH_4)_2SO_4$ in PBS) to 100% buffer B (30% v/v acetonitrile in PBS). Figure 2.1 shows the resulting chromatograms derived from pristine HL5 media and four different exosome isolation lots. In Fig. 2.1a, pristine HL5 was injected in order to establish a baseline chromatogram of the media components. The detector response shows a broadly eluting peak from ~2 – 10 minutes, composed of a myriad of proteins derived from yeast extract and peptone, various salts, and sugars. In Fig. 2.1b, exosomes previously isolated via differential centrifugation were injected onto the fiber column. The resulting HIC chromatogram displays two major peaks, a very broad band between 2 – 11 minutes, and a fairly sharp feature reflecting more strongly retained (hydrophobic) species with an elution time of ~13 – 13.5 mins. In Fig. 2.1c, exosomes previously isolated via the exoEasy kit were injected for HIC separation. The resulting chromatogram displays four prominent peaks. In this case, the first three broad peaks eluting within the same same time frame of 2 – 11 minutes bands in Figs. 2.1a and b. As in Fig. 2.1b, a discrete feature eluting in the ~13 – 13.5 min window is seen. Based on the structure of the respective chromatograms (Figs. 2.1a-c), it is not unreasonable to suggest that the peaks eluting between 2 – 11 minutes represent remaining HL5 media

components, host cell (*D. discoideum*) proteinaceous and genetic material, salts, and other small molecules left behind during the previous isolation procedures, with the later eluting (13 – 13.5 min) smaller, sharper peak representing exosomes. One cannot rule out that there may be some EV-related material in the broad elution band, but one would expect that such species would be very hydrophobic in comparison to other media and cellular byproducts.

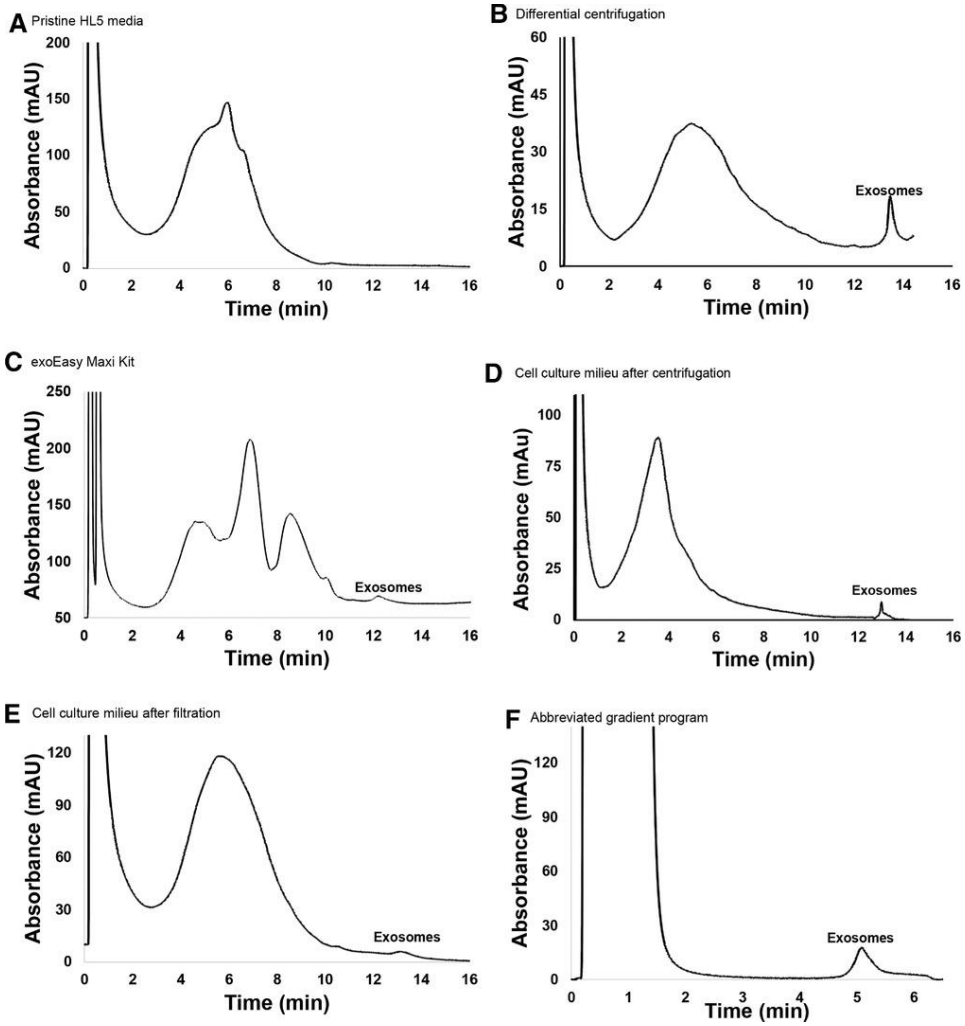

Figure 2.1. Representative HIC chromatograms of exosome isolation using using PET C-CP fibers. Separations were performed with a mobile phase flow rate of 0.5 mL min^{-1}, 60 µL aliquot injections, and a 20 min gradient from 100% buffer A (1.8 M $(NH_4)_2SO_4$ solution dissolved in PBS; pH = 7.4) to 100% buffer B (30% acetonitrile (v/v) dissolved in PBS). a) Baseline chromatogram of pristine HL5 media. b) *D. discoideum*-derived exosomes previously isolated via differential centrifugation. c) *D. discoideum*-derived exosomes previously isolated via the Qiagen exoEasy Maxi Kit. d) *D. discoideum*-derived exosomes following centrifugation to remove cells and large debris. e) *D. discoideum*-derived exosomes following filtration through a 0.8 µm filter to remove cells and large debris. f) Abbreviated gradient program (injection at A (0.8 M $(NH_4)_2SO_4$ solution dissolved in PBS; pH = 7.4), gradient initiated at t= 2 min., gradient to 100% buffer B (30% acetonitrile (v/v) dissolved in PBS) in 10 min.

Indeed, simple Bradford assays revealed very high protein/amino acid content in these bands. Further confirmation of the latter assignment is presented in particle tracking data and SEM images presented in subsequent sections. These results suggest that the PET C-CP HIC method is effective at separating the population of exosomes from other chemical species inherent in the spent cell media. Indeed, the presence of the broad concomitant elution bands in the HIC chromatograms reflects the non-specificity and carryover towards proteins, etc. that exists in the DC and exoEasy isolates. It is believed that the far greater abundance of such species (based on the integrated absorbance of the bands) for the exoEasy case versus the DC is due to non-specific binding to the hydrophobic matrix versus the differential centrifugation where proteins and exosomes are more discretely segregated. HIC results prove that the exosome fractions can indeed be readily isolated from those otherwise undesirable components, as in the protein carryover in the exoEasy. Removal of such proteins would require further processing for both the DC and exoEasy isolation methods. The eluted exosome fractions from these isolations were collected and saved for NTA.

To more realistically compare the efficiencies of the C-CP fiber method with the benchmark methods, *D. discoideum* cell cultures were processed in similar fashions in terms of removing whole cells and cellular debris. In the case of DC, simple centrifugation is the first step, while macroscale debris is filter-removed prior to exoEasy Kit isolation. The resulting culture milieu solutions, having the exosomes in their native (relatively dilute) concentrations, were then subjected to HIC on the PET C-CP fiber columns using the previous gradient. The chromatogram of the centrifuged *D.*

discoideum cell culture milieu (Fig. 2.1d), displays two prominent peaks at elution times of 2 - 11 and approximately 13 minutes, respectively. The differences in retention time (<5 % relative) and shapes among the exosome eluents may be due to slight differences in the surface chemistries of the exosomes based on how they were processed prior to the HIC separation, especially solvent composition. This is certainly a point for further investigation. As before, the broader peak is attributed to various media components and cellular metabolites and debris, with the smaller second peak attributed to more hydrophobic species, likely exosomes. The relative responses for the concomitant species and the exosomes make sense as there is apt to be more debris and proteinaceous material, and lower exosome concentrations, in the milieu sample than the DC isolate suspended in PBS. The exosome peak from the milieu reflects their more dilute concentration in this stage of media processing. The corresponding HIC chromatogram taken of the filtered cell culture media is structurally the same as those seen in Figs. 2.1b-d, though with a lower relative exosome yield versus the other media components. This suggests that there may be some exosome loss in the initial filtration process in the exoEasy kit protocol, which is not unreasonable as the filter material itself is composed of both hydrophobic and hydrophilic layers.

As in any new chromatographic method, there are many aspects of the separation that can be optimized. The ability to improve the HIC method throughput is illustrated in Fig. 2.1f, where the initial DC milieu sample was injected at a reduced salt concentration of 0.8 M ammonium sulfate. In this way, the components making up the broad elution peak are not retained on the column. Following passage of the injection peak, the reverse

salt gradient was then initiated, with clean elution of the exosomes. A simple comparison to the analogous full gradient (Fig. 2.1b) reveals that there is little or no difference in the exosome recovery for the abbreviated gradient method. Thus, there is an expectation that further improvements in throughput may be realized. Certainly, larger column formats would also improve processing speeds.

Comparison of exosome recoveries for the different isolation methodologies

NTA is a widely-accepted method for the evaluation of exosome concentration and size distribution, and so was used to characterize the exosome isolation from the DC and exoEasy kit procedures and those of the exosome fractions from the HIC isolations. Figure 2.2 provides a graphic overview of the procedural steps and NTA-determined exosome concentrations for each exosome isolation protocol. The initial entrees into the flow charts (starting milieu volumes) were chosen based on previous experience in the use of DC and exoEasy methods, with the ultimate particle densities normalized to a common 50 mL volume sample.

Since all particles counted during the NTA may not be exosomes (protein aggregates, other classes of extracellular vesicles, including microvesicles, and other cellular debris would also be counted), the resulting values (presented as particles-per-mL) in Fig. 2.2 should be compared to one another on an order-of-magnitude basis as opposed to absolute values. When compared in this manner, it can be seen that the differential centrifugation (Fig. 2.2a) and exoEasy kit (Fig. 2.2b) yield comparable exosome/particle recoveries. Figure 2.2 also shows that the PET C-CP HIC exosome isolation method, regardless of whether the cell culture was first centrifuged (Fig. 2.2c) or

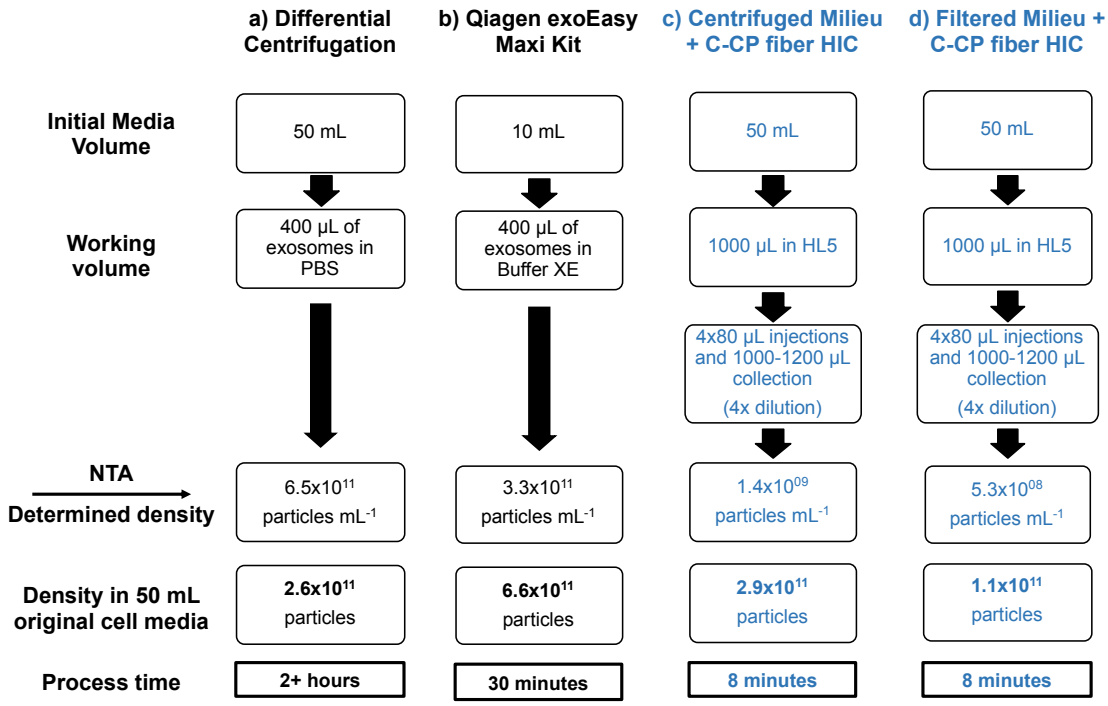

Figure 2.2. Comparison of NTA-determined particle population characteristics following the various exosome isolation methodologies. All values were normalized to number of particles (exosomes) derived from 50 mL of starting cell culture. Reported values are averages from triplicate isolations. a) Exosomes isolated via differential centrifugation. b) Exosomes isolated via Qiagen exoEasy Maxi Kit. c) Cell culture media cleared of cells and large debris via centrifugation, followed by exosome isolation via PET C-CP HIC. d) Cell culture media cleared of cells and large debris via filtration, followed by exosome isolation via PET C-CP HIC.

filtered (Fig. 2.2d) to remove cells and large debris, yields the same order of magnitude values as the benchmark methods following the initial debris removal steps.

The particle size distributions, as measured by NTA, were also very similar across all of the isolated exosome samples, regardless of the isolation method (Table 2.1). In general, the *D. discoideum* exosome size distributions were very similar to those previously reported by Tatischeff et al.[41] Histograms of the NTA size distributions (Fig. 2.3) each contained a prominant high concentration peak on the lower range of the size

distribution scale ranging from ~90 to 160 nm, typically representing ~70 % of the total population. Beyond this, a minor, larger-sized fraction is also seen in each distribution, most prominently in the DC-generated populations. These populations reflect protein and exosome agglomerates, as well as other classes of extracellular vesicles, including microvesicles, which would be most expected in the case of differential centrifugation.

Such populations would also reflect the time-lag associated with sampling, packaging, and shipping of the materials for NTA characterization. Performing NTA/SEM/TEM measurements immediately following exosome isolation may help remediate the level of potential exosome or protein aggregation. Collectively, the NTA results demonstrate that the PET C-CP fiber exosome isolation method does not adversely bias exosome population recoveries (density or sizing) versus the benchmark isolation methods.

As a final point of comparison, Fig. 2.2 also demonstrates the isolation time

Table 1 Comparison of exosome size population characteristics for the different isolation

Table 2.1 Comparison of EV size population characteristics for the different isolation procedures as determined by NTA

Exosome Isolation Method	Mean (nm)	Mode (nm)	Standard Deviation (nm)	10th Percentile (nm)	90th Percentile (nm)
Differential centrifugation	183	143	66.3	119	257
Qiagen exoEasy Maxi kit	154	97.1	80.2	87.6	263
Centrifuged milieu + PET C-CP fibers	155	121	60.1	106	228
Filtered milieu + PET C-CP fibers	142	108	60.4	87.6	206

required for each of the processes. Differential centrifugation is the most time-consuming method, requiring more than 2 hours to perform (Figs. 2.2a). In comparison, the exoEasy kit requires approximately 30 minutes (Figs. 2.2b), while the PET C-CP HIC method can be affected in only 8 minutes (Figs. 2.2 c,d). The C-CP fiber-based method is appreciably faster than either benchmark method, a major asset with regards to its potential usefulness for exosome isolation in a clinical setting. Indeed, the HIC method could be easilly affected in less than 3 minutes with the use of a step-gradient program as suggested in simple terms in Fig. 2.1f.

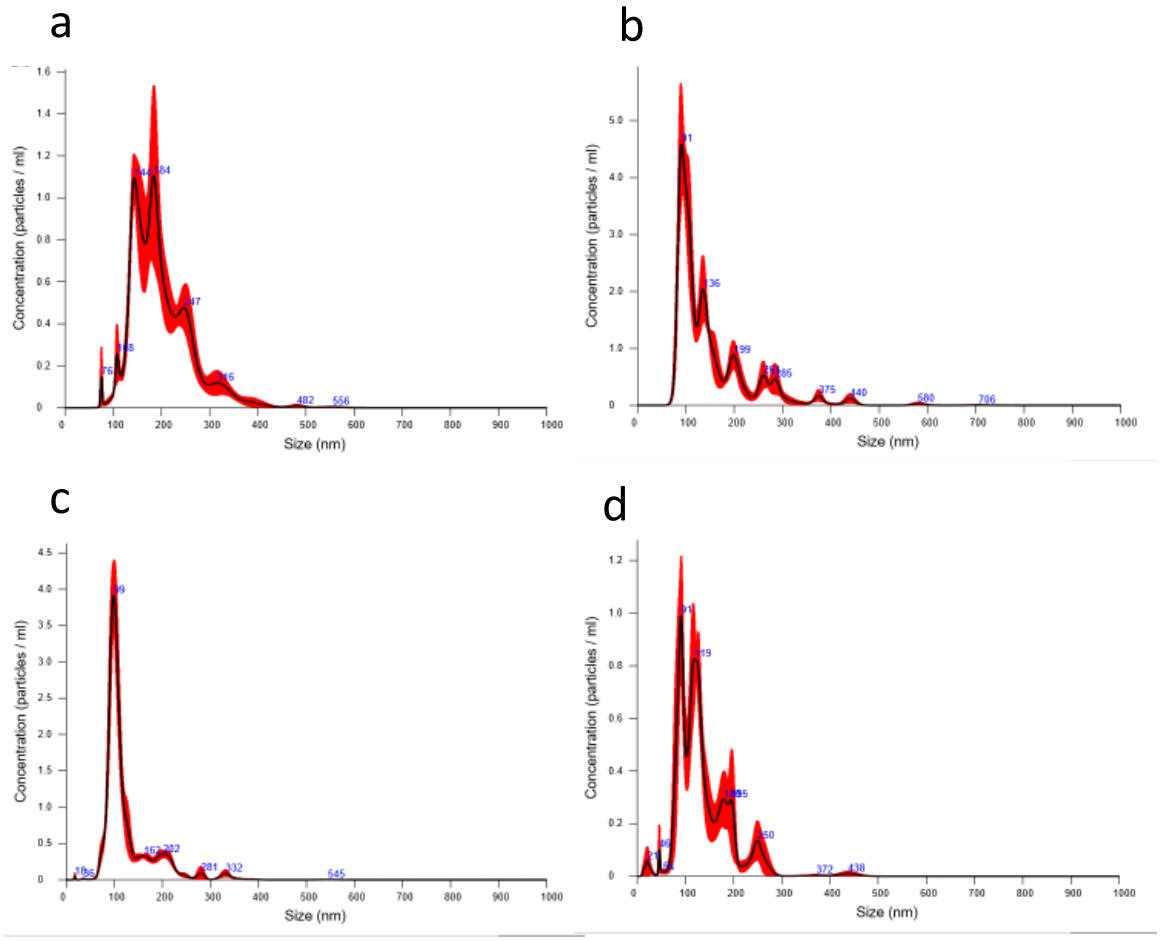

Figure 2.3. Representative nanoparticle tracking analysis (NTA) size distributions. a) differential centrifugation, b) Qiagen exoEasy Maxi kit, c) centrifuged milieu + PET C-CP fibers, and d) filtered Milieu + PET C-CP fibers.

Imaging of exosomes adsorbed onto C-CP fibers

While the size distributions of the *D. discoideum* EVs were very similar to those previously reported by Tatischeff et al. **38**, the standard method of verifying the presence of EVs or exosomes generally includes NTA size distribution results in conjunction with Western Blot verification of the presence of known exosomal protein markers, and a TEM micrograph to visualize and verify sizes of individual vesicles. However, this trio of

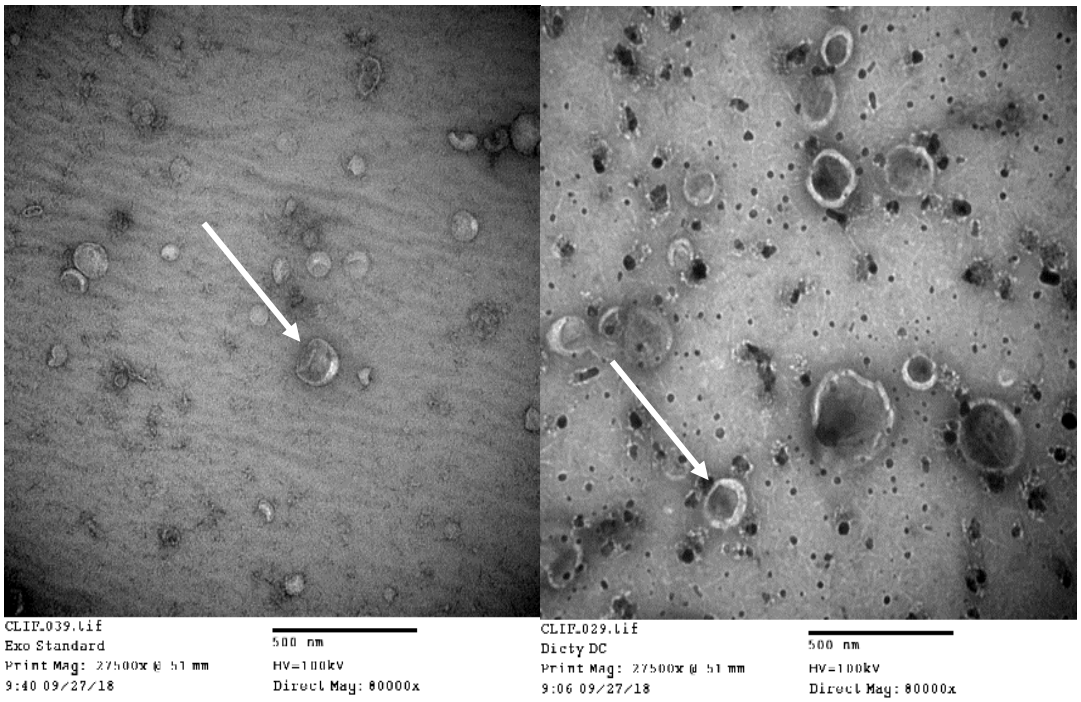

Figure 2.4. TEM images of exosomes immobilized on copper grids. (Left) Standard exosomes derived from human urine (Right) *D. discoideum*-derived exosomes previously isolated via differential centrifugation.

verification methodologies is for mammalian cell-derived exosomes, where exosomal marker proteins have been verified and antibodies to these proteins are commercially available. To this end, no commercial antibodies exist for *D. discoideum* EV surface proteins. Therefore, we rely herein upon the resultant NTA data in combination with TEM micrographs of the commercially available exosome standards as compared to *D. discoideum* EVs resulting from the differential centrifugation method employed for isolation throughout this study (Fig. 2.4).

The resulting micrographs show that the sizes and general morphology of the standard exosomes and those exosomes derived from *D. discoideum* are very similar.

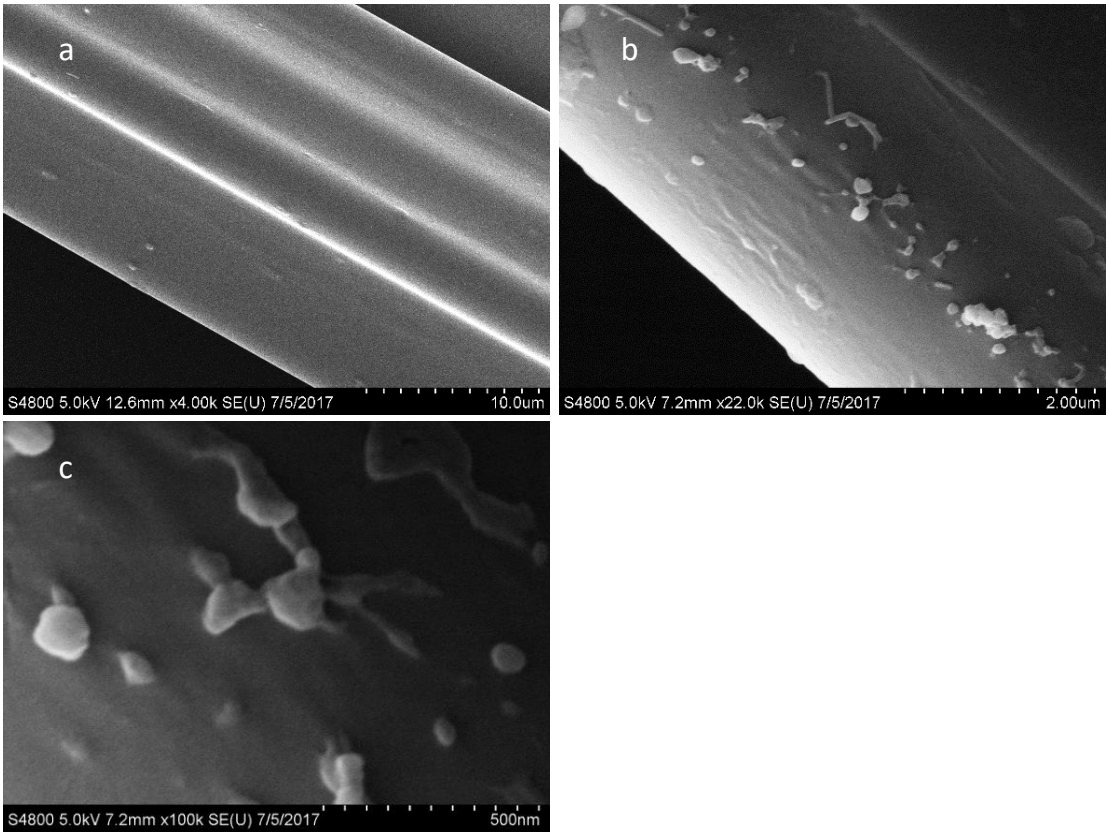

Figure 2.5. SEM images of exosomes immobilized on PET C-CP fibers. a) 2M ammonium sulfate control (no exosomes exposed). b) *D. discoideum*-derived exosomes previously isolated via differential centrifugation. c) Higher magnification image of exosomes depicted in micrograph b, showing detail of exosome interactions with each other and the fiber surface.

Therefore, we contend that the differential centrifugation method employed resulted in the isolation of *D. discoideum* exosomes. These purified exosomes were subsequently utilized to produce SEM images of the exosomes on the experimental columns as outlined below.

SEM images were collected to verify the presence and integrity of the exosomes and to investigate how they interact with the PET C-CP fiber channels. Exosomes that had been isolated from *D. discoideum* cell culture media via differential centrifugation

and re-suspended in PBS were added to 2M ammonium sulfate chromatographic mobile phase and then each spun through PET C-CP fiber micropipette tips using the described solid phase extraction technique.[33, 45] In addition, 2M ammonium sulfate was spun through a separate tip as a non-exosome control.

In each case, an aqueous wash step was employed following exposure to remove any accumulated media particulates. As seen in Fig. 2.5a, the fibers exposed only to the salt media show a very smooth surface, with multiple channels of the same fiber seen at this 10 µm-scale micrograph. Passage of the DC–derived media through the fibers results in the adsorption of vesicle material as seen in Fig. 2.5b (2.0 µm-scale). A large number of vesicles are present as individual entities, but some appear as aggregates. It remains to be confirmed whether or not the agglomerates were formed on the fiber surface or originated in the milieu. Further magnification of the DC-derived aliquot (Fig. 2.5c, 500 nm scale) shows exquisite detail of individual exosomes, with diameters of 100 nm or less, on the PET fiber surfaces with some neighboring exosomes touching one another, perhaps stretching or elongating as they adhere to the fiber. This morphology could be early signs of aggregation or exosome fusion. While the SEM imaging demonstrates the phenomenon of the immobilization of the exosomes on the fiber surfaces, it also suggests that the fiber platform might be a valuable means of studying exosome agglomeration or other phenomena.

Isolation of exosomes via HIC from a simulated urine matrix

Following verification that exosomes could be isolated directly from *D. discoideum* culture milieu, the ability to isolate exosomes from synthetic urine (an ability needed for

diagnostic applications) was investigated. For this experiment, exosomes that had been previously isolated via differential centrifugation were spiked into a simulated urine matrix which was also spiked with the model proteins Myo, Chymo, Ribo, BSA and Lyso, each at a concentration of 0.1 mg mL^{-1}. In this way, isolation from both urine matrix components and concomitant proteins is demonstrated using the same HIC gradient as employed in the Fig. 2.1 separations. Figure 2.6 shows the HIC chromatogram of the simulated urine matrix to establish baseline elution times for the matrix components and the spiked proteins. The five proteins are very well resolved in this case, with the other matrix species eluting as a band over the 8 – 10 min elution window. As seen in Fig. 2.6, when the simulated urine was spiked 50:50 with DC-isolated exosomes and subsequently run on the C-CP columns, HIC revealed the expected peaks for the spiked proteins along with an additional, later-eluting prominent peak attributed to the exosomes. Importantly, the added proteins appear as discrete peaks superimposed on a broader peak previously attributed to remnant proteins and debris associated with the spiked exosomes following their DC-isolation (Fig. 2.1b). (The 0.1 mg mL^{-1} concentrations spiked here are clearly higher than those present from the spiked, equal-volume, milieu isolate.) The ability to cleanly separate exosomes from other species in a urine matrix suggests that C-CP fiber HIC (or simple solid phase extraction[45]) may be a promising method of isolation in a clinical setting.

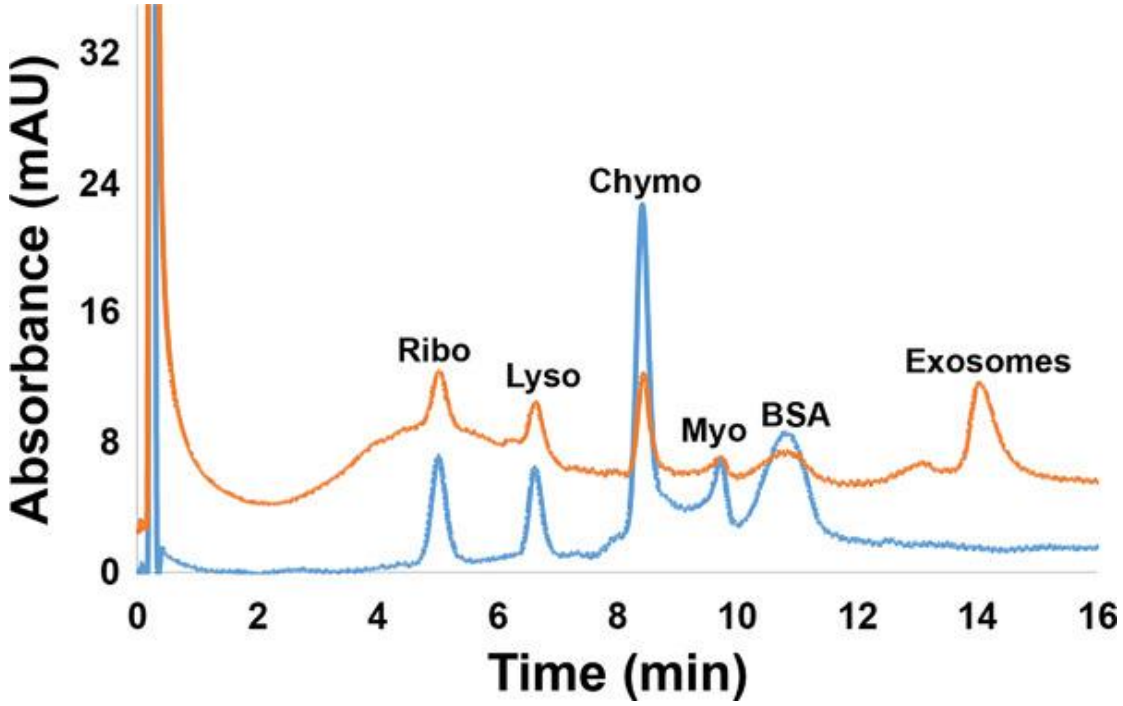

Figure 2.6. PET C-CP fiber HIC chromatograms of simulated urine matrix spiked at 0.1 mg ml^{-1} concentration of model proteins and 50:50 mixture of simulated urine and DC-isolated exosomes. Separations were performed with a mobile phase flow rate of 0.5 mL min^{-1}, 20 µL aliquot injections, and a 20 min gradient from 100% buffer A (1.8 M $(NH_4)_2SO_4$ solution dissolved in PBS; pH = 7.4) to 100% buffer B (30% acetonitrile (v/v) dissolved in PBS).

Potential for Exosome Quantification

In order to make exosome retrieval easier to verify and potentially quantify, a simple measure of recovery is needed. In the context of the HPLC isolation step, UV-vis absorbance at 216 nm is a viable approach. This is a common wavelength used in protein chromatography, and fortuitously, the exosomes absorb at this wavelength. It is most common to quantify exosomes based on lysing the vesicles and quantifying the total protein content via Western blot separations or a Bradford-type assay, or counting/sizing particles via NTA. Of course, this assumes no protein carryover in the isolation step, the protein content in each exosome is the same, and no extraneous cellular debris is present. Hook and co-workers have employed a surface plasmon resonance (SPR) approach to quantification [46], wherein target proteins are captured onto a gold substrate through a surface immobilized antibody. Solution concentrations were extrapolated from first principles relationships, but not verified by any external standards. To establish a quantitative relationship between exosome concentration and absorbance, increasingly larger aliquots of exosomes (previously isolated via DC) were added to 100 μL aliquots of the simulated urine and the culture milieu (HL5) matrices, and the integrated absorbance values for the peaks eluting between 13 - 14 minutes were recorded. As shown in Fig. 2.7, a direct proportionality exists, suggesting quantitative recovery of exosomes from the C-CP fiber separation method. While the robustness of the method as employed here requires far greater evaluation, the results plotted in Fig. 2.7 represent a total of 24 and 15 injections of the respective samples (urine and media), each on a single column, without showing deleterious effects

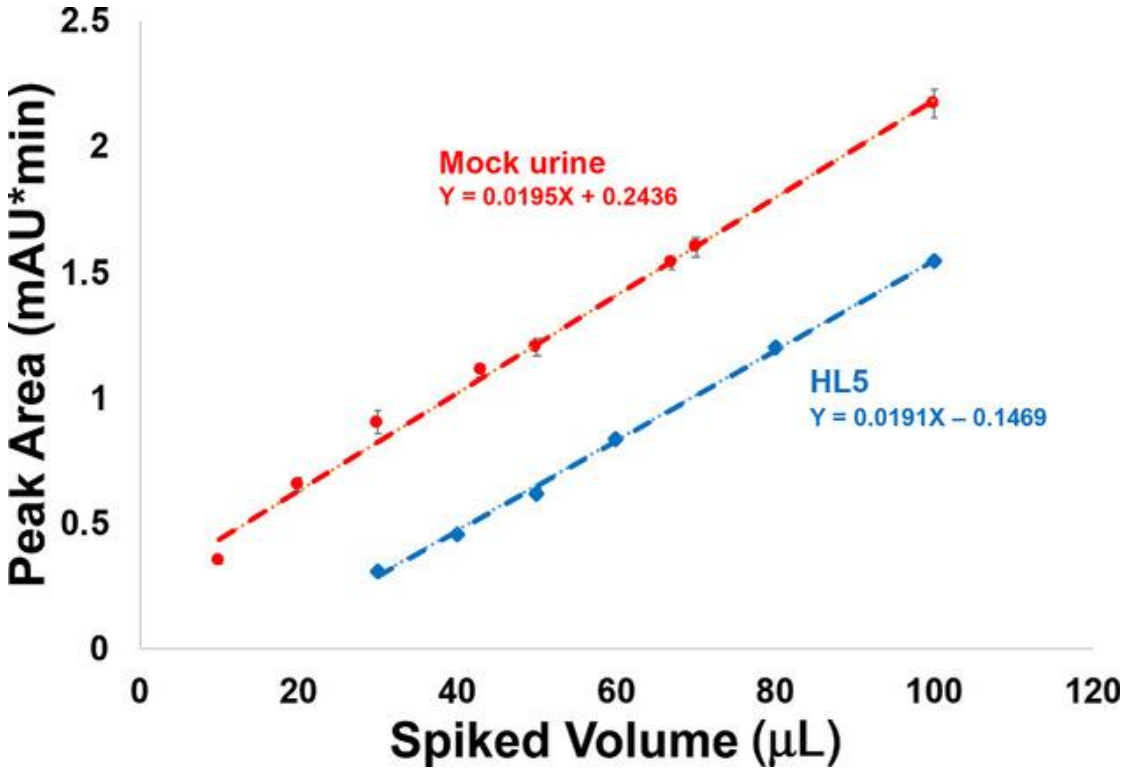

Figure 2.7. Analytical response curves for separations of mixtures of 100 µL of the test matrices (simulated urine and HL5 media) and the designated volumes of DC-isolated exosomes. Separations were performed with a mobile phase flow rate of 0.5 mL min^{-1}, 20 µL aliquot injections, and a 20 min gradient from 100% buffer A to 100% buffer B. Error bars reflect the standard deviation across n=3 injections.

regarding the analytical precision. This suggests insignificant carryover or irreversible binding of the exosome solutes. The number of cycles that milieu-derived samples might be run is a more stringent and practical metric which is currently under review.

Importantly, the slopes of the two response curves are virtually identical, implying that the purity of the isolated fractions is very consistent between the two matrix forms. Note, we are in no position to place firm concentration values on the results of these experiments, as no appropriate certified reference materials (CRMs) exists. Sources of quantified exosomes will be investigated to provide more definitive figures of

metrics. Based on the NTA values presented in Table 2.1, the working range presented in Fig. 2.7 is ~0.1 – 7 X10^9 particles for the 20 μL injections. Accordingly, it is not difficult to imagine limits of detection for this method to be approximately 5 X10^7 particles. Of course, UV-vis absorbance post-column quantification could also be applied for preparative purposes. One could also envision other LC-compatible detection methods, for example, multi-angle light scatter (MALS), which would also provide size information for the eluting particles.

Conclusions

In order for basic research and potential application of exosomes to continue to grow, lower cost, more time-efficient methods of exosome isolation are needed. This report introduces a promising new isolation platform using PET C-CP fibers as stationary phases for HIC isolation of exosomes. The method isolates exosome populations of similar number density and size distribution as currently accepted isolation methods involving advanced centrifugation or solid phase extraction. The fiber platform is inexpensive ($5 USD per column which can be used >20 times on the analytical scale), while providing comparatively high throughput. Additionally, the versatility of the C-CP fibers will allow for the addition of antibodies, surface chemistries, and other isolation modalities to transform the generic (hydrophobic interaction) exosome isolation method demonstrated here into a type-specific method. In an alternative approach, the fibers may be used in spin-down column format (i.e., micropipette tips) to isolate exosomes from body fluids such as urine [47], providing high purity, high throughput, and cost-effective exosome isolation for potential clinical use. Selective capture can be augmented with

spectroscopic or visual imaging as means of verifying the presence of target exosome species on the fiber surfaces.

Much fundamental work remains towards realizing the practical utility of the method on the clinical, analytical, and preparative scales. Each of these areas will pose challenges and require evaluation regarding selectivity, robustness, loading capacity, throughput, and column structure/operation parameters. Many basic challenges towards this end remain. For example, there exist no reference materials which contain quantitative amounts (either mass or number) of exosomes in defined media. Ultimately, the potential impact of exosomes in modern medicine is a tremendous driving force for these continued efforts.

References

1. Lässer C, Eldh M, Lötvall J. Isolation and characterization of RNA-containing exosomes. *J Vis Exp*. Jan 2012;(59):e3037. doi:10.3791/3037

2. Urbanelli L, Magini A, Buratta S, et al. Signaling pathways in exosomes biogenesis, secretion and fate. *Genes (Basel)*. Mar 2013;4(2):152-70. doi:10.3390/genes4020152

3. Raposo G, Stoorvogel W. Extracellular vesicles: exosomes, microvesicles, and friends. *J Cell Biol*. Feb 2013;200(4):373-83. doi:10.1083/jcb.201211138

4. Rashed M, Bayraktar E, Helal G, et al. Exosomes: From Garbage Bins to Promising Therapeutic Targets. Review. *International Journal of Molecular Sciences*. MAR 2017 2017;18(3)ARTN 538. doi:10.3390/ijms18030538

5. Yáñez-Mó M, Siljander PR, Andreu Z, et al. Biological properties of extracellular vesicles and their physiological functions. *J Extracell Vesicles*. 2015;4:27066.

6. Vlassov AV, Magdaleno S, Setterquist R, Conrad R. Exosomes: current knowledge of their composition, biological functions, and diagnostic and therapeutic potentials. *Biochim Biophys Acta*. Jul 2012;1820(7):940-8. doi:10.1016/j.bbagen.2012.03.017

7. Li M, Zeringer E, Barta T, Schageman J, Cheng A, Vlassov AV. Analysis of the RNA content of the exosomes derived from blood serum and urine and its potential as biomarkers. *Philos Trans R Soc Lond B Biol Sci*. Sep 2014;369(1652)doi:10.1098/rstb.2013.0502

8. Lee Y, El Andaloussi S, Wood MJ. Exosomes and microvesicles: extracellular vesicles for genetic information transfer and gene therapy. *Hum Mol Genet*. Oct 2012;21(R1):R125-34. doi:10.1093/hmg/dds317

9. Bellingham S, Coleman B, Hill A. Small RNA deep sequencing reveals a distinct miRNA signature released in exosomes from prion-infected neuronal cells. Article. *Nucleic Acids Research*. NOV 2012 2012;40(21):10937-10949. doi:10.1093/nar/gks832

10. Huang X, Yuan T, Tschannen M, et al. Characterization of human plasma-derived exosomal RNAs by deep sequencing. *BMC Genomics*. May 2013;14:319. doi:10.1186/1471-2164-14-319

11. Taylor D, Gercel-Taylor C. MicroRNA signatures of tumor-derived exosomes as diagnostic biomarkers of ovarian cancer. Article. *Gynecologic Oncology*. JUL 2008 2008;110(1):13-21. doi:10.1016/j.ygyno.2008.04.033

12. Rabinowits G, Gercel-Taylor C, Day J, Taylor D, Kloecker G. Exosomal MicroRNA: A Diagnostic Marker for Lung Cancer. Article. *Clinical Lung Cancer*. JAN 2009 2009;10(1):42-46. doi:10.3816/CLC.2009.n.006

13. Li A, Zhang T, Zheng M, Liu Y, Chen Z. Exosomal proteins as potential markers of tumor diagnosis. *J Hematol Oncol*. 12 2017;10(1):175. doi:10.1186/s13045-017-0542-8

14. An M, Wu J, Zhu J, Lubman DM. Comparison of an Optimized Ultracentrifugation Method versus Size-Exclusion Chromatography for Isolation of Exosomes from Human Serum. *J Proteome Res*. Oct 2018;17(10):3599-3605. doi:10.1021/acs.jproteome.8b00479

15. Li X, Wang X. The emerging roles and therapeutic potential of exosomes in epithelial ovarian cancer. Review. *Molecular Cancer*. MAY 15 2017 2017;16ARTN 92. doi:10.1186/s12943-017-0659-y

16. Momen-Heravi F, Balaj L, Alian S, et al. Current methods for the isolation of extracellular vesicles. *Biol Chem*. Oct 2013;394(10):1253-62. doi:10.1515/hsz-2013-0141

17. Furi I, Momen-Heravi F, Szabo G. Extracellular vesicle isolation: present and future. *Ann Transl Med*. Jun 2017;5(12):263. doi:10.21037/atm.2017.03.95

18. Van Deun J, Mestdagh P, Sormunen R, et al. The impact of disparate isolation methods for extracellular vesicles on downstream RNA profiling. *J Extracell Vesicles*. 2014;3doi:10.3402/jev.v3.24858

19. Jeppesen DK, Hvam ML, Primdahl-Bengtson B, et al. Comparative analysis of discrete exosome fractions obtained by differential centrifugation. *J Extracell Vesicles*. 2014;3:25011.

20. Zarovni N, Corrado A, Guazzi P, et al. Integrated isolation and quantitative analysis of exosome shuttled proteins and nucleic acids using immunocapture approaches. *Methods*. Oct 2015;87:46-58. doi:10.1016/j.ymeth.2015.05.028

21. Yang F, Liao X, Tian Y, Li G. Exosome separation using microfluidic systems: size-based, immunoaffinity-based and dynamic methodologies. *Biotechnol J*. Apr 2017;12(4)doi:10.1002/biot.201600699

22. Böing AN, van der Pol E, Grootemaat AE, Coumans FA, Sturk A, Nieuwland R. Single-step isolation of extracellular vesicles by size-exclusion chromatography. *J Extracell Vesicles*. 2014;3doi:10.3402/jev.v3.23430

23. Nordin JZ, Lee Y, Vader P, et al. Ultrafiltration with size-exclusion liquid chromatography for high yield isolation of extracellular vesicles preserving intact biophysical and functional properties. *Nanomedicine*. May 2015;11(4):879-83. doi:10.1016/j.nano.2015.01.003

24. Li P, Kaslan M, Lee SH, Yao J, Gao Z. Progress in Exosome Isolation Techniques. *Theranostics*. 2017;7(3):789-804. doi:10.7150/thno.18133

25. Marcus R, Davis W, Knippel B, et al. Capillary-channeled polymer fibers as stationary phases in liquid chromatography separations. Article. *Journal of Chromatography a*. JAN 31 2003 2003;986(1):17-31. PII S0021-9673(02)01835-6. doi:10.1016/S0021-9673(02)01835-6

26. Nelson D, Marcus R. A novel stationary phase: Capillary-channeled polymer (C-CP) fibers for HPLC separations of proteins. Article. *Journal of Chromatographic Science*. OCT 2003 2003;41(9):475-479. doi:10.1093/chromsci/41.9.475

27. Stanelle R, Marcus R. Nylon-6 capillary-channeled polymer (C-CP) fibers as a hydrophobic interaction chromatography stationary phase for the separation of proteins. Article. *Analytical and Bioanalytical Chemistry*. JAN 2009 2009;393(1):273-281. doi:10.1007/s00216-008-2457-2

28. Randunu KM, Marcus RK. Microbore polypropylene capillary channeled polymer (C-CP) fiber columns for rapid reversed-phase HPLC of proteins. *Anal Bioanal Chem*. Aug 2012;404(3):721-9. doi:10.1007/s00216-012-6163-8

29. Schadock-Hewitt A, Pittman J, Stevens K, Marcus R. Extrusion-Based Differences in Two Types of Nylon 6 Capillary-Channeled Polymer (C-CP) Fiber Stationary Phases as Applied to the Separation of Proteins via Ion Exchange Chromatography. Article. *Journal of Applied Polymer Science*. APR 15 2013 2013;128(2):1257-1265. doi:10.1002/app.38509

30. Jiang L, Marcus R. Microwave-assisted grafting polymerization modification of nylon 6 capillary-channeled polymer fibers for enhanced weak cation exchange protein separations. Article. *Analytica Chimica Acta*. FEB 15 2017 2017;954:129-139. doi:10.1016/j.aca.2016.11.065

31. Jiang L, Marcus R. Microwave-assisted, grafting polymerization preparation of strong cation exchange nylon 6 capillary-channeled polymer fibers and their chromatographic properties. Article. *Analytica Chimica Acta*. JUL 18 2017 2017;977:52-64. doi:10.1016/j.aca.2017.04.033

32. Jiang XC, Gao JQ. Exosomes as novel bio-carriers for gene and drug delivery. *Int J Pharm*. Apr 2017;521(1-2):167-175. doi:10.1016/j.ijpharm.2017.02.038

33. Schadock-Hewitt A, Marcus R. Initial evaluation of protein A modified capillary-channeled polymer fibers for the capture and recovery of immunoglobulin G. Article. *Journal of Separation Science*. MAR 2014 2014;37(5):495-504. doi:10.1002/jssc.201301205

34. Trang H, Marcus R. Application of protein A-modified capillary-channeled polymer polypropylene fibers to the quantitation of IgG in complex matrices. Article. *Journal of Pharmaceutical and Biomedical Analysis*. AUG 5 2017 2017;142:49-58. doi:10.1016/j.jpba.2017.04.028

35. Jiang L, Marcus R. Biotin-functionalized poly(ethylene terephthalate) capillary-channeled polymer fibers as HPLC stationary phase for affinity chromatography. Article. *Analytical and Bioanalytical Chemistry*. JAN 2015 2015;407(3):939-951. doi:10.1007/s00216-014-8235-4

36. Lavialle F, Deshayes S, Gonnet F, et al. Nanovesicles released by Dictyostelium cells: a potential carrier for drug delivery. *Int J Pharm*. Oct 2009;380(1-2):206-15. doi:10.1016/j.ijpharm.2009.06.039

37. Annesley SJ, Chen S, Francione LM, et al. Dictyostelium, a microbial model for brain disease. *Biochim Biophys Acta*. Apr 2014;1840(4):1413-32. doi:10.1016/j.bbagen.2013.10.019

38. QIAGEN. exoEasy Maxi Kit Handbook. Hilden, Germany2015.

39. Fey P, Dodson RJ, Basu S, Chisholm RL. One stop shop for everything Dictyostelium: dictyBase and the Dicty Stock Center in 2012. *Methods Mol Biol*. 2013;983:59-92. doi:10.1007/978-1-62703-302-2_4

40. Enderle D, Spiel A, Coticchia CM, et al. Characterization of RNA from Exosomes and Other Extracellular Vesicles Isolated by a Novel Spin Column-Based Method. *PLoS One*. 2015;10(8):e0136133. doi:10.1371/journal.pone.0136133

41. Tatischeff I, Larquet E, Falcón-Pérez JM, Turpin PY, Kruglik SG. Fast characterisation of cell-derived extracellular vesicles by nanoparticles tracking analysis, cryo-electron microscopy, and Raman tweezers microspectroscopy. *J Extracell Vesicles*. 2012;1doi:10.3402/jev.v1i0.19179

42. Bobaly B, Beck A, Veuthey J, Guillarme D, Fekete S. Impact of organic modifier and temperature on protein denaturation in hydrophobic interaction chromatography. Article. *Journal of Pharmaceutical and Biomedical Analysis*. NOV 30 2016 2016;131:124-132. doi:10.1016/j.jpba.2016.08.019

43. Fekete S, Veuthey JL, Beck A, Guillarme D. Hydrophobic interaction chromatography for the characterization of monoclonal antibodies and related products. *J Pharm Biomed Anal*. Oct 2016;130:3-18. doi:10.1016/j.jpba.2016.04.004

44. Bobály B, D'Atri V, Beck A, Guillarme D, Fekete S. Analysis of recombinant monoclonal antibodies in hydrophilic interaction chromatography: A generic method development approach. *J Pharm Biomed Anal*. Oct 2017;145:24-32. doi:10.1016/j.jpba.2017.06.016

45. Burdette CQ, Marcus RK. Solid phase extraction of proteins from buffer solutions employing capillary-channeled polymer (C-CP) fibers as the stationary phase. *Analyst*. Feb 2013;138(4):1098-106. doi:10.1039/c2an36126d

46. Rupert DL, Lässer C, Eldh M, et al. Determination of exosome concentration in solution using surface plasmon resonance spectroscopy. *Anal Chem*. Jun 2014;86(12):5929-36. doi:10.1021/ac500931f

47. Manard BT, Jones SM, Marcus RK. Capillary-channeled polymer (C-CP) fibers for the rapid extraction of proteins from urine matrices prior to detection with MALDI-MS. *Proteomics Clin Appl*. Jun 2015;9(5-6):522-30. doi:10.1002/prca.201400081

CHAPTER 3

A MODEL SYSTEM TO INVESTIGATE SELECTIVE EXTRACELLULAR VESICLE CAPTURE

Abstract

Ovarian cancer (OC) is one of the deadliest cancers for women, in part due to its often late stage discovery. Given current advanced treatment options, earlier diagnosis of OC could greatly improve overall survival rates. Presently, there are no routinely administered early OC screening techniques for non-symptomatic women. This is crucial, as there is no symptomology associated with early stage, and late stage OC symptomology is generally vague, including abdominal bloating, gastrointestinal upset, nausea and fatigue. Exosomes are a subpopulation of extracellular vesicles (EVs) approximately 30-150 nm in diameter that may hold promise for the development of early OC diagnostics. However, despite promising studies, exosome diagnosis has been mainly limited to research laboratories primarily due to inconsistencies in isolation and characterization methodologies. The poly(ethylene terephthalate) (PET) capillary-channeled polymer (C-CP) fiber-based EV isolation platform, discussed in Chapter 2, may result in quicker, cheaper, and easier exosome isolations, but requires refinement to improve the selectivity, specificity, and diagnostic accuracy required for clinical OC diagnostics. The model system of cancerous and non-cancerous fluorescent EVs and the immunoaffinity capture protocol developed and analyzed here will allow for quicker and

easier development and optimization of a selective PET C-CP EV isolation platform for use in OC diagnostics.

These investigations include collaborative work with Dr. Ken Marcus of the Clemson University Chemistry Department.

Introduction

Late stage diagnosis of severe maladies, particularly cancers, has led to poor outcomes and high mortality among patients.[1-3] Early diagnosis of these diseases, regardless of treatment strategies, can greatly increase survival and outcome for patients. For example, patients with melanomas, if diagnosed early, have an average 5-year survival rate of 98%. However, when the patient is diagnosed late and melanoma reaches the lymph nodes or metastasizes to other organs during later stages, the 5-year survival rate drops to 64% and 23%, respectively.[4] Likewise, pancreas, lung, ovarian, and breast cancer, among others, demonstrate similar 5-year survival patterns.[3, 5-13] Improvements in early diagnosis and standardization of preventative screening are crucial components in improving cancer survival rates.

Exosomes, a type of extracellular vesicle (EV), have recently garnered attention as diagnostic tools and have several unique properties that make them ideal candidates as biomarkers for early cancer diagnostics. First, as exosomes appear to be selectively packaged with particular contents, including exosomal protein, lipid, and RNA markers, they may be identified and traced back to the originating cell.[14, 15] In particular, protein marker identification and miRNA expression pattern recognition through advanced data analysis may help develop exosome marker profiles for particular diseased cell-derived exosomes.[5, 16, 17] Second, exosomes are released by nearly all types of cells and are found in nearly all types of body fluids.[18] The ability to identify the same category of biomarker from nearly all cell types may allow for development of a universal test to screen for a multitude of diseases. Furthermore, a wide variety of body fluids from which to isolate

EVs provides flexibility with regards to the types of exosome isolation methods that may be utilized. Finally, exosomes are very stable and can protect protein and RNA contents from protease and RNase degradation.[19-21] This high exosome stability may allow for the use of more severe isolation methods to enhance the speed and lower the cost of exosome isolations. In addition, this quality makes them a more reliable species for use in liquid biopsies than free DNA and RNA species that may be easily degraded.[22]

To date, the full potential of exosome-based diagnostics has yet to be realized in clinical trials. However, several groups have developed promising exosome-based diagnostic platforms using protein and miRNA markers. For example, Zhao et al. have developed a microfluidics device that uses microbeads to capture and identify ovarian cancer (OC) exosomal protein markers.[23] Similarly, Yokoi et al. have developed an analytical method to better diagnose OC using a combination of 8 exosome miRNAs with a sensitivity of 0.92 and a specificity of 0.91.[16] As evidenced by these studies, OC has emerged as a desirable exosome diagnostic target due to its morbidity and the diagnostic difficulties associated with the disease. OC, when diagnosed in stage 3 or 4, has a 5 year survival rate of 29%. However, when OC is diagnosed and treated in stage 1, the 5 year survival rate is 92%.[24] Unfortunately, due to lack of effective diagnostic technologies and indistinct early symptomology, most OC cases are diagnosed in stage 3 or 4.[25, 26] Exosome-based diagnostics may provide an opportunity for early stage OC detection, allowing treatments to be started earlier and potentially increasing the overall survival rate of OC patients.

There is now an ongoing effort to identify the patterns of protein and miRNA expression within malignant tumor-derived exosomes to establish biological pathways and discover new potential cancer biomarkers. By utilizing mass spectroscopy-based proteomics and miRNA sequencing analysis in conjunction with machine learning and pattern recognition algorithms, exosome expression patterns are being identified and categorized by cancer type, stage, malignancy, origin, and pathology.[5, 27-39] As the available data continues to amass, more patterns that can be used for diagnosis will emerge. However, the quickly changing classifications, isolations, and terminologies surrounding exosomes and EVs may require that these analyses be revisited. Despite these early challenges, it is anticipated that the differentiation of cancerous and non-cancerous exosome expression patterns from this data will ultimately be an important step in the development of quick, easy, and non-invasive exosome-based cancer diagnostics.

Complete exosome proteomes and miRNA profiles are excellent for identification of proteins and miRNAs enriched in cancerous exosomes, but not realistic for affordable and efficient clinical diagnostics. Development of comprehensive proteomes and miRNA profiles is expensive, time consuming, and would require extensive data analysis amounting to long time periods passing between sample collection and diagnosis. A much simpler, cheaper, and faster strategy has been to utilize identified enriched protein and miRNA exosomal biomarkers to capture subpopulations to determine the origins of the exosomes.[18, 22, 36, 37, 40-43] Through these kinds of efforts, OC tumor cells have been found to release exosomes enriched in protein biomarkers including, EpCAM (epithelial

adhesion molecule), CA-125 (cancer antigen 125), CD24 (cluster of differentiation 24), HER-2 (human epidermal growth factor receptor 2), CLDN3 (claudin 3), CLDN4 (claudin 4), L1CAM (L1 cell adhesion molecule), EGFR (epidermal growth factor receptor), PCNA (proliferating cell nuclear antigen), TGF-β1 (transforming growth factor - β1) , MAGE3/6 (melanoma antigen gene 3/6), FASN (fatty acid synthase), ERBB2 (receptor tyrosine-protein kinase), and APOE (apolipoprotein E).[43-47] Furthermore, antibodies to these biomarker proteins have demonstrated the ability to specifically capture and/or identify subpopulations of exosomes for potential disease diagnostics.

Despite the promising medical applications and biomarker discovery underway, reliable exosome isolation remains a large hurdle for their use in diagnostics.[18, 48-52] Slight variations in exosome isolation methods can greatly alter both the exosome proteome and miRNA profile[40, 52-54], making comparisons across datasets difficult. Additionally, different exosome isolations may alter the integrity of the vesicles and their contents, further contributing to alterations in proteome and miRNA signatures.[22, 36, 55] Although the EV community is working to create standards to increase consistency across the field, there remains a need for an improved exosome isolation method that can become a dominant protocol within the field. Current standards and commercially available isolation methods are often expensive, slow, inefficient, or retain non-exosomal impurities, making them unreliable in a clinical setting. A diagnostic test for early OC needs to be quick, easy, and cost effective so that it can be performed routinely as a preventative screening tool for women. Additionally, diagnostic accuracy has yet to be verified for each type of exosome isolation. Developing an improved exosome isolation

method that preserves exosome stability and integrity for downstream analysis is not only critical for clinical translation but will also improve the accuracy, speed, and cost of research laboratory protocols.

To increase the signal to noise ratio inherent in discovery of exosomal markers and further improve diagnostic accuracy, it will be essential to efficiently separate exosomes from healthy and diseased sources. Immunoaffinity capture will almost certainly play a large role in this; however, differentiating capture of healthy and diseased exosome populations may prove difficult. The separation will likely require time consuming, costly protein assays to verify the results of each test and involve variable and costly patient samples. Alternatively, model systems are frequently used to speed up the protocol optimization process and reduce costs for early research. In this case, a model system of cancerous and non-cancerous cell lines capable of producing fluorescently-labeled exosomes would enable efficient optimization of the poly(ethylene terephthalate)(PET) capillary-channeled polymer (C-CP) fiber-based EV isolation platform, developed by Bruce et al.[56], for use in OC diagnostics. This study details the development and analysis of two new cells lines, one cancerous and one non-cancerous, that constitutively express fluorescently-tagged exosomal marker proteins that allow for simple, colorimetric-based differentiation between their individually released exosomes.

As there are several known exosomal OC protein biomarkers and OC is a prime target for exosome-based diagnostics, cancerous (SKOV-3) and non-cancerous (IHOE) ovarian cell lines were selected for the development of a model system for the production of fluorescently-labeled exosomes. Each cell line was genetically transduced to express

known exosomal markers, CD81 and CD9, with fluorescent tags of different excitation and emission wavelengths (GFP and RFP, respectively). Exosomes isolated from each of the resulting cell lines, IHOE-CD81-GFP and SKOV-3-CD9-RFP, express fluorescent markers that allow for easier differentiation, separation, and detection of cancerous and non-cancerous ovarian cell-derived exosome populations. To test the ability of PET C-CP fibers to capture the model vesicles and to check for any potential adverse effects of the fluorescent tags on the binding of the exosomes to the fibers, IHOE-CD81-GFP and SKOV-3-CD9-RFP exosomes were used to evaluate adherence to the surface of the PET C-CP fibers and fluorescence images were collected. Finally, in a proof-of-concept investigation aimed at future efforts for the direct translation to OC diagnostics based upon the new PET C-CP fiber-based EV isolation platform, antibodies to known universal exosomal biomarkers and exosomal OC biomarkers were used to capture pre-enriched IHOE-CD81-GFP and SKOV-3-CD9-RFP exosomes on nitrocellulose membranes to demonstrate the specific capture of the cancerous and non-cancerous fluorescent exosomes. By utilizing these model cancer and non-cancer cell-derived exosomes, the accuracy, selectivity, and specificity of the new PET C-CP EV isolation platform may be studied without the need for more costly and difficult to obtain patient samples. With improvements as a result of the fluorescent exosome model system developed here, this diagnostic platform may be optimized for the identification of early stage ovarian cancer and hopefully provide a quick, easy-to-use, and inexpensive tool for routine and early ovarian cancer screening in the future.

As the EV research field expands, experts have expressed a growing concern that vesicles referred to generically as exosomes may actually be a mix of EV subtypes. Due to the complex debate surrounding EV classification and nomenclature currently underway, all EVs discussed herein will be referred to as small EVs (sEVs) rather than exosomes specifically.

Materials and Methods

Cell and culture conditions

Immortalized Human Ovarian Epithelial (IHOE) cells (Applied Biological Materials, Richmond, BC, Canada) were maintained in Prigrow I medium (Applied Biological Materials, Richmond, BC, Canada) supplemented with 10% exosome-depleted fetal bovine serum (FBS) (A2720801, Thermo Fisher Scientific, Waltham, MA), 100 IU/mL penicillin and 100 µg/mL streptomycin at 37˚C and 5% CO_2. Human ovarian adenocarcinoma epithelial SKOV-3 cells (ATCC, Manassas, VA) were maintained in McCoy's 5a Medium Modified supplemented with 10% exosome-depleted fetal bovine serum (FBS), 100 IU/mL penicillin and 100 µg/mL streptomycin at 37˚C and 5% CO_2. Additionally, IHOE-CD81-GFP and SKOV-3-CD9-RFP cells were supplemented with puromycin at a concentration of 2.5 µg/mL to maintain selection. All cells were passaged at 70-90% confluency.

SKOV-3 and IHOE plasmid transduction and clone development

Approximately $9x10^4$ SKOV-3 and IHOE cells were seeded in each well of a 96 well plate and incubated in media supplemented with 10% exosome-depleted FBS for 10-18 hours before transduction. IHOE cells were transduced using an HIV lentivector system pre-packaged with either pCT-CD81-GFP or pCT-Cyto-GFP plasmid (CYTO124-VA-1, CYTO118-VA-1, System Biosciences, Palo Alto, CA). SKOV-3 cells were transduced using an HIV lentivector system pre-packaged with either pCT-CD9-RFP or pCT-Cyto-RFP plasmid (CYTO123-VA-1, CYTO119-VA-1, System Biosciences, Palo Alto, CA). Both cell lines were transduced at a multiplicity of infections (MOI) of 1, 2, 5, and 10 using the TransDux MAX Lentivirus Transduction Reagent (LV860A-1, System Biosciences, Palo Alto, CA). After 72 hours of incubation at 37˚C and 5% CO_2, cells were screened for fluorescence using a GE INCell Analyzer 2500HS (General Electric, Boston, MA), and cell culture media was replaced and supplemented with 2.5 µg/mL puromycin for selection. All cells were incubated for 7-14 days until stable transduction produced confluent polyclonal cultures. Afterward, dilution cloning was used to obtain single cells for the development of monoclonal stable cell lines.

Small extracellular vesicle isolation using ultracentrifugation

All SKOV-3 and IHOE cells were cultured in Falcon 75 cm^2 cell culture flasks with vented caps (Corning, Corning, NY) to approximately 80% confluency and replenished with fresh media. Cultures were incubated for 3 days and then conditioned media was collected for sEV isolation. sEV isolation was performed in a series of differential centrifugation steps starting with 45 mL of conditioned cell culture media. Using an Eppendorf Centrifuge 5430R (Eppendorf, Hamburg, Germany), the conditioned

media was centrifuged at 700 x g for 5 minutes at 22˚C. The resulting supernatant was then centrifuged at 2,000 x g for 10 minutes at 22˚C. Next, the resulting supernatant was centrifuged at 10,000 x g for 30 minutes at 4˚C using a Beckman Coulter Avanti J-26S XPI Centrifuge equipped with a JA-25.50 rotor (Beckman Coulter, Brea, CA) and the supernatant was collected. Finally, the collected supernatant was centrifuged at 120,000 x g for 60 minutes at 4˚C using a Beckman Coulter Optima XPN-80 Ultracentrifuge equipped with a Type 45 Ti rotor (Beckman Coulter, Brea, CA) and the supernatant was discarded. The final pellet was then resuspended in 400 µL of phosphate buffered saline (PBS).

Fixation and staining of samples for transmission electron microscopy

Samples being prepared for transmission electron microscopy (TEM) were first fixed in 4% paraformaldehyde for 30 minutes on ice. Grid adhesion, staining, and washing steps were performed on parafilm by moving 200 mesh copper formvar grids (Electron Microscopy Sciences, Hatfield, PA) from drop to drop. Following fixation, grids were placed on 5 µL drops of each sample for 5 minutes. Grids were washed 3 times with DI water for 4 minutes each, stained with 2% Uranyl Acetate for 5 minutes, and then washed 3 times with DI water for 4 minutes each. Grids were air dried in a low-humidity environment and then imaged using a Hitachi H7600 TEM (Hitachi, Tokyo, Japan).

Production of cell lysate

Approximately 2.5 – 5 x 10^5 cells were resuspended in 1 mL of ice-cold 1X radioimmunoprecipitation assay (RIPA) lysis buffer (50672585, Thermo Fisher Scientific, Waltham, MA) and incubated with agitation for 30 minutes. Samples were then centrifuged at 13,000 x g for 20 minutes at 22˚C using an Eppendorf Centrifuge 5424 (Eppendorf, Hamburg, Germany). The resulting supernatant (lysate) was collected and saved for subsequent analysis.

Protein Quantification

All sEV and cell lysate samples were quantified using a NanoVue Plus UV-Vis spectrophotometer (GE Healthcare, Chicago, IL). The spectrophotometer was blanked between each sample using phosphate buffered saline and samples were quantified at 280 nm absorbance according to the manufacturer's instructions.

SDS-PAGE and western blot analysis of extracellular vesicles and cell lysates

All samples were separated using a 12% gel and NuPAGE XCell SureLock Mini-Cell electrophoresis system (Thermo Fisher Scientific, Waltham, MA) under reduced or non-reduced conditions. Cell lysate, recombinant TurboGFP protein (EVN-FP552, Axxora, Farmingdale, NY), and purified RFP protein (NBP199583, Fisher Scientific, Hampton, NH) were used as positive controls. All gels were run at 170 mV for approximately 45 minutes. Wet transfer was performed using a Genie Electrophoretic transfer system (Idea Scientific Co, Minneapolis, MN) with a polyvinylidene difluoride (PVDF) membrane in 1X Towbin buffer run at 12 V for approximately 90 minutes. PVDF membranes were blocked in 5% non-fat milk in 1X Tris buffered saline

supplemented with 0.5% Tween 20 (TBS-Tween) for 40 minutes at 37°C. Blocked membranes were rinsed with 0.5%Tween 20/TBS, and incubated overnight at 4°C with primary antibody (1:2000 rabbit anti-TurboGFP (PIPA522688, Fisher Scientific, Hampton, NH) or 1:1000 rabbit anti-RFP (600-401-379, Rockland Immunochemicals, Inc., Pottstown, PA)). After washing in TBS-Tween for 1 hour at 22°C with 6 buffer changes, membranes were incubated with secondary 1:5000 goat anti-mouse IgG horseradish peroxidase (1:5000; GTXMU004DHRPX, Immunoreagents, Inc., Raleigh, NC) or 1:10,000 goat anti-rabbit IgG horseradish peroxidase (GTXRB003FHRPX, Immunoreagents, Inc., Raleigh, NC) antibody for 1 hour at room temperature. Probed membranes were then washed in high salt tris buffered saline supplemented with 0.05% Tween (TS-Tween) for 1 hour at 22°C with 6 buffer changes. Finally, protein was detected using the Pierce ECL Western blotting substrate kit (32106, Thermo Fisher Scientific, Waltham, MA) following the manufacturer's instructions. Western blot gels were loaded according to the following scheme. IHOE-CD81-GFP, SKOV-3-CD9-RFP, IHOE, and SKOV-3 cell lysate lanes were loaded with 150 µg of protein each. IHOE-CD81-GFP, SKOV-3-CD9-RFP, IHOE, and SKOV-3 sEV lanes were loaded with 10 µg of protein each. Differences in cell lysate and sEV loading amounts are to account for differences in concentration of the protein of interest. Finally, the purified, control tGFP protein lane was loaded with 50 ng of protein and the purified, control RFP protein lane was loaded with 40 ng of protein.

C-CP fiber tip assembly

Polymer extruded polyethylene terephthalate capillary-channeled fibers (C-CP), produced by the Material Science and Engineering Department at Clemson University, were wound on a circular frame 8 times (450 fibers) then rinsed with hot water, acetonitrile, isopropanol, and ultra-pure water. Wound fibers were pulled through a 30 cm length, 0.762 mm internal diameter polyether ether ketone (PEEK)(IDEX Health & Science LLC, Oak Harbor, WA) tubing using a plastic monofilament. Packed tubing sections were attached to the end of 200 µl micropipette tips and subsequently inserted through pierced centrifuge tube caps for sample spin-down and wash collection.

sEV capture and isolation on C-CP tips

Following C-CP tip assembly, sEV or PBS samples of 100 µl were loaded into the tips and spun down at 300 x g for 1 minute using an Eppendorf Centrifuge 5430R (Eppendorf, Hamburg, Germany). Afterward, the loaded tubing was prepared for either SEM or fluorescence imaging.

C-CP Fiber sample preparation for scanning electron microscopy

C-CP fiber samples being prepared for SEM were fixed in 1% osmium tetroxide for 1 hour with shaking. After removing the osmium tetroxide, samples were washed in deionized water 3 times for 3-5 minutes. Next, the samples were washed in an ethanol-water mixture of the following ethanol percentages for 3 minutes each: 50%, 70%, 80%, 90%, 95%, 100%, 100%. The samples were then washed in a 50:50 hexamethyldisilazane(HMDS) –ethanol mixture for 3 minutes and then washed in 100%

HMDS and left to dry for 2-3 days. After drying, samples were attached to a metal stage using adhesive and platinum coated using the Hummer 6.2 Sputtering system (Anatech, Battle Creek, MI) at 70 millitorr for 2 minutes. A Hitachi SU5000 Field Emission Scanning Electron Microscope (FE-SEM) (Hitachi, Tokyo, Japan) was used to capture SEM images.

Immunoaffinity blot capture technique

Antibodies for turboGFP, RFP, CD63, CD24, Her2, L1CAM, and EGFR (Table 3.1) were used to capture sEVs on nitrocellulose membranes (See Figure 3.1 for visual experimental setup). To prepare the membranes, 0.25 μL of each primary antibody at a concentration of 1 mg/mL was applied to the nitrocellulose membrane and allowed to dry for 1 hour. Prepared membranes were blocked with 0.5% bovine serum albumin (BSA) in tris buffered saline supplemented with 0.5% Tween (TBS-Tween) for 30 minutes at 37˚ C to prevent non-specific binding. Blocked membranes were then exposed to IHOE-CD81-GFP and/or SKOV-3-CD9-RFP sEVs in TBS-Tween at a concentration of 125 μg/mL for 2 hours at room temperature with shaking. Finally, membranes were washed in TBS-Tween for 1 hour with 6 buffer changes to remove any excess sample and decrease background signal. Fluorescent images of membranes were captured immediately while wetted with TBS-Tween to minimize variation in background signal.

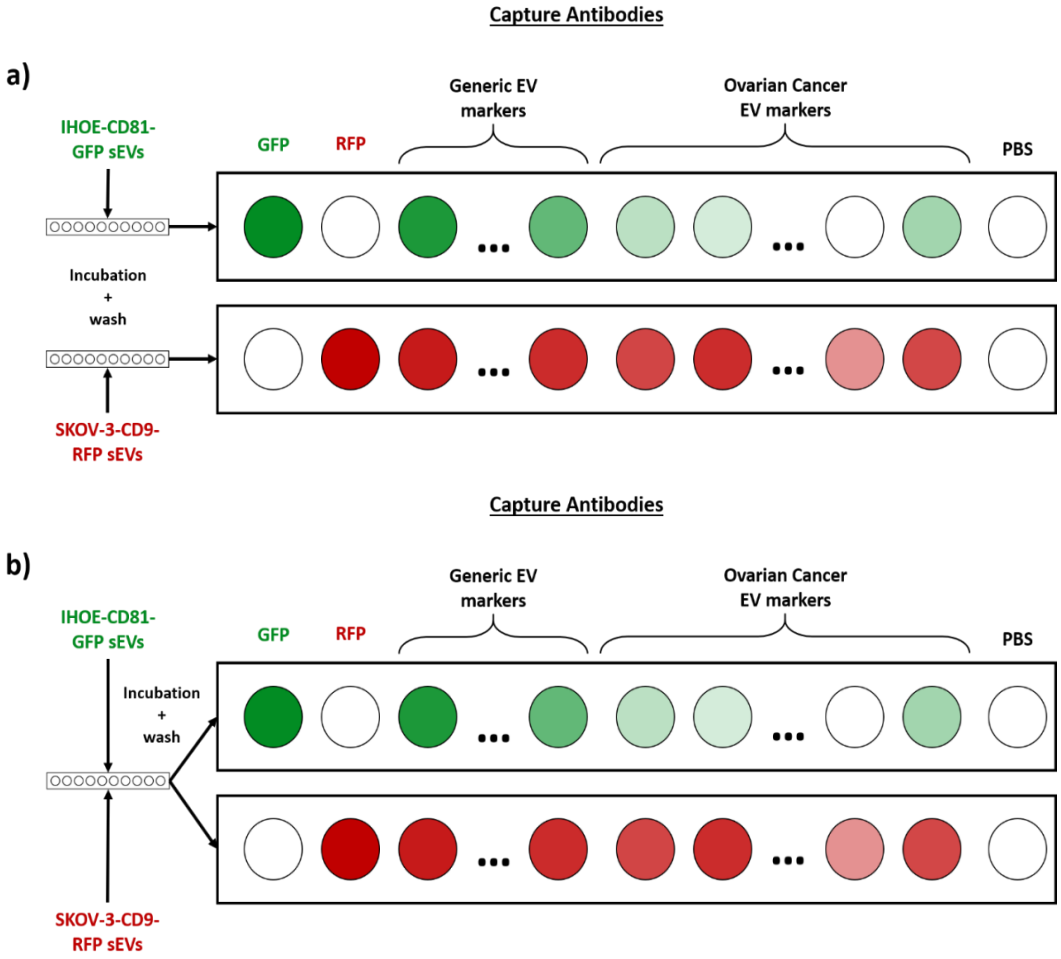

Figure 3.1. Diagram of sEV immunoaffinity blot capture experimental setup. IHOE-CD81-GFP and SKOV-3-CD9-RFP sEVs were incubated in solution with antibody-dotted nitrocellulose membranes. Capture studies were performed with IHOE-CD81-GFP and SKOV-3-CD9-RFP sEV samples in a) independent experiments and b) mixed sample experiments. Capture antibodies used in the complete experiment are detailed in Table 3.1.

Fluorescence Intensity, Super-Resolution Confocal Imaging, and Image Analysis

Confocal fluorescent and differential interference contrast (DIC) images were captured using a Leica SP8 confocal microscope with Hyvolution super-resolution (Leica, Wetzlar, Germany). IHOE, IHOE-Cyto-GFP, IHOE-CD81-GFP, SKOV-3, SKOV-3-cyto-RFP, and SKOV-3-CD9-RFP cells were seeded in 8-well, coverslip bottom imaging plates at a concentration of $1 – 5 \times 10^4$ cells/mL. Cells were fixed in 4% paraformaldehyde (EMS, Hatfield, PA) for 15 minutes at 22˚C and washed 3 times in 1X PBS. Cells were then stained with 300 nM DAPI (4',6-Diamidino-2-Phenylindole, Dihydrochloride) for 5 minutes at 22˚C and washed 3 times in PBS prior to imaging. All images were captured using an HC PL APO CS2 63x/1.40 oil immersion objective. DAPI images were obtained using 405 nm excitation (15% power; gain=50), and a gateable HyD detector (411-449 nm detection; time gate = 8.5-12 ns). GFP images were obtained using 488 nm excitation (15% power; gain=100), and a gateable HyD detector (512-564 nm detection, time gate = 0.01-6 ns). RFP images were obtained using 558 nm excitation (25% power; gain=300), and a gateable HyD detector (575-650 nm detection, timegate = 0.08-3.58 ns).

Relative fluorescence intensity measurements of IHOE-CD81-GFP and SKOV-3-CD9-RFP sEVs isolated by UC and resuspended in PBS were obtained using a Biotek Synergy H1 Hybrid Reader (Biotek, Winooski, VT) with a 100 ms exposure time for all samples. The suspended IHOE-CD81-GFP sEVs were excited at 488 nm with fluorescence measured at 525 nm and suspended SKOV-3-CD9-RFP sEVs were excited at 550 nm with fluorescence measured at 590 nm.

All fluorescent C-CP fiber images were captured using a Leica SP8 HyVolution confocal microscope (Leica, Wetzlar, Germany). PET C-CP fibers prepared with samples were removed from the packed columns and spread evenly across a slide prior to imaging. All green fluorescent protein (GFP) images were obtained using a 488 nm excitation laser line at 25% intensity, an emission detection range from 500-541 nm, with a detector gain of 300, and a time gate from 0.08-3.58 ns. All red fluorescent protein (RFP) images were obtained using a 558 nm excitation laser line at 25% intensity, an emission detection range from 564-628 nm, with a detector gain of 300, and a time gate from 0.3-6 ns.

Relative fluorescence intensity measurements of the dot blots on nitrocellulose membranes, prepared as described in the immunoaffinity blot capture technique above, were obtained using a Leica Thunder- Model Organism imaging system (Leica, Wetzlar, Germany). Single-channel images for GFP and RFP were captured using a Plan APO 1.0X objective (0.09 numeral aperture, no immersion) with a 5x zoom for a total of 50x magnification (GFP - 100 ms exposure; ET GFP filter set (450-490 nm excitation/500-550 nm detection); RFP- 2s exposure; ET mCherry filter set (540-580 nm excitation/592-667 nm detection). Following image capture, average relative fluorescence intensity was measured using ImageJ version 1.48 software (NIH, Bethesda, MD). Relative fluorescence intensity values were normalized to the average intensities of UC isolated sEVs from IHOE CD81-GFP and SKOV-3-CD9-RFP cells dotted (3 µl) on a nitrocellulose membrane at a protein concentration of 2,500 µg/mL and imaged under the

same conditions. All intensity values were adjusted using appropriate background subtractions.

Statistical Analysis

All numeric values are presented as sample means ± 1 standard deviation. Data were analyzed using a one-tailed t-test ($\alpha=0.05$) in Microsoft Excel's data analysis software (Microsoft, Redmond, WA). All tests with $p<0.05$ were considered statistically significant.

Table 3.1. Description and catalog number of antibodies used in western blot and immuno-affinity blot capture experiments.

Antibody	Antigen Description	Catalog Number
Rabbit anti-TurboGFP	Brighter variant of the traditional green fluorescent protein – a commonly used fluorescent marker.	AB513 (Evrogen, Moscow, Russia)
Rabbit anti-RFP	Red fluorescent protein – a commonly used fluorescent marker.	600-401-379 (Rockland Immunochemicals Inc., Limerick, PA)
Mouse anti-CD81	Tetraspanin involved in signal transduction and trafficking. Common sEV marker.[89]	sc-166029 (Santa Cruz Biotechnology, Dallas, TX)
Mouse anti-CD9	Tetraspanin involved in cell adhesion and migration. Common sEV marker.[89]	sc-13118 (Santa Cruz Biotechnology, Dallas, TX)
Rabbit anti-CD63	Tetraspanin involved in cell signaling cascades. Common sEV marker.[89]	11271-r142 (Sino Biological Inc., Beijing, China)
Mouse anti-CD24	Sialoglycoprotein associated with development, invasion, and metastasis of cancer cells. Overexpressed in ovarian cancer sEVs.[90]	14-0247-82 (Thermo Fisher Scientific, Waltham, MA)
Mouse anti-HER-2	Human Epidermal Growth Factor Receptor 2 - Tyrosine kinase receptor involved in cell proliferation and tumor cell metastasis. Associated with poor outcomes in ovarian cancer.[65]	BMS120 (ThermoFisher Scientific, Waltham, MA)
Mouse anti-L1CAM	Cell adhesion molecule involved in cell proliferation, adhesion, migration, and chemoresistance. Associated with poor prognosis in various carcinomas and ovarian cancer.[91]	L4543 (Sigma-Aldrich, St. Louis, MO)
Mouse anti-EGFR	Epidermal Growth Factor Receptor – Tyrosine kinase receptor involved in cell proliferation, migration, and invasion. Highly expressed in ovarian tumors.[92]	555996 (BD Biosciences, San Jose, CA)

Results

Establishment and verification of IHOE-CD81-GFP and SKOV-3-CD9-RFP model system

Initial lentiviral-mediated transduction of IHOE and SKOV-3 cells with pCT-Cyto-GFP (CYTO118-VA-1, SBI, Palo Alto, CA) and pCT-Cyto-RFP (CYTO119-VA-1, SBI, Palo Alto, CA), respectively, revealed an optimal transduction efficiency of 10 pCT-Cyto-GFP virus particles per IHOE cell and 5 pCT-Cyto-RFP virus particles per SKOV-3 cell. Transduction of IHOE cells with pCT-CD81-GFP or the pCT-Cyto-GFP control plasmid resulted in production of IHOE-CD81-GFP and IHOE-Cyto-GFP control cells, respectively. Transduction of SKOV-3 cells resulted in production of SKOV-3-CD9-RFP and SKOV-3-Cyto-RFP control cells, respectively. Confocal imaging of IHOE-CD81-GFP cells, stained with DAPI (see Figure 3.2), revealed punctate expression of GFP throughout the cytoplasm of the cell. Under the same imaging conditions, IHOE-Cyto-GFP control cells (see Figure 3.2) demonstrated even GFP distribution throughout the entire cell, including potential expression within the nucleus. Non-transduced control IHOE cells (see Figure 3.2) demonstrated no GFP expression while none of the samples demonstrated RFP expression (see Figure 3.2)

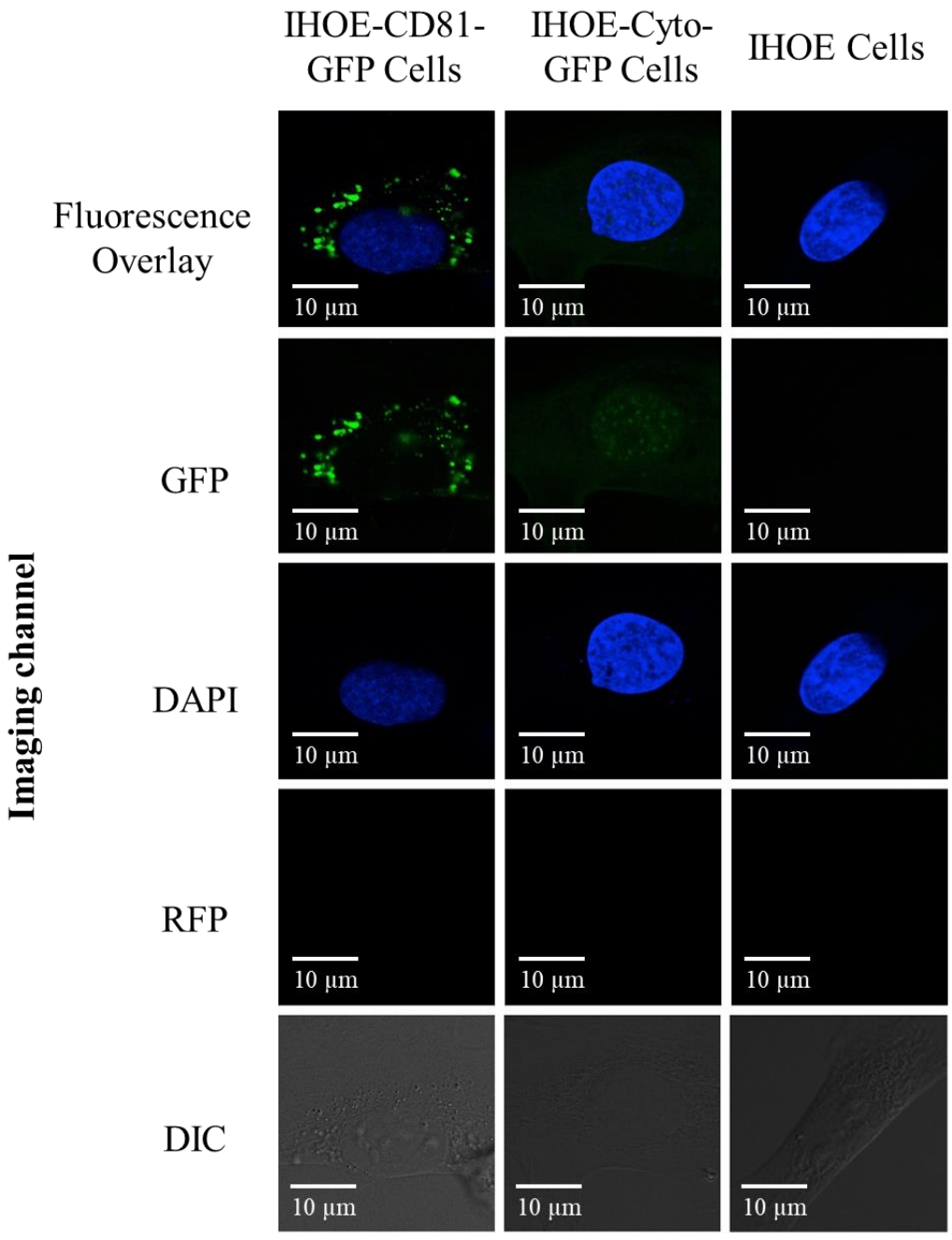

Figure 3.2. Confocal Fluorescence and DIC Images of transduced cells fixed and stained with DAPI. Fluorescence and DIC images of IHOE-CD81-GFP; IHOE-Cyto-GFP; and IHOE cells. Blue emission spectra (425-500 nm), green emission spectra (510-590 nm), and red emission spectra (575-650 nm) were captured in single channels and overlaid in confocal images.

Similarly, confocal imaging of SKOV-3-CD9-RFP cells, stained with DAPI (see Figure 3.3), showed punctate expression of RFP throughout the cytoplasm with little evidence of RFP expression in the nucleus. Imaging of the SKOV-3-Cyto-RFP control cells (see Figure 3.3) revealed even RFP expression throughout the entire cell, including strong expression overlapping the nucleus. Non-transduced control SKOV-3 cells displayed no evidence of RFP expression under the same imaging conditions (Figure 3.3). Additionally, none of the samples demonstrated GFP expression (see Figure 3.3)

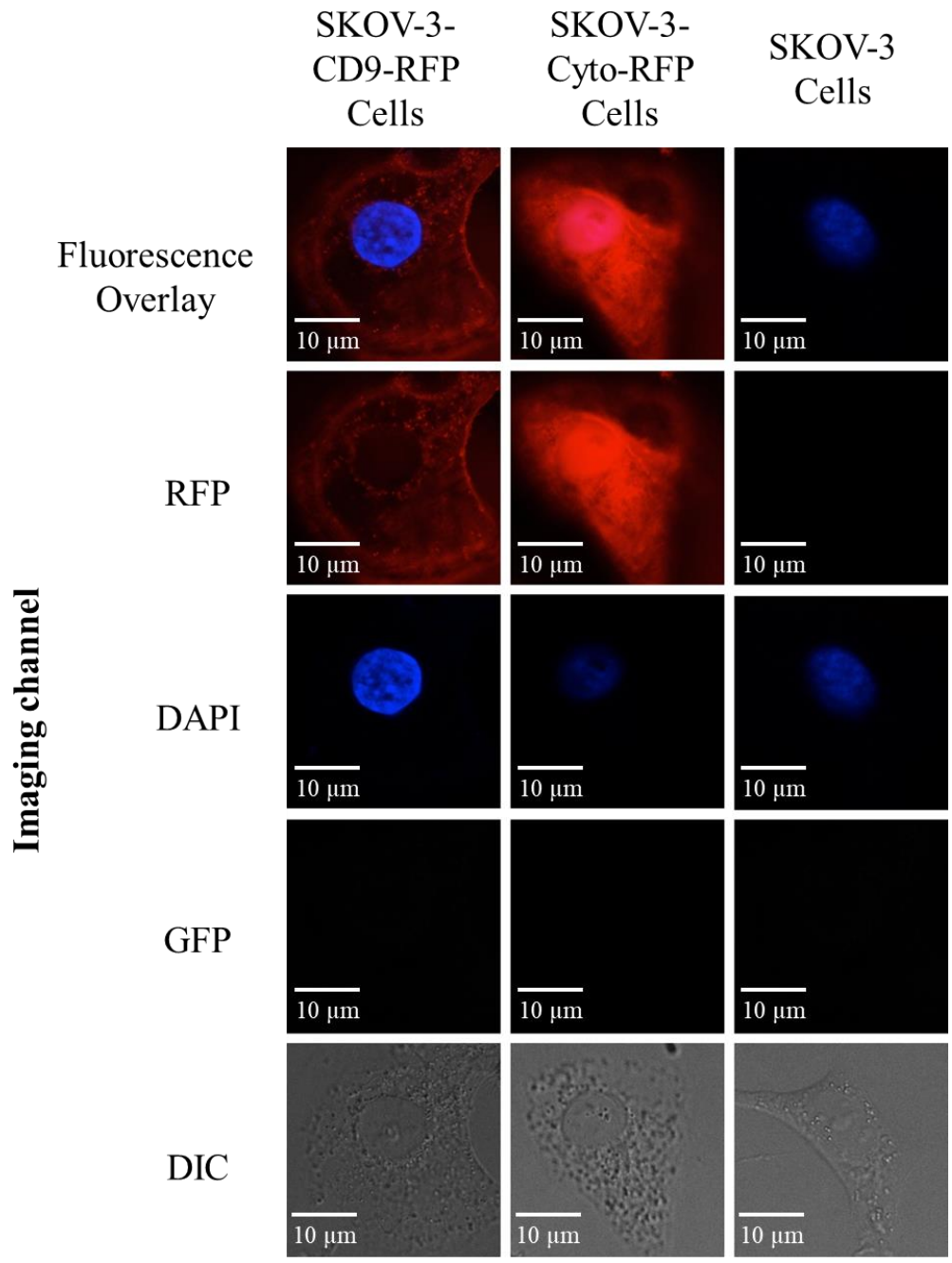

Figure 3.3. Confocal Fluorescence and DIC Images of transduced cells fixed and stained with DAPI. Fluorescence and DIC images of SKOV-3-CD9-RFP; SKOV-3-Cyto-RFP; and SKOV-3 cells. Blue emission spectra (425-500 nm), green emission spectra (510-590 nm), and red emission spectra (575-650 nm) were captured in single channels and overlaid in confocal images.

TEM of sEV samples isolated from IHOE-CD81-GFP and SKOV-3-CD9-RFP cells revealed the presence of single vesicles of approximately 80-140 nm in diameter (see Figure 3.4). Observed vesicles from both IHOE-CD81-GFP and SKOV-3-CD9-RFP cells demonstrated a slight "dimpled" morphology as well as darker staining around the exterior of the vesicle. The vesicles appeared intact and demonstrated no signs of damage such as deformation, cracks, or debris.

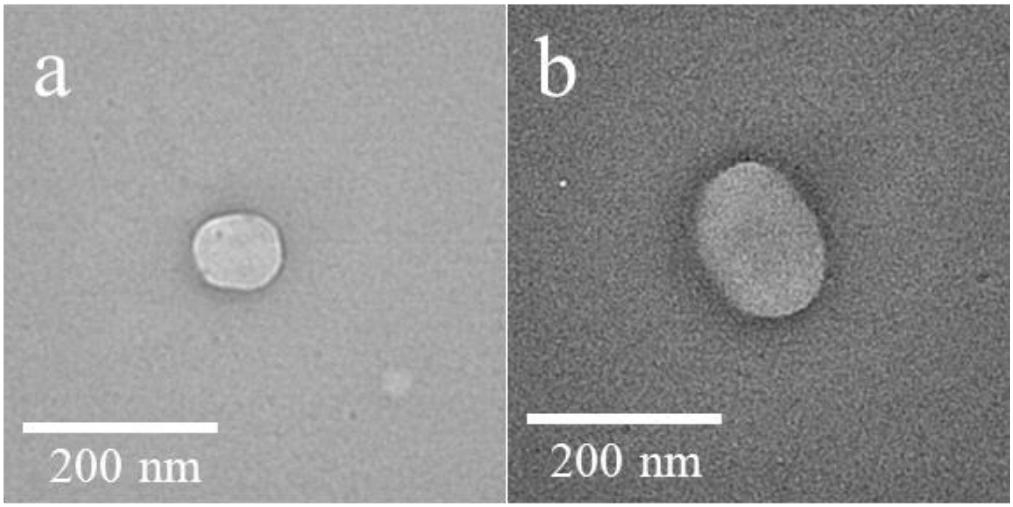

Figure 3.4. Transmission electron microscopy of small extracellular vesicles. TEM of sEVs isolated from (a) IHOE-CD81-GFP and (b) SKOV-3-RFP cells by ultracentrifugation.

Upon western blot analysis, GFP normally expresses a protein band size of ~26 kDa[57, 58], as does CD81[59], while RFP normally expresses a protein band size of ~ 27 kDa[60] and CD9 a protein band size of ~ 25 kDa.[61] As such, CD81-GFP should express a protein band size of ~ 52 kDa, as should CD9-RFP. Western blot analysis of IHOE-CD81-GFP sEVs and cell lysate using rabbit anti-turboGFP (tGFP) (see Figure 3.5a) revealed multiple bands at approximately 24 kDa (Band I), 41 kDa (Band II), 55 kDa (Band III), and > 62 kDa (Band IV), while non-transduced control IHOE sEVs and cell lysate showed no bands. Purified, control tGFP protein displayed bands at approximately 26 kDa and 43 kDa. SKOV-3-CD9-RFP sEVs and cell lysate probed with rabbit anti-RFP showed bands at ~ 45 kDa (Band V) and ~54 kDa (Band VI) (see Figure 3.5b), while non-transduced control SKOV-3 sEVs and cell lysate showed no bands. Purified, control RFP protein displayed a single band at ~28 kDa.

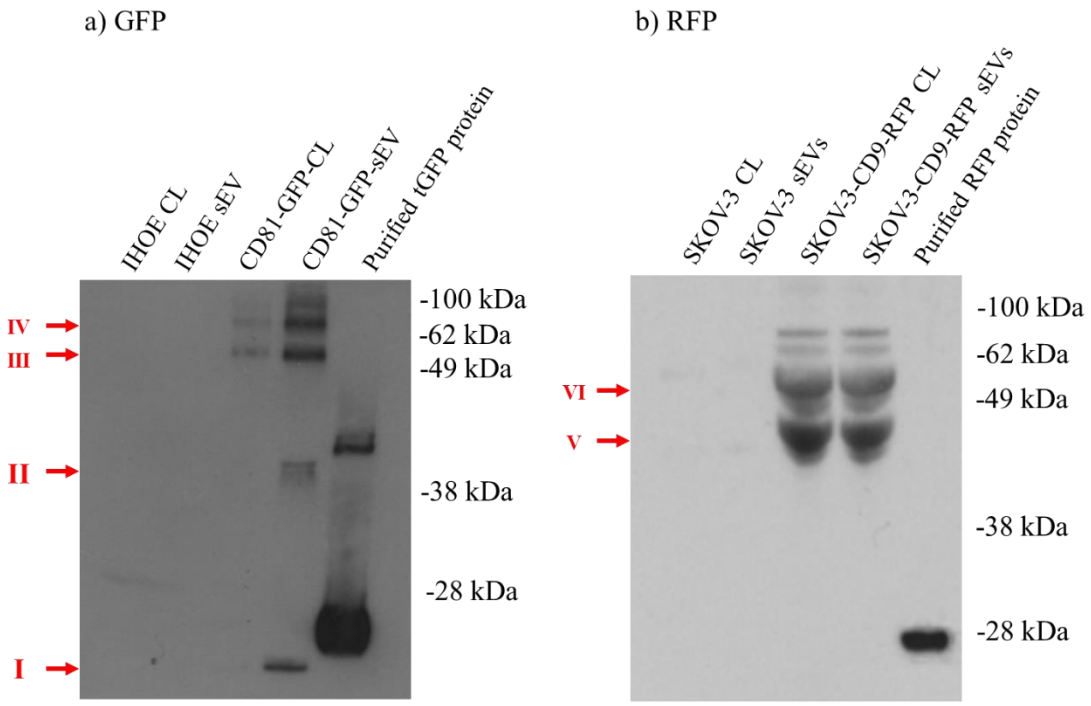

Figure 3.5. GFP and RFP western blots of IHOE-CD81-GFP sEVs and cell lysate and SKOV-3-CD9-RFP sEVs and cell lysate. a) Rabbit anti-tGFP and b) rabbit anti-RFP primary antibody probing. Arrows and Roman numeral indicate regions of interest.

The dotting of isolated, enriched IHOE-CD81-GFP sEVs and SKOV-3-CD9-RFP sEVs on a nitrocellulose membrane with protein concentrations of 2500 μg/mL revealed visibly greater relative fluorescence intensity for both sEV samples compared to the vesicle-free PBS controls (see Figure 3.6). The sample images (Figures 3.6a,c) also demonstrated distinct puncta. Average fluorescence intensities of these images (Figures 3.6a,c) were subsequently used for normalization of further nitrocellulose dotting and capture experiments.

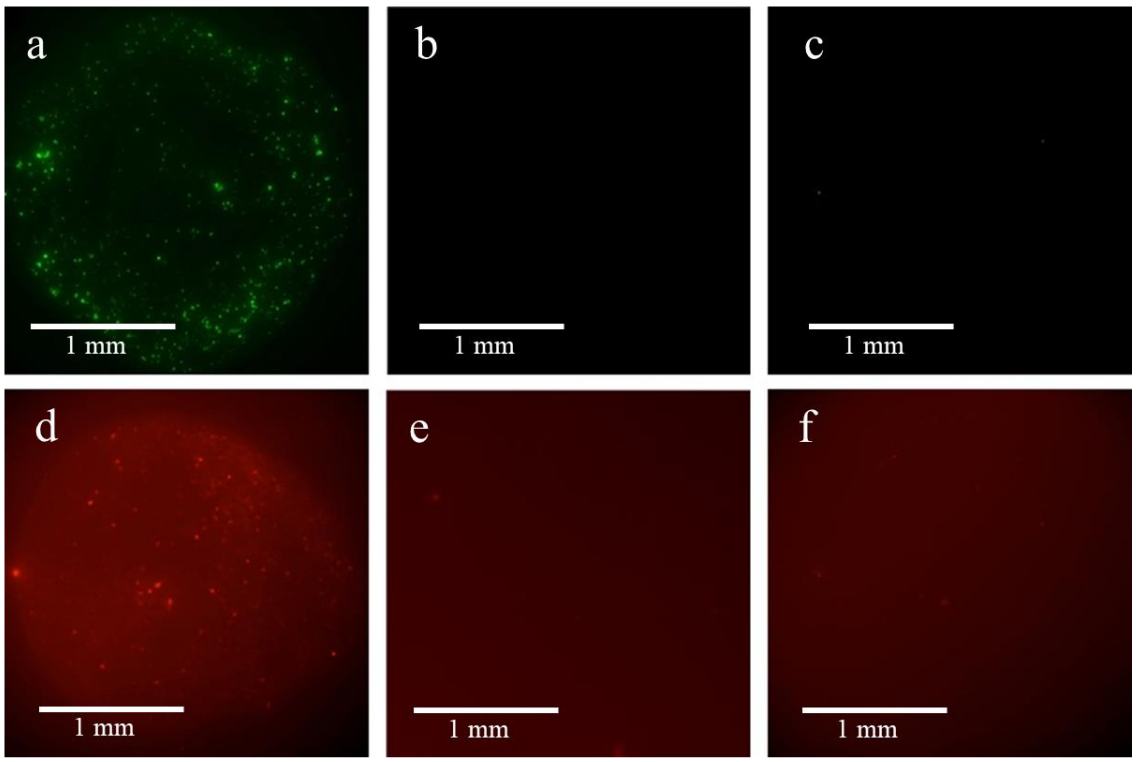

Figure 3.6. Fluorescence images of GFP and RFP tagged vesicles dotted on nitrocellulose membrane. (a) Immortalized Human Ovarian Epithelial (IHOE)-derived CD81-GFP tagged, (b) IHOE-derived, (d) SKOV-3-derived CD9-RFP tagged, and (d) SKOV-3-derived sEVs were isolated by ultracentrifugation and dotted on a nitrocellulose membrane. Extracellular vesicle isolations were dotted at a concentration of 2500 µg/mL of protein. (e, f) PBS controls dotted on nitrocellulose. Images were obtained using both a GFP filter with a 100 ms exposure (a,b,c) and an mCherry filter with a 2 s exposure (d,e,f).

Following imaging of the IHOE-CD81-GFP and SKOV-3-CD81-RFP sEVs on nitrocellulose (see Figure 3.7), average relative fluorescence intensity per μg of total protein of the IHOE-CD81-GFP and SKOV-3-CD81-RFP sEVs was compared to normal IHOE and SKOV-3 sEVs as well as to IHOE-CD81-GFP, SKOV-3-CD9-RFP, IHOE, and SKOV-3 cell lysates. Relative fluorescence intensities per μg of protein of IHOE-CD81-GFP and SKOV-3-CD9-RFP sEVs (see Figure 3.7) were significantly higher than those of their respective cell lysates and non-transduced control cell sEVs. Additionally, relative fluorescence intensities of IHOE-CD81-GFP and SKOV-3-CD9-RFP cell lysates were significantly higher than non-transduced IHOE and SKOV-3 cell lysates. It should be noted that while the relative fluorescence intensities of the fluorescent cell lysate samples were much higher than the corresponding fluorescent sEV samples, the total protein in the fluorescent cell lysate samples were much higher. Thus, relative fluorescence per μg of protein was much higher in the fluorescent sEV samples.

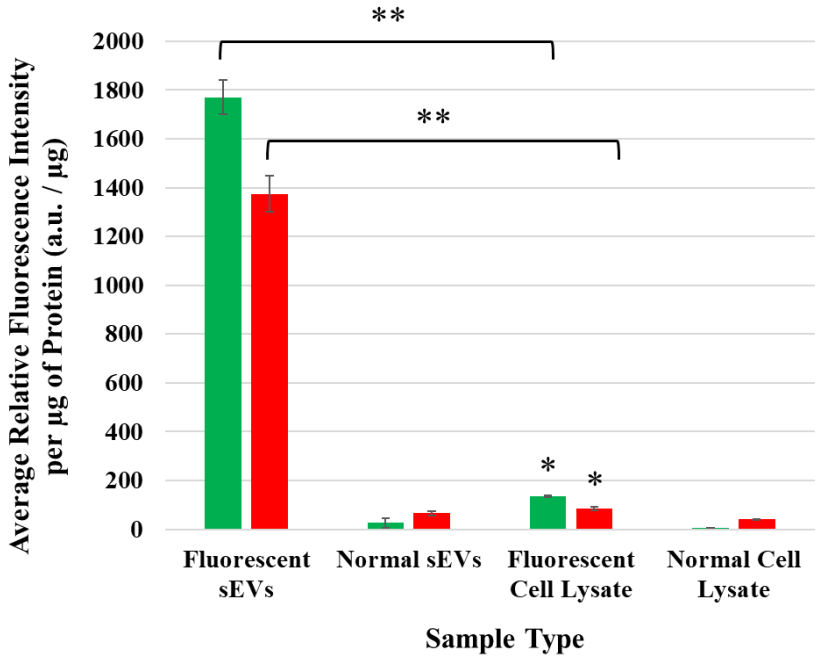

Average Fluorescence Intensity per µg of Protein (a.u. / µg)

IHOE-CD81-GFP sEVs	IHOE sEVs	IHOE-CD81-GFP Cell Lysate	IHOE Cell Lysate
1771 ± 69	26 ± 19	136 ± 2	5 ± 1

SKOV-3-CD9-RFP sEVs	SKOV-3 sEVs	SKOV-3-CD9-RFP Cell Lysate	SKOV-3 Cell Lysate
1375 ± 74	66 ± 8	86 ± 7	41 ± 2

Figure 3.7. Relative fluorescence intensity per µg of protein of sEVs and cell lysate imaged on nitrocellulose membranes. Green bars represent samples derived from IHOE cells and red bars represent samples derived from SKOV-3 cells. Fluorescent sEVs and cell lysate were derived from IHOE-CD81-GFP and SKOV-3-CD9-RFP cells. Normal sEVs and cell lysate were derived from non-transduced IHOE and SKOV-3 control cells. Corresponding samples were subjected to a student's t-test (** - significantly different from corresponding sample and control, $p<0.05$) (* - significantly different from control alone, $p<0.05$); error bars demonstrate one standard deviation, n=3.

The relative fluorescence intensity of IHOE-CD81-GFP sEVs in solution measured at 525 nm over varied protein concentrations (see Figure 3.8a) demonstrated consistent intensities and a coefficient of determination (R^2) of 0.9805. Similarly, the relative fluorescence intensity of SKOV-3-CD9-RFP sEVs in solution measured at 590 nm over varied protein concentrations (see Figure 8b) demonstrated consistent intensities and a coefficient of determination (R^2) of 0.9190.

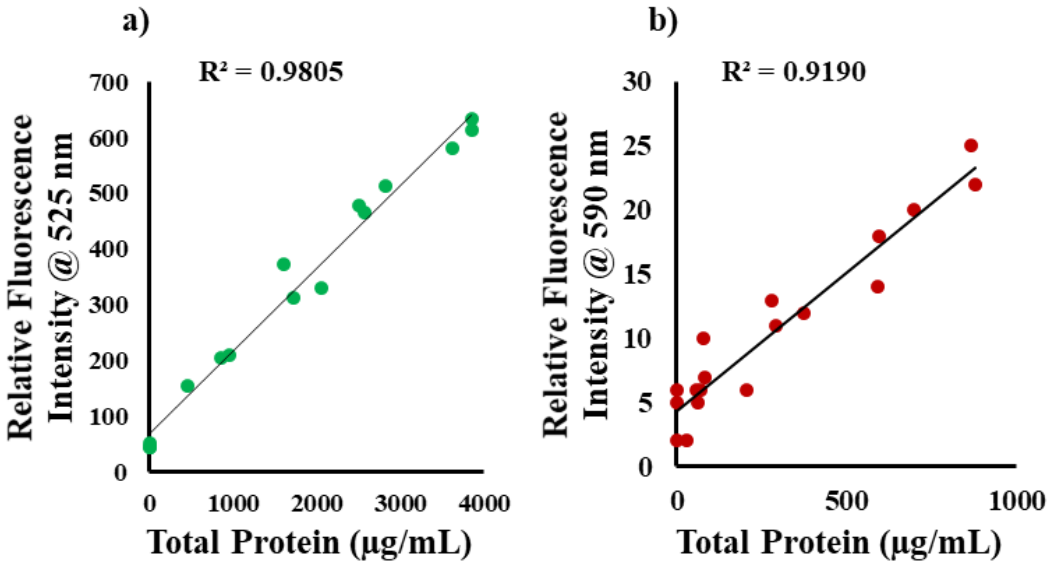

Figure 3.8. Relative fluorescence intensity per µg of suspended protein. a) IHOE-CD81-GFP sEVs excited at 488 nm with fluorescence measured at 525 nm and b) SKOV-3-CD9-RFP sEVs excited at 550 nm with fluorescence measured at 590 nm. Relative fluorescence intensity was measured with a 100 ms exposure time for all samples. Calculated coefficient of determination (R^2) represents the level of explained variability within the sample group. Coefficient of determination values: a) 0.9805 and b) 0.919.

PET C-CP fiber sEV capture

Following cell line establishment and verification, IHOE-CD81-GFP and SKOV-3-CD9-RFP sEVs, initially isolated and concentrated via UC, were spun down onto C-CP fibers in a micropipette tip format. Observation of the fibers under SEM revealed significant vesicle capture along the surfaces of the PET C-CP fibers loaded with the IHOE-CD81-GFP and SKOV-3-CD9-RFP sEV samples, while no vesicles were seen on the PET C-CP fiber surfaces exposed to the sEV-free PBS control (see Figure 3.9). IHOE-CD81-GFP vesicles on the fiber surface appeared more evenly distributed, while SKOV-3-CD9-RFP vesicles on the fiber surface appeared to have greater amounts of vesicle aggregation. Neither sample demonstrated significant vesicle damage.

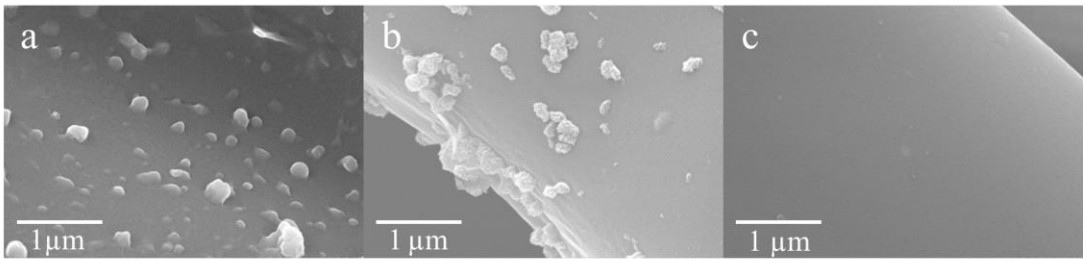

Figure 3.9. Scanning electron microscopy of small extracellular vesicles on PET C-CP fibers. SEM of sEVs isolated from (a) IHOE-CD81-GFP and (b) SKOV-3-CD9-RFP cells by ultracentrifugation and (c) an sEV-free PBS control spun down onto PET C-CP fibers in a micropipette tip format.

Super-resolution confocal microscopy of IHOE-CD81-GFP sEVs (see Figure 3.10a) revealed small fluorescent particles, approximately 0.2-1 μm in diameter, scattered across the surface of the PET C-CP fibers. While the fibers emitted significant autofluorescence in the observed GFP emission range (500-541 nm; see PBS control in Figure 3.10c), fluorescent puncta remained observable in micrographs of the IHOE-CD81-GFP samples. Non-transduced IHOE sEVs (non-fluorescent) captured on the fiber surfaces appeared no different than the PBS control-treated fibers (see Figure 3.10b). Similarly, super-resolution confocal microscopy of SKOV-3-CD9-RFP sEVs (see Figure 3.10d) revealed small fluorescent particles, approximately 0.2-1 μm in diameter, scattered across the surface of the PET C-CP fibers. While the fibers emitted significant autofluorescence in the observed RFP emission range (564-628 nm; see PBS control in Figure 13f), additional fluorescent puncta were visible in the micrographs of the SKOV-3-CD9-RFP samples. Non-transduced SKOV-3 sEVs (non-fluorescent) captured on the fiber surfaces appeared no different than the PBS control-treated fiber (see Figure 3.10e).

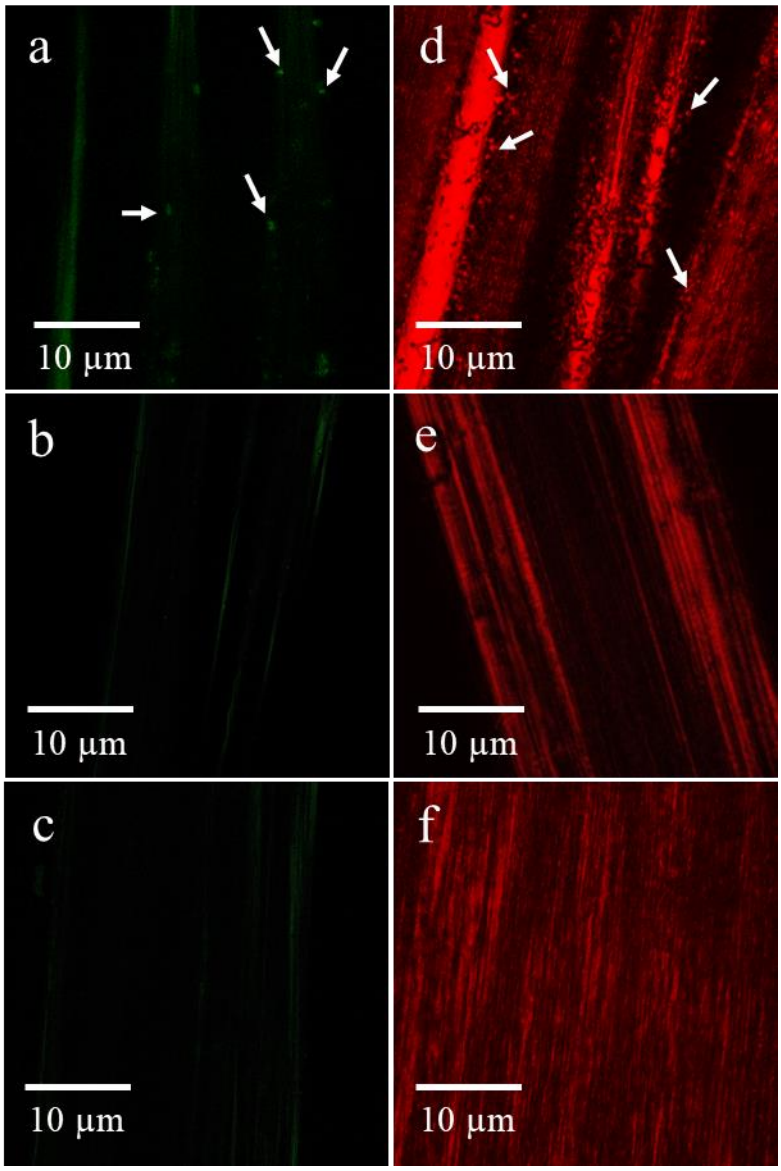

Figure 3.10. Super-resolution confocal fluorescence microscopy of IHOE-CD81-GFP and SKOV-3-CD9-RFP-expressing small extracellular vesicles on PET C-CP fibers. Super-resolution confocal fluorescence microscopy of (a) IHOE-CD81-GFP sEVs, (b) non-transduced IHOE sEVs (non-fluorescent), (c) PBS (d) SKOV-3-CD9-RFP sEVs, (e) non-transduced SKOV-3 sEVs (non-fluorescent) and (f) PBS spun down onto PET C-CP fibers in a micropipette tip format. Images a, b, and c were captured under GFP imaging conditions (see Materials and Methods) and images d, e, and f were captured under RFP imaging conditions. Arrows indicate distinct exosomal adherence regions along the fibers.

IHOE-CD81-GFP and SKOV-3-CD9-RFP sEV mixed samples spun onto PET C-CP fibers demonstrated similar patterns to the IHOE-CD81-GFP and SKOV-3-CD9-RFP samples alone (see Figure 3.11). The mixed samples demonstrated fluorescent particles within both the green emission range (500-541 nm, see Figure 3.11a) and red emission range (564-628 nm, see Figure 3.11b). An overlaid image of the green and red emission channels (see Figure 3.11c), revealed the presence of green and red fluorescent particles in both overlapping and distinct locations along the fibers (see arrows on Figure 3.11).

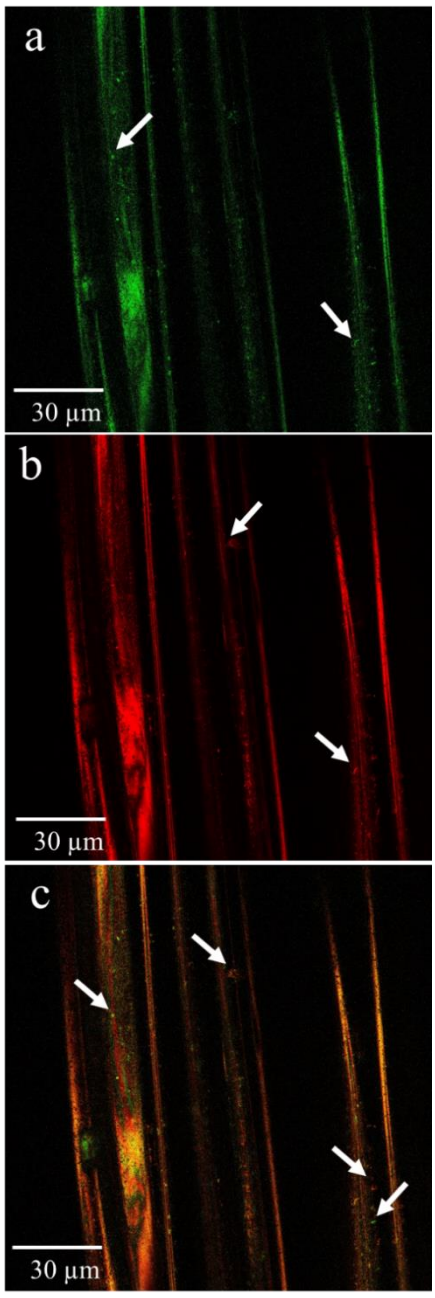

Figure 3.11. Super-resolution confocal fluorescence microscopy of IHOE-CD81-GFP and SKOV-3-CD9-RFP small extracellular vesicles on PET C-CP fibers. Super-resolution confocal fluorescence microscopy of IHOE-CD81-GFP and SKOV-3-CD9-RFP sEVs mixed prior to being spun down onto PET C-CP fibers in a micropipette format. Observations in (a) green and (b) red channels were (c) overlaid showing distinct exosomal adherence locations along the fibers (arrows)

Selective immunoaffinity capture of sEVs

Following determination of average fluorescence values for the sample area of the controls for normalization (Figure 3.6), immunoaffinity capture experiments were set up as described in Figure 3.1 using nitrocellulose strips dotted with the antibodies listed in Table 3.1. IHOE-CD81-GFP and SKOV-3-CD9-RFP sEV samples were added to separate nitrocellulose antibody-dotted capture strips (see Figure 3.1a and Table 3.1) and imaged with multichannel widefield fluorescence microscopy (see Figures 3.12-3.16, Table 3.2). In a separate experiment, IHOE-CD81-GFP and SKOV-3-CD9-RFP sEVs were mixed prior to addition to a single nitrocellulose antibody-dotted capture strip (see Figure 3.1b and Table 3.1) and imaged with multichannel widefield fluorescence microscopy (see Figures 3.17-3.18, Table 3.2). The positive control capture antibody against tGFP (rabbit anti-tGFP) demonstrated significant GFP fluorescence intensity when incubated with IHOE-CD81-GFP sEVs alone (see Figure 3.12a) or with a sample containing both IHOE-CD81-GFP and SKOV-3-CD9-RFP sEVs (see Figure 3.12c), as compared to the negative PBS controls (no antibody, IHOE-CD81-GFP or SKOV-3-CD9-RFP sEV samples; see Figure 3.12e,f). Similarly, the positive control capture antibody against RFP (rabbit anti-RFP) demonstrated significant mCherry fluorescence intensity when incubated with SKOV-3-CD9-RFP sEVs alone (see Figure 3.12h) or with a sample containing both IHOE-CD81-GFP and SKOV-3-CD9-RFP sEVs(see Figure 3.12j), as compared to the negative PBS controls (no antibody, IHOE-CD81-GFP or SKOV-3-CD9-RFP sEV samples; see Figure 3.12k,l). No spectral crossover was observed between the red and green channels (see Figure 3.12g,i,b,d) Fluorescence of the

captured IHOE-CD81-GFP and SKOV-3-CD9-RFP sEVs appeared to be more homogeneous as opposed to punctate in nature as compared to IHOE-CD81-GFP and SKOV-3-CD9-RFP sEV samples dotted directly onto a nitrocellulose surface without specific capture antibodies (Figure 3.6).

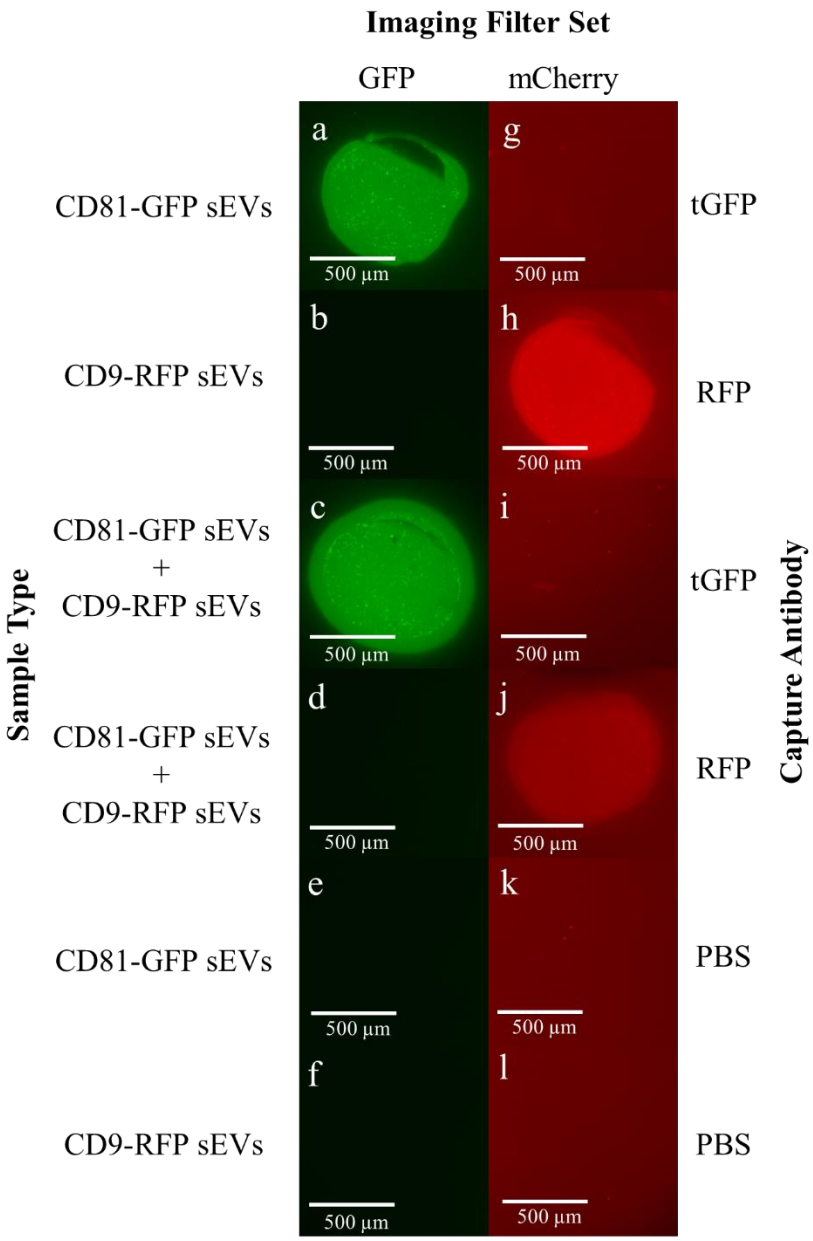

Figure 3.12. Immunoaffinity blot capture using rabbit anti-tGFP and rabbit anti-RFP antibodies. IHOE-CD81-GFP and/or SKOV-3-CD9-RFP sEVs were isolated by UC and captured on a nitrocellulose membrane using rabbit anti-tGFP or rabbit anti-RFP antibodies. Each type of sEV was exposed to antibody-dotted nitrocellulose for 2 hours at a protein concentration of 125 µg/mL followed by a 1 hour wash in TBS-Tween. GFP images were obtained using a 100 ms exposure and mCherry images were obtained using a 2 s exposure.

CD63 is a generic exosomal marker protein. When rabbit anti-CD63 antibodies were used to capture IHOE-CD81-GFP and SKOV-3-CD9-RFP sEVs, there was significant relative fluorescence intensity for IHOE-CD81-GFP sEVs (Figures 3.13-3.14, Table 3.2) and mixed IHOE-CD81-GFP and SKOV-3-CD9-RFP sEVs (Figures 3.17-3.18, Table 3.2) in the green channel. Rabbit anti-CD63 dots also demonstrated significant relative fluorescence intensity for SKOV-3-CD9-RFP sEVs (Figures 3.15-3.16, Table 3.2) and mixed IHOE-CD81-GFP and SKOV-3-CD9-RFP sEVs (Figures 3.17-3.18, Table 3.2) in the red channel. The rabbit anti-CD63 normalized relative fluorescence intensity for IHOE-CD81-GFP sEVs in the green channel and the normalized relative fluorescence intensity for SKOV-3-CD9-RFP sEVs in the red channel were not significantly different (see Figures 3.13-3.16). Likewise, the rabbit anti-CD63 normalized relative fluorescence intensities in both the green and red channels for mixed IHOE-CD81-GFP and SKOV-3-CD9-RFP sEVs were not significantly different (see Figures 3.17-3.18).

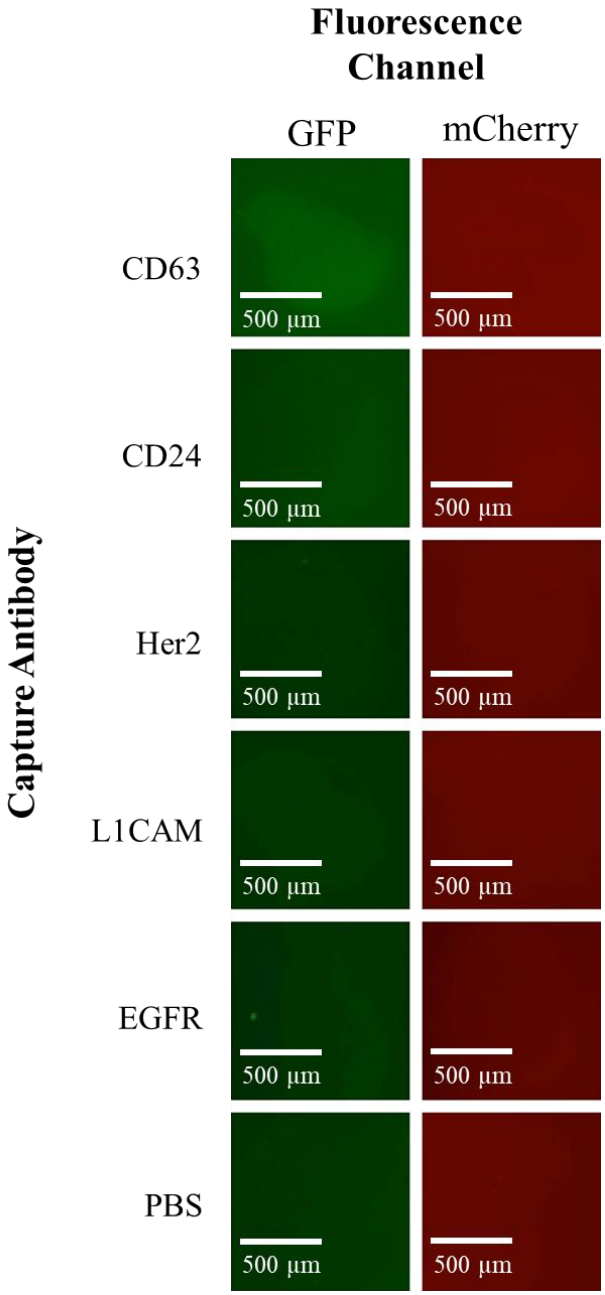

Figure 3.13. IHOE-CD81-GFP sEVs immuno-captured on a nitrocellulose membrane and imaged with multichannel microscopy. IHOE-CD81-GFP sEVs were exposed to antibody-dotted nitrocellulose for 2 hours at a protein concentration of 125 µg/mL followed by a 1 hour wash in TBS-Tween. GFP images were obtained using a 100 ms exposure and mCherry images were obtained using a 2 s exposure.

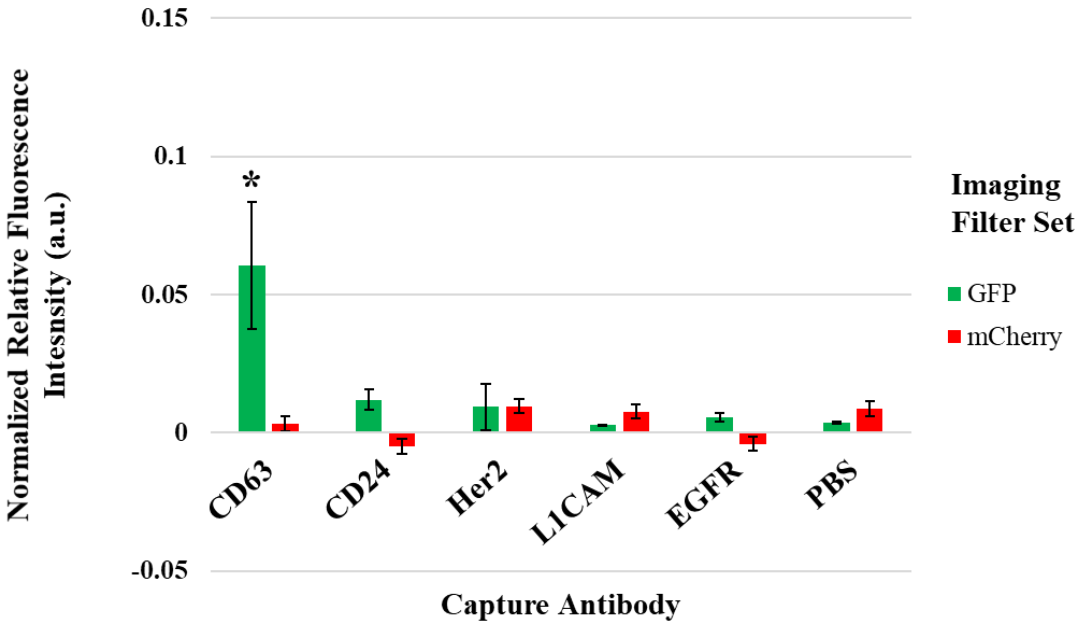

Figure 3.14. Normalized relative fluorescence intensities of IHOE-CD81-GFP immuno-captured on a nitrocellulose membrane and imaged with multichannel microscopy. IHOE-CD81-GFP sEVs were captured and imaged on a nitrocellulose test strips. sEVs were exposed to the multiple antibody-dotted nitrocellulose test strip for 2 hours at a protein concentration of 125 µg/mL followed by a 1 hour wash in TBS-Tween. GFP (green bar) images were obtained using a 100 ms exposure and mCherry (red bar) images were obtained using a 2 s exposure. (* - Significantly different from PBS control and corresponding fluorescence channel data based on a one-tailed t-test)

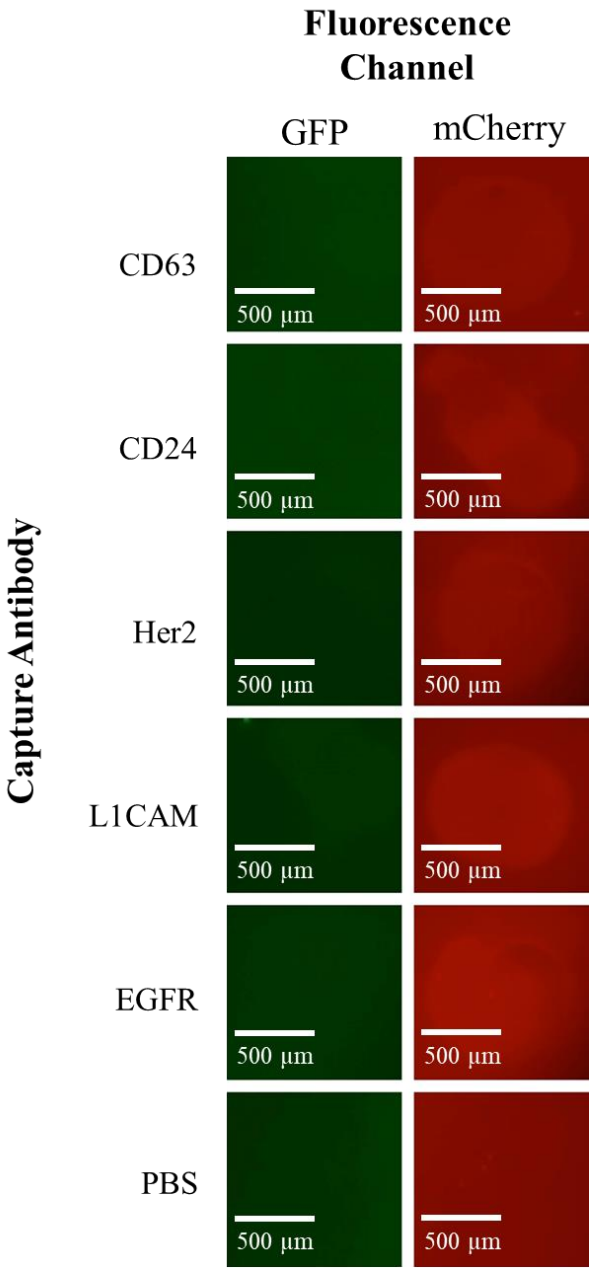

Figure 3.15. SKOV-3-CD9-RFP sEVs immuno-captured on a nitrocellulose membrane and imaged with multichannel microscopy. SKOV-3-CD9-RFP sEVs were exposed to antibody-dotted nitrocellulose for 2 hours at a protein concentration of 125 µg/mL followed by a 1 hour wash in TBS-Tween. GFP images were obtained using a 100 ms exposure and mCherry images were obtained using a 2 s exposure.

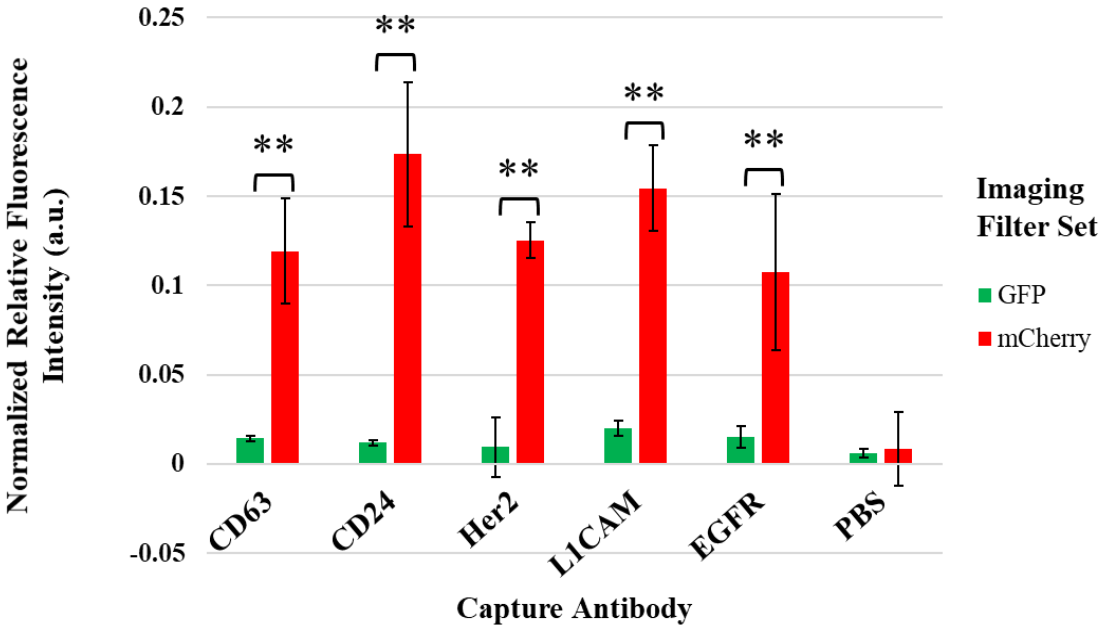

Figure 3.16. Normalized relative fluorescence intensities of SKOV-3-CD9-RFP sEVs immuno-captured on a nitrocellulose membrane and imaged with multichannel microscopy. SKOV-3-CD9-RFP sEVs were captured and imaged on nitrocellulose test strips. sEVs were exposed to multiple antibody-dotted nitrocellulose test strips for 2 hours at a protein concentration of 125 µg/mL followed by a 1 hour wash in TBS-Tween. GFP (green bar) images were obtained using a 100 ms exposure and mCherry (red bar) images were obtained using a 2 s exposure. (* - Significantly different from the PBS control, based on a one-tailed t-test; **- Significantly different from PBS control and corresponding fluorescence channel data based on a one-tailed t-test)

Dot blots with antibodies against the ovarian cancer sEV marker proteins, CD24, Her2, L1CAM, and EGFR, demonstrated significantly greater red relative fluorescence intensities when incubated with the SKOV-3-CD9-RFP sEVs than green relative fluorescence intensity when incubated with IHOE-CD81-GFP sEVs (see Figures 3.13-3.16, Table 3.2). Similarly, the dot blots demonstrated significantly greater red relative fluorescence intensity than green relative fluorescence intensities when incubated with mixed IHOE-CD81-GFP and SKOV-3-CD9-RFP sEVs (see Figures 3.17-3.18, Table 3.2). Dot blots with mouse anti-L1CAM antibody did not show significantly greater red relative fluorescence intensity than green fluorescent intensity when incubated with mixed IHOE-CD81-GFP and SKOV-3-CD9-RFP sEVs. However, the mouse anti-L1CAM dot blots did show slightly lower mean red relative fluorescence intensity with higher variance when incubated with mixed IHOE-CD81-GFP and SKOV-3-CD9-RFP sEVs compared to dot blots with mouse anti-Her2 and mouse anti-EGFR (see Figure 3.17-3.18, Table 3.2). Dot blots using ovarian cancer sEV marker antibodies demonstrating significant relative fluorescence intensities following sEV incubations had normalized relative fluorescence intensities ranging from approximately 0.10 to 0.24 (a.u.) (see Figures 3.15-3.18, Table 3.2).

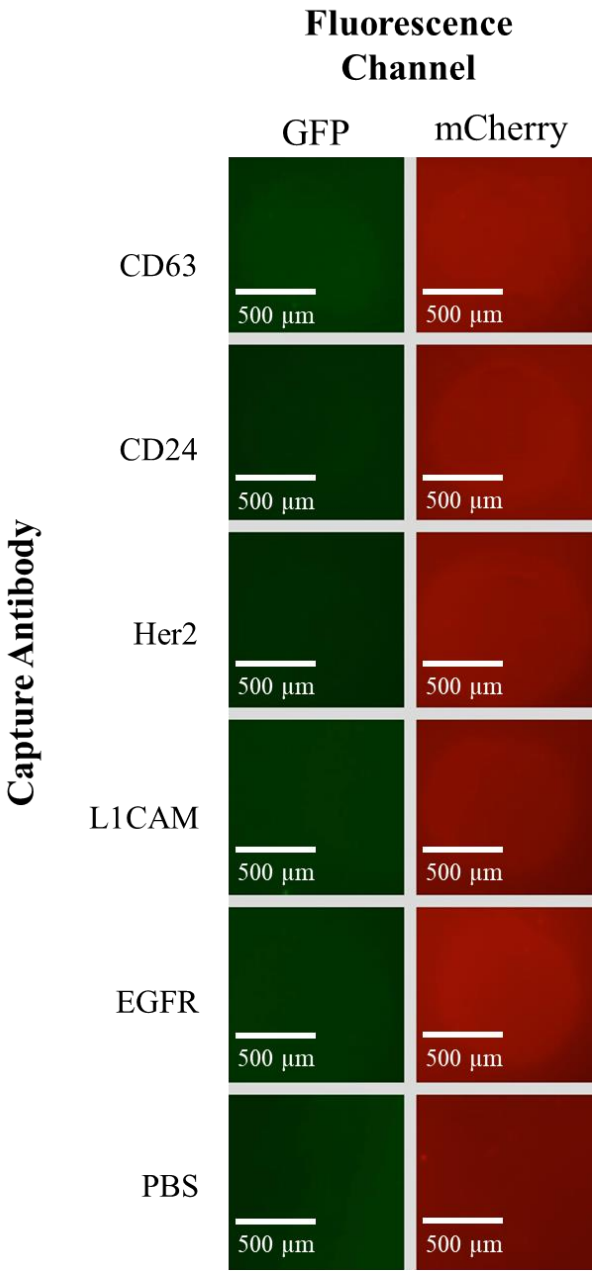

Figure 3.17. IHOE-CD81-GFP and SKOV-3-CD9-RFP sEVs immuno-captured on a nitrocellulose membrane and imaged with multichannel widefield fluorescence microscopy. IHOE-CD81-GFP and SKOV-3-CD9-RFP sEVs were mixed prior to capture on a single test strip. Mixed sEVs were exposed to multiple antibody-dotted nitrocellulose for 2 hours at a protein concentration of 125 µg/mL followed by a 1 hour wash in TBS-Tween. GFP images were obtained using a 100 ms exposure and mCherry images were obtained using a 2 s exposure.

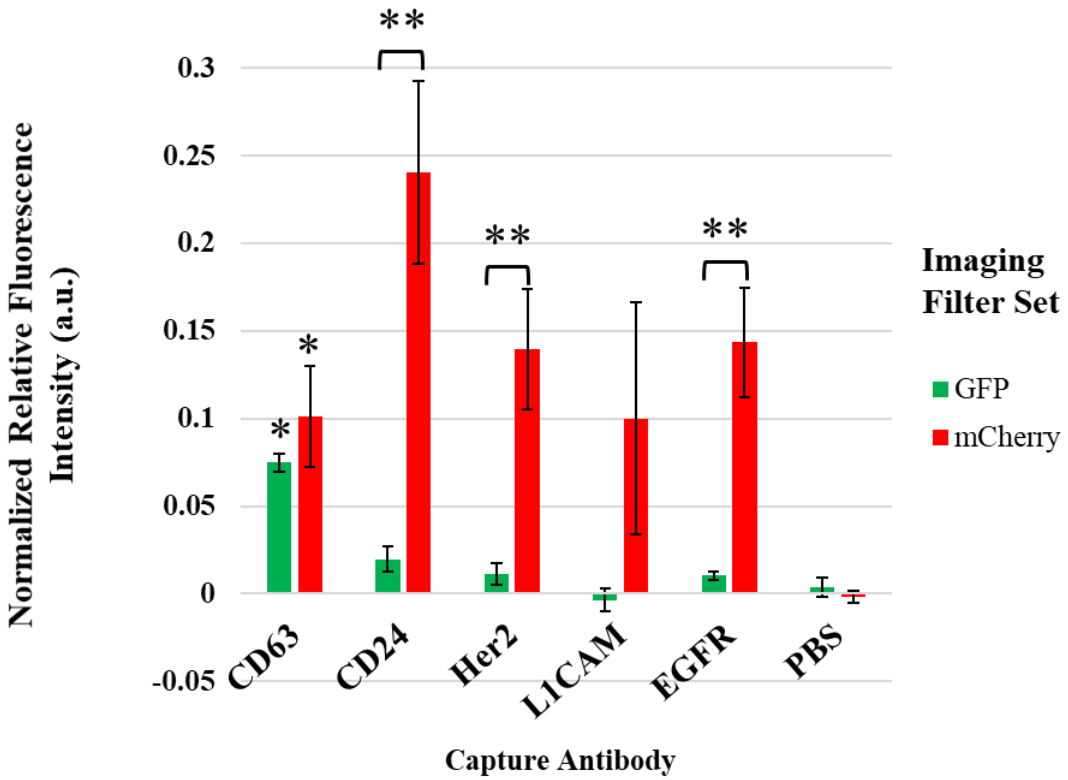

Figure 3.18. Normalized relative fluorescence intensities of mixed IHOE-CD81-GFP and SKOV-3-CD9-RFP sEVs captured by ovarian cancer EV marker antibodies. IHOE-CD81-GFP and SKOV-3-CD9-RFP sEVs were mixed prior to capture on a single test strip. Mixed sEVs were exposed to antibody-dotted nitrocellulose for 2 hours at a protein concentration of 125 µg/mL followed by a 1 hour wash in TBS-Tween and then imaged using multichannel widefield fluorescence microscopy. GFP (green bar) images were obtained using a 100 ms exposure and mCherry (red bar) images were obtained using a 2 s exposure. (* - Significantly different from the PBS control, based on a one-tailed t-test; **- Significantly different from PBS control and corresponding fluorescence channel data based on a one-tailed t-test)

Table 3.2. Relative fluorescence intensities (a.u.) of captured IHOE-CD81-GFP and SKOV-3-CD9-RFP sEVS using multichannel widefield fluorescence imaging with GFP filter set (450-490 nm excitation/500-550 nm detection) and mCherry filter set (540-580 nm excitation/592-667 nm detection)

	Sample Type			
	GFP Filter Set		mCherry Filter Set	
Capture Antibody	*IHOE-CD81-GFP*	*IHOE-CD81-GFP* + *SKOV-3-CD9-RFP*	*SKOV-3-CD9-RFP*	*IHOE-CD81-GFP* + *SKOV-3-CD9-RFP*
Rabbit anti-tGFP	1.082	1.592	0.001	0.007
Rabbit anti-RFP	-0.005	-0.002	0.843	1.109
Rabbit anti-CD63	0.061	0.075	0.119	0.101
Mouse anti-CD24	0.012	0.020	0.174	0.241
Mouse anti-Her2	0.009	0.011	0.125	0.139
Mouse anti-L1CAM	0.003	-0.004	0.154	0.100
Mouse anti-EGFR	0.006	0.010	0.108	0.144
PBS	0.004	0.004	0.009	-0.002

Discussion

Although there is currently no agreement or official guidelines on the classification of EV populations, there is consensus on the need for new EV isolation methods, particularly those with greater specificity, selectivity, purity, and yield. In response, immunoaffinity sEV isolation techniques have emerged as promising methods with respect to sEV specificity and selectivity and have demonstrated results similar to or better than those of ultracentrifugation.[50] Thus far, immunoaffinity capture techniques have largely been dominated by magnetic bead and microfluidics approaches. Magnetic bead approaches have demonstrated high capture efficiency and sensitivity due the to enhanced surface area available for capture and mixture homogeneity.[62] Microfluidics devices employing immunoaffinity approaches in tandem with other separation factors, including size, density, hydrophobicity, and biochemical profile, may allow for the greatest specificity and selectivity and may prove ideal for diagnostic purposes. Strategies employed in these methods include generic capture of sEVs using tetraspanin marker antibodies followed by tumor-specific marker identification, as well as sEV capture using tetraspanin and tumor-specific markers simultaneously. While both strategies have certain advantages, recent studies appear to primarily focus on tetraspanin capture alone prior to tumor-specific sEV marker identification. This workflow is likely due to low overall sEV yield values.

As new EV isolation and quantification methods are designed, they will require more systematic comparison protocols for overall efficacy evaluation. The overall goal of this study was to develop a model system (IHOE-CD81-GFP- and SKOV-3-CD9-RFP-

expressing cells) to produce fluorescent sEVs for use in optimization of the newly developed PET C-CP EV isolation platform. Specifically, this model system, by distinguishing between cancerous and non-cancerous cell-derived sEVs via fluorescence, will be used to develop the selective capture component of the PET C-CP EV isolation platform in a quick and cost-effective manner prior to patient sample investigation. Once refined, selective OC-specific capture antibodies coupled to the isolation platform may be able to streamline EV capture and be employed for early OC diagnosis. The aims of this work included establishment and verification of the IHOE-CD81-GFP- and SKOV-3-CD9-RFP-expressing cell lines for production of fluorescently-labelled sEVs, demonstration of the ability of PET C-CP fibers to capture IHOE-CD81-GFP and SKOV-3-CD9-RFP sEVs effectively, and demonstration of OC-specific antibody capture and discrimination of IHOE-CD81-GFP and SKOV-3-CD9-RFP sEVs, thus demonstrating the ability to distinguish between non-cancerous and cancerous cell-derived sEVs. This study details the development of a model system that can be used to further develop the PET C-CP EV isolation platform by improving selectivity and specificity and allowing for its optimization prior to testing with highly variable and costly patient samples.

Development and analysis of the cell line model system

In order to engineer non-cancerous (IHOE) and cancerous (SKOV-3) cell lines to release fluorescent sEVs for downstream selective capture, generic endosomal proteins were identified as candidates for addition of fluorescent tags. Both CD81 and CD9 are tetraspanin proteins that, due to their involvement in endosomal vesicle transport, are expressed on plasma membrane components of cells. They are both reported sEV

markers, are typically highly expressed in populations of sEVs, and are often used as protein controls in sEV experiments.[63, 64] Specifically, IHOE cell sEVs contain high amounts of CD81 and SKOV-3 cell sEVs are highly enriched in CD9.[65] Therefore, to create fluorescent sEVs from IHOE and SKOV-3 cells, IHOE and SKOV-3 cells were transduced with commercially obtained pCT-CD81-GFP (CYTO124-VA-1, System Biosciences, Palo Alto, CA) or pCT-CD9-RFP (CYTO125-VA-1, System Biosciences, Palo Alto, CA) plasmids, respectively. The plasmids were designed by System Biosciences to add fluorescent tags to the C-terminus, intracellular domains of the specific tetraspanin proteins (CD81 and CD9).[66] Each plasmid was independently prepackaged into an HIV lentiviral construct purchased from System Biosciences to be used for transduction of the appropriate cell line. To assess the optimal multiplicity of infection (MOI, the ratio of virus particles to cells) required, transduction efficiency was calculated using the pre-packaged control plasmids, pCT-Cyto-GFP (CYTO118-VA-1, SBI, Palo Alto, CA) and pCT-Cyto-RFP (CYTO119-VA-1, SBI, Palo Alto, CA) for the IHOE and SKOV-3 cells, respectively. pCT-Cyto-GFP showed an optimal transduction efficiency at an MOI of 5 and pCT-Cyto-RFP showed optimal and maximum transduction efficiency at an MOI of 10. Given these results, an MOI of 5 for pCT-CD81-GFP and IHOE cells and a MOI of 10 for pCT-CD9-RFP and SKOV-3 cells were chosen for future experiments.

IHOE cells and SKOV-3 cells were successfully transduced with either pCT-CD81-GFP or pCT-CD9-RFP, respectively, selected for plasmid expression with puromycin, and subjected to limited dilution cloning. Clones with the highest cell lysate

fluorescence intensities, as measured using a Biotek Synergy H1 Hybrid Reader (Biotek, Winooski, VT), from identical cell densities were chosen for use in subsequent experiments. Laser scanning confocal images of IHOE-CD81-GFP and SKOV-3-CD9-RFP cells, as seen in Figures 3.2 and 3.3, demonstrate the successful cell transductions and expression patterns of fluorescently-labelled CD81 and CD9 in the IHOE and SKOV-3 cell lines. As the CD81 and CD9 transmembrane proteins are typically enriched in extracellular vesicles, they would be expected to be expressed in many small, punctate transport vesicles across the cell, resulting in scattered, intense fluorescence spots as opposed to uniform fluorescence expression throughout the cytoplasm. The micrographs of the IHOE-CD81-GFP and SKOV-3-CD9-RFP expressing cells (see Figures 3.2 and 3.3) as compared to the micrographs of the IHOE-Cyto-GFP and SKOV-3-Cyto-RFP expressing control cells (general cytoplasm expression; see Figures 3.2 and 3.3) demonstrate these expected localization patterns. TEM imaging (see Figure 3.4) of sEVs isolated from IHOE-CD81-GFP and SKOV-3-CD9-RFP cells demonstrated typical "dimpled" EV morphology and maintenance of EV structure. Additionally, IHOE-CD81-GFP and SKOV-3-CD9-RFP sEV samples demonstrated higher relative fluorescence intensity per μg of protein than cell lysates from the corresponding cell types (see Figure 3.7), further indicating that the expressed CD81-GFP and CD9-RFP proteins are localized to extracellular vesicles, rather than generically expressed throughout the cytoplasm.

An important step in the development of a new cell line is to verify that the engineered cell line expresses the correct recombinant proteins using semi-quantitative

methods. However, there are several factors that make this challenging for sEV specific recombinant proteins. First, sEVs can be difficult to quantify due to their size and heterogeneous makeup and, to date, there is no reliable method for accurate quantification.[67] Thus, obtaining a correct measure of protein concentration per vesicle is difficult. Furthermore, it can be problematic to normalize protein data against standard loading controls when dealing with sEVs, as there is significant variation in sEV protein expression and enrichment, which can also be influenced by different sEV isolation methods.[68] Even when populations of sEVs are isolated from the same cell type, there can be considerable variation between resulting isolate densities due to the crude, and sometimes difficult, isolation processes often employed. While antibodies against standard loading control proteins, such as IgG or GAPDH, can be used in certain situations, the replication of samples is not always reliable or trustworthy for semi-quantification via western blot analysis.[40, 64, 69-71] Despite these issues, in an effort to move forward with fundamental research, the EV community has deemed certain sEV markers, such as CD81 and CD9, as suitable loading controls for sEV research.[72] However, when using these loading controls, it is important to understand that they are quite limited as they are only reliable when comparing sEVs from the same source or cell type. With this in mind, any attempt to normalize or quantify this data based on western blot band intensity would be unreliable. Therefore, there was no attempt to quantify or statistically compare intensity values among western blot results. All western blot results were evaluated only for specific protein presence or absence with limited relative comparison based on amount of total protein loaded in each well.

To verify the recombinant protein expression of CD81-GFP and CD9-RFP in the IHOE-CD81-GFP and SKOV-3-CD9-RFP cells and sEVs, western blots using primary antibodies against tGFP or RFP (see Figure 3.5) were performed. As seen in Figure 3.5a, probing IHOE-CD81-GFP sEVs with rabbit anti-tGFP reveals bands at approximately 24 kDa, 41 kDa, 55 kDa, and > 62 kDa as compared to the non-transduced control IHOE sEVs and cell lysate controls. The copGFP tag is a monomer with a molecular weight of 26 kDa and the CD81 protein has a molecular weight of 26 kDa.[57, 59] Thus, CD81 with the addition of a GFP molecule should have a molecular weight of ~52 kDa. According to the manufacturer's instructions, rabbit anti-tGFP antibody only detects copGFP under non-reduced conditions. During western blots, reduced conditions are used to break the disulfide bridges that maintain protein tertiary structure[73] but, in some cases, they may restrict antibody access to the protein epitope. Therefore, the western blot was run under non-reduced conditions to preserve protein disulfide bridges and maintain antibody access to the epitope. This can change the migration properties of the recombinant CD81-GFP protein as the two disulfide bonds of the CD81 portion do not unfold properly, causing an uneven charge distribution across the entire molecule.[59] A change in the migration properties can lead to a slightly higher indicated size than expected (~55kDa), as was observed. The IHOE-CD81-GFP cell lysate sample displayed a similar, albeit less intense band at ~55 kDa, representative of CD81-GFP as well. As non-transduced control IHOE sEVs and cell lysate did not display any bands, western blot evidence suggests that the CD81-GFP recombinant protein is being successfully expressed in the IHOE-CD81-GFP cells. Furthermore, GFP fluorescence is detected in the IHOE-CD81-GFP cell

micrographs (see Figure 3.2) and IHOE-CD81-GFP sEVs and cell lysate dotted on nitrocellulose (see Figure 3.6 and 3.7), suggesting CD81-GFP is being expressed in the IHOE-CD81-GFP cells.

The RFP tag used in this experiment has a molecular weight of approximately 27 kDa and CD9 molecules have a molecular weight of approximately 25 kDa.[17, 60, 61] Therefore, CD9-RFP molecules should have a theoretical molecular weight of ~52 kDa. SKOV-3-CD9-RFP sEVs and cell lysate probed with rabbit anti-RFP show a band at approximately 54 kDa (see Figure 3.5b, band VI), suggesting that CD9-RFP molecules are present in the sEV and cell lysate samples. Moreover, RFP fluorescence is also detected in SKOV-3-CD9-RFP cell images (see Figure 3.3) and in micrographs of SKOV-3-CD9-RFP sEVs and cell lysate (see Figure 3.6 and 3.7) dotted on nitrocellulose, further suggesting that CD9-RFP is being expressed in the SKOV-3-CD9-RFP cells.

To investigate the potential additional feature of using IHOE-CD81-GFP and SKOV-3-CD9-RFP sEVs for testing the PET C-CP EV isolation platform, protein concentrations were compared to relative fluorescence intensities as a means for simple sEV quantification. The fluorescently-labeled IHOE-CD81-GFP and SKOV-3-CD9-RFP sEVs demonstrated a high correlation between protein content and relative fluorescence compared to non-fluorescent IHOE and SKOV-3 sEV controls (see Figure 3.8), suggesting that the relative fluorescence of IHOE-CD81-GFP and SKOV-3-CD9-RFP sEVs may be an alternative means of sEV quantification. Although protein concentration is by no means considered an accurate method of sEV quantification, it does provide an sEV concentration approximation and is widely reported in literature. With the use of

fluorescence detectors (which are already incorporated into the PET C-CP fiber HIC isolation platform reported in Chapter 2), sEV fluorescence protein correlation may hold value as a simple method of sEV quantification approximation during PET C-CP fiber-based EV isolation.

Taken together, these results demonstrate that IHOE-CD81-GFP and SKOV-3-CD9-RFP cells were successfully established and verified to express the fluorescent tags on the appropriate proteins (CD81-GFP and CD9-RFP). Therefore, IHOE-CD81-GFP and SKOV-3-CD9-RFP cells may assist in the development of the PET C-CP EV isolation platform through EV binding verification via fluorescence imaging and EV quantitative analysis through fluorescence detection. However, in order for the sEVs derived from the IHOE-CD81-GFP and SKOV-3-CD9-RFP cells to be utilized for evaluation of PET C-CP fibers, they must first be captured on the fiber surfaces.

PET C-CP fiber-based sEV capture

To evaluate the PET C-CP fiber utility for EV separation of and compatibility with IHOE-CD81-GFP and SKOV-3-CD9-RFP sEVs, IHOE-CD81-GFP and SKOV-3-CD9-RFP sEVs were isolated by UC and spun down through PET C-CP fibers in a micropipette tip format (see Materials and Methods). Under SEM observation, IHOE-CD81-GFP (see Figure 3.9a) and SKOV-3-CD9-RFP (see Figure 3.9b) sEVs demonstrate capture without significant morphological damage. Some vesicle aggregation on the fibers is observed but is likely due to the tendency for UC to cause vesicles to aggregate prior to spinning through the C-CP fibers.

While this study did observe GFP and RFP extracellular vesicle aggregates and vesicles in close proximity through fluorescent microscopy, it is important to note that single vesicle observation is not possible with a limit of resolution of approximately 150 nm using the Leica SP8 Hyvolution super-resolution imaging system and software. However, in future studies, the addition of stimulated emission depletion (STED) super-resolution to the existing Leica SP8, with resolutions down to 50 nm, may make individual vesicle imaging of fluorescent sEVs possible and allow samples to be more easily distinguishable.[74, 75] With this in mind, IHOE-CD81-GFP and SKOV-3-CD9-RFP vesicles, again collected by UC and spun down through PET C-CP fibers, were observed using super-resolution (~150 nm) fluorescence confocal microscopy. Initial observation of PBS controls revealed significant autofluorescence from the PET fibers in both the green (see Figure 3.10c) and red (see Figure 3.10f) channels with RFP emission wavelengths displaying greater intensity than GFP emission wavelengths. However, after application of the IHOE-CD81-GFP (see Figure 3.10a) and SKOV-3-CD9-RFP (see Figure 3.10a) sEVs, groups of fluorescent particles could be observed beyond the fiber autofluorescence. To verify that the IHOE-CD81-GFP and SKOV-3-CD9-RFP samples were not emitting significant autofluorescence, non-transduced IHOE (see Figure 3.10b) and SKOV-3 (see Figure 3.10e) sEVs, collected by UC and spun down through PET C-CP fibers were observed under the same fluorescence imaging conditions. Non-transduced IHOE and SKOV-3 sEVs did not display any evidence of additional fluorescence as compared to the PBS controls. This further demonstrates that the fluorescent particles observed in the IHOE-CD81-GFP and SKOV-3-CD9-RFP sEV

sample micrographs are fluorescently-labelled sEVs captured on the PET C-CP fiber surfaces (Figures 3.10a,c). This observation is further confirmed by SEM images (see Figure 3.9) and the previous protein and fluorescence analyses of the IHOE-CD81-GFP and SKOV-3-CD9-RFP sEVs (see Figures 3.2, 3.3, 3.5-3.7). In addition, mixed IHOE-CD81-GFP and SKOV-3-CD9-RFP sEV samples were spun down on PET C-CP fibers and imaged under the same conditions as the IHOE-CD81-GFP and SKOV-3-CD9-RFP samples alone (see Figure 3.11). After overlaying the channels, both GFP and RFP sEVs can be observed in separate and coinciding locations, suggesting that, while there is significant overlap, IHOE-CD81-GFP and SKOV-3-CD9-RFP vesicle groupings may be distinguished from each other on fiber surfaces using super-resolution confocal microscopy.

As these results show, IHOE-CD81-GFP and SKOV-3-CD9-RFP sEVs are captured on the surface of PET C-CP fibers and can be detected and distinguished using fluorescence microscopy. The addition of the fluorescent labels do not appear to impede the adherence of the tagged sEVs to the PET C-CP fiber surfaces, therefore, the model fluorescent sEVs provide a useful tool for validation and optimization of the PET C-CP fiber-based EV isolation platform. Additionally, the ability to readily distinguish between non-cancerous and cancerous cell-derived sEVs via green and red fluorescence provides a means of evaluating the specificity of exosomal biomarker antibodies for use in lateral flow assay-based ovarian cancer diagnostics.

Selective immunoaffinity capture of sEVs

Like any complex system, access to a complete dataset would be ideal when observing the properties of a population. However, as sampling can rarely, if ever, include every member of a population, statistical analysis is used to look for patterns and correlations that may explain or predict characteristics and sub-populations based on a few variables. In lieu of technology capable of selectively identifying the proteome of individual sEVs and for clinical practicality, only a few parameters are employed to distinguish cancerous and non-cancerous sEVs. Although the number of parameters is limited, as OC is a heterogeneous disease with many subtypes and origins, multiple markers would be more effective for early screening. Here, selective immunoaffinity capture provides a means to identify sEV sub-populations via multiple biomarker antibodies with the goal of distinguishing between cancerous and non-cancerous ovarian cell-derived sEVs and translating that technology to the PET C-CP EV isolation platform.

As only a fraction of an sEV population may express a specific OC tumor-specific sEV marker, such as CD24 or Her2[46, 76], sEV capture using only one of these sEV OC markers may lead to lower numbers of captured sEVs, resulting in low signal and decreased disease screening success. Generic sEV markers, such as CD9, CD81, and CD63 are present in a higher proportion of sEVs[31, 64, 77] and would likely lead to higher capture yields. However, ovarian cancer tumor-specific sEV marker capture may allow for greater sEV population selectivity. The immunocapture experiment described here

employs strategies from other sEV lateral flow and immunoaffinity blot techniques and provides a means for validating the model sEV system for use in the development of immunoaffinity capture and isolation techniques for ovarian cancer diagnostics.[78, 79]

To provide a means of appropriate comparison and normalization of sEV immunocapture, dotting of concentrated IHOE-CD81-GFP and SKOV-3-CD9-RFP sEVs on nitrocellulose was used to set a threshold of maximum fluorescence intensity (Figure 3.6). (Of note, IHOE-CD81-GFP and SKOV-3-CD9-RFP sEV samples captured on nitrocellulose were imaged with exposure times of 100 ms and 2 s, respectively. The discrepancy in these exposure times was appropriated to account for the differences in documented brightness between copGFP (42 cm^{-1} M^{-1})[57, 58] and mRFP (12.5 cm^{-1} M^{-1})[60] molecules and any potential quenching due to the molecular environment *in vitro*). The ability to selectively capture GFP- or RFP-expressing sEVs from independent and mixed IHOE-CD81-GFP and SKOV-3-CD9-RFP sEV (see Figure 3.1 for experimental setup) samples via a dot blot immunoaffinity assay using rabbit anti-tGFP and rabbit anti-RFP antibodies was successfully demonstrated These positive controls show that the dot blot technique can be used to visually confirm the capture of specific sEVs based on their protein expression.

Once it was demonstrated that selective capture of IHOE-CD81-GFP and SKOV-3-CD9-RFP sEVs was possible via rabbit anti-tGFP and rabbit anti-RFP antibodies (see Figure 3.12, Table 3.2) the next step was to show that specific capture of the cancer and non-cancer cell-derived sEVs could be performed using antibodies to known ovarian cancer exosomal biomarkers. In addition to using specific ovarian cancer biomarkers, a

known universal exosomal biomarker was also investigated as a capture antibody. In this manner, the capture results from mixed cancer and non-cancer cell-derived sEV samples may be interpreted in terms of capture specificity. The universal exosomal biomarker, CD63, was selected as a positive control for the validation of the study dot blot assays. For the control assays, IHOE-CD81-GFP and SKOV-3-CD9-RFP sEVs were immunocaptured from both independent (see Figures 3.13-3.16, Table 3.2) and mixed (see Figures 3.17-3.18 , Table 3.2) samples on dot blots with rabbit anti-CD63 antibody.[64] When imaged, the dot blots displayed similar fluorescence intensities for all of the samples. Although CD63 expression likely differs somewhat between the IHOE-CD81-GFP and SKOV-3-CD9-RFP cells, positive fluorescence in both the red and green channels for the mixed samples indicates that CD-63 can be used as a positive control for the immunocapture assays. This positive control antibody may be used to show that sEVs are present and that the capture assay is working properly, just as the positive control line functions in a lateral flow immunoassay.

The potential to differentiate between IHOE-CD81-GFP and SKOV-3-CD9-RFP sEVs was assessed using antibodies to various known ovarian cancer tumor-specific exosomal marker proteins. CD24, Her2, EGFR, and L1CAM molecular markers have all been identified in previous studies as candidate biomarkers for the diagnosis and prognosis of ovarian cancer.[17, 23, 46, 76, 80-82] Therefore, dot blots using antibodies to these ovarian cancer exosomal marker proteins were designed to test whether or not immunoaffinity assays could be used to specifically capture cancer-cell derived sEVs (see Figures 3.13-3.18, Table 3.2). For these assays, individual and mixed samples of

IHOE-CD81-GFP (non-cancerous cell-derived) and SKOV-3-CD9-RFP (cancerous cell-derived) sEVs were added to the dot blots. Dot blot results for the non-cancer cell-derived (IHOE-CD81-GFP) sEVs alone showed no red fluorescence and significant green fluorescence only for dots containing antibodies to CD63 (control). This indicates that these non-cancer cell-derived sEVs were captured by the antibody to the generic exosomal marker tetraspanin protein, CD63, but were not captured by antibodies to any of the ovarian cancer exosomal marker proteins (CD24, Her2, EGFR, L1CAM). Conversely, the dot blot results for the cancer cell-derived (SKOV-3-CD9-RFP) sEVs alone showed no green fluorescence and significant red fluorescence for the dots containing antibodies to the CD63 control and for all of the dots containing antibodies to the ovarian cancer exosomal marker proteins (CD24, Her2, EGFR, LICAM). Finally, the dot blot results of a mixture of the non-cancer and cancer cell-derived sEVs showed significant green and red fluorescence for the dots containing antibody to CD63, while significant fluorescence was only seen in the red channel for the dots containing antibodies to the ovarian cancer marker proteins. These results indicate that sEVs from the model cell lines may be employed in the future development and optimization of lateral flow immunocapture assays for rapid, early ovarian cancer diagnostics.

Compared to the utilization of single markers, use of a multiplexed approach to identify multiple exosomal biomarkers at once may diagnose a greater proportion of ovarian cancers.[16] In this case, a panel of tumor-specific protein markers was successfully used to differentiate between cancerous and non-cancerous sEVs. Multiple marker “hits” provides greater assurance that less false negative test results will occur. As cells in the

tumor environment may undergo changes that can lead to differences in exosomal biomarker expression[83-85], screening for a panel of biomarkers can increase the overall robustness of an exosomal liquid biopsy-based diagnostic test.[9, 22, 38, 40]

The impact of IHOE-CD81-GFP and SKOV-3-CD9-RFP cell lines and immunoaffinity capture on development of a PET C-CP fiber-based EV isolation platform

The IHOE-CD81-GFP and SKOV-3-CD9-RFP cell lines developed in this study provide an extremely valuable tool for the development, optimization, and proof of concept testing of the PET C-CP EV isolation platform, and its potential use in a simple, cost effective, early ovarian cancer diagnostics test. As the Marcus group has previously shown, antibodies may be grafted onto the surfaces of the PET C-CP fibers or alternatively to channeled films for selective protein capture.[86-90] This study shows that sEVs expressing biomarker proteins may be selectively captured using immobilized antibodies. The model system may be used to produce sEVs for laboratory use instead of having to rely on expensive, limited availability human patient samples. Specifically, the incorporation of fluorescent markers into sEVs and the proven utility of the tagged sEVs for self-reporting immunocapture characterization studies provide a framework to further investigate selective sEV capture parameters, PET C-CP fiber and film-based sEV selective capture and separation, diagnostic accuracy, and clinical replication. Moreover, multiplexed immunoaffinity capture using OC tumor-specific EV markers has demonstrated the potential for these methods to distinguish between malignant and benign tumor cell-derived sEVs. The IHOE-CD81-GFP and SKOV-3-CD9-RFP cell model system may also allow for advancement of EV imaging and quantification via

efficient sample prep, easier live cell imaging, and quantitative fluorescence correlations. The versatility of the sEVs generated by these cell lines will prove useful as new applications come to light and the EV community begins to focus more on selective EV capture and super-resolution microscopy.

References

1. Doubeni CA, Doubeni AR, Myers AE. Diagnosis and Management of Ovarian Cancer. *Am Fam Physician*. Jun 2016;93(11):937-44.

2. Taylor D, Gercel-Taylor C. MicroRNA signatures of tumor-derived exosomes as diagnostic biomarkers of ovarian cancer. Article. *Gynecologic Oncology*. JUL 2008 2008;110(1):13-21. doi:10.1016/j.ygyno.2008.04.033

3. Tørring ML, Falborg AZ, Jensen H, et al. Advanced-stage cancer and time to diagnosis: An International Cancer Benchmarking Partnership (ICBP) cross-sectional study. *Eur J Cancer Care (Engl)*. Sep 2019;28(5):e13100. doi:10.1111/ecc.13100

4. American Cancer Society. Survival Rates for Melanoma Skin Cancer: Early Detection, Diagnosis, and Staging.

5. Jin X, Chen Y, Chen H, et al. Evaluation of Tumor-Derived Exosomal miRNA as Potential Diagnostic Biomarkers for Early-Stage Non-Small Cell Lung Cancer Using Next-Generation Sequencing. *Clin Cancer Res*. Sep 2017;23(17):5311-5319. doi:10.1158/1078-0432.CCR-17-0577

6. Yamashita T, Kamada H, Kanasaki S, et al. Epidermal growth factor receptor localized to exosome membranes as a possible biomarker for lung cancer diagnosis. *Pharmazie*. Dec 2013;68(12):969-73.

7. Beach A, Zhang H, Ratajczak M, Kakar S. Exosomes: an overview of biogenesis, composition and role in ovarian cancer. Review. *Journal of Ovarian Research*. JAN 25 2014 2014;7ARTN 14. doi:10.1186/1757-2215-7-14

8. Chen IH, Xue L, Hsu CC, et al. Phosphoproteins in extracellular vesicles as candidate markers for breast cancer. *Proc Natl Acad Sci U S A*. 03 2017;114(12):3175-3180. doi:10.1073/pnas.1618088114

9. de la Torre Gomez C, Goreham RV, Bech Serra JJ, Nann T, Kussmann M. "Exosomics"-A Review of Biophysics, Biology and Biochemistry of Exosomes With a Focus on Human Breast Milk. *Front Genet*. 2018;9:92. doi:10.3389/fgene.2018.00092

10. Eichelser C, Stückrath I, Müller V, et al. Increased serum levels of circulating exosomal microRNA-373 in receptor-negative breast cancer patients. *Oncotarget*. Oct 2014;5(20):9650-63. doi:10.18632/oncotarget.2520

11. American Cancer Society. Survival Rates for Pancreatic Cancer: Early Detection, Diagnosis, and Staging.

12. Melo SA, Luecke LB, Kahlert C, et al. Glypican-1 identifies cancer exosomes and detects early pancreatic cancer. *Nature*. Jul 2015;523(7559):177-82. doi:10.1038/nature14581

13. Qiu J, Yang G, Feng M, et al. Extracellular vesicles as mediators of the progression and chemoresistance of pancreatic cancer and their potential clinical applications. *Mol Cancer*. 01 2018;17(1):2. doi:10.1186/s12943-017-0755-z

14. Sancho-Albero M, Navascués N, Mendoza G, et al. Exosome origin determines cell targeting and the transfer of therapeutic nanoparticles towards target cells. *J Nanobiotechnology*. Jan 2019;17(1):16. doi:10.1186/s12951-018-0437-z

15. Properzi F, Logozzi M, Fais S. Exosomes: the future of biomarkers in medicine. *Biomark Med*. Oct 2013;7(5):769-78. doi:10.2217/bmm.13.63

16. Yokoi A, Yoshioka Y, Hirakawa A, et al. A combination of circulating miRNAs for the early detection of ovarian cancer. *Oncotarget*. Oct 2017;8(52):89811-89823. doi:10.18632/oncotarget.20688

17. Sandfeld-Paulsen B, Aggerholm-Pedersen N, Bæk R, et al. Exosomal proteins as prognostic biomarkers in non-small cell lung cancer. *Mol Oncol*. 12 2016;10(10):1595-1602. doi:10.1016/j.molonc.2016.10.003

18. Urbanelli L, Buratta S, Sagini K, Ferrara G, Lanni M, Emiliani C. Exosome-based strategies for Diagnosis and Therapy. *Recent Pat CNS Drug Discov*. 2015;10(1):10-27.

19. Boukouris S, Mathivanan S. Exosomes in bodily fluids are a highly stable resource of disease biomarkers. *Proteomics Clin Appl*. Apr 2015;9(3-4):358-67. doi:10.1002/prca.201400114

20. Cheng L, Sharples RA, Scicluna BJ, Hill AF. Exosomes provide a protective and enriched source of miRNA for biomarker profiling compared to intracellular and cell-free blood. *J Extracell Vesicles*. 2014;3doi:10.3402/jev.v3.23743

21. Koga Y, Yasunaga M, Moriya Y, et al. Exosome can prevent RNase from degrading microRNA in feces. *J Gastrointest Oncol*. Dec 2011;2(4):215-22. doi:10.3978/j.issn.2078-6891.2011.015

22. Di Meo A, Bartlett J, Cheng Y, Pasic MD, Yousef GM. Liquid biopsy: a step forward towards precision medicine in urologic malignancies. *Mol Cancer*. 04 2017;16(1):80. doi:10.1186/s12943-017-0644-5

23. Zhao Z, Yang Y, Zeng Y, He M. A microfluidic ExoSearch chip for multiplexed exosome detection towards blood-based ovarian cancer diagnosis. *Lab Chip*. Feb 2016;16(3):489-96. doi:10.1039/c5lc01117e

24. Reid BM, Permuth JB, Sellers TA. Epidemiology of ovarian cancer: a review. *Cancer Biol Med*. Feb 2017;14(1):9-32. doi:10.20892/j.issn.2095-3941.2016.0084

25. Jacobs IJ, Menon U, Ryan A, et al. Ovarian cancer screening and mortality in the UK Collaborative Trial of Ovarian Cancer Screening (UKCTOCS): a randomised controlled trial. *Lancet*. Mar 2016;387(10022):945-956. doi:10.1016/S0140-6736(15)01224-6

26. Menon U, Ryan A, Kalsi J, et al. Risk Algorithm Using Serial Biomarker Measurements Doubles the Number of Screen-Detected Cancers Compared With a Single-Threshold Rule in the United Kingdom Collaborative Trial of Ovarian Cancer Screening. *J Clin Oncol*. Jun 2015;33(18):2062-71. doi:10.1200/JCO.2014.59.4945

27. Bandu R, Oh JW, Kim KP. Mass spectrometry-based proteome profiling of extracellular vesicles and their roles in cancer biology. *Exp Mol Med*. Mar 2019;51(3):30. doi:10.1038/s12276-019-0218-2

28. Hegmans JP, Bard MP, Hemmes A, et al. Proteomic analysis of exosomes secreted by human mesothelioma cells. *Am J Pathol*. May 2004;164(5):1807-15. doi:10.1016/S0002-9440(10)63739-X

29. Li Y, Zhang Y, Qiu F, Qiu Z. Proteomic identification of exosomal LRG1: a potential urinary biomarker for detecting NSCLC. *Electrophoresis*. Aug 2011;32(15):1976-83. doi:10.1002/elps.201000598

30. Pietrowska M, Funk S, Gawin M, et al. Isolation of Exosomes for the Purpose of Protein Cargo Analysis with the Use of Mass Spectrometry. *Methods Mol Biol*. 2017;1654:291-307. doi:10.1007/978-1-4939-7231-9_22

31. Zhang W, Ou X, Wu X. Proteomics profiling of plasma exosomes in epithelial ovarian cancer: A potential role in the coagulation cascade, diagnosis and prognosis. *Int J Oncol*. May 2019;54(5):1719-1733. doi:10.3892/ijo.2019.4742

32. Bellingham S, Coleman B, Hill A. Small RNA deep sequencing reveals a distinct miRNA signature released in exosomes from prion-infected neuronal cells. Article. *Nucleic Acids Research*. NOV 2012 2012;40(21):10937-10949. doi:10.1093/nar/gks832

33. Huang X, Yuan T, Tschannen M, et al. Characterization of human plasma-derived exosomal RNAs by deep sequencing. *BMC Genomics*. May 2013;14:319. doi:10.1186/1471-2164-14-319

34. Kobayashi M, Salomon C, Tapia J, Illanes SE, Mitchell MD, Rice GE. Ovarian cancer cell invasiveness is associated with discordant exosomal sequestration of Let-7 miRNA and miR-200. *J Transl Med*. Jan 2014;12:4. doi:10.1186/1479-5876-12-4

35. Lässer C, Eldh M, Lötvall J. Isolation and characterization of RNA-containing exosomes. *J Vis Exp*. Jan 2012;(59):e3037. doi:10.3791/3037

36. Nakamura K, Sawada K, Yoshimura A, Kinose Y, Nakatsuka E, Kimura T. Clinical relevance of circulating cell-free microRNAs in ovarian cancer. Review. *Molecular Cancer*. JUN 24 2016 2016;15ARTN 48. doi:10.1186/s12943-016-0536-0

37. Rabinowits G, Gercel-Taylor C, Day J, Taylor D, Kloecker G. Exosomal MicroRNA: A Diagnostic Marker for Lung Cancer. Article. *Clinical Lung Cancer*. JAN 2009 2009;10(1):42-46. doi:10.3816/CLC.2009.n.006

38. Sharma S, Zuñiga F, Rice GE, Perrin LC, Hooper JD, Salomon C. Tumor-derived exosomes in ovarian cancer - liquid biopsies for early detection and real-time monitoring of cancer progression. *Oncotarget*. Nov 2017;8(61):104687-104703. doi:10.18632/oncotarget.22191

39. Sueta A, Yamamoto Y, Tomiguchi M, Takeshita T, Yamamoto-Ibusuki M, Iwase H. Differential expression of exosomal miRNAs between breast cancer patients with and without recurrence. *Oncotarget*. Sep 2017;8(41):69934-69944. doi:10.18632/oncotarget.19482

40. Kanwar SS, Dunlay CJ, Simeone DM, Nagrath S. Microfluidic device (ExoChip) for on-chip isolation, quantification and characterization of circulating exosomes. *Lab Chip*. Jun 2014;14(11):1891-900. doi:10.1039/c4lc00136b

41. Mathivanan S, Lim JW, Tauro BJ, Ji H, Moritz RL, Simpson RJ. Proteomics analysis of A33 immunoaffinity-purified exosomes released from the human colon tumor cell line LIM1215 reveals a tissue-specific protein signature. *Mol Cell Proteomics*. Feb 2010;9(2):197-208. doi:10.1074/mcp.M900152-MCP200

42. Sharma P, Ludwig S, Muller L, et al. Immunoaffinity-based isolation of melanoma cell-derived exosomes from plasma of patients with melanoma. *J Extracell Vesicles*. 2018;7(1):1435138. doi:10.1080/20013078.2018.1435138

43. Pan C, Stevic I, Müller V, et al. Exosomal microRNAs as tumor markers in epithelial ovarian cancer. *Mol Oncol*. Nov 2018;12(11):1935-1948. doi:10.1002/1878-0261.12371

44. Cheng L, Wu S, Zhang K, Qing Y, Xu T. A comprehensive overview of exosomes in ovarian cancer: emerging biomarkers and therapeutic strategies. *J Ovarian Res*. Nov 2017;10(1):73. doi:10.1186/s13048-017-0368-6

45. Li J, Sherman-Baust CA, Tsai-Turton M, Bristow RE, Roden RB, Morin PJ. Claudin-containing exosomes in the peripheral circulation of women with ovarian cancer. *BMC Cancer*. Jul 2009;9:244. doi:10.1186/1471-2407-9-244

46. Luo H, Xu X, Ye M, Sheng B, Zhu X. The prognostic value of HER2 in ovarian cancer: A meta-analysis of observational studies. *PLoS One*. 2018;13(1):e0191972. doi:10.1371/journal.pone.0191972

47. Wu Y, Deng W, Klinke DJ. Exosomes: improved methods to characterize their morphology, RNA content, and surface protein biomarkers. *Analyst*. Oct 2015;140(19):6631-42. doi:10.1039/c5an00688k

48. Diaz G, Bridges C, Lucas M, et al. Protein Digestion, Ultrafiltration, and Size Exclusion Chromatography to Optimize the Isolation of Exosomes from Human Blood Plasma and Serum. *J Vis Exp*. 04 2018;(134)doi:10.3791/57467

49. Helwa I, Cai J, Drewry M, et al. A Comparative Study of Serum Exosome Isolation Using Differential Ultracentrifugation and Three Commercial Reagents. Article. *Plos One*. JAN 23 2017 2017;12(1)ARTN e0170628. doi:10.1371/journal.pone.0170628

50. Li P, Kaslan M, Lee SH, Yao J, Gao Z. Progress in Exosome Isolation Techniques. *Theranostics*. 2017;7(3):789-804. doi:10.7150/thno.18133

51. Tang YT, Huang YY, Zheng L, et al. Comparison of isolation methods of exosomes and exosomal RNA from cell culture medium and serum. *Int J Mol Med*. Sep 2017;40(3):834-844. doi:10.3892/ijmm.2017.3080

52. Van Deun J, Mestdagh P, Sormunen R, et al. The impact of disparate isolation methods for extracellular vesicles on downstream RNA profiling. *J Extracell Vesicles*. 2014;3doi:10.3402/jev.v3.24858

53. Prendergast EN, de Souza Fonseca MA, Dezem FS, et al. Optimizing exosomal RNA isolation for RNA-Seq analyses of archival sera specimens. *PLoS One*. 2018;13(5):e0196913. doi:10.1371/journal.pone.0196913

54. Quek C, Bellingham SA, Jung CH, et al. Defining the purity of exosomes required for diagnostic profiling of small RNA suitable for biomarker discovery. *RNA Biol*. 02 2017;14(2):245-258. doi:10.1080/15476286.2016.1270005

55. Heinemann ML, Ilmer M, Silva LP, et al. Benchtop isolation and characterization of functional exosomes by sequential filtration. *J Chromatogr A*. Dec 2014;1371:125-35. doi:10.1016/j.chroma.2014.10.026

56. Bruce TF, Slonecki TJ, Wang L, Huang S, Powell RR, Marcus RK. Exosome isolation and purification via hydrophobic interaction chromatography using a polyester, capillary-channeled polymer fiber phase. *Electrophoresis*. 2018;40(4):571-581.

57. Shagin DA, Barsova EV, Yanushevich YG, et al. GFP-like proteins as ubiquitous metazoan superfamily: evolution of functional features and structural complexity. *Mol Biol Evol*. May 2004;21(5):841-50. doi:10.1093/molbev/msh079

58. Evdokimov AG, Pokross ME, Egorov NS, et al. Structural basis for the fast maturation of Arthropoda green fluorescent protein. *EMBO Rep*. Oct 2006;7(10):1006-12. doi:10.1038/sj.embor.7400787

59. Kitadokoro K, Bordo D, Galli G, et al. CD81 extracellular domain 3D structure: insight into the tetraspanin superfamily structural motifs. *EMBO J*. Jan 2001;20(1-2):12-8. doi:10.1093/emboj/20.1.12

60. Campbell RE, Tour O, Palmer AE, et al. A monomeric red fluorescent protein. *Proc Natl Acad Sci U S A*. Jun 2002;99(12):7877-82. doi:10.1073/pnas.082243699

61. Umeda R, Nishizawa T, Nureki O. Crystallization of the human tetraspanin protein CD9. *Acta Crystallogr F Struct Biol Commun*. Apr 2019;75(Pt 4):254-259. doi:10.1107/S2053230X1801840X

62. Contreras-Naranjo JC, Wu HJ, Ugaz VM. Microfluidics for exosome isolation and analysis: enabling liquid biopsy for personalized medicine. *Lab Chip*. 10 2017;17(21):3558-3577. doi:10.1039/c7lc00592j

63. Yáñez-Mó M, Siljander PR, Andreu Z, et al. Biological properties of extracellular vesicles and their physiological functions. *J Extracell Vesicles*. 2015;4:27066.

64. Kowal J, Arras G, Colombo M, et al. Proteomic comparison defines novel markers to characterize heterogeneous populations of extracellular vesicle subtypes. *Proc Natl Acad Sci U S A*. Feb 2016;113(8):E968-77. doi:10.1073/pnas.1521230113

65. Hwang JR, Jo K, Lee Y, Sung BJ, Park YW, Lee JH. Upregulation of CD9 in ovarian cancer is related to the induction of TNF-α gene expression and constitutive NF-κB activation. *Carcinogenesis*. Jan 2012;33(1):77-83. doi:10.1093/carcin/bgr257

66. Hulme RS, Higginbottom A, Palmer J, Partridge LJ, Monk PN. Distinct regions of the large extracellular domain of tetraspanin CD9 are involved in the control of human multinucleated giant cell formation. *PLoS One*. 2014;9(12):e116289. doi:10.1371/journal.pone.0116289

67. Koritzinsky EH, Street JM, Star RA, Yuen PS. Quantification of Exosomes. *J Cell Physiol*. Jul 2017;232(7):1587-1590. doi:10.1002/jcp.25387

68. Patel GK, Khan MA, Zubair H, et al. Comparative analysis of exosome isolation methods using culture supernatant for optimum yield, purity and downstream applications. *Sci Rep*. Mar 2019;9(1):5335. doi:10.1038/s41598-019-41800-2

69. Lobb RJ, Becker M, Wen SW, et al. Optimized exosome isolation protocol for cell culture supernatant and human plasma. *J Extracell Vesicles*. 2015;4:27031. doi:10.3402/jev.v4.27031

70. Baranyai T, Herczeg K, Onódi Z, et al. Isolation of Exosomes from Blood Plasma: Qualitative and Quantitative Comparison of Ultracentrifugation and Size Exclusion Chromatography Methods. *PLoS One*. 2015;10(12):e0145686. doi:10.1371/journal.pone.0145686

71. Tauro BJ, Greening DW, Mathias RA, et al. Comparison of ultracentrifugation, density gradient separation, and immunoaffinity capture methods for isolating human colon cancer cell line LIM1863-derived exosomes. *Methods*. Feb 2012;56(2):293-304. doi:10.1016/j.ymeth.2012.01.002

72. Théry C, Witwer KW, Aikawa E, et al. Minimal information for studies of extracellular vesicles 2018 (MISEV2018): a position statement of the International Society for Extracellular Vesicles and update of the MISEV2014 guidelines. *J Extracell Vesicles*. 2018;7(1):1535750. doi:10.1080/20013078.2018.1535750

73. Braakman I, Helenius J, Helenius A. Manipulating disulfide bond formation and protein folding in the endoplasmic reticulum. *EMBO J*. May 1992;11(5):1717-22.

74. Chen C, Zong S, Wang Z, et al. Imaging and Intracellular Tracking of Cancer-Derived Exosomes Using Single-Molecule Localization-Based Super-Resolution Microscope. *ACS Appl Mater Interfaces*. Oct 2016;8(39):25825-25833. doi:10.1021/acsami.6b09442

75. Schermelleh L, Ferrand A, Huser T, et al. Super-resolution microscopy demystified. *Nat Cell Biol*. 01 2019;21(1):72-84. doi:10.1038/s41556-018-0251-8

76. Tarhriz V, Bandehpour M, Dastmalchi S, Ouladsahebmadarek E, Zarredar H, Eyvazi S. Overview of CD24 as a new molecular marker in ovarian cancer. *J Cell Physiol*. Mar 2019;234(3):2134-2142. doi:10.1002/jcp.27581

77. Escola JM, Kleijmeer MJ, Stoorvogel W, Griffith JM, Yoshie O, Geuze HJ. Selective enrichment of tetraspan proteins on the internal vesicles of multivesicular endosomes and on exosomes secreted by human B-lymphocytes. *J Biol Chem*. Aug 1998;273(32):20121-7. doi:10.1074/jbc.273.32.20121

78. Oliveira-Rodríguez M, López-Cobo S, Reyburn HT, et al. Development of a rapid lateral flow immunoassay test for detection of exosomes previously enriched from cell culture medium and body fluids. *J Extracell Vesicles*. 2016;5:31803. doi:10.3402/jev.v5.31803

79. Paolini L, Orizio F, Busatto S, et al. Exosomes Secreted by HeLa Cells Shuttle on Their Surface the Plasma Membrane-Associated Sialidase NEU3. *Biochemistry*. Dec 2017;56(48):6401-6408. doi:10.1021/acs.biochem.7b00665

80. Fang S, Tian H, Li X, et al. Clinical application of a microfluidic chip for immunocapture and quantification of circulating exosomes to assist breast cancer diagnosis and molecular classification. *PLoS One*. 2017;12(4):e0175050. doi:10.1371/journal.pone.0175050

81. Mehner C, Oberg AL, Goergen KM, et al. EGFR as a prognostic biomarker and therapeutic target in ovarian cancer: evaluation of patient cohort and literature review. *Genes Cancer*. May 2017;8(5-6):589-599. doi:10.18632/genesandcancer.142

82. Bondong S, Kiefel H, Hielscher T, et al. Prognostic significance of L1CAM in ovarian cancer and its role in constitutive NF-κB activation. *Ann Oncol*. Jul 2012;23(7):1795-802. doi:10.1093/annonc/mdr568

83. Shen J, Zhu X, Fei J, Shi P, Yu S, Zhou J. Advances of exosome in the development of ovarian cancer and its diagnostic and therapeutic prospect. *Onco Targets Ther*. 2018;11:2831-2841. doi:10.2147/OTT.S159829

84. Milane L, Singh A, Mattheolabakis G, Suresh M, Amiji MM. Exosome mediated communication within the tumor microenvironment. *J Control Release*. Dec 2015;219:278-294. doi:10.1016/j.jconrel.2015.06.029

85. Conigliaro A, Cicchini C. Exosome-Mediated Signaling in Epithelial to Mesenchymal Transition and Tumor Progression. *J Clin Med*. Dec 2018;8(1)doi:10.3390/jcm8010026

86. Jiang L, Marcus R. Microwave-assisted grafting polymerization modification of nylon 6 capillary-channeled polymer fibers for enhanced weak cation exchange protein separations. Article. *Analytica Chimica Acta*. FEB 15 2017 2017;954:129-139. doi:10.1016/j.aca.2016.11.065

87. Jiang L, Marcus R. Microwave-assisted, grafting polymerization preparation of strong cation exchange nylon 6 capillary-channeled polymer fibers and their chromatographic properties. Article. *Analytica Chimica Acta*. JUL 18 2017 2017;977:52-64. doi:10.1016/j.aca.2017.04.033

88. Trang H, Marcus R. Application of protein A-modified capillary-channeled polymer polypropylene fibers to the quantitation of IgG in complex matrices. Article. *Journal of Pharmaceutical and Biomedical Analysis*. AUG 5 2017 2017;142:49-58. doi:10.1016/j.jpba.2017.04.028

89. Jiang L, Marcus R. Biotin-functionalized poly(ethylene terephthalate) capillary-channeled polymer fibers as HPLC stationary phase for affinity chromatography. Article. *Analytical and Bioanalytical Chemistry*. JAN 2015 2015;407(3):939-951. doi:10.1007/s00216-014-8235-4

90. Schadock-Hewitt A, Marcus R. Initial evaluation of protein A modified capillary-channeled polymer fibers for the capture and recovery of immunoglobulin G. Article. *Journal of Separation Science*. MAR 2014 2014;37(5):495-504. doi:10.1002/jssc.201301205

CHAPTER 4

POTENTIAL IMPACTS OF ISOLATION METHOD AND SAMPLE SOURCE ON SMALL EXTRACELLULAR VESICLE MORPHOLOGY AND BIOMARKER PROFILING

Abstract

Extracellular vesicles (EVs) have emerged as promising diagnostic, drug delivery, and therapeutic agents, particularly with regards to cancer. Although research is progressing quickly, progression of EV applications is hindered by the limitations of EV isolation and separation technologies. Current EV isolation techniques are in need of standardization across the industry for translational progression to continue. In particular, sample source is an important factor that may influence EV isolation choice and outcome. In this research, urine and cervical mucus are compared as potential sources for EV isolation and downstream EV analysis for potential ovarian cancer diagnostic and treatment applications. In addition, a larger study of microRNA (miRNA) content of EVs isolated from cervical mucus samples from patients with and without ovarian cancer revealed several potential miRNA biomarkers. In-depth analysis of this miRNA data, along with corresponding proteomic data, is ongoing in an attempt to reveal pathology and characteristic-specific miRNA and protein biomarkers for early ovarian cancer detection. Together, these studies demonstrate that cervical mucus may be useful for ovarian cancer-specific EV diagnostics. Ultimately, investigations of sample source-

specific applications, such as this, may lead to more accurate and specific EV diagnostics and therapeutic outcomes, as well as greater standardization across the EV field.

It should be noted that this is collaborative work and was performed with Dr. Brian Dean of the Clemson University Biomedical Data Science and Informatics Program. The bioinformatics work outlined in this chapter was primarily performed by Ms. Paritra Mandal. All patient samples used in this work were provided by Dr. Larry Puls, who serves as the Head of Gynecological Oncology at Prisma Health Systems in Greenville, SC.

Introduction

Extracellular vesicle (EV) and exosome research has quickly developed into an expansive area of study focusing on vesicle biogenesis, classification, transport, uptake, dissemination, isolation and separation, biomarker discovery, drug delivery, and therapeutics.[2-6] Broadly, these areas of focus can be divided into basic research and knowledge discovery and medical application development. Both sides of EV research are making significant progress but lack a strong base to make definitive and repeatable claims. Every discovery and development is highly dependent on the source of the vesicles, the method of separation, and the micro- and macro-environments from which the vesicles originate. With so many sources and methods of isolating EVs, paired with the diverse subcategories of EVs, it is both remarkable and encouraging that such significant progress has been made in the understanding of these bio-nanoparticles.

However, with each new discovery, the complexities surrounding EVs grow ever more intricate.

Before investigating either basic research or medical application development, it is important for the EV community to come to agreement by setting standards in classification and isolation methods. While Thery et al. and the International Society for Extracellular Vesicles (ISEV) have made significant progress toward formulating vesicle classifications and benchmarks of identification, the standards are still continually debated and evolving.[7, 8] There are many commonly used isolation techniques, including ultracentrifugation (UC), ultrafiltration (UF), chromatography, precipitation, and immunocapture, but very little agreement upon which technique should be used for principal comparison.[9-11] Perhaps the best way to develop greater consistency and experimental reproducibility is to develop standards for EV separation and isolation. Classification of EV isolation strategies into methods better suited for particular applications may be a good place to start.

Of the most common EV isolation methods, ultracentrifugation is perhaps the most readily available technique, requiring equipment that is already found at most biology research institutions.[12-14] Although UC output can vary greatly depending on sample viscosity, sample source, pellet disturbance, and rotor characteristics,[15-17] UC has proven to be a useful starting point for EV research and applications.[14] Furthermore, although other EV separation methods have shown greater promise, UC still holds value as a tool of comparison when developing new EV isolation methods.[12, 16, 18, 19] UC has demonstrated the ability to isolate EVs from conditioned cell media and most body fluids

including urine, blood plasma, cerebrospinal fluid, amniotic fluid, saliva, and cervical mucus.[11, 16, 17, 20-25] The flexibility and ease with which UC can be performed make it an excellent tool for comparison as it serves as an acceptable standard across the industry.

Unlike UC, which relies on vesicle density and molecular weight to separate cell components and EVs, UF and size exclusion chromatography (SEC) rely on vesicle diameter.[26-28] Stratification based on size allows for greater control of EV sub-populations compared to UC, but struggles to classify larger vesicles. Vesicle size provides a general picture of vesicle classification, but discounts many key characteristics including biogenesis, protein, RNA, lipid profiles, density, zeta potential, and morphology. That said, any EV isolation technique using only one metric of comparison will likely struggle with classification. Size exclusion EV separation techniques have demonstrated high throughput, fast isolation, and high yield[26-29], but, due to the use of force, have struggled to limit vesicle deformation and may cause damage to larger vesicles.[9] The use of size limit thresholds and multiple filtration or exclusion steps has greatly improved the purity and population selection of these techniques.[27, 28, 30] With increased EV purity and population selection, size exclusion techniques may serve best in applications requiring high through-put and large samples.

Due to the presence and diversity of proteins in EV membranes, immunoaffinity capture techniques have emerged as popular methods for increasing EV population specificity and purity. Immunoaffinity steps have been incorporated into microfluidics devices and combined with other effective EV isolation methods with great success.[31-35] For example, Mathivanan et al. identified several colon cancer-related proteins and

potential EV diagnostic markers using a combination of UC, UF, and immune-affinity approaches[35], while Ueda et al. coupled antibodies to mass spectroscopy to create an immuno-assay useful for increasing specificity and quickly identifying proteins for biomarker discovery.[36] With the ability to increase specificity and purity, immunoaffinity methods are continually being incorporated into EV diagnostic techniques and will likely play an important role in developing EV isolation methods for specific and unique applications, particularly disease diagnostics.

From diagnosis of cancer, neurodegenerative diseases, and cardiovascular disease to treatment of Parkinson's Disease through drug delivery, EV applications can vary widely.[3, 37-39] In particular, ovarian cancer is a prime candidate for EV-based early diagnostics due to its propensity for late stage diagnosis and poor 5-year survival rate.[40] Each application may require vastly different EV population purity, consistency, specificity, proteomics, transcriptomics, lipidomics, and morphology. Ideally, different EV separation methods may be able to control these characteristics with limited vesicle damage. Additionally, sample source (urine, plasma, etc.) may influence the effectiveness, efficiency, practicality, and accuracy of EV separation. While consistency across samples is always important, it is unclear whether it is necessary to calibrate each EV population characteristic for each application or sample source and whether an EV separation dominant design will emerge as the most practical method.

While developing individualized EV separation methods for each application may prove useful, practicality, speed, and ease of use are important considerations that may push EV isolation research in a different direction. A single consistent isolation, while

less individualized for applications or sample sources, may ultimately be the most useful in clinical settings and for vesicle comparison in the EV community. However, just as immunocapture EV isolation may separate sub-populations of EVs, it is hypothesized that body fluid samples originating from or near a region of interest may contain more relevant EV information for specific conditions. For instance, urinary EVs have been frequently investigated as biomarkers for prostate cancer and kidney diseases as a means of improving the accuracy and sensitivity of diagnostics.[20, 41-46] Additionally, breast milk-derived EVs have been shown to directly promote the epithelial-mesenchymal transition in breast cancer tumor cells and breast milk-derived EVs with high expression of TGFβ2 may be associated with a higher risk of breast cancer.[47, 48] Diagnosis via EVs isolated from plasma may use a more generic EV population and demonstrate lower specific disease detection accuracy due to low signal to noise ratios. Therefore, establishing a consistent dominant design for EV isolation, while easier to study and evaluate, may prove impractical for many applications. Finding a balance between consistency in EV separation and customization for a given EV application will be required to advance EV understanding and achieve clinical translation.

Much of the EV community has focused on improving or comparing isolation and diagnostic methods and has focused very little on comparing EV sample sources.[49] While several studies have compared urine and plasma EV diagnostic potential[10, 25, 50, 51], comparison of region-specific sources, such as cervical mucus, breast milk, amniotic fluid, tears, semen, and cerebrospinal fluid, is uncommon. The size distributions and RNA makeup of urine and blood plasma EVs have been shown to vary significantly

when isolated via ultracentrifugation[52] potentially due to the presence of Tamm–Horsfall protein (THP, one of the most common glycoproteins in urine), albumin, and other protein contaminants in urine and blood.[14, 53] Removal or reduction of THP and other contaminating agents may decrease the variance in size distribution and biomarker detection from urine and blood EV samples.[54] However, if elimination of contamination proves difficult, other sample sources may allow EV isolation with reduced or manageable contaminants. Although no individual study has compared the characteristics of EVs from different sources (other than urine and blood plasma) under controlled conditions, sample source comparison across studies reveals variance in EV size distribution and RNA makeup.[24, 52, 55-68]

With such variation in EV characteristics and transcriptomics, it is difficult to determine which body fluid matrix is optimal for each isolation method and downstream application. Furthermore, it is unclear whether sample proximity to a region of interest may improve diagnostic accuracy. More analysis and comparison across studies is needed before any conclusions can be drawn. However, this study aims to compare the morphology and miRNA content of EVs isolated from urine and cervical mucus samples of patients with benign or malignant ovarian tumors. In doing so, this study highlights the differences in morphology and miRNA content between urine and cervical mucus EVs and may provide evidence for increased use of sample sources near regions of interest with regard to diagnostic accuracy. Furthermore, this study contributes ovarian cancer EV miRNA differential expression analysis that can be used to develop more accurate and potentially earlier EV-based diagnoses for ovarian cancer. Notably, early diagnosis

(stage 1 or 2) of ovarian cancer, may increase the 5-year survival rate of the disease to 92% from 29% when discovered in stage 3 or 4.[40]

Due to concerns over the classification and nomenclature of EVs among the EV community, all EVs discussed in this study will be referred to as small extracellular vesicles (sEVs) rather than exosomes specifically.

Materials and Methods

Urine, cervical mucus, and plasma collection and storage

Urine, cervical mucus (CM), and blood plasma samples were obtained from patients through the Prisma Health System (Greenville Campus, Institute for Translational Oncology Research (ITOR) biorepository responsible for sample processing and storage). All procedures were approved and performed with adherence to the Prisma Health Institutional Review Board and Clemson University Institutional Biosafety Committee safety guidelines. Upon collection, 50 mL urine samples were supplemented with 1.67 mL of 100 mM sodium azide, 2.5 mL of 2 mg/mL phenylmethylsulfonyl fluoride (PMSF), and 50 µL of 1 mg/mL Leupeptin. After supplementation, urine samples were frozen and stored at -80˚C until further processing. To collect CM samples, the cervical mucus plug and a swab of cervical mucus were placed in 10 mL of phosphate buffered saline (PBS) supplemented with 334 µL of 100 mM sodium azide, 500 µL of 2 mg/mL PMSF, and 10 µL of 1 mg/mL Leupeptin. After supplementation, CM samples were placed on ice for 30 minutes, vortexed for 30

seconds, frozen and stored at -80˚C until further processing. Blood samples were collected via standard phlebotomy procedures in an ethylenediaminetetraacetic acid (EDTA) coated tube. Within 30 minutes of sample collection, blood samples were inverted 8 to 10 times and centrifuged at 1500 x g at 22˚C for at least 15 minutes. Supernatant of centrifuged blood samples were aliquoted into 1.5 mL cryovials, frozen and stored at -80˚C.

sEV isolation via ultracentrifugation

Patient urine and cervical mucus were thawed at 22°C prior to sEV isolation. After thawing completely, urine samples were vortexed for 30 seconds while CM samples were vortexed for 3 minutes to ensure even mixing, breakup of mucus, and removal of mucus from the collection swab. After being vortexed, collection swabs were removed from the CM and scraped into the tube to retain any excess mucus still on the swab. Briefly, 8 mL of urine or CM was centrifuged at 2,000 x g for 20 minutes at 22˚C using an Eppendorf Centrifuge 5430R (Eppendorf, Hamburg, Germany). The resultant supernatant was centrifuged at 10,000 x g for 30 minutes at 4˚C using a Beckman Coulter Avanti J-26S XPI Centrifuge with a JA-25.50 rotor (Beckman Coulter, Brea, CA). The resultant supernatant was filtered using a 0.2 µm sterile syringe filter (Thermo Fisher Scientific, Waltham, MA). After filtration, the supernatant was transferred to a compatible ultracentrifuge tube (Beckman Coulter, Brea, CA) and centrifuged at 120,000 x g for 60 minutes at 4˚C using a Beckman Coulter Optima XPN-80 Ultracentrifuge and a Type 45 Ti rotor (Beckman Coulter, Brea, CA). Finally, the resultant pellet was resuspended in 400 µL of 1x PBS and stored at -80ºC for downstream analysis.

C-CP fiber sEV isolation method

Chemicals used during sEV separation include ammonium sulfate ($(NH_4)_2\ SO_4$) (VWR, Radnor, PA), 10x PBS (Hyclone Laboratories Inc., Logan, UT), acetonitrile (ACN) (EMD Millipore, Burlington, MA), glycerol (Fisher Scientific, Waltham, MA), and ultra-pure water (obtained using a Milli-Q water system, Millipore, Burlington, MA). Extruded polyethylene terephthalate (PET) capillary-channeled polymer (C-CP) fibers, produced by the Material Science and Engineering Department at Clemson University, were wound on a circular frame 8 times (450 fibers) then rinsed with hot water, acetonitrile, isopropanol, and ultra-pure water. Wound fibers were pulled through a 30 cm length, 0.762 mm internal diameter polyether ether ketone (PEEK)(IDEX Health & Science LLC, Oak Harbor, WA) tubing using a plastic monofilament. Using a Dionex Ultimate 3000 HPLC system (LPG-3400SD quaternary pump and MWD-3000 UV–Vis absorbance detector; Thermo Fisher Scientific, Sunnyvale, CA, USA), packed columns were washed using ultra-pure water, acetonitrile, and then ultra-pure water at 0.5 mL min^{-1}. Chromatography was performed using the Dionex Ultimate 3000 HPLC system and controlled by the Chromeleon 7 software system. Samples were injected using a Rheodyne model 8125 low dispersion injector with a 60 μL injection loop (Rheodyne, Rohnert Park, CA). The baseline case (no sample, step gradient mobile phase) was performed with mobile phase flow rate of 0.5 mL min^{-1} and subtracted from sample chromatograms. After being flushed with 1X PBS, the column was equilibrated with 2 M ammonium sulfate solution dissolved in 1X PBS, pH = 7.4. A step gradient mobile phase of 25% glycerol with 1M $(NH_4)_2\ SO_4$ (0.5 mL min^{-1}) was introduced 3 minutes following

sample injection. Column elution was initiated by a second step gradient of 50% glycerol in 1X PBS (0.5 mL min^{-1}) 5 minutes after sample injection. Eluting species (proteins and sEVs) were detected at 216 nm and recovered using an R1 fraction collector (Teledyne Isco, Lincoln, NE, USA) based on detector absorbance response.

C-CP Fiber-based film wicking sample preparation

Samples used in the film wicking experiments included patient urine and blood plasma, obtained through Prisma Health and standard exosomes (HBM-PEU-100, HansaBioMed, Tallinn, Estonia) diluted in mock urine, reconstituted milk, and mock saliva to a concentration of 9.3 x 10^5 particles/mL. Mock urine and saliva were prepared according to recipes from previous studies[69, 70], while reconstituted milk was prepared as 2% non-fat dry milk (Bio-Rad, Hercules, CA) dissolved in DI water. All samples were supplemented with 1% red food coloring (McCormick, Baltimore, MD) by volume.

C-CP channeled film wicking studies

C-CP channeled films, produced by the Material Science and Engineering Department at Clemson University, were cut into 5 cm strips and taped down to 1 x 3 inch glass microscope slides, ridges face-up. A micropipette was used to apply 10 µl of patient urine, patient plasma, 1X PBS diluted standard exosomes, or 1X PBS directly to the center of the film. The applied drop was allowed to wick along the film for 20 minutes at 22˚C while exposed to air. Following wicking, the films were removed from the glass slides and the film regions where sample visibly wicked were clipped off using scissors and prepared for scanning electron microscopy (SEM).

In a separate experiment, 3 μl of 1X PBS, patient urine, patient plasma, or standard exosomes diluted in mock urine, mock saliva, reconstituted milk, or 1X PBS were applied directly to the center of the C-CP films via micropipette and allowed to wick for 15 minutes at 22˚C while exposed to air and under 5X magnification (Plan APO 1.0X objective, 0.09 numeral aperture, no immersion) stereoscopic observation using a Leica Thunder Model Organism Imaging System (Leica, Wetzlar, Germany). Images were captured at a rate of one frame per second and compiled into time-lapse movies. Tracker Video Analysis and Modeling Tool, available through Open Source Physics (https://www.compadre.org), was used to track the fluid front in order to determine the velocity of sample wicking on the films. Any velocities below $2x10^{-7}$ m/s (periods of little to no movement) were not included in the average (n=8) calculations (see Figure 4.4a). Flow rate was calculated as velocity multiplied by the C-CP film cross-sectional area as measured by SEM.

Sample preparation for scanning electron microscopy

C-CP films being prepared for SEM were fixed in 1% osmium tetroxide for 1 hour with shaking immediately after sample wicking. After removing the osmium tetroxide, samples were washed in deionized water 3 times for 3-5 minutes per wash. Next, the samples were washed in an ethanol-water mixture of the following ethanol percentages for 3 minutes each: 50%, 70%, 80%, 90%, 95%, 100%, 100%. The samples were then washed in a 50:50 hexamethyldisilazane(HMDS) –ethanol mixture for 3 minutes and then finally washed in 100% HMDS and left to dry at 20˚C in a chemical fume hood for 2-3 days. After drying was complete, samples were attached to a metal

stage using adhesive and platinum coated using the Hummer 6.2 Sputtering system (Anatech, Battle Creek, MI) at 70 millitorr for 2 minutes. Images were captured using a Hitachi SU5000 Field Emission Scanning Electron Microscope (FE-SEM) (Hitachi, Tokyo, Japan).

Sample preparation for transmission electron microscopy

To prepare for transmission electron microscopy (TEM), 40 µL of urine or CM sEVs isolated by UC or C-CP fiber separation were fixed in 4% paraformaldehyde for 30 minutes on ice. All grid adhesion and staining steps were performed by pipetting drops of sample, stain, or wash onto parafilm and moving 200 mesh copper formvar coated grids (Electron Microscopy Sciences, Hatfield, PA) from one drop to the next. After sample fixation, grids were placed coated side down on 5 µL drops of each sample for 5 minutes. Grids were washed 3 times with DI water for 4 minutes each, stained with 2% uranyl acetate for 5 minutes, and then washed 3 times with DI water for 4 minutes each. Grids were air dried in a low-humidity environment and then imaged using a Hitachi H7600 TEM (Hitachi, Tokyo, Japan). SEM measurements were made using ImageJ version 1.48 software (NIH, Bethesda, MD)

RNA sequencing

After isolation via ultracentrifugation, 4 patient urine sEV samples of 200 µL (2 cancerous and 2 non-cancerous) and 4 patient cervical mucus sEV samples of 200 µL (2 cancerous and 2 non-cancerous) were sent to Qiagen (Hilden, Germany) for RNA isolation, quality control, and differential expression analysis.

In a second study, 42 patient cervical mucus-derived sEV samples (26 cancerous and 16 non-cancerous), isolated by ultracentrifugation were sent to Qiagen (Hilden, Germany) for RNA isolation, quality control, and differential expression analysis. In both studies, sample quality was assessed via average read quality and average base quality, prior to next generation sequencing.

miRNA analysis

Analysis, (completed by Qiagen) included adaptor trimming, sequence mapping, principal component analysis, and miRNA differential expression analysis.

Statistical Analysis

C-CP film sample flow velocity means were presented with ± 1 standard deviation. A one-tailed t-test with $\alpha=0.05$, using Microsoft Excel's data analysis software (Microsoft, Redmond, WA), was used to analyze film flow velocity numeric values. Tests with $p<0.05$ were considered statistically significant. RNAseq data, analyzed using the EdgeR package in R statistical software (r-project.org), was evaluated using a statistical test analogous to Fisher's exact test following a negative binomial distribution.[71]

Results

SEM imaging was performed on the C-CP films following wicking of 1X PBS-diluted standard exosomes, patient urine, and patient plasma (Figure 4.1). The 1X PBS-diluted standard exosomes demonstrated adherence along the length of the films while wicking and displayed typical vesicular morphology when adhered to the film surface (Figure 4.1a,b). The patient urine sample, much like the standard exosome sample, demonstrated sEV adherence along the length of the film surface and demonstrated sEV morphology similar to the standard exosome sample (Figure 4.1c,d). Finally, the patient plasma sample, while containing vesicular structures similar in morphology to the standard exosome sample, also included other plasma components, which were potentially a mixture of cellular debris and blood clotting proteins (Figure 4.1e,f).

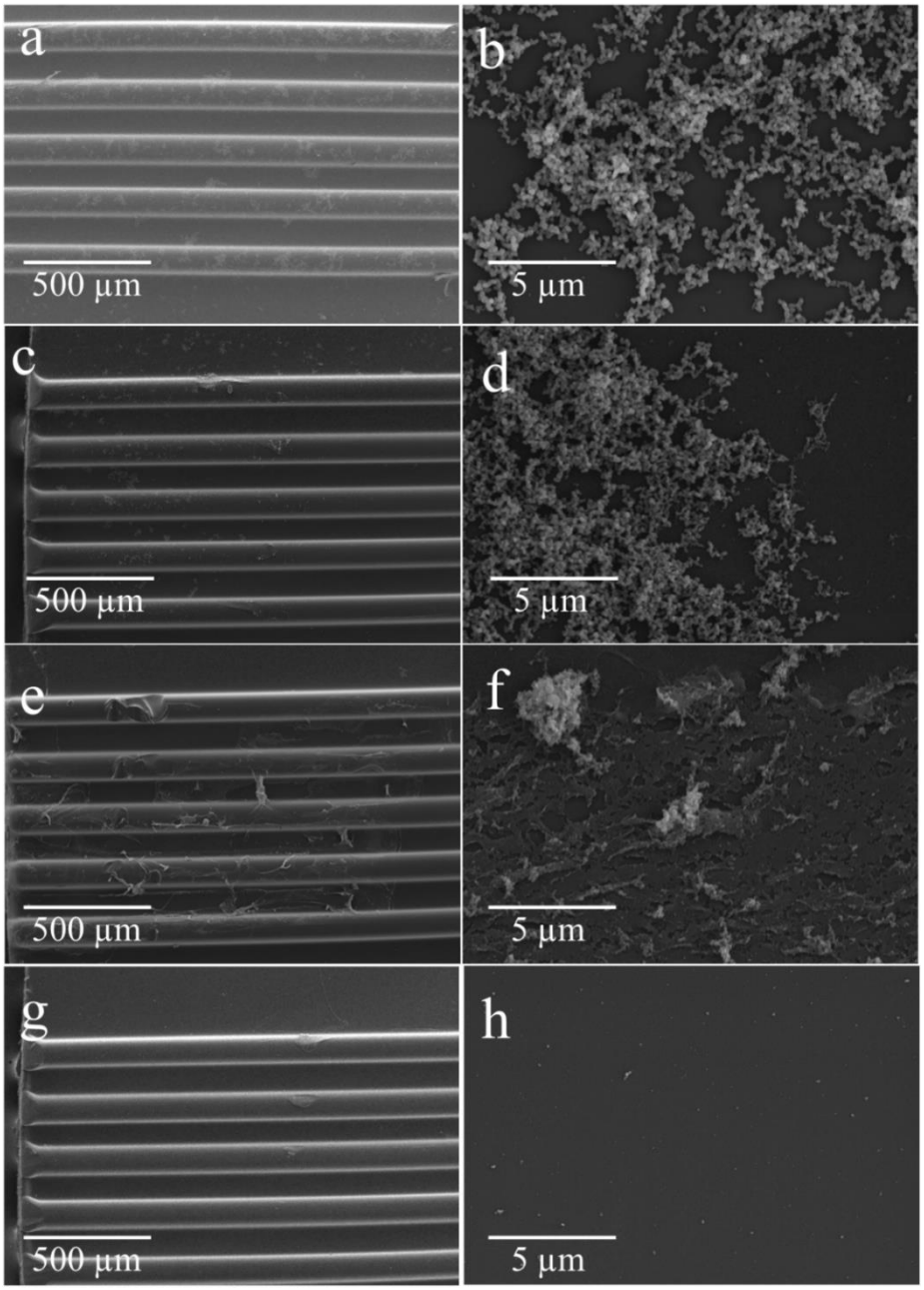

Figure 4.1. Scanning electron microscopy of C-CP films after wicking of various media. Film wicking of (a,b) 1X PBS-diluted standard exosomes, (c,d) patient urine, (e,f) patient plasma, and (g,h) 1X PBS, no sEV control. Images were captured at 70x magnification (a, c, e, g) and 7,000x magnification (b, d, f, h).

Next, the flow rates of patient urine, patient plasma, and standard exosomes diluted in PBS, mock urine, reconstituted milk, or mock saliva on the films were measured and calculated using videos of sample wicking under stereoscopic observation. The average and maximum volumetric flow rates were calculated by multiplying the velocity of each sample observed during sample movement (see Figure 4.2)(Table 4.1) and the cross-sectional area of the film as measured from SEM images (see Figure 4.3, cross-section area: 9,310 μm^2). Velocities during periods of minimal movement (velocity $< 2x10^{-7}$ m/s)(see Figure 4.4a and Materials and Methods for explanation) were not included in the average flow calculations. Halting of fluid flow was due to the limited source pool and uneven sample distribution. PBS control samples demonstrated a significantly higher flow rate than all other samples. Patient urine average volumetric flow was significantly higher than mock urine + Std Exo, patient plasma, reconstituted milk + Std Exo, and mock saliva + Std Exo. Although PBS + Std Exo demonstrated a significantly lower average volumetric flow rate as compared to PBS, its average volumetric flow rate was significantly higher than those of patient plasma, mock urine + Std Exo, reconstituted milk + Std Exo, and mock saliva + Std Exo. Patient urine and PBS + Std Exo flow rates were not significantly different. Additionally, the maximum volumetric flow rates for less viscous samples (PBS, patient urine, PBS + Std Exo, mock urine + Std Exo, and reconstituted milk + Std Exo) were generally higher than more viscous matrices (patient plasma and mock saliva + Std Exo)(Table 4.1).

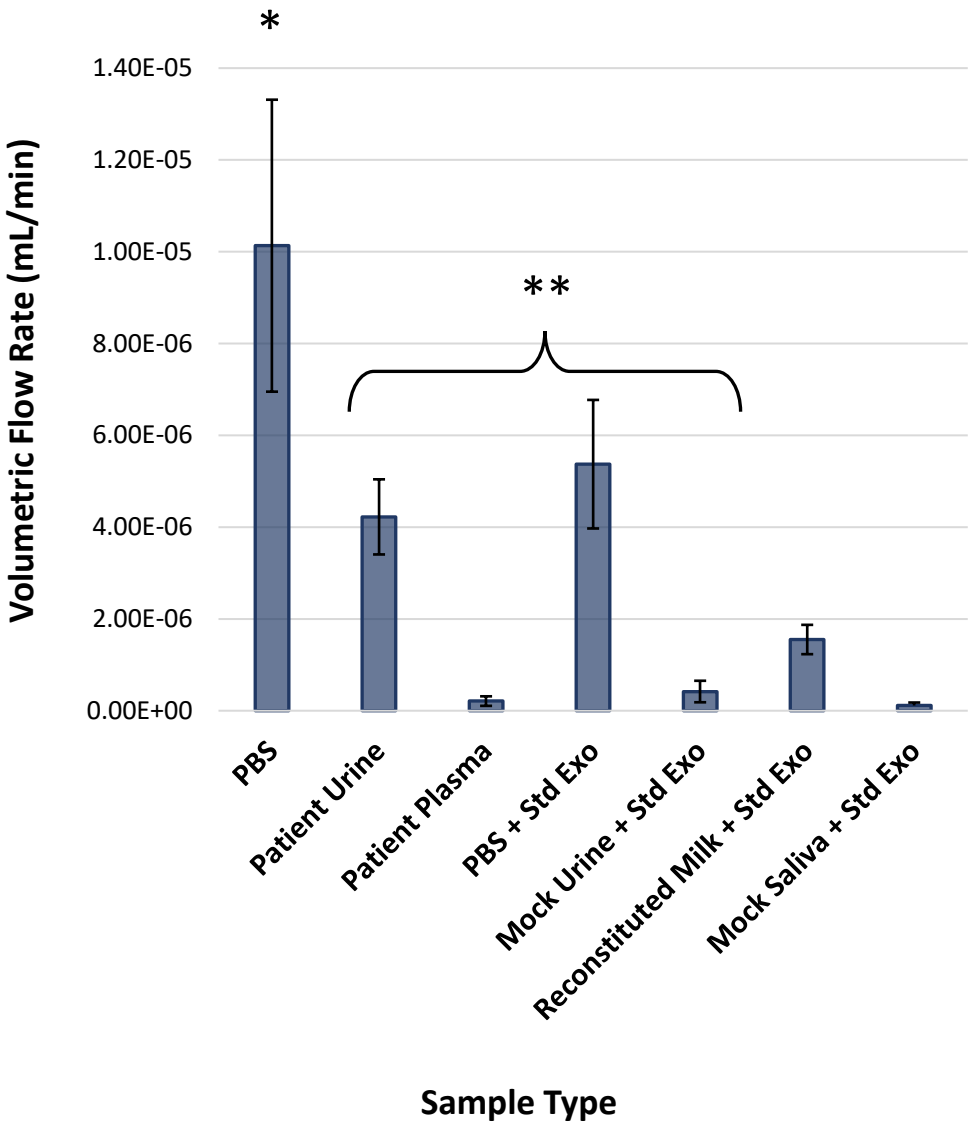

Figure 4.2. Average volumetric flow rates of C-CP film wicking. Results demonstrating the average volumetric flow rates for various matrices, including phosphate buffered saline (PBS), patient urine, patient plasma, PBS + standard exosomes (Std Exo), mock urine + Std Exo, reconstituted milk + Std Exo, and mock saliva + Std Exo (* - PBS; significantly different from all samples, $p<0.05$) (** - patient urine; significantly different from mock urine +Std Exo, $p<0.05$, $n=8$).

Table 4.1. Average and maximum volumetric flow rates of C-CP film wicking. Matrices wicked on C-CP films include phosphate buffered saline (PBS), patient urine, patient plasma, PBS + standard exosomes (Std Exo), mock urine + Std Exo, reconstituted (Reconst) milk + Std Exo, and mock saliva + Std Exo. Error is represented by 1 standard deviation from the mean, n=8.

	Average Flow Rate (mL/min)	Maximum Flow Rate (mL/min)	Standard Deviation
PBS	1.01E-05	2.15E-05	3.18E-06
Patient Urine	4.22E-06	6.09E-06	8.19E-07
Plasma	2.10E-07	5.48E-07	1.04E-07
PBS + Std Exo	5.37E-06	9.73E-06	1.40E-06
Mock Urine + Std Exo	4.18E-07	1.44E-06	2.34E-07
Reconst Milk + Std Exo	1.55E-06	2.18E-06	3.20E-07
Mock Saliva + Std Exo	1.12E-07	3.82E-07	6.57E-08

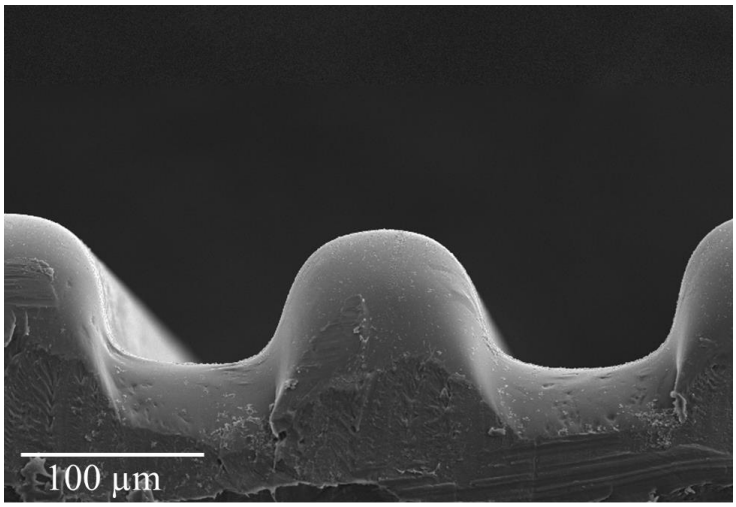

Figure 4.3. SEM of C-CP film cross-section. A cross-sectional image was captured of a C-CP film using SEM at 315x magnification. Area measurements (made using ImageJ 1.48) were used to calculate flow rate in the C-CP film wicking experiments.

a)

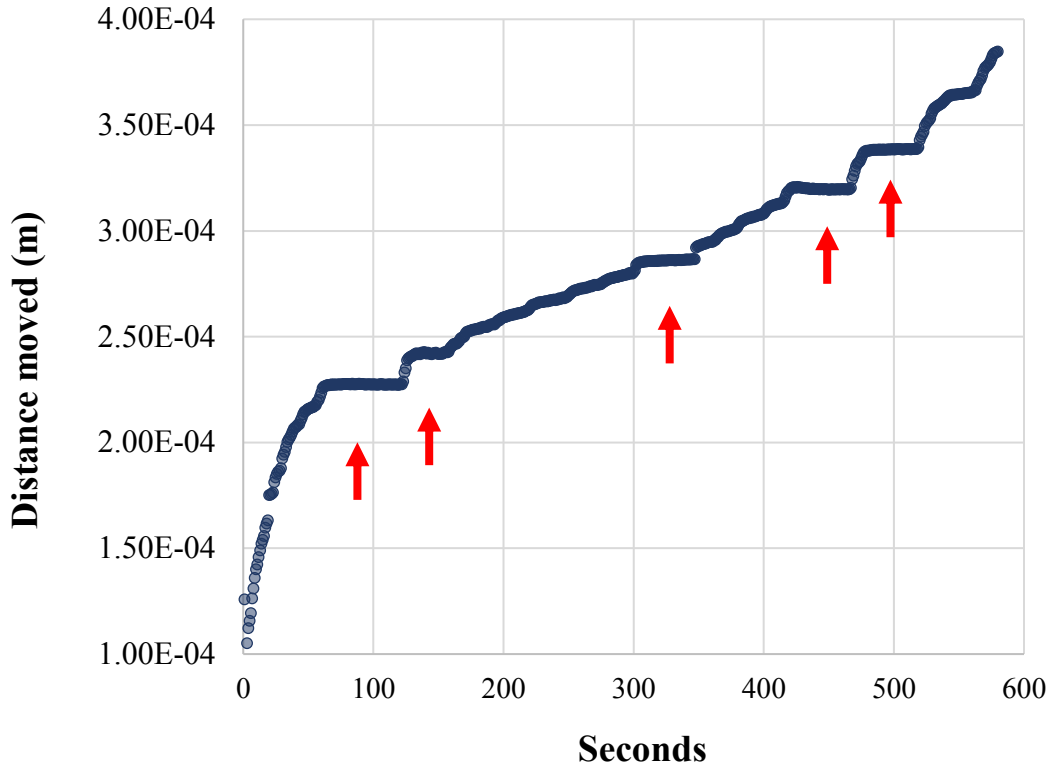

b)

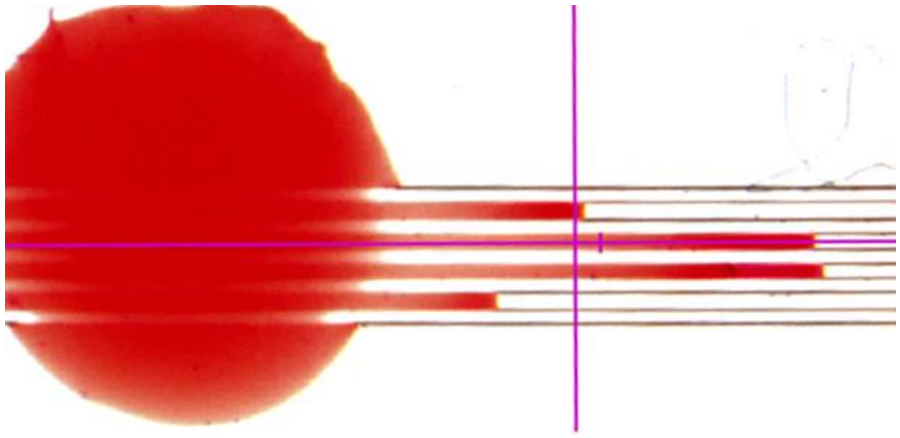

Figure 4.4. Patient urine C-CP fiber-based film wicking velocity and stereoscopic image. (a) Change in distance over time of patient urine wicking on C-CP film. Time points with a velocity below $2x10^{-7}$ m/s (periods of little movement, marked by red arrows) were removed from average velocity and flow calculations. (b) C-CP film stereoscopic image (5x magnification) of patient urine wicking experiment measured using Tracker video analysis software.

When imaged via TEM, patient urine and CM sEVs isolated using a C-CP fiber column and the glycerol stepwise elution protocol (see Materials & Methods; Figure 4.5) revealed similar morphologies to those isolated from the same sample type by UC. Patient urine sEVs isolated by UC (Figure 4.5a) ranged in size from approximately 50-200 nm, while the patient urine sEVs isolated by C-CP fiber-based HIC (Figure 4.5b) were approximately 200 nm in diameter. CM sEVs isolated by UC (Figure 4.5c) ranged in size from approximately 30-70 nm, while CM sEVs isolated by C-CP fiber-based HIC (Figure 4.5d) ranged in size from 60-100 nm. Samples derived from patient urine retained similar staining characteristics regardless of isolation protocol (Figure 4.5a,b), but CM sEVs isolated by C-CP fiber-based HIC appeared much darker than CM sEVs isolated by UC.

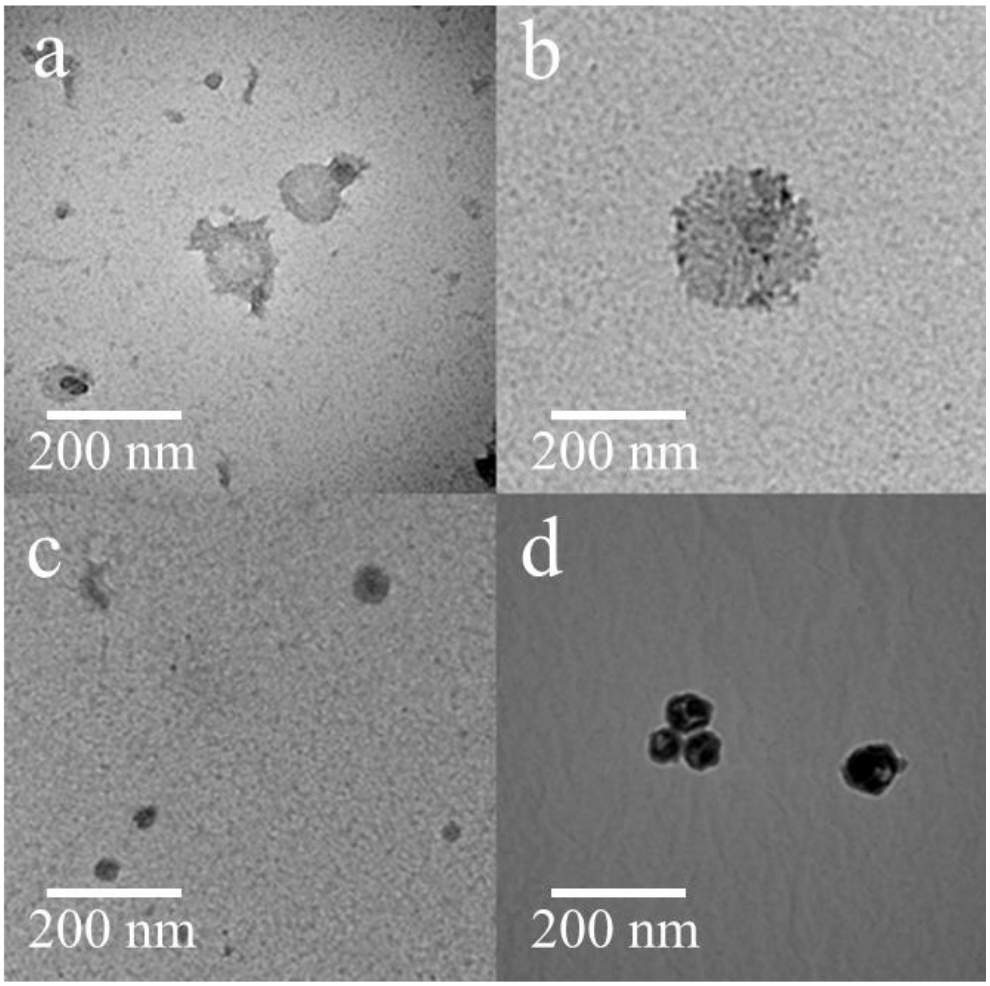

Figure 4.5. Transmission electron microscopy of small extracellular vesicles derived from urine and cervical mucus via UC or C-CP fiber HIC. Samples include sEVs from a) patient urine, isolated by UC, b) patient urine, isolated by C-CP fibers using HIC with glycerol elution, c) cervical mucus, isolated by UC, and d) cervical mucus, isolated by C-CP fibers using HIC with glycerol elution.

Initial pilot study sEVs (2 CM-derived – cancerous, 2 CM-derived – benign, 2 urine-derived – cancerous, 2 urine-derived – benign) were run through quality control, library prepped, sequenced for miRNA, and analyzed for miRNA expression patterns. Principal component analysis (PCA), which dimensionally reduces and clusters samples based on the most influential variables (largest coefficient of variation), was used to look at similarities between samples (Figure 4.6). Principal component 1 is weighed more heavily than principal component 2, meaning sample proximity within principal component 1 indicates higher sample similarity than comparable sample proximity within principal component 2. Cancerous CM-derived sEV miRNA appeared to be grouping together with cancerous urine-derived sEV miRNA. Benign urine-derived sEV miRNA appeared to be comparable to cancerous CM- and urine-derived sEV miRNA in one sample, but not similar in the other sample. Both benign CM-derived sEV miRNA samples did not appear to group well together, but also differed significantly from cancerous CM-derived sEV miRNA.

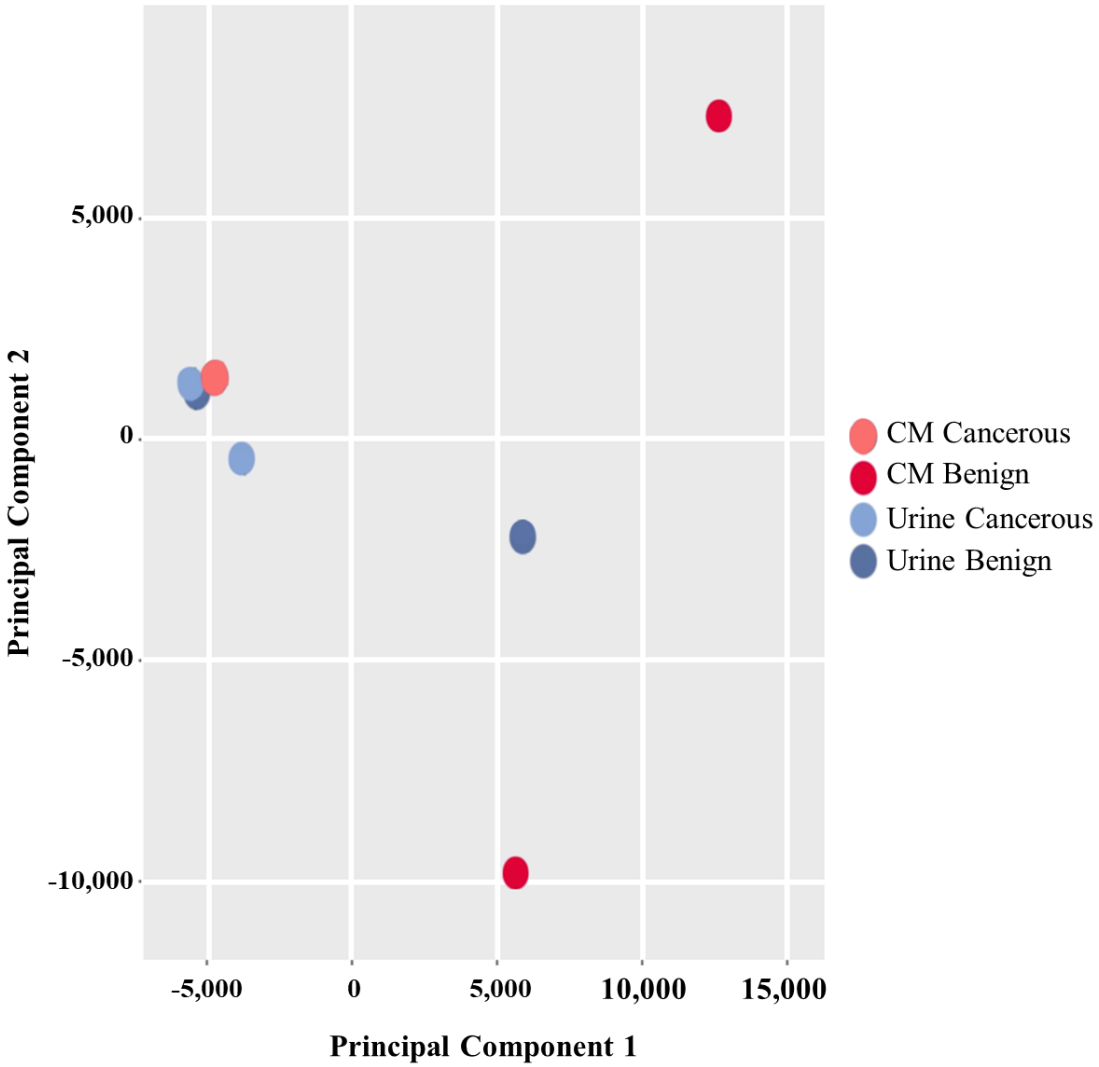

Figure 4.6. Principal Component Analysis (PCA) plot of benign and cancerous cervical mucus- or urine-derived sEV miRNA expression (Pilot Study). Cancerous CM- (n=2), benign CM- (n=2), cancerous urine- (n=2), and benign urine- (n=2) derived sEV miRNAs were dimensionally reduced and clustered for easier interpretation. Data was normalized using the weighted trimmed mean of M-values (TMM) method.[1] PCA completed using 50 miRNAs with the largest coefficient of variation based on TMM. Principal component 1 is the largest component in the variation and principal component 2 is the second largest component in the variation.

Differential expression analysis between pilot study benign (n=2) and cancerous (n=2) urine-derived sEV miRNA revealed numerous miRNAs that were highly differentially expressed and statistically different (Figure 4.7). Several cancerous urine-derived sEV miRNAs appeared significantly upregulated or downregulated in comparison to benign counterparts. Specifically, 2 cancerous urine-derived miRNAs were highly downregulated and statistically significant (log10(p-value)>1.301) and 5 cancerous urine-derived miRNAs were highly upregulated and statistically significant when compared to benign miRNA counterparts. The maximum log2 fold change magnitude between benign and cancerous urine-derived sEV miRNA was 3.85. Of those miRNAs that were highly differentially expressed and statistically significant in the cancerous urine-derived sEV samples, highly expressed miRNAs (high log of counts per million – logCPM) with tumor-related published literature were identified as potential indicators of pathogenesis (Table 4.2).

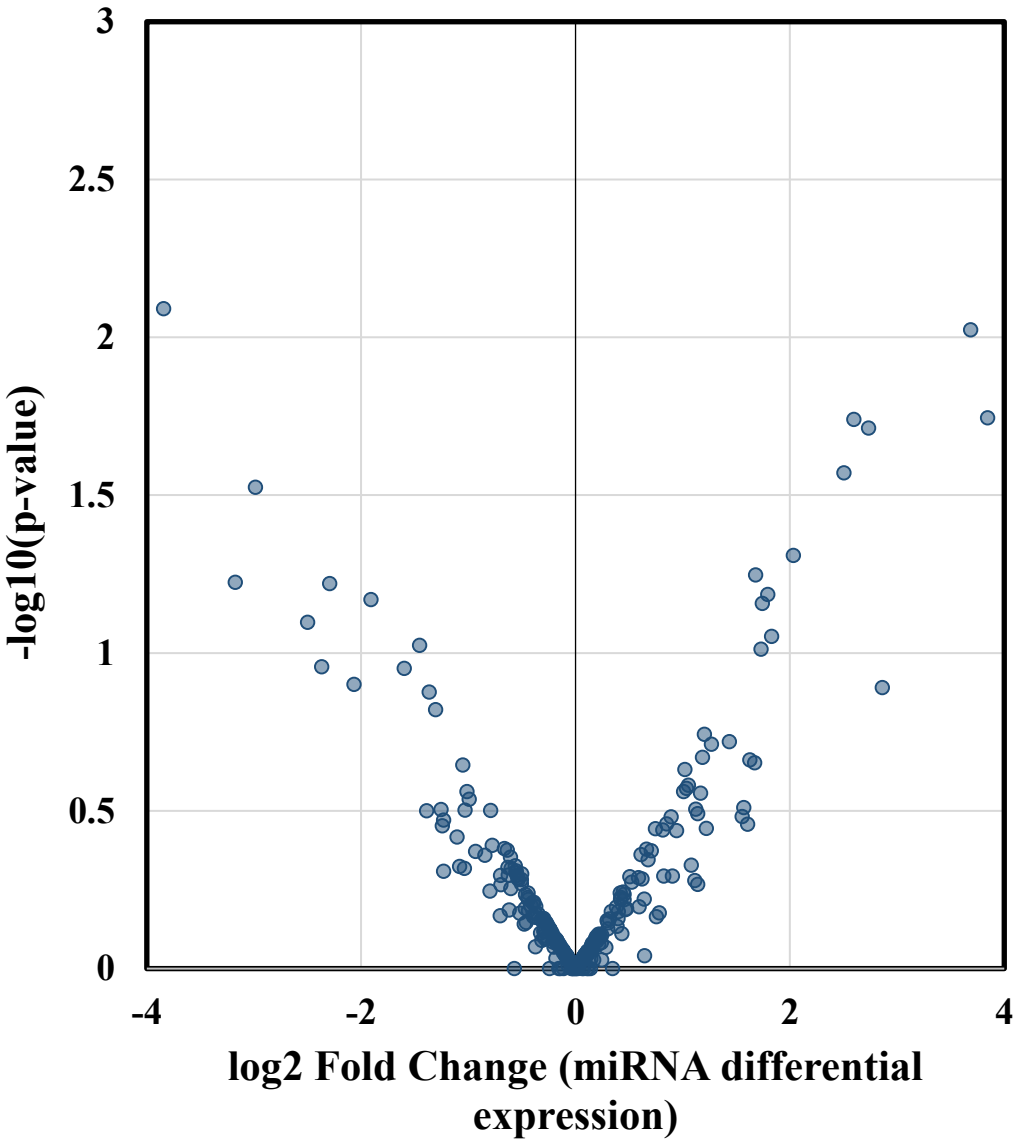

Figure 4.7. Volcano plot of miRNA differential expression of benign vs cancerous urine-derived sEVs (Pilot Study). Benign urine-derived sEV samples (n = 2) serve as the basis of comparison against cancerous urine-derived sEV samples (n=2). A log2 fold change > 0 indicates miRNA expression upregulation while a log2 fold change < 0 indicates miRNA expression downregulation. Differential expression and statistical significance ($p<0.05$ or $-\log_{10}(p\text{-value})>1.301$) determined using the EdgeR package for R and statistical test analogous to Fisher's exact test that follows a negative binomial distribution.

Table 4.2. Differentially expressed miRNAs of interest from benign (n=2) vs cancerous (n=2) urine-derived sEVs (Pilot Study). Significantly different miRNAs of interest were selected by looking for a high absolute value log2 fold change (Log2 FC), a high log of counts per million (logCPM), a p-value<0.05, and tumor-related literature.

miRNA Name	Log2 FC	LogCPM	p-value	Direction
hsa-mir-299-5p	-3.842	4.161	0.0081	Downregulated
hsa-mir-205-5p	3.687	10.807	0.0095	Upregulated
hsa-mir-320d	2.597	4.281	0.018	Upregulated

Differential expression analysis of pilot study benign (n=2) and cancerous (n=2) CM-derived sEV miRNAs primarily demonstrated high upregulation of miRNAs (Figure 4.8). In the cancerous CM-derived sEV samples, 4 miRNAs were downregulated and statistically significant and 72 miRNAs were upregulated and statistically significant compared to benign CM-derived miRNAs. The maximum log2 fold change magnitude between benign and cancerous CM-derived sEV miRNA observed was 7.34 (Figure 4.8). Several miRNAs were identified as being highly expressed (high log CPM), highly differentially expressed (log2 fold change) and statistically significant (p-value <0.05) (Table 4.3) between benign and cancerous CM-derived sEVs.

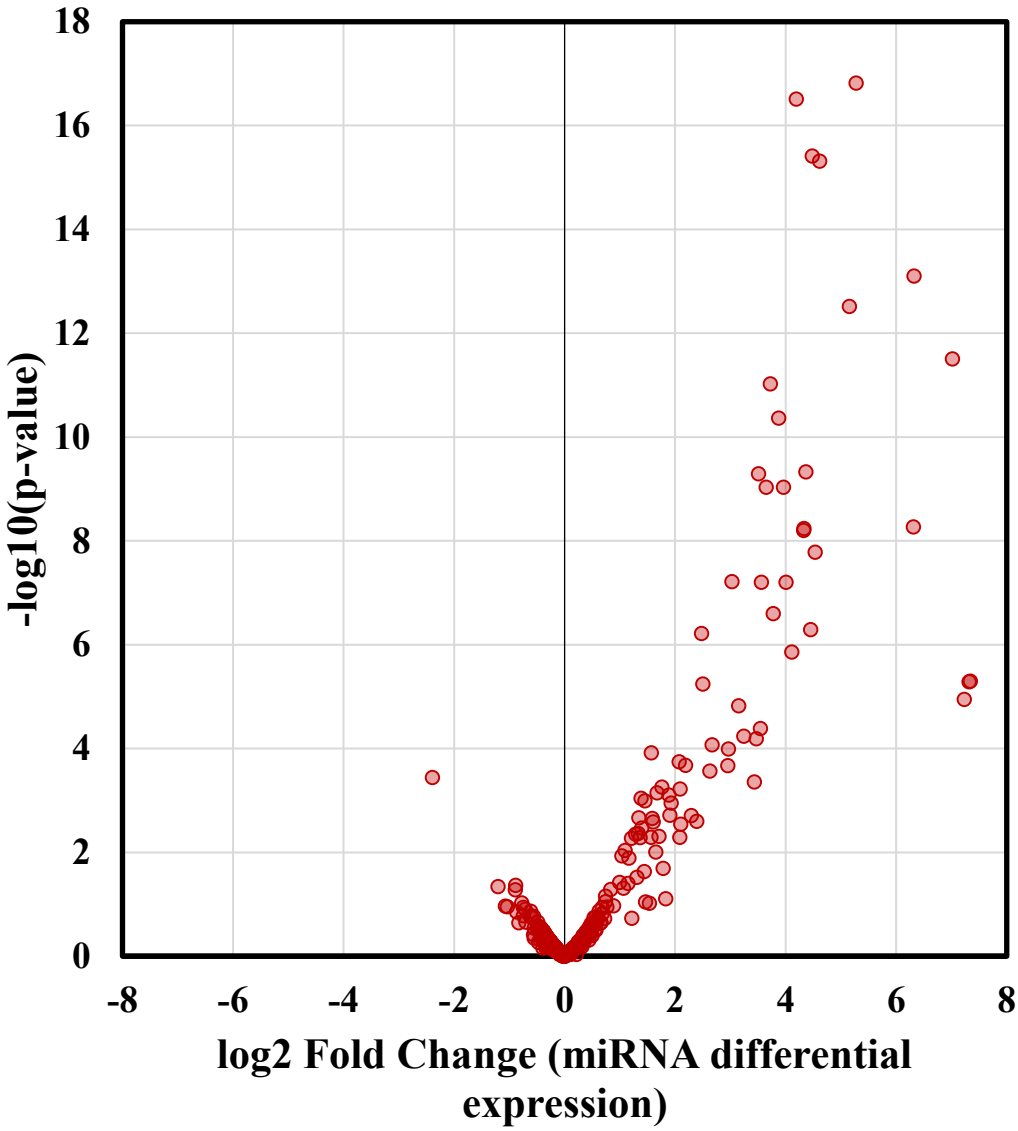

Figure 4.8. Volcano plot of miRNA differential expression of benign vs cancerous cervical mucus-derived sEVs (Pilot Study). Benign CM-derived sEV samples (n=2) serve as the basis of comparison against cancerous CM-derived sEV samples (n=2). Upregulation of miRNA expression (log2 fold change >0), downregulation of miRNA expression (log2 fold change <0), and statistical significance ($p<0.05$ or $-\log10(\text{p-value})>1.301$) determined using the EdgeR package for R and statistical test analogous to Fisher's exact test that follows a negative binomial distribution.

Table 4.3. Differentially expressed miRNAs of interest from benign (n=2) vs cancerous (n=2) cervical mucus-derived sEVs (Pilot Study). Significantly different miRNAs of interest were selected by looking for a high absolute value log2 fold change (Log2 FC), a high log of counts per million (logCPM), a p-value<0.05, and tumor-related literature.

miRNA Name	Log2 FC	LogCPM	p-value	Direction
hsa-mir-95-3p	5.274	5.877	1.53E-17	Upregulated
hsa-mir-184	6.320	7.528	8.01E-14	Upregulated
hsa-mir-429	4.617	9.056	4.88E-16	Upregulated

As part of a larger study, 42 CM-derived sEV (16 benign, 26 cancerous) samples were sequenced and analyzed (by Qiagen) for miRNA expression. After quality control, library prep, and sequencing, sample miRNA expression levels were analyzed using principal component analysis (PCA) to more easily understand clustering and similarities in expression between samples (Figure 4.9).Visually, cancerous CM-derived sEV miRNA profiles appeared to cluster closer along the first principal component compared to benign CM-derived sEV miRNAs. Overall, much of the variance in expression for all 43 miRNAs appear very similar for both cancerous and benign CM-derived sEVs, as indicated by PCA overlap and close proximity.

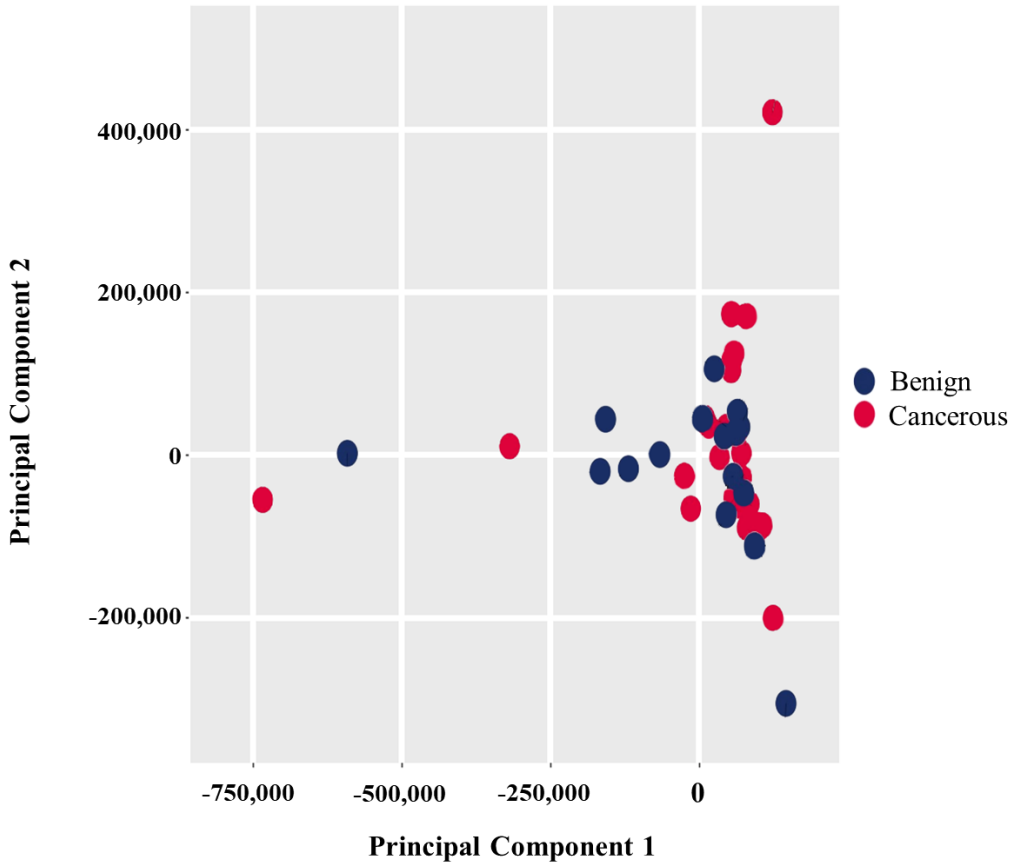

Figure 4.9. Principal Component Analysis (PCA) plot of benign and cancerous CM-derived sEV miRNA expression. Dimensional reduction and clustering was used to analyze miRNA expression similarities between benign CM-derived sEV samples (n=16) and cancerous CM-derived sEV samples (n=26). Data was normalized using the weighted trimmed mean of M-values (TMM) method.[1] PCA completed using 43 miRNAs with the largest coefficient of variation based on TMM. Principal component 1 is the largest component in the variation and principal component 2 is the second largest component in the variation.

In a larger analysis, benign (n=16) and cancerous (n=26) CM-derived sEV miRNAs were analyzed for differential expression based on benign CM-derived sEV miRNAs (Figure 4.10). Of the miRNAs analyzed, 18 were downregulated and statistically significant (log10(p-value) >1.301) and 4 were upregulated and statistically significant in the cancerous CM-derived sEVs. Additionally, the maximum log2 fold change magnitude observed between benign and cancerous CM-derived sEV miRNA expression was 3.14. By filtering miRNA expression by high fold change (log2 FC), high log of counts per million (logCPM), and statistical significance (p-value<0.05) as well as looking for cancer-related published literature, several potential biomarker candidates were identified (Table 4.4). Notably, hsa-mir-184 was identified with these qualifications in both the pilot study (2 benign, 2 cancerous, Figure 4.8, Table 4.3) and larger study (16 benign, 26 cancerous, Figures 4.10, 4.11 Table 4.4) of CM-derived sEV miRNAs.

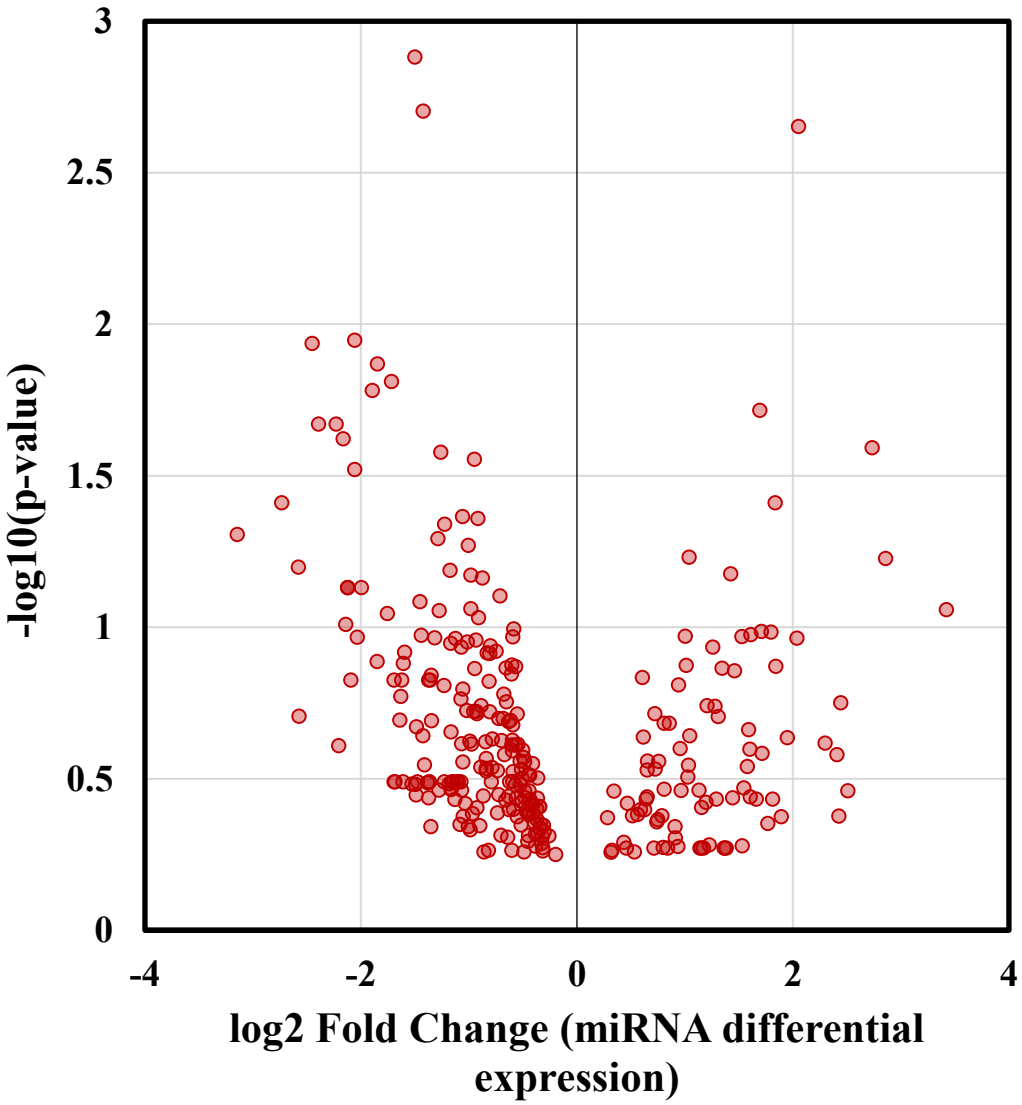

Figure 4.10. Volcano plot of miRNA differential expression of benign vs cancerous cervical mucus-derived sEVs. Benign CM-derived sEV samples (n=16) serve as the basis of comparison against cancerous CM-derived sEV samples (n=26). MicroRNA expression upregulation (log2 fold change >0), downregulation (log2 fold change <0), and statistical significance ($p<0.05$ or –log10(p-value)>1.301) determined using the EdgeR package for R and statistical test analogous to Fisher's exact test that follows a negative binomial distribution.

Table 4.4. Differentially expressed miRNAs of interest from benign vs cancerous cervical mucus-derived sEVs. Differential expression determined using 16 benign and 26 cancerous CM-derived sEV samples. Significantly different miRNAs of interest were selected by looking for a high absolute value log2 fold change (Log2 FC), a high log of counts per million (logCPM), a p-value<0.05, and tumor-related literature.

miRNA Name	Log2 FC	LogCPM	p-value	Direction
hsa-mir-142-3p	-1.500	12.628	0.0013	Downregulated
hsa-mir-34c-3p	-1.718	8.530	0.0154	Downregulated
hsa-mir-184	1.694	10.170	0.0191	Upregulated
hsa-mir-223-3p	-1.288	15.523	0.0500	Downregulated

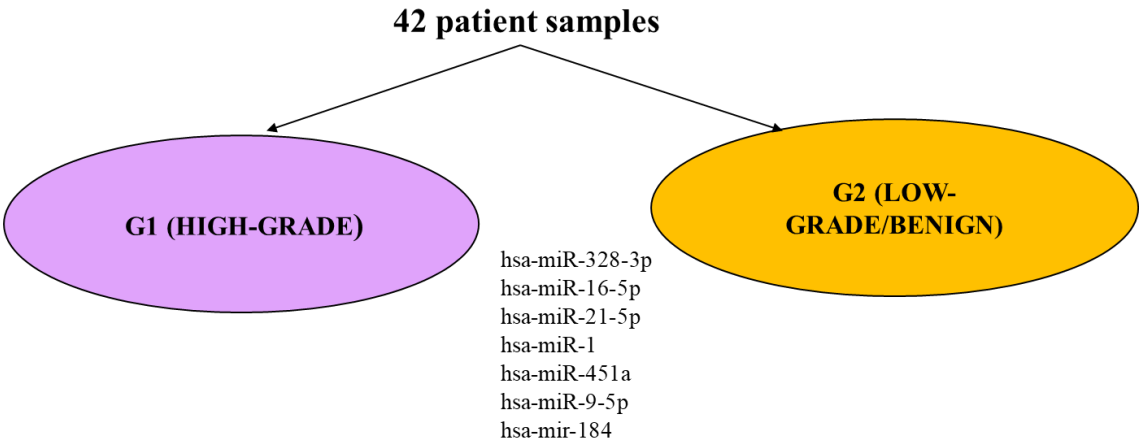

Figure 4.11. Re-clustering of cervical mucus miRNA expression data. Ongoing research has observed clustering of samples into high-grade (G1) and low-grade/benign (G2) rather than cancerous and non-cancerous. Top differentially expressed miRNAs between correctly grouping samples (n=42).

Discussion

The impact that EVs may have on disease diagnostics and therapies is becoming more apparent. As EV biogenesis and classifications become clearer, more efficient, and effective EV isolations emerge, and EV technology moves closer to clinical translation.[2, 72] Specifically, EV isolation maintains a great deal of promise for early cancer detection.[46] Due to frequent late stage discovery and severity, ovarian cancer (OC) is a prime candidate for EV-based diagnostics. According to a recent epidemiology review, patients diagnosed with OC at stages 3 or 4 have a 5-year survival rate of 29% and a 5-year survival rate of 92% when diagnosed at stages 1 or 2.[40, 73] As most OC patients are diagnosed in stages 3 or 4[74], early stage discovery via EV-based diagnosis may be used to greatly improve OC survival rates. Clinical routine screening for cancer cell-derived EVs is plausible, practical, inexpensive, and could substantially reduce instances of cancer-related deaths.

Although EVs have demonstrated promising and powerful therapeutic and diagnostic abilities *in vitro*, only a handful of clinical trials have reported results from phase 1-3 (dosage, safety, and efficacy)[75-79] studies. The trials reporting results have demonstrated that therapeutic EV dosing has been well-tolerated in most instances with only a few cases of moderate adverse events.[80] To date, no clinical trials regarding EV diagnostic ability have reported results. While these trials are promising, the number of trial applications has been limited primarily due to EV isolation inconsistencies, changing EV characterization definitions, and mutable good manufacturing practices (GMP). For EV technology to be translated to the clinic, it is vitally important that the EV community

establish greater consistency within EV isolation, classification, characterization, and sample source selection. The International Society of Extracellular Vesicles (ISEV) has thus far done an excellent job establishing standards of classification and characterization[8], but much more research and discussion will be required to fully understand the complexities surrounding EV biogenesis and classification.

A large hurdle impeding consistency across EV research is choice of EV source. The majority of EVs used in clinical trials come from either autologous or allogeneic dendritic cells (DCs), mesenchymal stem cells (MSCs) or patient body fluids.[80] Sources of EVs investigated *in vitro* may include human, plant, or other eukaryotic cell lines and numerous human body fluids.[2, 3, 52, 80-89] Sample source can greatly impact the results of a study and should be carefully chosen for each application. By defining isolation strategies starting with sample source, the EV community may be able to improve EV diagnostic consistency, precision, and accuracy needed to progress toward clinical translation. While several studies have demonstrated diagnostic correlations using urine or plasma, more body fluids are worth investigating for region-specific diagnostic potential. For instance, hypothetically speaking, urine may provide the most accurate diagnosis for renal cell or bladder carcinomas, while breast milk may provide the most accurate diagnosis for breast cancer. Moreover, the strategies employed to isolate EVs should largely depend on the sample source and application desired. By investigating how EV separation techniques using various sample sources impacts downstream EV applications, the EV community may find correlations that help develop improved guidelines and standards for EV isolation and diagnostics.

When choosing an EV isolation design, both physical characteristics and potential application should be considered. Vesicle properties including size, morphology, concentration, and protein, nucleotide, and lipid content can influence EV separation parameters.[12, 15, 30, 48, 90, 91] Furthermore, the EV source fluid viscosity, protein profile, volume, and contaminants can affect process efficiency or resulting sample purity. For instance, a highly viscous source, such as blood plasma or cervical mucus, may not flow through microfluidics devices under the same conditions as urine, thus potentially influencing capture efficiency. As applications are considered, it is important to understand the EV sub-populations and contaminants present in each EV source. For instance, blood sample EV separations have demonstrated the highest level of contamination (proteins, non-vesicular membranous species, lipoproteins), which may influence downstream proteomics, lipidomics, or therapies.[92, 93] Even while considering the EV physical characteristics, source, and application, with the lack of comparison of EV isolation techniques and sources, it can be difficult to ascertain the optimal approach. This study aims to compare the effects of separation method and sEV source (urine or cervical mucus), on recovered sEV morphology, and RNA sequencing (miRNA) results. In particular, this study provides important preliminary data for the study of ovarian cancer diagnostic potential of urine- and cervical mucus-derived sEV miRNA. The ultimate aim of these investigations and those of the cohort is to determine which EV source is optimal for downstream predictive ovarian cancer diagnostics and to optimize EV separation for that source.

The Case for Urine-derived EVs

Urine was chosen first for EV investigation as it has become a popular choice for EV study due to its availability and ease of collection. Urine-derived EVs have been characterized by morphology, proteome, and miRNA content numerous times, providing an abundance of information for comparison.[42, 52, 94] Furthermore, ultracentrifugation, size exclusion, microfluidics, polymer precipitation, and immunoaffinity separation approaches have been used to isolate urine-derived EVs.[20, 52, 56, 95, 96] Given the lack of standards within the EV community, size characterization and quantification of urinary EVs appears heavily dependent on isolation protocol, purification steps, sample preparation, and characterization method. However, when developed under identical protocols, different size distribution and concentrations of urinary EVs could indicate underlying disease states.[42] Urinary EVs may be particularly useful for downstream miRNA analysis as the abundant protein content in urine does not prohibit RNA extraction[43] and extravesicular RNA does not tend to co-precipitate with urinary EVs.[43, 97] Moreover, publications have identified more than 5,000 urinary EV proteins (many of which can be analyzed online at EVpedia and Vesiclepedia) that researchers can investigate further as potential biomarkers.[42] Compared to other body fluids, urine and blood have amassed the most EV-related literature and, given the large amount of data available and ease of access, may be ideal for biomarker discovery and disease diagnostics.

Since plasma EVs cannot easily cross the glomerular filtration apparatus, the majority of urinary EVs are derived from the kidneys.[58] Based on the premise that EV

sources in close proximity to diseased tissue may allow for better diagnostic accuracy, most studies of urinary EV diagnostic potential have focused on urinary tract diseases.[20, 44, 45, 55, 97, 98] However, proteomics analysis of urinary EVs has demonstrated significant diagnostic potential for urogenital tract diseases, metastatic cancers, and non-urologic diseases. For instance, Wang et al found that SNAP23 and calbindin were elevated in Parkinson's Disease urinary EVs and predicted disease 86% of the time.[57] The suggestion that urinary EVs can be used to diagnose urogenital tract diseases is valid, but, likely due to glomerular filtration of proteins, urinary EVs may also have the potential to diagnose distant diseases or injuries, such as neurodegenerative diseases, cardiovascular diseases, liver injury, and cancers.[35, 57, 92, 95, 99, 100]

The early results of this study suggest that urine may be an excellent EV source for isolation techniques involving wicking or capillary movement. Initial TEM images of sample wicking on C-CP fiber-based films (Figure 4.1) demonstrated high similarity in EV capture and morphology between PBS-diluted standard exosomes (Figure 4.1a,b) and patient urine (Figure 4.1c,d) samples. Vesicles in both PBS-diluted standard exosomes and patient urine samples appeared to adhere to the film surface in large aggregates. Although, it remains to be seen if capturing vesicles in aggregates or with even surface distribution is more or less beneficial for easy vesicle detection. When compared to patient plasma wicked on C-CP films (Figure 4.1e,f), urine presented clearer and cleaner capture of EVs, suggesting that urine may be more compatible with wicking-based EV separation and capture. Plasma samples may require further purification or supplementation (to reduce protein contamination or viscosity) in this format in order to

wick and separate plasma sEVs. Analysis of the flow rates of the various matrices on C-CP films (see Figure 4.2) revealed that PBS-diluted standard exosomes and urine flow at significantly lower rates than PBS, but significantly higher rates than patient plasma and standard exosomes diluted in mock urine, reconstituted milk, or mock saliva. The presence of standard exosomes in PBS appeared to decrease the sample flow rate compared to PBS alone. The significant difference in flow rates of patient urine and mock urine suggests that the samples have significantly different composition. As the mock urine is not capable of representing the large range and variation of patient urine (especially in regard to water content and solute concentrations), the difference in flow rates is not surprising. Additionally, it seems unlikely that the urine collection preservatives (protease inhibitors and a bacteriostatic) may be altering the sample surface tension, viscosity, or interaction with the fiber surface. However, as urine samples can vary widely from patient to patient, more sample replicates would be required to make substantial claims.

Due to its widespread use, availability of proteomic information , compatibility with wicking and capillary flow applications, and diverse EV population, urine may act as an optimal EV source in most situations. However, as one of the primary goals of these investigations is to determine which EV source is optimal for downstream predictive ovarian cancer diagnosis, body fluids more closely associated with the female reproductive tract needed to be explored. While urine may provide heterogenous EV populations useful for a variety of applications, greater homogeneity in EV population

may provide enhanced diagnostic sensitivity for certain diseases. Hence, the next logical step was to investigate a body fluid with greater proximity to the ovaries.

The Case for Cervical Mucus-derived EVs

Recently, cervical mucus (CM) has generated interest as an EV source for diagnosis of diseases or injury in the female reproductive tract. Like urine, CM proximity to potential diseased areas (cervix, endometrial lining, ovaries, fallopian tubes, etc.) may allow for greater diagnostic specificity. While blood-derived EV disease diagnosis is promising, low specificity, heterogeneous EV populations, and EV sub-population masking by other EV populations may affect diagnostic accuracy in certain applications. In the case of ovarian cancer, the potential of CM specificity may outweigh diagnostic potential of more heterogenous EV population sources, such as blood and urine.

Although CM may be an appealing source of EVs for diagnosis, there has been very little investigation into CM-derived EVs by researchers. Since EVs are found in most body fluids[6, 101], are heavily involved in placental barrier communication during pregnancy[102, 103], and Flori et al. found that cervical mucus from pregnant and non-pregnant women contain membranous vesicles having exosome-like structure,[24] there is reasonable evidence that CM contains EVs. However, the CM-derived vesicle concentrations and characteristics are not well documented. With so little available information, it can be challenging to develop new protocols that produce consistent EV populations and downstream results from CM. However, the lack of CM-derived EV research offers an opportunity to expand understanding of EV separation, morphology,

and downstream analysis of CM. The practicality or ease of collection of CM may also generate concern, especially compared to urine; however, CM can be easily obtained during routine gynecological examinations.

In this study, initial analysis suggests that sEVs may be separated from CM in a similar fashion to urine. TEM imaging of urine and CM samples subjected to UC and glycerol elution (see Figure 4.5) all revealed small dimpled vesicles meeting the description of sEVs. The similarity in morphology between UC and glycerol elution samples for each sample type suggests that the glycerol elution method may provide an alternative to UC isolation. Furthermore, the similarity in morphology across CM UC and glycerol elution samples suggests that CM may be compatible with chromatography techniques despite high sample viscosity.

After literature investigation and experimental demonstration of CM sEV separation, the potential of CM sEV downstream analysis needed to be investigated. With an eye toward comparison of urine and CM downstream analyses and ensuing OC diagnostics investigations, an sEV miRNA sequencing pilot study was designed to examine miRNA differential expression of cancerous and benign urine and CM sEV samples.

Comparison of urine- and CM-derived EV miRNA sequencing

Urine and CM-derived EV samples were prepared via UC prior to miRNA isolation, sequencing, and analysis. The pilot study consisted of 2 cancerous urine-derived, 2 non-cancerous urine-derived, 2 cancerous CM-derived, and 2 non-cancerous

CM-derived EV samples with all 4 urine-derived and 4 CM-derived EV samples sourced from the same 4 patients (one urine and one CM sample from each patient). Although the sample sizes were not large enough to make conclusive statements, the pilot study allowed for assessment of sample source compatibility with the given protocol and provided small insights into the miRNA differential expression of urine- and CM-derived EVs.

Initial completion of quality control and observation of the PCA (see Figure 4.6) suggests that the UC method used here can produce viable urine- and CM-derived EVs for downstream miRNA analysis. A more thorough analysis of the quality and differential expression of miRNA may be required when developing or comparing new isolation methods. In this case, UC is already a well-established EV isolation protocol with many studies demonstrating viable miRNA analysis.[16, 19, 59, 65, 104] For this study, as CM-derived EVs have never been sequenced for miRNA, it was very important to verify miRNA quality in the CM-derived EV samples.

The pilot study PCA of benign and cancerous cervical mucus- or urine-derived sEV miRNA expression (see Figure 4.6), although based on small sample size, suggested that CM-derived EV miRNAs may cluster better into benign and cancerous groups than urine-derived EV miRNAs. Both urine- (Figure 4.7) and CM-derived (Figure 4.8) sEV miRNA profiles demonstrated several miRNAs that were highly differentially expressed and statistically different; however, the number of miRNAs meeting this criteria was much greater for CM-derived sEVs than urine-derived sEVs (CM-derived: 4 downregulated, 72 upregulated; Urine-derived: 2 downregulated, 5 upregulated).

Moreover, the maximum log2 fold change for CM-derived sEV miRNAs was 7.34 while the maximum log2 fold change for urine-derived sEV miRNAs was 3.85. It is unclear why the differentially expressed CM-derived sEV miRNAs are skewed toward upregulation, but a larger sample size would provide more extensive data and possible insights. It is notable that several of the miRNAs identified as highly expressed and highly differentially expressed in urine- and CM-derived sEVs were found in tumor-related literature (see Table 4.2 and Table 4.3). This suggests that both urine- and CM-derived sEVs may facilitate diagnosis of cancerous tumors using specific miRNA markers. However, the greater number of differentially expressed and statistically different miRNAs, and the greater maximum log2 fold change suggests that CM-derived sEVs may provide clearer demonstrations of benign and cancerous sEV miRNA differential expression. Thus, CM-derived sEV-identified miRNA markers may enable more accurate and specific downstream OC diagnoses than urine-derived sEV miRNA markers.

After discussion and comparison of urine- and CM-derived sEVs, CM-derived sEVs were chosen for a subsequent, more comprehensive miRNA study. The larger study group was comprised of 16 benign CM-derived sEV and 26 cancerous CM-derived sEV samples. Ideally, the control benign patient samples would comprise half of the group; however, the total number of potential benign CM samples were difficult to predict ahead of time as patients who were asked to supply samples were undergoing hysterectomies because they had ovarian tumors were not biopsied until after surgery. PCA of all 42 samples (see Figure 4.9) did not reveal distinct groupings between benign and cancerous.

Although this is concerning, especially regarding differential expression, more in-depth analysis of groupings based on cancer type, stage, and physical characteristics revealed more representative clustering. Early bioinformatics indicates that high-grade tumor sample cluster together, while low-grade tumor and benign samples are more similar in expression (see Figure 4.11). This may be an indication that low-grade tumors and benign samples may be more difficult to distinguish based on these parameters. As ovarian cancer is a highly heterogeneous disease, this is not surprising, and additional categorization beyond these simplistic cancerous and non-cancerous groupings will likely be required to fully characterize the complexities of the data. Concerning this observation, more research is ongoing to classify and discriminate characteristics between these groups to better analyze biomarker candidates. However, differential expression analysis of the 42 samples (see Figure 4.10) based on simple benign and cancerous groupings still provided insightful patterns and demonstrated significant miRNA upregulation (4 miRNAs) and downregulation (18 miRNAs). Significant differential expression, even with simple benign and cancerous groupings, is evidence that specific miRNA markers may be used either in single or multiplexed formats to identify ovarian cancer CM-derived sEVs. Similar to the pilot study, these 22 significantly differentially expressed miRNAs were cross-referenced with tumor-related literature and the markers that were highly differentially expressed and relevant to ovarian cancer were identified (see Table 4.4).

Of the markers identified, hsa-miR-184 was of particular interest as it was highly upregulated in both the pilot and 42-sample miRNA studies and early indications from

ongoing research suggest that it is also highly upregulated in the clustered high-grade tumor samples as compared to the low-grade tumor and benign samples. Further investigation into published research revealed that hsa-miR-184 has been identified as a potential prognostic marker in epithelial ovarian cancer.[105] Functionally, hsa-miR-184 has been categorized as a tumor suppressor for renal cell carcinoma, colorectal cancer, retinoblastoma, and epithelial ovarian cancer and, accordingly, is typically downregulated in these tumor environments.[105-107] While the exact mechanism is unclear, hsa-miR-184 appears to regulate cell proliferation, apoptosis, and inflammation.[105] However, this study suggests that hsa-miR-184 is highly upregulated in ovarian tumor sEVs, a marked difference from most investigations. This appears puzzling at first, but there are several rationales that may explain the disparity. First, no study has used sEV-derived miRNA to link hsa-miR-184 to a tumor environment. While sEV contents are derived from the cell cytoplasm, specific molecules are often selectively packaged into sEVs to direct exact cell communication.[4, 108, 109] Second, while most investigations have found that hsa-miR-184 is downregulated in tumor tissues, Chen et al.[106] found that tongue squamous cell carcinoma had upregulated levels of hsa-miR-184 compared to corresponding non-tumorous tissue and that upregulation of hsa-miR-184 may promote tongue squamous cell carcinoma migration and metastasis. Therefore, since sEVs are a mode of microenvironmental communication and are known to be involved in tumor microenvironment progression and metastasis, it is possible that hsa-miR-184, a potential promoter of cell migration and metastasis, may be released into the microenvironment where it could serve to promote disease spread. Lastly, the variety of types and stages of

ovarian cancer involved in this study may influence hsa-miR-184 expression. For instance, late stage (III/IV) epithelial ovarian cancer tissues have demonstrated lower hsa-miR-184 expression,[105] which may skew the differential expression results if samples are not more specifically categorized for analysis. While the intracellular mechanisms of hsa-miR-184 require further investigation, especially for therapeutic applications, hsa-miR-184 differential expression and its known involvement in ovarian cancer mechanisms may prove to be a useful biomarker for diagnostic or disease progression monitoring applications. It is hoped that more insight into this possible biomarker and the discovery of others may be realized during an ongoing Phase II patient study that focuses on patients who have identified BRCA1 mutations.

Frequently denoted as BRCA1 "positive," a mutation in the BRCA1 tumor suppressor gene is associated with a much higher risk of developing ovarian, breast, fallopian tube, peritoneal, and pancreatic cancer.[110] As a result of a BRCA1 mutation, the homologous recombination system responsible for repairing double strand DNA breaks may fail and cell cycle arrest may be impaired with consequence of a higher risk of tumor development.[111] For women with a BRCA1 mutation, the lifetime risk of developing OC is 40% and late stage OC discovery survival rates remain low.[110] In the currently ongoing study, cervical mucus samples from patients undergoing prophylactic surgery as well as those with tumors, both cancerous and non-cancerous, will be processed for EV isolation for subsequent characterization via RNA sequencing and proteomics. The resulting miRNA expression and protein data from these samples will be used to identify novel protein biomarkers for early stage OC. Moreover, machine learning algorithms are being

constructed that will be used to correlate miRNA and protein expression data to uncover specific biological pathways involved in tumor initiation and progression. In this manner, intermediary proteins may be identified that may prove to be diagnostically useful biomarkers or potential cancer therapy targets.

Sample source selection and OC sEV diagnostic potential

These investigations have compared the resultant sEV morphology and miRNA profiles for different sEV separation methodologies and sample sources (urine and cervical mucus). The apparent distinctions between urine and CM-derived sEVs, particularly concerning miRNA expression, highlight the need to consider sample source when selecting sEV separation method, downstream analysis, and biomarker discovery. Both urine- and CM-based diagnostic approaches have great potential and are worthy of consideration for downstream sEV analysis. However, for these investigations, CM was chosen based on proximity to the cancer origin and preliminary results. Resulting sEV miRNA data suggests that CM-derived sEV miRNA sequencing can be used to construct a panel of OC diagnostic biomarkers. With the correct sEV isolation methods, CM-derived sEV miRNA may deliver a simple test that could be seamlessly integrated into routine gynecological examinations. Such a test would greatly increase the number of early-stage OC diagnoses and potentially increase the average 5-year survival rate of OC patients. While the lofty aims of this assay are still far from accomplished, future investigations are being designed to address the diagnostic accuracy of specific biomarkers. These investigations should include more CM-derived sEV miRNA sequencing and analysis, CM-derived sEV proteomics analysis, CM-derived sEV C-CP

film-based separation, and colorimetric assay development. Continued development of C-CP film-based sEV isolation could benefit from even sample application and increased wicking capacity using sample and absorption pads (similar to standard lateral flow assays, e.g. pregnancy test strips). Uniform sample application and wicking would improve the consistency of C-CP film-based sEV separation and elucidate the prospects of the sEV isolation strategy for use in diagnostics. Further transcriptomics and proteomics investigations should focus on clustering patients based on carcinoma subtype or underlying pathophysiology and analyzing data using bioinformatic machine learning algorithms to reveal expression patterns. These expression patterns may then be used to develop a panel of diagnostic biomarkers to predict OC occurrence. Paired with the appropriate sEV isolation, predictive OC biomarkers could lead to more accurate, easier to perform, and inexpensive OC detection assays. Clinical translation of this technology has the potential to reach clinical or home settings and would truly revolutionize early cancer detection and improve cancer survival rates for one of the deadliest cancers for women.

References

1. Robinson MD, Oshlack A. A scaling normalization method for differential expression analysis of RNA-seq data. *Genome Biol*. 2010;11(3):R25. doi:10.1186/gb-2010-11-3-r25

2. Hessvik NP, Llorente A. Current knowledge on exosome biogenesis and release. *Cell Mol Life Sci*. 01 2018;75(2):193-208. doi:10.1007/s00018-017-2595-9

3. Rashed M, Bayraktar E, Helal G, et al. Exosomes: From Garbage Bins to Promising Therapeutic Targets. Review. *International Journal of Molecular Sciences*. MAR 2017 2017;18(3)ARTN 538. doi:10.3390/ijms18030538

4. Abels ER, Breakefield XO. Introduction to Extracellular Vesicles: Biogenesis, RNA Cargo Selection, Content, Release, and Uptake. *Cell Mol Neurobiol*. Apr 2016;36(3):301-12. doi:10.1007/s10571-016-0366-z

5. Johnsen KB, Gudbergsson JM, Skov MN, Pilgaard L, Moos T, Duroux M. A comprehensive overview of exosomes as drug delivery vehicles - endogenous nanocarriers for targeted cancer therapy. *Biochim Biophys Acta*. Aug 2014;1846(1):75-87. doi:10.1016/j.bbcan.2014.04.005

6. Li X, Wang X. The emerging roles and therapeutic potential of exosomes in epithelial ovarian cancer. Review. *Molecular Cancer*. MAY 15 2017 2017;16ARTN 92. doi:10.1186/s12943-017-0659-y

7. Lötvall J, Hill AF, Hochberg F, et al. Minimal experimental requirements for definition of extracellular vesicles and their functions: a position statement from the International Society for Extracellular Vesicles. *J Extracell Vesicles*. 2014;3:26913.

8. Théry C, Witwer KW, Aikawa E, et al. Minimal information for studies of extracellular vesicles 2018 (MISEV2018): a position statement of the International Society for Extracellular Vesicles and update of the MISEV2014 guidelines. *J Extracell Vesicles*. 2018;7(1):1535750. doi:10.1080/20013078.2018.1535750

9. Li P, Kaslan M, Lee SH, Yao J, Gao Z. Progress in Exosome Isolation Techniques. *Theranostics*. 2017;7(3):789-804. doi:10.7150/thno.18133

10. Zeringer E, Barta T, Li M, Vlassov AV. Strategies for isolation of exosomes. *Cold Spring Harb Protoc*. Apr 2015;2015(4):319-23. doi:10.1101/pdb.top074476

11. Momen-Heravi F, Balaj L, Alian S, et al. Current methods for the isolation of extracellular vesicles. *Biol Chem*. Oct 2013;394(10):1253-62. doi:10.1515/hsz-2013-0141

12. Helwa I, Cai J, Drewry M, et al. A Comparative Study of Serum Exosome Isolation Using Differential Ultracentrifugation and Three Commercial Reagents. Article. *Plos One*. JAN 23 2017 2017;12(1)ARTN e0170628. doi:10.1371/journal.pone.0170628

13. Théry C, Amigorena S, Raposo G, Clayton A. Isolation and characterization of exosomes from cell culture supernatants and biological fluids. *Curr Protoc Cell Biol*. Apr 2006;Chapter 3:Unit 3.22. doi:10.1002/0471143030.cb0322s30

14. Konoshenko MY, Lekchnov EA, Vlassov AV, Laktionov PP. Isolation of Extracellular Vesicles: General Methodologies and Latest Trends. *Biomed Res Int*. 2018;2018:8545347. doi:10.1155/2018/8545347

15. Patel GK, Khan MA, Zubair H, et al. Comparative analysis of exosome isolation methods using culture supernatant for optimum yield, purity and downstream applications. *Sci Rep*. Mar 2019;9(1):5335. doi:10.1038/s41598-019-41800-2

16. Tauro BJ, Greening DW, Mathias RA, et al. Comparison of ultracentrifugation, density gradient separation, and immunoaffinity capture methods for isolating human colon cancer cell line LIM1863-derived exosomes. *Methods*. Feb 2012;56(2):293-304. doi:10.1016/j.ymeth.2012.01.002

17. Livshits MA, Livshts MA, Khomyakova E, et al. Isolation of exosomes by differential centrifugation: Theoretical analysis of a commonly used protocol. *Sci Rep*. Nov 2015;5:17319. doi:10.1038/srep17319

18. An M, Wu J, Zhu J, Lubman DM. Comparison of an Optimized Ultracentrifugation Method versus Size-Exclusion Chromatography for Isolation of Exosomes from Human Serum. *J Proteome Res*. Oct 2018;17(10):3599-3605. doi:10.1021/acs.jproteome.8b00479

19. Tang YT, Huang YY, Zheng L, et al. Comparison of isolation methods of exosomes and exosomal RNA from cell culture medium and serum. *Int J Mol Med*. Sep 2017;40(3):834-844. doi:10.3892/ijmm.2017.3080

20. Lee J, McKinney KQ, Pavlopoulos AJ, et al. Altered Proteome of Extracellular Vesicles Derived from Bladder Cancer Patients Urine. *Mol Cells*. Mar 2018;41(3):179-187. doi:10.14348/molcells.2018.2110

21. Lamparski HG, Metha-Damani A, Yao JY, et al. Production and characterization of clinical grade exosomes derived from dendritic cells. *J Immunol Methods*. Dec 2002;270(2):211-26.

22. Tatischeff I, Lavialle F, Pigaglio-Deshayes S, Péchoux-Longin C, Chinsky L, Alfsen A. Dictyostelium extracellular vesicles containing hoechst 33342 transfer the dye into the nuclei of living cells: a fluorescence study. *J Fluoresc*. Mar 2008;18(2):319-28. doi:10.1007/s10895-007-0271-4

23. Soares Martins T, Catita J, Martins Rosa I, A B da Cruz E Silva O, Henriques AG. Exosome isolation from distinct biofluids using precipitation and column-based approaches. *PLoS One*. 2018;13(6):e0198820. doi:10.1371/journal.pone.0198820

24. Flori F, Secciani F, Capone A, et al. Menstrual cycle-related sialidase activity of the female cervical mucus is associated with exosome-like vesicles. *Fertil Steril*. Oct 2007;88(4 Suppl):1212-9. doi:10.1016/j.fertnstert.2007.01.209

25. Urbanelli L, Buratta S, Sagini K, Ferrara G, Lanni M, Emiliani C. Exosome-based strategies for Diagnosis and Therapy. *Recent Pat CNS Drug Discov*. 2015;10(1):10-27.

26. Diaz G, Bridges C, Lucas M, et al. Protein Digestion, Ultrafiltration, and Size Exclusion Chromatography to Optimize the Isolation of Exosomes from Human Blood Plasma and Serum. *J Vis Exp*. 04 2018;(134)doi:10.3791/57467

27. Benedikter BJ, Bouwman FG, Vajen T, et al. Ultrafiltration combined with size exclusion chromatography efficiently isolates extracellular vesicles from cell culture media for compositional and functional studies. *Sci Rep*. Nov 2017;7(1):15297. doi:10.1038/s41598-017-15717-7

28. Nordin JZ, Lee Y, Vader P, et al. Ultrafiltration with size-exclusion liquid chromatography for high yield isolation of extracellular vesicles preserving intact biophysical and functional properties. *Nanomedicine*. May 2015;11(4):879-83. doi:10.1016/j.nano.2015.01.003

29. Xu R, Simpson RJ, Greening DW. A Protocol for Isolation and Proteomic Characterization of Distinct Extracellular Vesicle Subtypes by Sequential Centrifugal Ultrafiltration. *Methods Mol Biol*. 2017;1545:91-116. doi:10.1007/978-1-4939-6728-5_7

30. Heinemann ML, Ilmer M, Silva LP, et al. Benchtop isolation and characterization of functional exosomes by sequential filtration. *J Chromatogr A*. Dec 2014;1371:125-35. doi:10.1016/j.chroma.2014.10.026

31. He M, Crow J, Roth M, Zeng Y, Godwin AK. Integrated immunoisolation and protein analysis of circulating exosomes using microfluidic technology. *Lab Chip*. Oct 2014;14(19):3773-80. doi:10.1039/c4lc00662c

32. Kanwar SS, Dunlay CJ, Simeone DM, Nagrath S. Microfluidic device (ExoChip) for on-chip isolation, quantification and characterization of circulating exosomes. *Lab Chip*. Jun 2014;14(11):1891-900. doi:10.1039/c4lc00136b

33. Oksvold MP, Neurauter A, Pedersen KW. Magnetic bead-based isolation of exosomes. *Methods Mol Biol*. 2015;1218:465-81. doi:10.1007/978-1-4939-1538-5_27

34. Zhang P, He M, Zeng Y. Ultrasensitive microfluidic analysis of circulating exosomes using a nanostructured graphene oxide/polydopamine coating. *Lab Chip*. 08 2016;16(16):3033-42. doi:10.1039/c6lc00279j

35. Mathivanan S, Lim JW, Tauro BJ, Ji H, Moritz RL, Simpson RJ. Proteomics analysis of A33 immunoaffinity-purified exosomes released from the human colon tumor cell line LIM1215 reveals a tissue-specific protein signature. *Mol Cell Proteomics*. Feb 2010;9(2):197-208. doi:10.1074/mcp.M900152-MCP200

36. Ueda K, Ishikawa N, Tatsuguchi A, Saichi N, Fujii R, Nakagawa H. Antibody-coupled monolithic silica microtips for highthroughput molecular profiling of circulating exosomes. *Sci Rep*. Aug 2014;4:6232. doi:10.1038/srep06232

37. Haney MJ, Klyachko NL, Zhao Y, et al. Exosomes as drug delivery vehicles for Parkinson's disease therapy. *J Control Release*. Jun 2015;207:18-30. doi:10.1016/j.jconrel.2015.03.033

38. Chen Y, Li G, Liu ML. Microvesicles as Emerging Biomarkers and Therapeutic Targets in Cardiometabolic Diseases. *Genomics Proteomics Bioinformatics*. 02 2018;16(1):50-62. doi:10.1016/j.gpb.2017.03.006

39. Soria FN, Pampliega O, Bourdenx M, Meissner WG, Bezard E, Dehay B. Exosomes, an Unmasked Culprit in Neurodegenerative Diseases. *Front Neurosci*. 2017;11:26. doi:10.3389/fnins.2017.00026

40. Reid BM, Permuth JB, Sellers TA. Epidemiology of ovarian cancer: a review. *Cancer Biol Med*. Feb 2017;14(1):9-32. doi:10.20892/j.issn.2095-3941.2016.0084

41. Pisitkun T, Shen RF, Knepper MA. Identification and proteomic profiling of exosomes in human urine. *Proc Natl Acad Sci U S A*. Sep 2004;101(36):13368-73. doi:10.1073/pnas.0403453101

42. Merchant ML, Rood IM, Deegens JKJ, Klein JB. Isolation and characterization of urinary extracellular vesicles: implications for biomarker discovery. *Nat Rev Nephrol*. Dec 2017;13(12):731-749. doi:10.1038/nrneph.2017.148

43. Lv LL, Cao Y, Liu D, et al. Isolation and quantification of microRNAs from urinary exosomes/microvesicles for biomarker discovery. *Int J Biol Sci*. 2013;9(10):1021-31. doi:10.7150/ijbs.6100

44. Skotland T, Ekroos K, Kauhanen D, et al. Molecular lipid species in urinary exosomes as potential prostate cancer biomarkers. *Eur J Cancer*. 01 2017;70:122-132. doi:10.1016/j.ejca.2016.10.011

45. McKiernan J, Donovan MJ, O'Neill V, et al. A Novel Urine Exosome Gene Expression Assay to Predict High-grade Prostate Cancer at Initial Biopsy. *JAMA Oncol*. Jul 2016;2(7):882-9. doi:10.1001/jamaoncol.2016.0097

46. Huang T, Deng CX. Current Progresses of Exosomes as Cancer Diagnostic and Prognostic Biomarkers. *Int J Biol Sci*. 2019;15(1):1-11. doi:10.7150/ijbs.27796

47. Qin W, Tsukasaki Y, Dasgupta S, Mukhopadhyay N, Ikebe M, Sauter ER. Exosomes in Human Breast Milk Promote EMT. *Clin Cancer Res*. Sep 2016;22(17):4517-24. doi:10.1158/1078-0432.CCR-16-0135

48. de la Torre Gomez C, Goreham RV, Bech Serra JJ, Nann T, Kussmann M. "Exosomics"-A Review of Biophysics, Biology and Biochemistry of Exosomes With a Focus on Human Breast Milk. *Front Genet*. 2018;9:92. doi:10.3389/fgene.2018.00092

49. Davis ME. Exosomes: What Do We Love So Much About Them? *Circ Res*. 12 2016;119(12):1280-1282. doi:10.1161/CIRCRESAHA.116.309942

50. Nakamura K, Sawada K, Yoshimura A, Kinose Y, Nakatsuka E, Kimura T. Clinical relevance of circulating cell-free microRNAs in ovarian cancer. Review. *Molecular Cancer*. JUN 24 2016 2016;15ARTN 48. doi:10.1186/s12943-016-0536-0

51. Properzi F, Logozzi M, Fais S. Exosomes: the future of biomarkers in medicine. *Biomark Med*. Oct 2013;7(5):769-78. doi:10.2217/bmm.13.63

52. Li M, Zeringer E, Barta T, Schageman J, Cheng A, Vlassov AV. Analysis of the RNA content of the exosomes derived from blood serum and urine and its potential as biomarkers. *Philos Trans R Soc Lond B Biol Sci*. Sep 2014;369(1652)doi:10.1098/rstb.2013.0502

53. Fernández-Llama P, Khositseth S, Gonzales PA, Star RA, Pisitkun T, Knepper MA. Tamm-Horsfall protein and urinary exosome isolation. *Kidney Int*. Apr 2010;77(8):736-42. doi:10.1038/ki.2009.550

54. Xu X, Barreiro K, Musante L, et al. Management of Tamm-Horsfall Protein for Reliable Urinary Analytics. *Proteomics Clin Appl*. 11 2019;13(6):e1900018. doi:10.1002/prca.201900018

55. Bandu R, Oh JW, Kim KP. Mass spectrometry-based proteome profiling of extracellular vesicles and their roles in cancer biology. *Exp Mol Med*. Mar 2019;51(3):30. doi:10.1038/s12276-019-0218-2

56. Channavajjhala SK, Rossato M, Morandini F, et al. Optimizing the purification and analysis of miRNAs from urinary exosomes. *Clin Chem Lab Med*. Mar 2014;52(3):345-54. doi:10.1515/cclm-2013-0562

57. Wang S, Kojima K, Mobley JA, West AB. Proteomic analysis of urinary extracellular vesicles reveal biomarkers for neurologic disease. *EBioMedicine*. Jul 2019;45:351-361. doi:10.1016/j.ebiom.2019.06.021

58. Barros ER, Carvajal CA. Urinary Exosomes and Their Cargo: Potential Biomarkers for Mineralocorticoid Arterial Hypertension? *Front Endocrinol (Lausanne)*. 2017;8:230. doi:10.3389/fendo.2017.00230

59. Rekker K, Saare M, Roost AM, et al. Comparison of serum exosome isolation methods for microRNA profiling. *Clin Biochem*. Jan 2014;47(1-2):135-8. doi:10.1016/j.clinbiochem.2013.10.020

60. Boukouris S, Mathivanan S. Exosomes in bodily fluids are a highly stable resource of disease biomarkers. *Proteomics Clin Appl*. Apr 2015;9(3-4):358-67. doi:10.1002/prca.201400114

61. Eichelser C, Stückrath I, Müller V, et al. Increased serum levels of circulating exosomal microRNA-373 in receptor-negative breast cancer patients. *Oncotarget*. Oct 2014;5(20):9650-63. doi:10.18632/oncotarget.2520

62. Beach A, Zhang H, Ratajczak M, Kakar S. Exosomes: an overview of biogenesis, composition and role in ovarian cancer. Review. *Journal of Ovarian Research*. JAN 25 2014 2014;7ARTN 14. doi:10.1186/1757-2215-7-14

63. Dixon CL, Sheller-Miller S, Saade GR, et al. Amniotic Fluid Exosome Proteomic Profile Exhibits Unique Pathways of Term and Preterm Labor. *Endocrinology*. 05 2018;159(5):2229-2240. doi:10.1210/en.2018-00073

64. Antounians L, Tzanetakis A, Pellerito O, et al. The Regenerative Potential of Amniotic Fluid Stem Cell Extracellular Vesicles: Lessons Learned by Comparing Different Isolation Techniques. *Sci Rep*. 02 2019;9(1):1837. doi:10.1038/s41598-018-38320-w

65. Grigor'eva AE, Tamkovich SN, Eremina AV, et al. [Characteristics of exosomes andmicroparticles discovered in human tears]. *Biomed Khim*. 2016 Jan-Feb 2016;62(1):99-106. doi:10.18097/PBMC20166201099

66. Street JM, Barran PE, Mackay CL, et al. Identification and proteomic profiling of exosomes in human cerebrospinal fluid. *J Transl Med*. Jan 2012;10:5. doi:10.1186/1479-5876-10-5

67. Stuendl A, Kunadt M, Kruse N, et al. Induction of α-synuclein aggregate formation by CSF exosomes from patients with Parkinson's disease and dementia with Lewy bodies. *Brain*. Feb 2016;139(Pt 2):481-94. doi:10.1093/brain/awv346

68. Chiasserini D, van Weering JR, Piersma SR, et al. Proteomic analysis of cerebrospinal fluid extracellular vesicles: a comprehensive dataset. *J Proteomics*. Jun 2014;106:191-204. doi:10.1016/j.jprot.2014.04.028

69. Khan LB, Read HM, Ritchie SR, Proft T. Artificial Urine for Teaching Urinalysis Concepts and Diagnosis of Urinary Tract Infection in the Medical Microbiology Laboratory. *J Microbiol Biol Educ*. 2017;18(2)doi:10.1128/jmbe.v18i2.1325

70. Burdette CQ, Marcus RK. Solid phase extraction of proteins from buffer solutions employing capillary-channeled polymer (C-CP) fibers as the stationary phase. *Analyst*. Feb 2013;138(4):1098-106. doi:10.1039/c2an36126d

71. Robinson MD, McCarthy DJ, Smyth GK. edgeR: a Bioconductor package for differential expression analysis of digital gene expression data. *Bioinformatics*. Jan 2010;26(1):139-40. doi:10.1093/bioinformatics/btp616

72. Cheng L, Wu S, Zhang K, Qing Y, Xu T. A comprehensive overview of exosomes in ovarian cancer: emerging biomarkers and therapeutic strategies. *J Ovarian Res*. Nov 2017;10(1):73. doi:10.1186/s13048-017-0368-6

73. American Cancer Society. Ovarian Cancer: Early Detection, Diagnosis, and Staging.

74. Elias KM, Guo J, Bast RC. Early Detection of Ovarian Cancer. *Hematol Oncol Clin North Am*. 12 2018;32(6):903-914. doi:10.1016/j.hoc.2018.07.003

75. Besse B, Charrier M, Lapierre V, et al. Dendritic cell-derived exosomes as maintenance immunotherapy after first line chemotherapy in NSCLC. *Oncoimmunology*. Apr 2016;5(4):e1071008. doi:10.1080/2162402X.2015.1071008

76. Dai S, Wei D, Wu Z, et al. Phase I clinical trial of autologous ascites-derived exosomes combined with GM-CSF for colorectal cancer. *Mol Ther*. Apr 2008;16(4):782-90. doi:10.1038/mt.2008.1

77. Escudier B, Dorval T, Chaput N, et al. Vaccination of metastatic melanoma patients with autologous dendritic cell (DC) derived-exosomes: results of thefirst phase I clinical trial. *J Transl Med*. Mar 2005;3(1):10. doi:10.1186/1479-5876-3-10

78. Morse MA, Garst J, Osada T, et al. A phase I study of dexosome immunotherapy in patients with advanced non-small cell lung cancer. *J Transl Med*. Feb 2005;3(1):9. doi:10.1186/1479-5876-3-9

79. Nassar W, El-Ansary M, Sabry D, et al. Umbilical cord mesenchymal stem cells derived extracellular vesicles can safely ameliorate the progression of chronic kidney diseases. *Biomater Res*. 2016;20:21. doi:10.1186/s40824-016-0068-0

80. Chen YS, Lin EY, Chiou TW, Harn HJ. Exosomes in clinical trial and their production in compliance with good manufacturing practice. *Ci Ji Yi Xue Za Zhi*. 2019 Apr-Jun 2019;32(2):113-120. doi:10.4103/tcmj.tcmj_182_19

81. Wang J, Hendrix A, Hernot S, et al. Bone marrow stromal cell-derived exosomes as communicators in drug resistance in multiple myeloma cells. *Blood*. Jul 2014;124(4):555-66. doi:10.1182/blood-2014-03-562439

82. Zhang W, Bai X, Zhao B, et al. Cell-free therapy based on adipose tissue stem cell-derived exosomes promotes wound healing via the PI3K/Akt signaling pathway. *Exp Cell Res*. Sep 2018;370(2):333-342. doi:10.1016/j.yexcr.2018.06.035

83. Alvarez-Erviti L, Seow Y, Yin H, Betts C, Lakhal S, Wood MJ. Delivery of siRNA to the mouse brain by systemic injection of targeted exosomes. *Nat Biotechnol*. Apr 2011;29(4):341-5. doi:10.1038/nbt.1807

84. Kim MS, Haney MJ, Zhao Y, et al. Engineering macrophage-derived exosomes for targeted paclitaxel delivery to pulmonary metastases: in vitro and in vivo evaluations. *Nanomedicine*. Jan 2018;14(1):195-204. doi:10.1016/j.nano.2017.09.011

85. El-Andaloussi S, Lee Y, Lakhal-Littleton S, et al. Exosome-mediated delivery of siRNA in vitro and in vivo. Article. *Nature Protocols*. DEC 2012 2012;7(12):2112-2126. doi:10.1038/nprot.2012.131

86. Sahoo S, Klychko E, Thorne T, et al. Exosomes from human CD34(+) stem cells mediate their proangiogenic paracrine activity. *Circ Res*. Sep 2011;109(7):724-8. doi:10.1161/CIRCRESAHA.111.253286

87. Mineo M, Garfield SH, Taverna S, et al. Exosomes released by K562 chronic myeloid leukemia cells promote angiogenesis in a Src-dependent fashion. *Angiogenesis*. Mar 2012;15(1):33-45. doi:10.1007/s10456-011-9241-1

88. Soo CY, Song Y, Zheng Y, et al. Nanoparticle tracking analysis monitors microvesicle and exosome secretion from immune cells. *Immunology*. Jun 2012;136(2):192-7. doi:10.1111/j.1365-2567.2012.03569.x

89. Tatischeff I, Larquet E, Falcón-Pérez JM, Turpin PY, Kruglik SG. Fast characterisation of cell-derived extracellular vesicles by nanoparticles tracking analysis, cryo-electron microscopy, and Raman tweezers microspectroscopy. *J Extracell Vesicles*. 2012;1doi:10.3402/jev.v1i0.19179

90. Enderle D, Spiel A, Coticchia CM, et al. Characterization of RNA from Exosomes and Other Extracellular Vesicles Isolated by a Novel Spin Column-Based Method. *PLoS One*. 2015;10(8):e0136133. doi:10.1371/journal.pone.0136133

91. Wang Z, Wu HJ, Fine D, et al. Ciliated micropillars for the microfluidic-based isolation of nanoscale lipid vesicles. *Lab Chip*. Aug 2013;13(15):2879-82. doi:10.1039/c3lc41343h

92. Grigor'eva AE, Dyrkheeva NS, Bryzgunova OE, Tamkovich SN, Chelobanov BP, Ryabchikova EI. [Contamination of exosome preparations, isolated from biological fluids]. *Biomed Khim*. Jan 2017;63(1):91-96. doi:10.18097/PBMC2017630191

93. Karimi N, Cvjetkovic A, Jang SC, et al. Detailed analysis of the plasma extracellular vesicle proteome after separation from lipoproteins. *Cell Mol Life Sci*. 08 2018;75(15):2873-2886. doi:10.1007/s00018-018-2773-4

94. Vlassov AV, Magdaleno S, Setterquist R, Conrad R. Exosomes: current knowledge of their composition, biological functions, and diagnostic and therapeutic potentials. *Biochim Biophys Acta*. Jul 2012;1820(7):940-8. doi:10.1016/j.bbagen.2012.03.017

95. Li Y, Zhang Y, Qiu F, Qiu Z. Proteomic identification of exosomal LRG1: a potential urinary biomarker for detecting NSCLC. *Electrophoresis*. Aug 2011;32(15):1976-83. doi:10.1002/elps.201000598

96. Cheruvanky A, Zhou H, Pisitkun T, et al. Rapid isolation of urinary exosomal biomarkers using a nanomembrane ultrafiltration concentrator. *Am J Physiol Renal Physiol*. May 2007;292(5):F1657-61. doi:10.1152/ajprenal.00434.2006

97. Miranda KC, Bond DT, McKee M, et al. Nucleic acids within urinary exosomes/microvesicles are potential biomarkers for renal disease. *Kidney Int*. Jul 2010;78(2):191-9. doi:10.1038/ki.2010.106

98. Di Meo A, Bartlett J, Cheng Y, Pasic MD, Yousef GM. Liquid biopsy: a step forward towards precision medicine in urologic malignancies. *Mol Cancer*. 04 2017;16(1):80. doi:10.1186/s12943-017-0644-5

99. Sato K, Meng F, Glaser S, Alpini G. Exosomes in liver pathology. *J Hepatol*. 07 2016;65(1):213-221. doi:10.1016/j.jhep.2016.03.004

100. Sung S, Kim J, Jung Y. Liver-Derived Exosomes and Their Implications in Liver Pathobiology. *Int J Mol Sci*. Nov 2018;19(12)doi:10.3390/ijms19123715

101. Li A, Zhang T, Zheng M, Liu Y, Chen Z. Exosomal proteins as potential markers of tumor diagnosis. *J Hematol Oncol*. 12 2017;10(1):175. doi:10.1186/s13045-017-0542-8

102. Saadeldin IM, Oh HJ, Lee BC. Embryonic-maternal cross-talk via exosomes: potential implications. *Stem Cells Cloning*. 2015;8:103-7. doi:10.2147/SCCAA.S84991

103. Mitchell MD, Peiris HN, Kobayashi M, et al. Placental exosomes in normal and complicated pregnancy. *Am J Obstet Gynecol*. Oct 2015;213(4 Suppl):S173-81. doi:10.1016/j.ajog.2015.07.001

104. Lässer C, Eldh M, Lötvall J. Isolation and characterization of RNA-containing exosomes. *J Vis Exp*. Jan 2012;(59):e3037. doi:10.3791/3037

105. Qin CZ, Lou XY, Lv QL, et al. MicroRNA-184 acts as a potential diagnostic and prognostic marker in epithelial ovarian cancer and regulates cell proliferation, apoptosis and inflammation. *Pharmazie*. Oct 2015;70(10):668-73.

106. Chen D, Li J, Li S, et al. miR-184 promotes cell proliferation in tongue squamous cell carcinoma by targeting SOX7. *Oncol Lett*. Aug 2018;16(2):2221-2228. doi:10.3892/ol.2018.8906

107. He TG, Xiao ZY, Xing YQ, Yang HJ, Qiu H, Chen JB. Tumor Suppressor miR-184 Enhances Chemosensitivity by Directly Inhibiting SLC7A5 in Retinoblastoma. *Front Oncol*. 2019;9:1163. doi:10.3389/fonc.2019.01163

108. Colombo M, Moita C, van Niel G, et al. Analysis of ESCRT functions in exosome biogenesis, composition and secretion highlights the heterogeneity of extracellular vesicles. *J Cell Sci*. Dec 2013;126(Pt 24):5553-65. doi:10.1242/jcs.128868

109. Tricarico C, Clancy J, D'Souza-Schorey C. Biology and biogenesis of shed microvesicles. *Small GTPases*. 10 2017;8(4):220-232. doi:10.1080/21541248.2016.1215283

110. Doubeni CA, Doubeni AR, Myers AE. Diagnosis and Management of Ovarian Cancer. *Am Fam Physician*. Jun 2016;93(11):937-44.

111. Toss A, Tomasello C, Razzaboni E, et al. Hereditary ovarian cancer: not only BRCA 1 and 2 genes. *Biomed Res Int*. 2015;2015:341723. doi:10.1155/2015/341723

CHAPTER 5:
CONCLUSIONS

The primary goal of these studies is to ultimately create a "liquid biopsy" system for exosome-based diagnosis of ovarian cancer. Exosomes are an excellent "liquid biopsy" candidate species as they are found in a variety of body fluids, making invasive or surgical diagnostic procedures unnecessary. In addition, they are inherently more stable than other liquid biopsy targets, such as free DNA, RNA, and proteins. While promising, exosome applications have been limited by inconsistent, expensive and time-consuming isolation techniques. To alleviate this problem, we have developed a PET C-CP fiber-based EV isolation method that is quick and inexpensive and have compared it to standard EV isolation protocols.

For ovarian cancer diagnostics to be possible using this new isolation platform, we must devise methods of selective EV isolation based on specific EV-associated ovarian cancer biomarkers. These efforts will require the use of model sEVs derived from normal and malignant ovarian cells. To this end, we have engineered a model system consisting of two ovarian cell lines, one normal and one cancerous, to produce green and red fluorescent sEVs, respectively, that may be employed in the testing and optimization of the PET C-CP EV isolation platform for specific sEV capture. The model sEVs can be easily visualized via fluorescence microscopy and provide a simple, cost-effective, consistent system to verify specificity and sensitivity of antibodies to OC biomarker proteins grafted to the PET C-CP fiber surfaces for use in lateral flow-based diagnostics

for OC. In order to ensure selective capture potential and imaging compatibility, the model EVs were generically captured on the PET C-CP fibers and selectively captured on nitrocellulose using ovarian cancer marker-specific antibodies.

With future experiments in mind, we demonstrated that urine or cervical mucus can be used as a sample source for EV isolation and for EV miRNA differential expression analysis. The miRNA data collected during these investigations and in ongoing proteomics investigation will be used to identify novel ovarian cancer EV biomarkers. Additionally, a new clinical investigation of BRCA1 mutation patients with or without ovarian cancer of varying stages will continue to bolster biomarker discovery. Newly discovered ovarian cancer biomarkers will be incorporated into the new PET C-CP platform selective EV capture method to improve early ovarian cancer detection. To support clinical translation of the PET C-CP fiber technology, a PET C-CP fiber-based film is being refined to capture and detect ovarian cancer EVs as a colorimetric lateral flow assay, similar to a pregnancy test. With a new EV isolation method, model sEVs designed to test it, a protocol for ovarian cancer biomarker identification and incorporation, we have a clear path toward clinical translation. Future work will focus on the development of a prototype for a quick, inexpensive, and easy-to-use colorimetric ovarian cancer diagnostic test that can be routinely performed in the clinical or home setting.

APPENDICES

APPENDIX A:
EXTRACELLULAR VESICLE CHARACTERIZATION IN BUFFERS

Materials and Methods

Extracellular Vesicles (EV) isolation

Caov-3 cells were grown to 80% confluency, refreshed with new media, and incubated for 3 days. Conditioned media was then aspirated from the culture flask and processed using an ultracentrifugation protocol. Briefly, conditioned culture media was centrifuged at 700 x g for 5 minutes at 22˚C using an Eppendorf Centrifuge 5430R (Eppendorf, Hamburg, Germany). The resulting supernatant was centrifuged at 2,000 x g for 10 minutes at 22˚C using an Eppendorf Centrifuge 5430R (Eppendorf, Hamburg, Germany). Again, the resultant supernatant was centrifuged at 10,000 x g for 30 minutes at 4˚C using a Beckman Coulter Avanti J-26S XPI Centrifuge with a JA-25.50 rotor (Beckman Coulter, Brea, CA). Lastly, the supernatant resulting after centrifugation at 10,000 x g was centrifuged at 120,000 x g for 60 minutes at 4˚C using a Beckman Coulter Optima XPN-80 Ultracentrifuge and a Type 45 Ti rotor (Beckman Coulter, Brea, CA). Finally, 400 µL of 1x PBS was used to resuspend and store the resultant pellet for downstream analysis.

EV buffer characterization

Caov-3 ultracentrifugation EV samples in PBS were mixed with several buffers at a ratio of 1:1. Mixing buffer working concentrstions included 1X PBS, 5%,10%, 20%, and 30% glycerol, 25 mM trehalose, 20% acetonitrile, mixed 20% acetonitrile and 25 mM trehalose,, 1 M ammonium sulfate, and mixed 1 M ammonium sulfate and 20% acetonitrile diluted in PBS. EVs were mixed with each buffer and stored briefly on ice prior to fixation and staining for transmission electron microscopy (TEM) imaging.

Sample preparation for transmission electron microscopycaov-3 EVs isolated by UC were fixed in 4% paraformaldehyde for 30 minutes on ice. All grid adhesion and staining steps were performed by pipetting drops of sample, stain, or wash onto parafilm and moving 200 mesh copper formvar coated grids (Electron Microscopy Sciences, Hatfield, PA) from one drop to the next. After sample fixation, grids were placed coated side down on 5 μL drops of each sample for 5 minutes. Grids were washed 3 times with DI water for 4 minutes each, stained with 2% uranyl acetate for 5 minutes, and then washed 3 times with DI water for 4 minutes each. Grids were air dried in a low-humidity environment and then imaged using a Hitachi H7600 TEM (Hitachi, Tokyo, Japan).

Results

Caov-3 small EVs (sEVs) isolated by UC were subjected to a various buffers and imaged using TEM to assess morphological structure and damage. Caov-3 sEVs in PBS (see Figure A1b) demonstrated sEV characteristics under this staining methodology. Caov-3 sEVs in PBS maintain a "dimpled" structure with a slight shadow surrounding the vesicle and are within 30-150 nm in diameter as compared to the negative control. Caov-3 sEVs diluted in 5%, 10%, 20%, and 30% glycerol (see Figure A1c-f) demonstrated similar morphology to Caov-3 sEVs in PBS and displayed no evidence of structural damage. Glycerol samples demonstrated significant non-vesicular imaging artifacts compared to the positive and negative controls. Next, Caov-3 sEVs diluted in 25 mM trehalose (see Figure A1g) demonstrated morphology similar to Caov-3 sEVs in PBS, but appeared in a smaller size range and stained much darker. Samples diluted in 25 mM trehalose also displayed significant non-vesicular imaging artifacts compared to the positive and negative controls. Caov-3 sEVs diluted in 20% acetonitrile (see Figure A1h) demonstrated very little morphological similarities to Caov-3 sEVs in PBS and contained large amounts of organic debris while Caov-3 sEVs diluted in 20% acetonitrile with addition of 25 mM trehalose (see Figure A1i) saw some retention of sEV morphological structure in addition to altered staining and organic debris. Addition of 1M ammonium sulfate to Caov-3 UC samples (see Figure A1j) resulted in morphological change and possible crenation of vesicles as well as altered staining and non-vesicular artifacts. Finally, addition of 1M ammonium sulfate and 20% acetonitrile to Caov-3 UC samples (see Figure A1k) resulted in morphological change, possible crenation or vesicles, altered

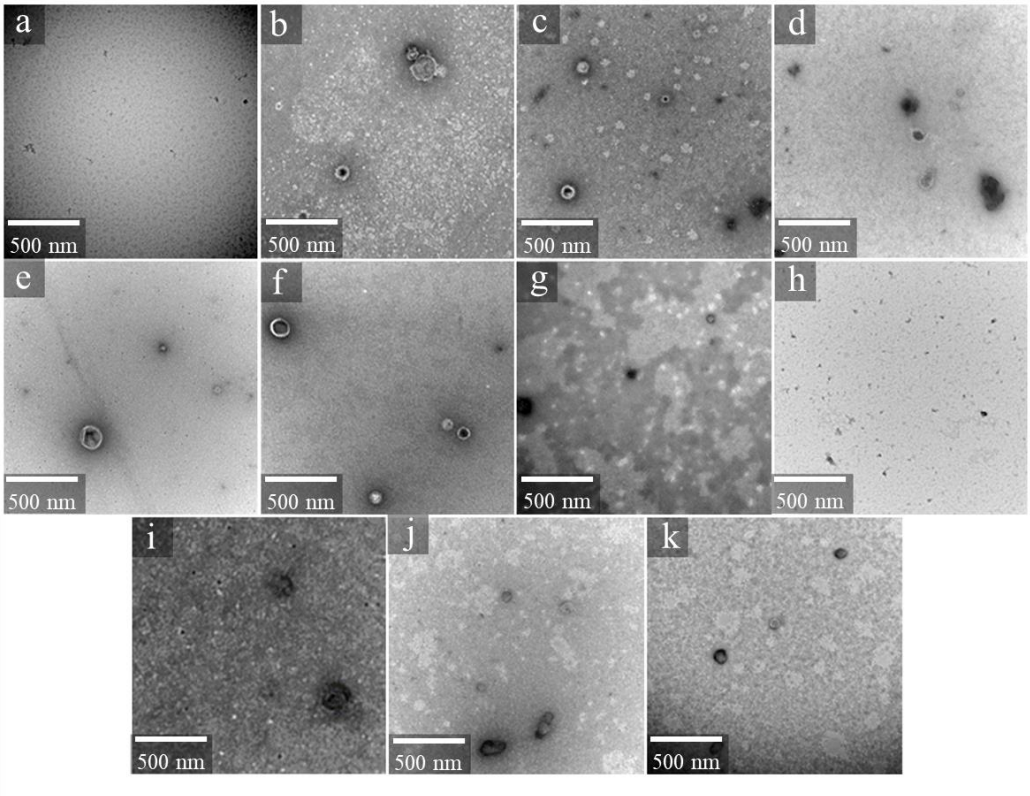

Figure A1. Scanning electron microscopy of Caov-3 small extracellular vesicles isolated by UC and diluted in various buffers. PBS negative control containing a) no sEVs and Caov-3 sEVs diluted in b) PBS, c) 5% glycerol, d) 10% glycerol, e) 20% glycerol, f) 30% glycerol, g) 25 mM trehalose, h) 20% acetonitrile, i) 20% acetonitrile and 25 mM trehalose, j) 1 M ammonium sulfate, and k) 1 M ammonium sulfate and 20% acetonitrile.

staining, and non-vesicular imaging artifacts, similar to Caov-3 vesicles subjected to 1M ammonium sulfate alone.

Discussion

As the parameters surrounding binding affinity of sEVs to poly(ethylene terephthalate) capillary-channeled polymer (C-CP) fibers are being further investigated, it is important to determine which media components may work best for eventual elution and separation of sEVs from the PET C-CP fibers. Ideally, all reagents used during the separation process should be compatible with the technical aspects of the chromatography process, while also retaining the morphology, structure, and informatic components of the sEVs. Damage to the vesicles could result in misinterpretation of downstream results. Therefore, TEM imaging was used to look at morphology and potential damage to vesicles in various buffers. As discussed before, intact sEVs observed under TEM tend to flatten out slightly, showing a circular structure with a "dimpled" interior.[1, 2] Additionally, vesicles in this format tend to show a darker ring or shadow around the circular structure due to the uranyl acetate employed while staining.[3] Of note, observed differences in the intensity of staining may be due in part to slight variation within the staining process. Any significant structural variation or lack thereof may indicate significant damage to or lysing of the vesicles.

Caov-3 sEVs collected via UC and diluted in 5%, 10%, 20%, and 30% glycerol (see Figure A1c-f) appeared to maintain normal sEV morphology within this description when compared to Caov-3 sEVs diluted in PBS. Glycerol, frequently used as a cryo-protectant in biological laboratories[4], is an organic osmolyte that helps maintain cell integrity and protein structure through reduction of intracellular non-organic ions.[5-7]

Furthermore, because it is a highly polar protic solvent, glycerol has been used as a solvent in hydrophobic interaction chromatography.[8, 9] Dilution of sEVs in 5-30% glycerol revealed conserved sEV morphology under TEM (see Figure A1c-f). Small EV protectant and organic solvent properties make glycerol an ideal candidate for further biological liquid chromatography investigations.

Caov-3 sEVs diluted in 25 mM trehalose showed limited damage based on morphology but appeared in much lower concentrations and smaller vesicle diameters, suggesting that damage or vesicle lysing may be occurring (see Figure A1g). Small EVs in 20% acetonitrile alone appeared to be severely damaged, lysed, and fragmented (see Figure A1h). While addition of 25 mM trehalose to 20% acetonitrile appeared to protect sEVs from some of the effects of 20% acetonitrile, there remained significant changes in vesicle staining and morphology among most vesicles (see Figure A1i). Addition of 25 mM trehalose to storage buffers has been shown to prevent aggregation and cryodamage in exosomes while narrowing the size distribution of the vesicles.[10] In this study, sEVs diluted in or supplemented with 25 mM trehalose demonstrated conserved morphology and structure (see Figure A1g,i). Therefore, 25 mM trehalose may be worth further investigation as a stabilizing agent for downstream sEV analysis and sEVs undergoing liquid chromatography separation.

As sEVs are comprised of a semi-permeable phospholipid bilayer, they are susceptible to disruption with organic solvents and small changes to osmotic pressure. Acetonitrile is a polar aprotic organic solvent that is particularly useful for chromatographic separations. However, its organic dissolution properties may severely

disrupt the phospholipid bilayer of sEVs, even in low concentrations.[11] This is clearly demonstrated in Figure A1h, where only organic fragments remain after application of 20% acetonitrile to sEVs and in Figure A1i where the vesicles are disfigured. Dilution of Caov-3 sEVs in 1 M ammonium sulfate demonstrated significant changes in vesicle shape and staining, but did not fragment the vesicles to the same degree as 20% acetonitrile (see Figure A1j). Finally, sEVs diluted in a solution of 20% acetonitrile and 1 M ammonium sulfate demonstrated significant changes in vesicle shape and staining, but, again, did not fragment the vesicles to the same degree as 20% acetonitrile alone (see Figure A1k). Ammonium sulfate is an inorganic salt commonly used in chromatographic separations that reduces protein solubility without denaturing the proteins.[12, 13] However, semipermeable phospholipid bilayers are highly susceptible to variations in salt concentrations in solution. For example, human osmoregulation maintains NaCl in the blood at 0.9 % w/v and any variations can lead to changes in osmotic pressure and crenation or lysing of cells.[14] Ammonium sulfate, while not frequently tested with living cells due to toxicity concerns, has demonstrated inhibitory effects toward *C. Albicans* with a concentration greater than 0.3 g/L.[15] In perspective, 1 M ammonium sulfate is equivalent to 132.14 g/L and, for these reasons, will likely affect the stability of the phospholipid bilayer of sEVs.

Together, these results indicate that glycerol in moderate concentrations ranging from 5-30% may help protect sEV morphology if used as a diluting reagent. Furthermore, addition of 25 mM trehalose, while results are not as conclusive, may help retain EV morphology as well. However, 20% acetonitrile and 1 M ammonium sulfate, when

applied separately and in conjunction may severely alter sEV structure and would likely influence potential downstream sEV analysis.

References

1. Yao Y, Wang C, Wei W, et al. Dendritic cells pulsed with leukemia cell-derived exosomes more efficiently induce antileukemic immunities. *PLoS One*. 2014;9(3):e91463. doi:10.1371/journal.pone.0091463

2. Yao Y, Wei W, Sun J, et al. Proteomic analysis of exosomes derived from human lymphoma cells. *Eur J Med Res*. Jan 2015;20:8. doi:10.1186/s40001-014-0082-4

3. Rikkert LG, Nieuwland R, Terstappen LWMM, Coumans FAW. Quality of extracellular vesicle images by transmission electron microscopy is operator and protocol dependent. *J Extracell Vesicles*. 2019;8(1):1555419. doi:10.1080/20013078.2018.1555419

4. Pegg DE. Principles of cryopreservation. *Methods Mol Biol*. 2007;368:39-57. doi:10.1007/978-1-59745-362-2_3

5. Gekko K, Timasheff SN. Thermodynamic and kinetic examination of protein stabilization by glycerol. *Biochemistry*. Aug 1981;20(16):4677-86. doi:10.1021/bi00519a024

6. Yancey PH. Organic osmolytes as compatible, metabolic and counteracting cytoprotectants in high osmolarity and other stresses. *J Exp Biol*. Aug 2005;208(Pt 15):2819-30. doi:10.1242/jeb.01730

7. Burg MB, Ferraris JD. Intracellular organic osmolytes: function and regulation. *J Biol Chem*. Mar 2008;283(12):7309-13. doi:10.1074/jbc.R700042200

8. Li JJ, Liu YD, Wang FW, Ma GH, Su ZG. Hydrophobic interaction chromatography correctly refolding proteins assisted by glycerol and urea gradients. *J Chromatogr A*. Dec 2004;1061(2):193-9. doi:10.1016/j.chroma.2004.11.002

9. Wang F, Liu Y, Ma G, Su Z. Glycerol-assisted hydrophobic interaction chromatography improving refolding of recombinant human granulocyte colony-stimulating factor. *Appl Biochem Biotechnol*. Dec 2009;159(3):634-41. doi:10.1007/s12010-008-8495-6

10. Bosch S, de Beaurepaire L, Allard M, et al. Trehalose prevents aggregation of exosomes and cryodamage. *Sci Rep*. 11 2016;6:36162. doi:10.1038/srep36162

11. Bobaly B, Beck A, Veuthey J, Guillarme D, Fekete S. Impact of organic modifier and temperature on protein denaturation in hydrophobic interaction chromatography. Article. *Journal of Pharmaceutical and Biomedical Analysis*. NOV 30 2016 2016;131:124-132. doi:10.1016/j.jpba.2016.08.019

12. Wingfield P. Protein precipitation using ammonium sulfate. *Curr Protoc Protein Sci*. May 2001;Appendix 3:Appendix 3F. doi:10.1002/0471140864.psa03fs13

13. Duong-Ly KC, Gabelli SB. Salting out of proteins using ammonium sulfate precipitation. *Methods Enzymol*. 2014;541:85-94. doi:10.1016/B978-0-12-420119-4.00007-0

14. Kültz D. Cellular osmoregulation: beyond ion transport and cell volume. *Zoology (Jena)*. 2001;104(3-4):198-208. doi:10.1078/0944-2006-00025

15. Vidotto V, Benech S, Maina AM, Bruatto M. Influence of different levels of ammonium concentrations on cell growth, RNA and protein production by Candida albicans. *Mycopathologia*. Jul 1993;123(1):19-25. doi:10.1007/BF01103484

APPENDIX B:
EXOSOME UPTAKE EXPERIMENT

Materials and Methods

Passage of Dictyostelium discoideum

Dictyostelium discoideum AX2 cell culture flasks were passaged when cells reached at least 70-90% confluency. Media from the old 25 cm^2 flask was replaced with 7 mL of fresh HL5 (Recipe on DictyBase.org) and the flask was vigorously beaten against the palm 5-7 times to detach the amoeba in solution. Next, 7 mL of fresh HL5 was added to each new culture flask and supplemented with 7 µL of 1000X Ampicillin (or appropriate selection). Finally, 0.1- 0.3 mL of the cell culture media from the old flask was added to any new flasks. Passage of cells into 75 cm^2 culture flasks follows the same protocol with exception of using 15 mL of fresh HL5 and 15 µL of 1000x Ampicillin (or appropriate selection) instead.

Exosome isolation

All centrifugation steps performed below 12,000X*g* were performed using an Eppendorf Centrifuge 5430R (Eppendorf, Hamburg, Germany). Centrifugations of 12,000X*g* or more were performed using a Beckman Coulter Avanti J-26S XPI Centrifuge with a JA-25.50 rotor (Beckman Coulter, Brea, CA). The first centrifugation step was performed at 700X*g* (5 min., 22˚C) in a full 50 mL conical centrifuge tube. After centrifugation, 45 mL of the supernatant was transferred to a new 50 mL conical centrifuge tube for further centrifugation, with the remaining 5 mL of supernatant saved

for exosome isolation via the C-CP HIC method. The second centrifugation was performed at 2,000X*g* (10 min., 22ºC.) The final centrifugation step was performed at 12,000X*g* (30 min., 4ºC.) The supernatant was carefully removed and the final pellet was re-suspended in 400 µL of PBS and stored at 4ºC.

GFP-Vacuolin-β AX2 transfection

Escherichia coli containing GFP-Vacuolin-β plasmid were obtained from Dr. Marcus Maniak, University of Kassel, Germany. GFP-Vacuolin-β presence in *E. coli* was verified via Polymerase Chain Reaction (PCR) with primers matching the GFP-Vacuolin-β nucleotide sequence. A Plasmid Maxi Kit (QIAGEN, Hilden, Germany) was used to isolate the GFP-Vacuolin-β plasmid followed by gel electrophoresis and PCR to verify the presence of the plasmid. AX2 *Dictyostelium discoideum* cells were transfected with the GFP-Vacuolin- β plasmid by electroporation. *D. discoideum* cells were centrifuged for 5 minutes at 500Xg and 4˚C, washed in 1 mL of H50 solution (Recipe on DictyBase.org) twice and resuspended to a concentration of $2x10^7$ cells/mL. After washing, 100µl of the cells in H50 were added to a pre-chilled 1 mm gap cuvette. Next, 2 µg of GFP-Vacuolin-β plasmid DNA was added to the cuvette and allowed to incubate on ice for 5 minutes. The cuvette underwent two consecutive pulses of 0.85 kV and capacitance 25 µF with 5 seconds recovery between pulses. Electroporated cells sat on ice for 5 minutes before being transferred to culture flasks with 7 mL of HL5 media. G418 selection was added to the culture flask the next day. Upon sufficient growth, GFP-Vacuolin-β AX2 cells were sorted using a BIORAD S3e cell sorter to obtain a higher percentage of high intensity fluorescent cells.

Exosome uptake experiment

GFP-Vacuolin- β AX2 cells were centrifuged for 5 minutes at 500Xg and 22˚C and then resuspended in HL5 media to a concentration of $1x10^6$ cells/mL. Next, 400 µL of the cell solution was added to live cell imaging well plates and cells attached to the dish for 1 hour. Exosomes isolated from normal AX2 cells were stained for 90 minutes at 37 ˚C using Cell Mask Orange (Thermo Fisher Scientific Inc, Waltham, MA) at a concentration of 5 µg/mL. Following staining, exosomes were filtered using a 30 kDa cutoff (Amicon Ultra-0.5 Centrifugal Filter unit, MilliporeSigma, Burlington, MA) to remove excess stain following manufacturer instructions. Prior to imaging, GFP-Vacuolin-β AX2 cell nuclei were stained with Hoechst 33342 at a concentration of 5 µg/mL for 5 minutes followed by washing and covering cells with PBS. Stained AX2 exosomes were added to the GFP-Vacuolin-β AX2 cell wells (5, 10, or 20 µL) and imaged every 60 seconds for 30 minutes.

Imaging conditions

Confocal fluorescent images were captured using a Leica SP8 confocal microscope with Hyvolution super-resolution (Leica, Wetzlar, Germany). All images were captured using an HC PL APO CS2 63x/1.40 oil immersion objective. Hoechst images were obtained using 405 nm excitation (15% power; gain=50), and a HyD detector (411-449 nm detection;). GFP images were obtained using 488 nm excitation (15% power; gain=100), and a HyD detector (512-564 nm detection). RFP images were obtained using 558 nm excitation (25% power; gain=300), and a HyD detector (575-650 nm detection). Images were captured every 60 seconds for a total of 30 minutes.

Results

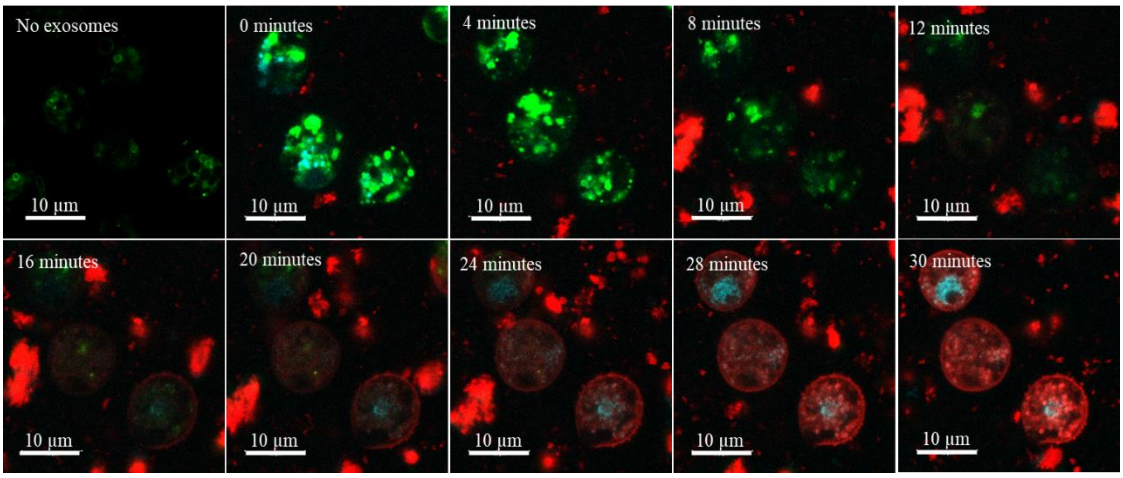

Figure B1. Exosome uptake experiment. GFP-Vacuolin *Dictyostelium discoideum* cells (Green) with Hoechst stain (cyan) exposed to cellMask Orange stained *D. discoideum* exosomes (Red) time lapse, Leica SP8 confocal microscope 63x magnification over a 30-minute period.

Discussion

The purpose of this experiment was to investigate exosome uptake mechanisms within a recipient cell using fluorescence microscopy. With little knowledge of the uptake and dissemination mechanisms surrounding exosomes in recipient cells, further investigation is required. Knowledge of these mechanisms will be particularly important for future exosome drug delivery investigations. The recipient cells used during the uptake experiment were engineered to express a GFP tag on Vacuolin-β, a protein expressed within the endocytic pathway of *D. discoideum*. Any overlap of fluorescent exosomes and GFP-Vacuolin-β expression may suggest that exosome dissemination is occurring throughout the endocytic pathway. Although this experiment likely needs refinement to obtain clearer results, exosomes (red, Figure B1) were observed entering the GFP-Vacuolin-β AX2 cells (green, Figure B1). Further investigation may be required to determine if the cellMask orange stain is remaining adhered to the exosome surface and whether the exosome lipid bilayer is mixing with the cell plasma membrane. It is unclear why the GFP expression disappeared around 8-12 minutes during exosome incubation. Furthermore, Hoechst staining of the GFP-Vacuolin-β AX2 cell was inconsistent likely due to *D. discoideum* tendency to expel foreign stains. Although this experiment produced very interesting images, it should be performed again with adjusted staining and uptake parameters. Investigators revisiting this experiment may look to adjust the live/dead cell imaging choice, resolution of the microscope used, stain concentrations, Hoechst and cellMask Orange stain choices, incubation time, cell concentrations, or exosome isolation technique. Alternatively, a similar experiment can

be performed using the IHOE-CD81-GFP or SKOV-3-CD9-RFP cells developed in chapter 2.

APPENDIX C:
EXTRACELLULAR VESICLE DRUG DELIVERY PROPOSAL

Hypothesis and Specific Aims

Exosomes are a class of extracellular vesicles, typically 30-100 nm in diameter, that facilitate cell-to-cell communication via paracrine and autocrine signal transduction.[1, 2] Exosome research has quickly developed into a flourishing research topic over the last 15 years and we are only now discovering the numerous roles of exosomes within regular homeostasis and the metastasis of cancers. To date, the scientific community has envisioned multitudes of exosome applications from cancer diagnosis to treatment of neurodegenerative diseases, some of which are coming to fruition.[3-5]

Exosomes are emerging as a potential Drug Delivery System (DDS) due to their size, encapsulating ability, natural biocompatibility, and potential for membranous marker manipulation.[6-8] Specifically, exosomes have been shown to cross the blood-brain barrier (BBB), which may allow for drug delivery to specific portions of the brain, a significant advantage over many other DDSs.[9] Our *long term goal* is to continue examining the potential for an exosome DDS that will deliver pharmaceutical or gene modifying agents past the BBB to specific regions of the brain for treatment of neurodegenerative diseases.

However, as exosome research is still in its early stages, there is a significant problem with isolating exosomes quickly, efficiently, and with sufficient purity in order to implement effective down-stream analysis and applications.[10] In previous research, our

cohort has developed a method of exosome isolation via Capillary-Channeled Polymer (C-CP) fibers using Hydrophobic Interaction Chromatography (HIC) for small-scale disease diagnostic purposes.[11-20] We plan to convert to and test this method of exosome isolation on a larger scale using batches of allogeneic cells grown in a bioreactor and modified to contain specific targeting moieties.

Specifically, our research group has imagined mass-producing exosomes to be used for drug delivery of catalase as a treatment for Parkinson's disease. ***We hypothesize*** that exosomes isolated via Capillary-Channeled Polymer fibers using Hydrophobic Interaction Chromatography, modified to express a rabies virus glycoprotein (RVG)-targeting peptide, and loaded with catalase will decrease brain inflammation in Parkinson's disease model mice. In order to assess this hypothesis, we will investigate these *three specific aims*.

Specific Aims:

Aim 1:

Investigate the capability of Capillary-Channeled Polymer fibers using Hydrophobic Interaction Chromatography to isolate exosomes from mammalian cell culture grown on large scales.

Aim 2:

Genetically modify mammalian cells to include modified exosomal membrane protein RVG-targeting peptides and investigate the loading capacity of catalase into RVG-targeted exosomes.

Aim 3:

Evaluate the effects of RVG-targeted and catalase loaded exosomes on cell cytotoxicity and brain inflammation in Parkinson's disease model mice using Intravenous injection.

Research Strategy

A. Significance

Parkinson's disease (PD) is among the most common neurodegenerative disease affecting adults worldwide. In the United States, 680,000 adults of over the age of 45 have developed this physically and mentally debilitating disorder and an increasingly older population and increased lifespan will likely escalate the number of neurodegenerative cases seen every year.[21] PD is characterized by degeneration of the dopaminergic neurons of the substantia nigra region of the brain. The degeneration of these neurons leads to decreased downstream production of dopamine, a neurotransmitter involved in significant pathways controlling reward-motivated behavior and motor function. As a result, patients with PD exhibit symptoms including loss or disruption of motor control and mental cognition.[22, 23] Most clinical treatments for PD still focus on replacement of the missing dopamine by administering pharmaceutical precursors that can be converted into dopamine. For example, levodopa is a precursor to dopamine that can cross the BBB, where it is converted to dopamine by DOPA decarboxylase.[24] Despite the alleviation of symptoms, dopamine replacement therapies do not significantly slow the degeneration of dopaminergic neurons or the development of PD.[25]

The pathology and development of PD is still a topic that is poorly understood, but evidence suggests that a variety of pathways may lead to a final common pathway of neuronal cell death. Altered mitochondrial activity, inflammatory changes, proteolysis modifications, and the formation of reactive oxygen species (ROS) have all been

implicated in the pathogenesis of neuronal cell death. Specifically, oxidative stress due to the formation of ROS is considered a cornerstone of the ideas surrounding dopaminergic cell death and has been implicated to contribute to a variety of neurodegenerative diseases. As such, PD has been associated with a reduction of redox enzymes including catalase, glutathione, superoxide dismutase, and others.[23, 26] Therefore, replacement or supplementation of redox enzymes has been theorized to slow the pathogenesis of dopaminergic cell death.[27] Furthermore, catalase, a powerful antioxidant capable of eliminating 1 million ROS per second per molecule, has been implicated as a potential treatment for PD.[6]

Unfortunately, 98% of drugs suspected to remedy various disease states of the central nervous system (CNS) cannot cross the BBB efficiently, catalase included.[6] Therefore, a DDS capable of crossing the BBB may be required to deliver catalase to the CNS for treatment of PD. Exosomes, a class of extracellular vesicles involved in cell-to-cell communication, have demonstrated drug delivery capabilities with increased biocompatibility and are able to cross the BBB.[6-9] Furthermore, Haney et al.[6] have specifically demonstrated the ability of exosomes to deliver catalase to the CNS. Taken a step further, to improve the capacity of exosomes targeting the CNS, several research groups have engineered cell cultures to secrete exosomes that express RVG peptide on their surface.[8, 28, 29] RVG peptide targeting has shown to improve CNS drug uptake and delivery across many DDSs, including exosomes.[30]

Previously, we have developed a method of exosome isolation using C-CP fibers and HIC that is quicker, more efficient, and cheaper than conventional methods.

Furthermore, HIC can be scaled up to process much larger volumes of cell culture media that may prove ideal for downstream analysis.[14] The major goals of this proposal are to investigate the ability of C-CP fibers and HIC to isolate exosomes on a large scale and investigate the ability of RVG-peptide expressing exosomes loaded with catalase to target the CNS and affect brain inflammation in Parkinson's disease model mice. We believe that this proposed research is significant because it will help develop a promising exosome isolation method capable for use in clinical settings and investigate the capability of exosomes as a DDS and the ability of catalase to treat Parkinson's disease.

A1) Our proposal investigates a method of exosome isolation via C-CP fibers and HIC on large scales: We have shown previously that C-CP fibers and HIC can be used to isolate exosomes on small scales for diagnostic purposes. Conventional methods of exosome isolation, ultracentrifugation, ultrafiltration, and others, have been proven to isolate exosomes, but with high inefficiency, cost, and time requirements. Furthermore, current methods of exosome isolation do not always produce high purity exosomes that are viable and consistent enough for clinical use.[10, 31, 32] Our technology, which we believe is capable of processing large volumes of media, provides a faster, cheaper, and more efficient method of isolating exosomes in clinical settings.

A2) Our proposal aims to create an allogeneic dendritic cell line engineered to express RVG-peptide targeted exosomes: A considerable hurdle to employing engineered exosomes in a clinic is the need to use autologous cells. Exosomes must be isolated after autologous cells are harvested, engineered, and grown from each individual patient. Exosomes derived from autologous sources are likely to produce a smaller

immune reaction. However, evidence suggests that allogeneic exosomes may avoid significant detection by the innate and adaptive immune systems due to the size of the vesicles.[33-36] An allogeneic exosome source could allow for pre-production, concentration, and lyophilization of exosomes for faster clinical application and more consistent drug development.

A3) Our proposal investigates the ability of catalase to treat Parkinson's disease with an enhanced RVG-peptide targeted exosome DDS: The absence or reduction of redox enzymes in PD is a potential target point for drug therapeutics. Catalase, a powerful antioxidant, could potentially mitigate or slow down the effects that ROS have on degeneration of dopaminergic neurons and reduce inflammation in the brain.[6] An RVG-targeted exosome DDS could allow for enhanced delivery of catalase across the BBB into the central and peripheral nervous systems for treatment and prevention of various neurodegenerative disorders.[8, 29, 30, 37]

B) Innovation

B1) Our method of exosome isolation is unique and may contribute to translational exosome research: Standard methods of exosome isolation lack the qualities to be consistently used in small clinical settings and on large scales for drug development. Ultracentrifugation, perhaps the most common method of exosome isolation, is too costly, time consuming, and difficult for most translational applications.[4, 10, 32, 38-40] Our method of exosome isolation using C-CP fibers and HIC is extremely cost

effective, quick, and easy to use. These C-CP fibers, developed by the Marcus research group at Clemson University, has been previously used to isolate other small molecules and proteins from solution.[13-16] Our exosome isolation method has the potential to transform exosome translational applications and galvanize clinical exosome research.

B2) Allogeneic, engineered exosomes will allow for more consistency and quality control in drug development: Consistency and quality control in regards to DDS development and drug treatment are essential for pharmaceutical approval and advancement to clinical trials. Autologous exosomes have been used in clinical trials due to identical DNA expression and histocompatibility.[7, 41, 42] However, allogeneic exosomes, if shown to be hypo-immunogenic or engineered to have reduced immunogenicity, could allow for greater, more specific manipulation and mass-production for pharmaceutical DDS development. We will engineer and modify a cell line that produces biocompatible allogeneic exosomes ideal for immune system avoidance and eventual clinical approval.

B3) Our methodology integrates an innovative exosome isolation technique with a unique targeted DDS to realize a translational treatment: We have partnered with experts in high performance liquid chromatography and bioengineering to implement techniques suitable for our goals including HIC, mass-production of cell lines in bioreactors, and DDS development. A multidisciplinary approach encompassing innovative strategies and complementary experts will allow us to investigate the feasibility of our technology and push it toward clinical application and relevance.

C) Approach

Our cohort has previously demonstrated the capability of C-CP fibers and HIC to isolate exosomes on small scales for diagnostic purposes (Figure C1). As it has been done previously with protein isolation, we believe that we can scale up our exosome isolation procedure using C-CP fibers and HIC to separate exosomes from larger volumes of milieu. Furthermore, based on previous experiments performed by other research groups[43-45], we believe we can engineer a cell line appropriate for allogeneic exosome separation and subsequently develop an exosome DDS for alleviation of Parkinson's disease degeneration and symptoms. Specifically, we hope to: (Aim 1) evaluate the ability of C-CP fibers and HIC to isolate exosomes from large volumes of human induced pluripotent stem cell (HiPSC)-derived dendritic cell (DC) culture milieu; (Aim 2) engineer and modify HiPSC-derived DCs to release RVG-peptide targeted exosomes and investigate the loading capacity of catalase into RVG-targeted exosomes; (Aim 3) investigate the effects of RVG-peptide targeted exosomes loaded with catalase on Parkinson's disease brain inflammation.

C1) Introduction

Exosomes are extracellular vesicles, approximately 30-100 nm in diameter, involved in various methods of autocrine and paracrine cell communication. Fortuitously, the messages carried by exosomes can potentially be traced back to the originating cell, allowing for many biomedical applications, such as disease diagnostics. Furthermore, the

ability of exosomes to load and pass cargo to many portions of the body, including the central nervous system, has led to investigation into exosome drug delivery applications.[1, 4, 10, 32, 46, 47] With so many potential applications and encouraging studies, exosome research has exploded onto the scene and has become a hot topic over the past 5 years. As a result, early progress has made toward developing exosomes as potential disease diagnostic biomarkers. Ideally, by identifying either the internal or external makeup of patient exosomes, clinicians may be able to provide a cancer diagnosis without the need to perform an invasive biopsy. Investigation into exosome origins has revealed several proteins and steps involved in the biogenesis of exosomes, but exosome uptake mechanisms, despite several investigations, still remain elusive.[1, 47, 48] Remarkably, Alvarez et al.[8] have demonstrated the ability of exosomes to perform as an efficient DDS for neurodegenerative diseases using modified RVG peptide exosomes, which may further the development of a translatable exosome DDS.

However, despite the promising advancements, the methods with which most investigators isolate exosomes are inefficient, time consuming, and costly. The "gold-standard" of exosome isolation, ultracentrifugation, is a proven method, but is expensive, time-consuming, results in low purity samples, and most importantly, is not easily translatable to the clinic.[31, 32, 38, 49, 50] With greater development of these exosome applications comes a greater need to improve exosome isolation methods. Using HIC in conjunction with C-CP fibers provides a promising alternative to standard exosome isolation procedures. Hydrophobic interaction chromatography and packed C-CP columns use innate hydrophobicity properties to isolate exosomes from the surrounding

environment. Particles of varying hydrophobicity will attach to and elute from the column at different salt concentrations, allowing for easy separation. This technique, especially when using solid phase extraction spin down columns, is extremely quick, cheap, easy, and suitable for clinical translation. Modification and scaling of this procedure could potentially result in a process that could mass-produce exosomes for other down-stream applications, including drug delivery.

Several clinical trials have used exosomes derived from dendritic cells for immunostimulatory purposes to prime the host immune system to target cancer cells producing neoantigens.[36] Down the line, dendritic-derived exosomes could be loaded with cancer therapeutics and be used to stimulate the immune system to target cancer cells and, in conjunction, deliver cancer drugs to the desired target. However, most exosome trials involve exosomes derived from autologous sources, which limits the replicability and quality control of the biological treatment.[41, 42] Allogeneic-derived exosomes have demonstrated hypo-immunogenic properties and could increase the quality, consistency, and replicability of an exosome biological treatment.[34, 51] Development of exosomes from an allogeneic dendritic cell line could result in a DDS that can be used to treat any number of cancers and neurological disorders and stimulate the immune system for enhanced outcomes.

Specifically, PD, which results in dopaminergic neurodegeneration in the subtantia nigra, has been pinned as a potential target for an exosome DDS. Although the pathology of PD is poorly understood, several factors, including excess ROS, have been implicated in the disease development. Therefore, treatment with powerful antioxidants

may help remediate or slow down the neurodegeneration associated with PD.[22, 23] Specifically, catalase, a powerful antioxidant, has shown promise in alleviation of PD, but, like most drugs, cannot cross the BBB.[6] An exosome DDS, capable of crossing the BBB and targeting the CNS, may allow for specific delivery of catalase to the CNS. Furthermore, exosomes engineered to contain an RVG-peptide targeting system may allow for increased efficiency and efficacy of delivery to the CNS.

C2) Preliminary Studies

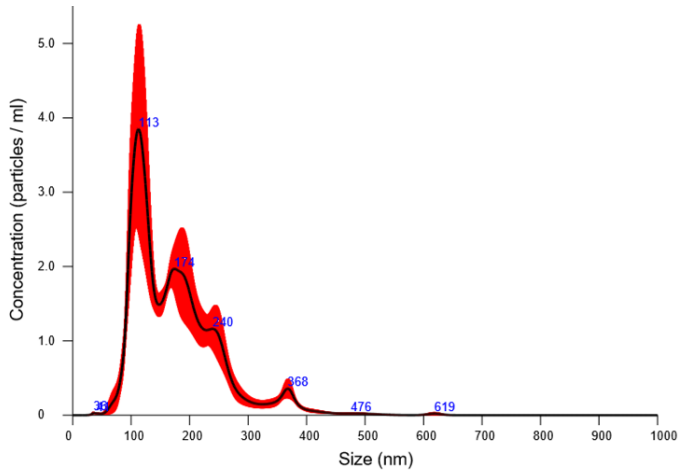

Figure C1. Average exosome concentration and particle size distribution measured by NTA. Exosomes isolated sequentially by differential centrifugation and HIC with Poly(ethylene terephthalate) C-CP fibers.

Previously, Marcus et al.[52] have demonstrated the potential for fast protein separation using C-CP fibers. Using C-CP fibers developed by the Marcus lab, we have used hydrophobic interaction chromatography to separate cell culture media components from *dictyostelium Discoideum* and Caov-3 cell lines. Specifically, we have demonstrated the ability to separate extracellular vesicles from cell culture after cells have been removed by either centrifugation or filtration. Nanoparticle Tracking Analysis (NTA)

allows for characterization of nanoparticle size distributions and concentrations using light scattering and Brownian motion properties. Using NTA (Figure C1), we have shown

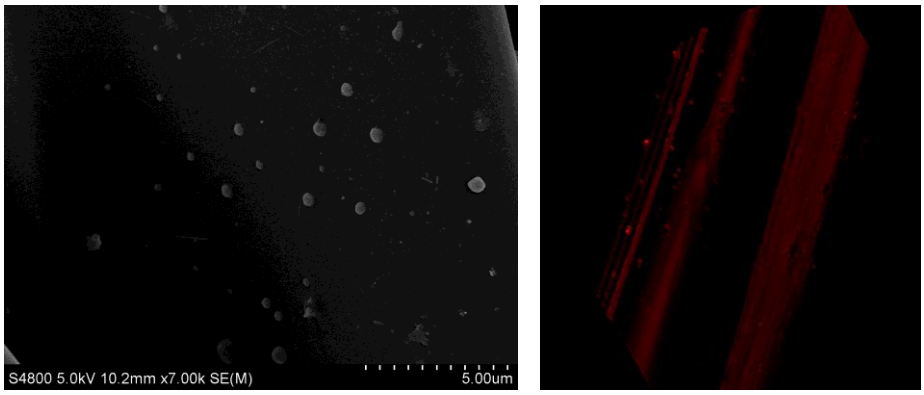

Figure C2. SEM and Fluorescent images of extracellular vesicles adhered to C-CP fiber surfaces. (a) SEM image of Caov-3 ultracentrifuge derived extracellular vesicles and (b) fluorescent image of Caov-3 cellMask orange stained ultracentrifuge derived extracellular vesicles.

that the separation technique we have developed isolates extracellular vesicles of approximately 100-200 nm. Furthermore, we have demonstrated that the extracellular vesicles are adhering to the solid-phase component of the HIC method via scanning electron microscopy (SEM) and fluorescent microscopy (Figure C2).

C3) Research Plan

Aim 1: Investigate the capability of Capillary-Channeled Polymer fibers using Hydrophobic Interaction Chromatography to isolate exosomes from mammalian cell culture grown on large scales**.** The goal of this aim is to determine whether scaled up C-CP fiber columns using HIC can isolate exosomes of high purity, quality, and quantity. To do this we will perform a number of chemical and physical verification steps to ensure effective total quality management of the separation method.

Aim 1.1: Verify the presence of exosome-associated markers in the C-CP fiber and HIC elution**.** Rationale: Although there is no "gold standard" to characterize exosomes, according to the International Society of Extracellular Vesicles, extracellular vesicles must be characterized by both protein composition and physical traits.[53] Samples must be characterized not only to determine the presence of exosomes, but also to determine the quality, quantity, and purity of the exosome samples. Our method of exosome isolation has demonstrated the ability to isolate well-characterized exosomes for diagnostic purposes. Therefore, we ***hypothesize*** that large-scale exosome isolation via C-CP fibers and HIC will produce high purity exosome samples with typical exosome-enriched proteins.

Experimental Design: In order to investigate the protein composition of C-CP fiber and HIC isolated exosomes, we will perform standard protein Bradford assays and western blots of exosome-enriched proteins. Specifically, using a western blot, we will look for the presence of CD9, CD81, CD63, TSG101, calnexin, and Grp94 to characterize the presence and purity of exosomes.

Expected Outcomes: As there are many types of extracellular vesicles, exosomes included, it is important for us to be able to first, verify the presence of extracellular vesicles and then second, verify that the sample is exosome-enriched. Since extracellular vesicles are derived from the phospholipid bilayer membrane of cells, transmembrane proteins are typically used to characterize their presence. Therefore, we would expect samples to contain the transmembrane proteins CD9, CD81, and CD63, all of which are typically used to characterize extracellular vesicles. Furthermore, cytosolic proteins that

are involved in extracellular vesicle biogenesis can be used to identify exosomes. In this instance, we will use TSG101, which is involved in the development of multivesicular bodies that generate exosomes, as a positive marker. A positive appearance of TSG101 further verifies the existence of extracellular vesicles and further suggests that the sample may be exosome-enriched. Additionally, to further characterize our samples as exosome-enriched, we will look for microvesicle markers calnexin and Grp94. These two markers are typically found enriched in the endoplasmic reticulum, a common place of origin for microvesicles. Therefore, we would expect our isolated exosome samples to contain little to no amounts of calnexin and Grp94. Lower amounts of calnexin and Grp94 would indicate that our exosome samples do not contain other types of extracellular vesicles including microvesicles, ectosomes, and apoptotic bodies.[53] If we can detect at least one transmembrane protein marker, one cytosolic protein marker and minimize the amount of negative exosome marker detected for each sample, we will have found chemical evidence that our sample contains exosomes and not another type of extracellular vesicle. Furthermore, we would expect a Bradford assay to find higher amounts of protein in each sample as compared to our previous research of exosome isolation on a small scale.

Potential Pitfalls and Alternatives: We do not expect to encounter significant difficulties with the western blot process as it is a very well developed technology and commonplace procedure in our lab. Furthermore, we have previously found that C-CP fiber and HIC exosome isolation produces samples with exosome-enriched markers, so we would anticipate to find these markers again. However, upon scaling up the procedure and using larger chromatography columns we may not encounter exosome isolation using the same

properties and framework. Mass isolation of exosomes may shift the expected adsorption and elution values of the columns due to oversaturation or vesicle aggregation. Although, with some adjustment and saturation analysis we should be able to overcome any alteration to the HIC procedure. Additionally, with a larger column, we might expect the concentration of exosomes isolated to scale linearly based on the size of the column or the amount of media injected through the column. We will test many column sizes and injection volumes to find the most efficient and effective procedure for producing pure, high concentration exosomes for down-stream analysis.

It is well known that western blot analysis is not a terribly quick procedure and performing protein analysis with this method on many samples may require a significant amount of resources and time. Furthermore, western blot analysis only detects the proteins of interest and ignores the presence of any other potentially important proteins. Therefore, we may consider using protein mass-spectrometry to identify the entire protein spectrum of each sample. Complete protein analysis would allow us to further analyze each sample and potentially differentiate between different types of exosomes for down-stream application.

Aim 1.2: Further characterize the presence, quality, and quantity of exosomes in the C-CP and HIC elution by physical properties**.** Rationale: As mentioned in aim 1.1, although there is no perfect process, exosomes can be reasonably characterized and identified using both protein composition and physical traits. Physical trait analysis can be used to further investigate the quality, quantity, and purity of the samples. Therefore, we ***hypothesize*** that large-scale exosome isolation via C-CP fibers and HIC will produce

exosomes with uniform size and density, high and consistent concentration, and sufficient purity.

Experimental Design: In order to investigate this aim we will inject cellular milieu samples into the scaled up C-CP fiber columns, perform HIC, and analyze the elution using nanoparticle tracking analysis (NTA), scanning electron microscope (SEM) imaging, transmission electron microscope (TEM) imaging and fluorescent imaging. Performing each of these techniques will allow us to verify the presence, quality, purity, and concentration of exosomes in each eluted sample. Furthermore, these techniques will also allow us to analyze the solid-phase surface interactions of the exosomes and C-CP fibers.

Expected Outcomes: By using several techniques to characterize the physical traits of our samples, we would expect a complete and replicated profile for each sample. Each of these procedures unveils information about the sample from a slightly different perspective. Specifically, from NTA, we would expect a size distribution similar to our previous research with the highest concentration of nanoparticles at approximately 100 nm. As we will be working with much larger volumes of media, we would also expect a nanoparticle concentration much higher than our previous research and on par with other standard exosome isolation methods. SEM imaging of the vesicles attached to the C-CP fibers pre- and post-elution will reveal information about the surface interactions between the vesicles and solid-phase C-CP fibers. We would expect similar images as compared to our previous research (Figure C2). Specifically, vesicles should be evenly distributed across the surface of the fiber with little aggregation, should be free of any visible

damage or deformity, and should no longer be present after elution from the fiber. TEM imaging will be used to further characterize the general shape, size, and structure of the eluted vesicles post-elution. We would expect TEM imaging to display highly concentrated vesicles of approximately 30-100 nm in diameter with the highly characteristic 'dimple' or 'cupped' appearance of exosomes. We would not expect to see broken, damaged, or deformed vesicles with TEM imaging due to the moderate nature of our exosome isolation. Finally, fluorescent imaging will be used to further verify vesicle and C-CP fiber interaction. Cellular stains CellMask and CellTracker will be used to fluorescently stain exosome samples prior to incubation with C-CP fibers and imaging. Similar to SEM, we would expect fluorescent images obtained using Leica SP8 with HyVolution, a super resolution software enhancement, to show vesicles evenly distributed across the fiber with little aggregation and the absence of vesicles post-elution.

Potential Pitfalls and Alternatives: As we have performed all of these techniques in previous research with C-CP fibers, we would expect fewer hurdles in collecting this information. NTA is commonly used to quantitatively and qualitatively assess exosome properties, but admittedly is not a perfect method. Many articles have addressed this issue[54, 55], but few better quantitative methods have emerged. Alternatively, to quantify exosome samples, we could use dynamic light scattering (DLS) or a newer technique such as tunable resistive pulse sensing (TRPS). Both DLS and TRPS have advantages and disadvantages, but the main point is that there is no perfect single method to analyze exosome properties. Therefore, it is best to assess the quality and quantity of our samples

using several techniques. SEM and TEM are very robust and informative techniques that will help assess the size and deformity of vesicles, but are limited to single vesicle analysis and do not incorporate the entire sample. As SEM and TEM imaging quality is almost entirely dependent on sample preparation, poor fixation and staining protocols may need to be adjusted based on the needs of the sample. If required, we may consider using cryogenic electron microscopy if TEM and SEM imaging do not produce adequate or quality results. Fluorescent imaging using Leica SP8 with HyVolution has a limit a resolution of approximately 140 nm, which is larger than the diameter of exosomes. Therefore, collecting images of individual vesicles via this method is very difficult, but possible when observing juxtaposed or collections of vesicles. Alternatively, as our lab is highly ingrained in the light microscopy community, we could send fiber and elution samples for super resolution imaging with a lower limit of resolution.

Aim 2: Genetically modify mammalian cells to include modified exosomal membrane protein RVG-targeting peptides and investigate the loading capacity of catalase into RVG-targeted exosomes. The goal of this aim is to generate a modified HiPSC-derived dendritic cell line to further investigate exosomes as a DDS. Specifically, we will modify the targeting moiety of the exosomes and investigate the loading capacity of catalase into exosomes.

Aim 2.1: Manipulate HiPSCs to differentiate into dendritic cells**.** Rationale: Production of an allogeneic cell line will allow for down-stream production of allogeneic exosomes. Presently, several clinical exosome studies have used exosomes derived from autologous dendritic cells, but allogeneic exosomes have demonstrated hypo-immunogenic

properties.[34, 41, 42, 51] Therefore, we are aiming to develop an allogeneic dendritic cell line for exosome production. ***We hypothesize*** that HiPSC expression manipulation will result in fully functional allogeneic dendritic cells capable of producing allogeneic exosomes.

Experimental Design: Specifically, we will follow previously well-developed protocols to differentiate HiPSCs into DCs similar to the $CD141^+$ subtype.[45] Doing so involves a number of additions and removals of specific growth factors at certain time points. Formation of embryoid bodies (EBs) through differentiation of HiPSCs, as a first step toward differentiation of HiPSCs into DCs, has been demonstrated using several types of bioreactors with reduced mixing.[56] In this instance, we will use structured and scheduled treatments of HiPSCs with pre-determined growth and differentiation factors using a high throughput bioreactor to initiate and complete the differentiation process of HiPSCs into DCs. Specifically, cells will be cultured over a 30 day period with gradual removal of growth factors including Bone Morphogenetic Protein 4 (BMP4), Vascular Endothelial Growth Factor (VEGF), Stem Cell Factor (SCF), and Granulocyte Macrophage Colony-Stimulating Factor (GM-CSF). Finally, the culture will be supplemented with Interleukin 4 to support final differentiation.[45]

Expected Outcomes: Forced differentiation is a highly controlled and structured process that is more easily accomplished using a high throughput bioreactor. Several well developed published protocols have demonstrated the expected outcomes of each differentiation step during the process that we will follow. We would expect to observe a step-wise transformation of HiPSCs into hematopoietic stem cells, common myeloid progenitors, DC precursors, immature DCs, and finally mature DCs. Quality management

along each step of the differentiation process will be critical to achieve the expected outcomes. The final outcome should be a variety of DCs presenting qualities similar to the $CD141^+$ subtype as detailed in published protocols.[43, 45, 57]

Potential Pitfalls and Alternatives: Forcing differentiation of stem cells is a very structured and difficult process and meticulous monitoring will be required to complete an accurate differentiation into DCs. Therefore, there may be certain difficulties in finding the exact environmental variables, growth factors, and timing for the process. We would expect that if the initial HiPSCs are slightly different than in previous studies that the differentiation process may vary slightly. By using a high throughput bioreactor we will be able monitor the environmental variables and test several cell culture preparations at one time to ensure an adequate final product of suitable quality and expression. If the differentiation procedure from HiPSCs to DCs is not fully accomplished with satisfactory expression and quality we could consider completing the remaining goals using allogeneic HiPSCs. As exosomes have demonstrated hypo-immunogenic properties, a different source of allogeneic exosomes may be worth investigating. Furthermore, since even allogeneic cells may contain epigenetic variation depending on the source, we could investigate the epigenetic expression of the cells and the impact of epigenetic expression on exosome variation.

Aim 2.2: Engineer HiPSC-derived dendritic cells to display RVG-targeting peptide on exosome surface membranes. Rationale: Exosomes are capable of crossing the BBB, but are not specifically targeted to remain in the brain and could disperse throughout the remaining blood. Ideally, exosomes engineered to target the brain

specifically will increase the fraction of injected exosomes in the central nervous system and are more likely to meet the designed target. We aim to create a DDS that is more accurate for drugs being delivered to the central nervous system via exosome transport. Therefore, ***we hypothesize*** that HiPSC-derived dendritic cell exosomes can be engineered to display RVG-targeting peptides on the outside phospholipid bilayer surface.

Experimental Design: RVG-peptide targeted exosomes have been engineered from murine cells, but have yet to be developed in human cells.[8] We will clone the RVG peptide into the human Lamp2b gene, an exosome-enriched transmembrane protein, using plasmid cDNA. Specifically, Lamp2b plasmid cDNA will be isolated from storage *Escherichia coli* and engineered to contain the RVG codon sequence using DNA fragments, restriction sites, and restriction and ligation enzymes. The resulting RVG-Lamp2b plasmid will be transformed into *E. coli* for plasmid verification and storage. After isolating the engineered plasmid from *E. coli,* RVG-Lamp2b cDNA will be transfected into HiPSC-derived DCs and cultured using the Lipofectamine 3000 transfection kit. Subsequently, we will verify the presence of RVG-peptide in both the DCs and DC exosomes via anti-RVG western blot.

Expected Outcomes: The HiPSC-derived cell line that we are developing will be stably transfected with a human cDNA plasmid. As part of cloning procedure, we will verify that RVG is inserted into the Lamp2b cDNA in the correct location using selection agents. After isolation of the cDNA and transfection into HiPSC-derived DCs, we would expect successfully transfected cells to express the positive selection trait (gaining resistance to a drug) inserted into the plasmid cDNA. An anti-RVG western blot of the

transfected DCs and subsequent exosomes will further verify the expression of RVG-Lamp2b in the transfected cells and exosomes.

Potential Pitfalls and Alternatives: Stable plasmid cDNA transfection in mammalian cells is not a terribly efficient process and as such, we may run into difficulties while performing the transfection. Furthermore, transfection with RVG-Lamp2b cDNA is no guarantee that the transfected DC exosomes will contain RVG-Lamp2b protein. Transient plasmid transfection is much more efficient and easier than stable transfection and has previously been used for mass production of proteins in mammalian cells.[58] Thus, as an alternative, we could transiently transfect the DCs to express RVG-Lamp2b and then isolate the exosomes within 24-48 hours post-transfection. Furthermore, as there are many transmembrane proteins typically enriched on the surface of exosomes, we could use other peptides such as CD9, CD81, or CD63 to develop an RVG-targeted exosome.

Aim 2.3: Investigate loading capacity of catalase into various modified exosomes.

Rationale: Catalase is a powerful antioxidant that may help mitigate neuronal degradation in PD and other neurodegenerative diseases by limiting ROS. Like many drugs, catalase cannot cross the BBB and requires transport to reach the central nervous system.[6] We believe that exosomes can be used as an efficient DDS for catalase due to their natural ability to cross the BBB and hypo-immunogenicity.[7, 9] Therefore, ***we hypothesize*** that catalase can be loaded into RVG-targeted and normal exosomes with high efficiency for downstream drug delivery.

Experimental Design: There are a number of different approaches to loading enzymes, RNAs, and other pharmaceuticals into exosomes, yet no one technique has emerged as the standard option.[59] Therefore, we will investigate several exosome loading techniques with our specific cell line and exosomes. Specifically, we will investigate the loading efficiency of electroporation, sonication, saponin permeabilization, and room temperature incubation of exosomes with catalase. NTA, DLS, and TEM will be used to examine the physical structure and integrity of the vesicles after loading. To effectively measure the amount of catalase or antioxidant in a sample, we will measure the rate at which hydrogen peroxide decomposes. Hydrogen peroxide decomposes at a very slow rate when no antioxidants are present. This hydrogen peroxide decomposition assay and western blot will be used to demonstrate the loading capacity and stability of exosomes loaded with catalase.

Expected Outcomes: Exosome properties can vary based on cell type origin, environmental factors, and biochemical purpose. As such, we would expect exosomes derived from HiPSC-derived DCs to have different size, integrity, loading capacity, proteins, makeup, and internal content than any exosomes studied previously. Therefore, it is difficult to predict which method of exosome loading will ultimately demonstrate the most efficient loading. Electroporation, sonication, saponin permeabilization, and room temperature incubation have all demonstrated loading capability in exosomes from multiple sources.[6, 8, 59, 60] However, sonication has demonstrated high loading efficiency and sustained release with exosome and catalase formulations, so we would expect the highest efficiency with sonication.[6] Each loading procedure applies very different

physical stresses to the exosomes and therefore, will likely cause disruption, collapse, or deformation of the vesicles in varying amounts. NTA, DLS, and TEM will clarify the physical exosome disturbances of each loading technique. Furthermore, we would expect the hydrogen peroxide decomposition assay and western blot to reveal a high loading capacity and retention time for each of the techniques with room temperature incubation likely having the lowest efficiency.

Potential Pitfalls and Alternatives: Since each of the exosome loading techniques can potentially damage or deform the exosome membrane, we may run into problems with catalase loaded exosome downstream applications. To help mitigate these potential problems we will assess the physical quality, loading capacity, and retention time of each of the loading techniques. With the most promising loading techniques, we can further assess the uptake and delivery of the exosome-catalase formulations in cell culture. If none of the proposed techniques offer an appropriate efficiency we could also investigate exosome extrusion, freeze/thaw, and optically reversible protein-protein interactions as potential alternative methods for loading.

Aim 3: Evaluate the effects of RVG-targeted and catalase loaded exosomes on cell cytotoxicity and brain inflammation in Parkinson's disease model mice using Intravenous injection**.** The goal of this aim is to measure brain inflammation in Parkinson's disease model mice after treatment with catalase loaded and RVG-targeted exosomes. We will use various histological techniques and fluorescent techniques to evaluate the level of inflammation in the mice brain samples.

Aim 3.1: Evaluate the cytotoxicity of RVG-targeted exosomes loaded with catalase using cell cytotoxicity and proliferation assays. Rationale: Exosomes have not typically been found to have cytotoxic properties, but any material introduced into a cell environment, especially with engineered modifications, could potentially introduce some form of toxicity. Therefore, especially with RVG modification, it is important to assess the cytotoxicity and proliferation of cell lines in vitro prior to performing any animal studies. ***We hypothesize*** that RVG-targeted exosomes from HiPSC-derived DCs will not be toxic to or alter the proliferation of in vitro cell cultures.

Experimental Design: Using Neuro2a (murine neuronal cells) and C2C12 (murine muscle cells) cell lines, we will perform a Trypan Blue exclusion viability assay and an MTT cell toxicity and proliferation assay to determine the cytotoxicity of catalase alone and RVG-targeted and normal exosomes loaded with catalase. Furthermore, we will use the same two cell lines to perform a mixed lymphocyte reaction using CD3+ T cell proliferation to determine the immunogenicity of catalase alone and the RVG-targeted and normal exosomes loaded with catalase.

Expected Outcomes: As previously mentioned, exosomes have demonstrated hypo-immunogenic qualities and specifically, RVG-targeted exosomes have shown low immunogenicity in mice.[8, 51] Specifically, Trypan Blue exclusion can be used to determine cell viability and an MTT assay measures the level of cell metabolic activity, which can be used to quantify cell viability and proliferation. From these two assays, we would expect high viability and proliferation of cells treated with RVG-targeted exosomes loaded with catalase. Furthermore, to assess the immunogenicity of the

produced catalase loaded exosomes, we will use a mixed lymphocyte reaction using CD3+ T cell proliferation. After treatment with RVG-targeted exosomes loaded with catalase, we would expect low T cell proliferation, indicating low immunogenicity.

Potential Pitfalls and Alternatives: Cell viability, proliferation, and immunogenicity assays are standard and custom procedures for any substance being introduced as a novel drug or pharmaceutical agent. An exosome DDS, as an engineered pharmaceutical component, will require cell viability, proliferation, and immunogenicity assessment. We would not expect significant difficulties performing the assays, as they are very standard practice and well developed. However, if we find that any assay does not produce appropriate or sufficient results, we will perform subsequent additional experiments such as colorimetric tetrazolium assays, luminogenic ATP assays, or DNA synthesis assays. If we find that RVG-targeted exosomes loaded with catalase generate unacceptable levels of cell viability, proliferation, or immunogenicity, we will readdress the engineering and source of the exosomes. We could potentially engineer the exosomes to be less immunogenic by disrupting beta-2-microglobulin and C2TA genes, which have been shown to affect MHC-I and MHC-II generation and immunogenicity, using CRISPR/cas9.[57] Cells modified to not express MHC-I and MHC-II molecules will in turn release exosomes without MHC-I and MHC-II molecules. Both MHC-I and MHC-II are involved in histocompatibility and immune response of foreign materials. If the MHC molecule does not match the unique MHC molecules of the host, then an immune response will be triggered. Removal of the MHC molecules will help increase histocompatibility and decrease immune response in the host.

Aim 3.2: Use histology and fluorescence techniques to stain and quantify inflammation and evaluate biodistribution in Parkinson's disease model mice brain sections treated with RVG-targeted exosomes loaded with catalase. Rationale: Parkinson's disease and other neurodegenerative diseases are often associated with brain inflammation in addition to physical and cognitive degeneration.[22, 23] Histological and fluorescent imaging techniques can be used to quantify the amount of inflammation in brain sections and help determine the level of neurodegeneration in the affected subject. Treatment with RVG-targeted exosomes loaded with catalase, which aims to eliminate or reduce ROS in the central nervous system, could reduce the downstream effects of Parkinson's disease, including inflammation. Therefore, ***we hypothesize*** that RVG-targeted exosomes loaded with catalase will reduce inflammation in Parkinson's disease model mice.

Experimental Design: We will use both intranasal (*i.n.*) and intravenous (*i.v.*) injection to assess the effects of RVG-targeted exosomes loaded with catalase on Parkinson's disease model mice. All exosome samples will be stained with fluorescent dye prior to injection to help assess biodistribution using fluorescent microscopy. After injection with either RVG-targeted catalase exosomes, normal catalase exosomes, unloaded exosomes, or catalase alone, mice will be sacrificed and perfused at several time points ranging from 4 to 48 hours. After fixation, mice brains will be sectioned and prepared for staining. To assess the general cell composition and level of inflammation we will stain the sections with hematoxylin and eosin (H&E) and observe the tissue using standard wide-field light microscopy. Additionally, we will perform anti-CD11b

immunohistochemistry (IHC) to further assess the level of inflammation in the brain sections.

Expected Outcomes: Given that catalase has previously been shown to reduce brain inflammation when loaded into exosomes, we would expect the RVG-targeted exosomes loaded with catalase to achieve similar or better reduction in inflammation and targeting.[6] With H&E staining, we would expect to observe an array of neuronal and microglial cells in addition to other immune cells. In general, higher concentrations of immune cells in the tissue indicate greater levels of inflammation. Various amounts of neutrophils, basophils, eosinophils, monocytes, lymphocytes, or macrophages could help determine the stage of inflammation, type of inflammation, or other potential causes of inflammation. For instance, a high level of eosinophils and basophils is typically associated with anaphylactic reaction.[61] CD11b antibody is typically used as a marker for microglial cells, macrophages, and other granulocytes within nervous tissue.[6] We would expect Immunohistochemistry using CD11b to show moderate, but reduced concentrations of immune cells and activated microglial cells in mice brain sections with RVG-targeted catalase exosomes as compared to normal catalase exosomes and untreated mice.

Potential Pitfalls and Alternatives: H&E and IHC are very common and established staining techniques, so we don't expect any significant hurdles. Furthermore, we work with cell staining and imaging experts that will help improve and expedite the process. With both imaging techniques, we would expect to see inflammation in the brain sections. Furthermore, we would expect to see targeted biodistribution of exosomes.

However, the inflammation may vary depending on the region of the brain that is imaged. We must be careful to identify and document each region of the brain and compare and contrast the inflammation. As Parkinson's disease develops in the substantia nigra, we may expect higher levels of inflammation in the areas surrounding the substantia nigra. If H&E or IHC fail to produce accurate or consistent images, then we may consider immunophenotyping spleen tissue derived from the subject mice to get a sense of the overall immune reaction to the treatments.

Conclusion

We believe that with further development of exosome isolation via C-CP fibers and HIC we will be able to create a clinically translatable technique that can be applied to any number of exosome applications. Further development of this technique, coupled with development of an allogeneic cell line for exosome isolation, could have a large impact on the development of an exosome DDS. Many ailments, including cancers and neurodegenerative diseases, could benefit from more specific and capable drug delivery system. With the methods we have outlined here, we hope to achieve our goal of contributing to exosome research and the development of an exosome DDS.

Timeline

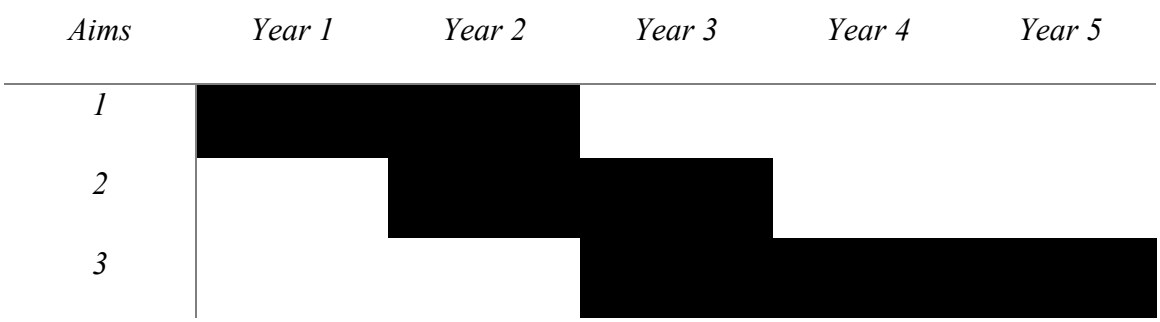

Vertebrate Animals

The animals and protocols used in this study will be approved by the Clemson University Institutional Animal Care and Use Committee (IACUC). Clemson University follows strict guidelines to maintain adherence to the protocols and procedures laid out by the IACUC. Specific designated areas within the Godley-Snell Research Center will be used to maintain and treat the mice used in this proposal.

This study will require the use of mice in Aim 3. Both Parkinson's disease model mice ($Nrf2^-$) and wild type mice (C57BL) will be used to assess the effects of the developed DDS. A total of 160 $Nrf2^-$ and 160 C57LB mice will be required for completion of this portion of the study.

Aim 3: Evaluate the effects of RVG-targeted and catalase loaded exosomes on cell cytotoxicity and brain inflammation in Parkinson's disease model mice using Intravenous injection.

Aim 3.2: Use histology and fluorescence techniques to stain and quantify inflammation and evaluate biodistribution in Parkinson's disease model mice brain sections treated with RVG-targeted exosomes loaded with catalase

80 $Nrf2^-$ mice for dose inflammation quantification = 5 mice per group x 4 groups (PBS injection, no treatment, RVG-exosome dose, and RVG-exosome w/ catalase dose) x 4 dosages.

80 C57LB mice for dose inflammation quantification = 5 mice per group x 4 groups (PBS injection, no treatment, RVG-exosome dose, and RVG-exosome w/ catalase dose) x 4 dosages.

80 $Nrf2^-$ mice for time point inflammation quantification = 5 mice per group x 4 groups (PBS injection, no treatment, RVG-exosome dose, and RVG-exosome w/ catalase dose) x 4 time points.

80 C57LB mice for time point inflammation quantification = 5 mice per group x 4 groups (PBS injection, no treatment, RVG-exosome dose, and RVG-exosome w/ catalase dose) x 4 time points.

Use of a mouse model in exosome research is essential prior to human clinical trials due to the young age of the potential therapies. Particularly, testing treatment of RVG-exosomes loaded with catalase will require investigation in a mouse model. Nrf2- mice are useful for studying oxidative stress in the pathogenesis of Parkinson's disease. All mice will be housed at the Godley-Snell Research Center and handled and cared for by experienced technicians and veterinarians.

All procedures and experiments on mice will be performed in a manner such as to minimize discomfort, distress, pain, and injury. All mice exhibiting excessive pain or discomfort will be euthanized. Euthanasia will be performed by CO2 asphyxiation.

Biohazards

Engineered or innate exosomes are not known to be infections to humans or animals. Direct exposure or ingestion of exosome samples may cause mild cellular level inflammation. All experiments will be performed in a laboratory meeting the biosafety level 2 requirements.

Resources and Environment

All fluorescent microscopy equipment and BSL2 lab space will be provided by the Clemson Light Imaging Facility. Procedures requiring the use of bioreactors and BSL2 lab space is available through the Clemson department of Bioengineering. The Clemson Electron Microscopy facility will assist in the staining and gathering of SEM and TEM images. Finally, all procedures requiring the use of mice will be performed at the Godley Snell Research Center, which is a Clemson University approved location for research using vertebrate animals.

References

1. Rashed M, Bayraktar E, Helal G, et al. Exosomes: From Garbage Bins to Promising Therapeutic Targets. Review. *International Journal of Molecular Sciences*. MAR 2017 2017;18(3)ARTN 538. doi:10.3390/ijms18030538

2. Raposo G, Stoorvogel W. Extracellular vesicles: exosomes, microvesicles, and friends. *J Cell Biol*. Feb 2013;200(4):373-83. doi:10.1083/jcb.201211138

3. D'Souza-Schorey C, Clancy JW. Tumor-derived microvesicles: shedding light on novel microenvironment modulators and prospective cancer biomarkers. *Genes Dev*. Jun 2012;26(12):1287-99. doi:10.1101/gad.192351.112

4. Li M, Zeringer E, Barta T, Schageman J, Cheng A, Vlassov AV. Analysis of the RNA content of the exosomes derived from blood serum and urine and its potential as biomarkers. *Philos Trans R Soc Lond B Biol Sci*. Sep 2014;369(1652)doi:10.1098/rstb.2013.0502

5. Lee Y, El Andaloussi S, Wood MJ. Exosomes and microvesicles: extracellular vesicles for genetic information transfer and gene therapy. *Hum Mol Genet*. Oct 2012;21(R1):R125-34. doi:10.1093/hmg/dds317

6. Haney MJ, Klyachko NL, Zhao Y, et al. Exosomes as drug delivery vehicles for Parkinson's disease therapy. *J Control Release*. Jun 2015;207:18-30. doi:10.1016/j.jconrel.2015.03.033

7. Kim MS, Haney MJ, Zhao Y, et al. Engineering macrophage-derived exosomes for targeted paclitaxel delivery to pulmonary metastases: in vitro and in vivo evaluations. *Nanomedicine*. Jan 2018;14(1):195-204. doi:10.1016/j.nano.2017.09.011

8. Alvarez-Erviti L, Seow Y, Yin H, Betts C, Lakhal S, Wood MJ. Delivery of siRNA to the mouse brain by systemic injection of targeted exosomes. *Nat Biotechnol*. Apr 2011;29(4):341-5. doi:10.1038/nbt.1807

9. Yang T, Martin P, Fogarty B, et al. Exosome Delivered Anticancer Drugs Across the Blood-Brain Barrier for Brain Cancer Therapy in Danio Rerio. Article. *Pharmaceutical Research*. JUN 2015 2015;32(6):2003-2014. doi:10.1007/s11095-014-1593-y

10. Li P, Kaslan M, Lee SH, Yao J, Gao Z. Progress in Exosome Isolation Techniques. *Theranostics*. 2017;7(3):789-804. doi:10.7150/thno.18133

11. Burdette C, Marcus R. Solid phase extraction of proteins from buffer solutions employing capillary-channeled polymer (C-CP) fibers as the stationary phase. Article. *Analyst*. 2013 2013;138(4):1098-1106. doi:10.1039/c2an36126d

12. Jiang L, Marcus R. Biotin-functionalized poly(ethylene terephthalate) capillary-channeled polymer fibers as HPLC stationary phase for affinity chromatography. Article. *Analytical and Bioanalytical Chemistry*. JAN 2015 2015;407(3):939-951. doi:10.1007/s00216-014-8235-4

13. Jiang L, Marcus R. Microwave-assisted grafting polymerization modification of nylon 6 capillary-channeled polymer fibers for enhanced weak cation exchange protein separations. Article. *Analytica Chimica Acta*. FEB 15 2017 2017;954:129-139. doi:10.1016/j.aca.2016.11.065

14. Jiang L, Marcus R. Microwave-assisted, grafting polymerization preparation of strong cation exchange nylon 6 capillary-channeled polymer fibers and their chromatographic properties. Article. *Analytica Chimica Acta*. JUL 18 2017 2017;977:52-64. doi:10.1016/j.aca.2017.04.033

15. Marcus R, Davis W, Knippel B, et al. Capillary-channeled polymer fibers as stationary phases in liquid chromatography separations. Article. *Journal of Chromatography a*. JAN 31 2003 2003;986(1):17-31. PII S0021-9673(02)01835-6. doi:10.1016/S0021-9673(02)01835-6

16. Nelson D, Marcus R. A novel stationary phase: Capillary-channeled polymer (C-CP) fibers for HPLC separations of proteins. Article. *Journal of Chromatographic Science*. OCT 2003 2003;41(9):475-479. doi:10.1093/chromsci/41.9.475

17. Schadock-Hewitt A, Pittman J, Stevens K, Marcus R. Extrusion-Based Differences in Two Types of Nylon 6 Capillary-Channeled Polymer (C-CP) Fiber Stationary Phases as Applied to the Separation of Proteins via Ion Exchange Chromatography. Article. *Journal of Applied Polymer Science*. APR 15 2013 2013;128(2):1257-1265. doi:10.1002/app.38509

18. Schadock-Hewitt A, Marcus R. Initial evaluation of protein A modified capillary-channeled polymer fibers for the capture and recovery of immunoglobulin G. Article. *Journal of Separation Science*. MAR 2014 2014;37(5):495-504. doi:10.1002/jssc.201301205

19. Stanelle R, Marcus R. Nylon-6 capillary-channeled polymer (C-CP) fibers as a hydrophobic interaction chromatography stationary phase for the separation of proteins. Article. *Analytical and Bioanalytical Chemistry*. JAN 2009 2009;393(1):273-281. doi:10.1007/s00216-008-2457-2

20. Trang H, Marcus R. Application of protein A-modified capillary-channeled polymer polypropylene fibers to the quantitation of IgG in complex matrices. Article. *Journal of Pharmaceutical and Biomedical Analysis*. AUG 5 2017 2017;142:49-58. doi:10.1016/j.jpba.2017.04.028

21. Marras C, Beck JC, Bower JH, et al. Prevalence of Parkinson's disease across North America. *NPJ Parkinsons Dis*. 2018;4:21. doi:10.1038/s41531-018-0058-0

22. Ding W, Ding LJ, Li FF, Han Y, Mu L. Neurodegeneration and cognition in Parkinson's disease: a review. *Eur Rev Med Pharmacol Sci*. Jun 2015;19(12):2275-81.

23. Dexter D, Jenner P. Parkinson disease: from pathology to molecular disease mechanisms. Review. *Free Radical Biology and Medicine*. SEP 2013 2013;62:132-144. doi:10.1016/j.freeradbiomed.2013.01.018

24. Devos D, Lejeune S, Cormier-Dequaire F, et al. Dopa-decarboxylase gene polymorphisms affect the motor response to L-dopa in Parkinson's disease. *Parkinsonism Relat Disord*. Feb 2014;20(2):170-5. doi:10.1016/j.parkreldis.2013.10.017

25. Olanow CW. Levodopa: effect on cell death and the natural history of Parkinson's disease. *Mov Disord*. Jan 2015;30(1):37-44. doi:10.1002/mds.26119

26. Paul R, Choudhury A, Kumar S, Giri A, Sandhir R, Borah A. Cholesterol contributes to dopamine-neuronal loss in MPTP mouse model of Parkinson's disease: Involvement of mitochondrial dysfunctions and oxidative stress. *PLoS One*. 2017;12(2):e0171285. doi:10.1371/journal.pone.0171285

27. Gilgun-Sherki Y, Melamed E, Offen D. Oxidative stress induced-neurodegenerative diseases: the need for antioxidants that penetrate the blood brain barrier. Review. *Neuropharmacology*. JUN 2001 2001;40(8):959-975. doi:10.1016/S0028-3908(01)00019-3

28. El-Andaloussi S, Lee Y, Lakhal-Littleton S, et al. Exosome-mediated delivery of siRNA in vitro and in vivo. Article. *Nature Protocols*. DEC 2012 2012;7(12):2112-2126. doi:10.1038/nprot.2012.131

29. Liu Y, Li D, Liu Z, et al. Targeted exosome-mediated delivery of opioid receptor Mu siRNA for the treatment of morphine relapse. Article. *Scientific Reports*. DEC 3 2015 2015;5ARTN 17543. doi:10.1038/srep17543

30. Oswald M, Geissler S, Goepferich A. Targeting the Central Nervous System (CNS): A Review of Rabies Virus-Targeting Strategies. Review. *Molecular Pharmaceutics*. JUL 2017 2017;14(7):2177-2196. doi:10.1021/acs.molpharmaceut.7b00158

31. Momen-Heravi F, Balaj L, Alian S, et al. Current methods for the isolation of extracellular vesicles. *Biol Chem*. Oct 2013;394(10):1253-62. doi:10.1515/hsz-2013-0141

32. Lässer C, Eldh M, Lötvall J. Isolation and characterization of RNA-containing exosomes. *J Vis Exp*. Jan 2012;(59):e3037. doi:10.3791/3037

33. Su S, Xie Y, Fu Z, Wang Y, Wang J, Xiang M. Emerging role of exosome-mediated intercellular communication in vascular remodeling. Review. *Oncotarget*. APR 11 2017 2017;8(15):25700-25712. doi:10.18632/oncotarget.14878

34. Barile L, Moccetti T, Marban E, Vassalli G. Roles of exosomes in cardioprotection. Review. *European Heart Journal*. MAY 7 2017 2017;38(18):1372-1379. doi:10.1093/eurheartj/ehw304

35. Cervio E, Barile L, Moccetti T, Vassalli G. Exosomes for Intramyocardial Intercellular Communication. Review. *Stem Cells International*. 2015 2015;ARTN 482171. doi:10.1155/2015/482171

36. Shenoda BB, Ajit SK. Modulation of Immune Responses by Exosomes Derived from Antigen-Presenting Cells. *Clin Med Insights Pathol*. 2016;9(Suppl 1):1-8. doi:10.4137/CPath.S39925

37. Cooper JM, Wiklander PB, Nordin JZ, et al. Systemic exosomal siRNA delivery reduced alpha-synuclein aggregates in brains of transgenic mice. *Mov Disord*. Oct 2014;29(12):1476-85. doi:10.1002/mds.25978

38. Jeppesen DK, Hvam ML, Primdahl-Bengtson B, et al. Comparative analysis of discrete exosome fractions obtained by differential centrifugation. *J Extracell Vesicles*. 2014;3:25011.

39. Van Deun J, Mestdagh P, Sormunen R, et al. The impact of disparate isolation methods for extracellular vesicles on downstream RNA profiling. *J Extracell Vesicles*. 2014;3doi:10.3402/jev.v3.24858

40. Vlassov AV, Magdaleno S, Setterquist R, Conrad R. Exosomes: current knowledge of their composition, biological functions, and diagnostic and therapeutic potentials. *Biochim Biophys Acta*. Jul 2012;1820(7):940-8. doi:10.1016/j.bbagen.2012.03.017

41. Dai S, Wei D, Wu Z, et al. Phase I clinical trial of autologous ascites-derived exosomes combined with GM-CSF for colorectal cancer. Article. *Molecular Therapy*. APR 2008 2008;16(4):782-790. doi:10.1038/mt.2008.1

42. Willis GR, Kourembanas S, Mitsialis SA. Toward Exosome-Based Therapeutics: Isolation, Heterogeneity, and Fit-for-Purpose Potency. *Front Cardiovasc Med*. 2017;4:63. doi:10.3389/fcvm.2017.00063

43. Li Y, Liu M, Yang ST. Dendritic cells derived from pluripotent stem cells: Potential of large scale production. *World J Stem Cells*. Jan 2014;6(1):1-10. doi:10.4252/wjsc.v6.i1.1

44. Pitt JM, André F, Amigorena S, et al. Dendritic cell-derived exosomes for cancer therapy. *J Clin Invest*. Apr 2016;126(4):1224-32. doi:10.1172/JCI81137

45. Sachamitr P, Leishman AJ, Davies TJ, Fairchild PJ. Directed Differentiation of Human Induced Pluripotent Stem Cells into Dendritic Cells Displaying Tolerogenic Properties and Resembling the $CD141^{+}$ Subtype. *Front Immunol*. 2017;8:1935. doi:10.3389/fimmu.2017.01935

46. Rabinowits G, Gercel-Taylor C, Day J, Taylor D, Kloecker G. Exosomal MicroRNA: A Diagnostic Marker for Lung Cancer. Article. *Clinical Lung Cancer*. JAN 2009 2009;10(1):42-46. doi:10.3816/CLC.2009.n.006

47. Urbanelli L, Magini A, Buratta S, et al. Signaling pathways in exosomes biogenesis, secretion and fate. *Genes (Basel)*. Mar 2013;4(2):152-70. doi:10.3390/genes4020152

48. Beach A, Zhang H, Ratajczak M, Kakar S. Exosomes: an overview of biogenesis, composition and role in ovarian cancer. Review. *Journal of Ovarian Research*. JAN 25 2014 2014;7ARTN 14. doi:10.1186/1757-2215-7-14

49. Böing AN, van der Pol E, Grootemaat AE, Coumans FA, Sturk A, Nieuwland R. Single-step isolation of extracellular vesicles by size-exclusion chromatography. *J Extracell Vesicles*. 2014;3doi:10.3402/jev.v3.23430

50. Zarovni N, Corrado A, Guazzi P, et al. Integrated isolation and quantitative analysis of exosome shuttled proteins and nucleic acids using immunocapture approaches. *Methods*. Oct 2015;87:46-58. doi:10.1016/j.ymeth.2015.05.028

51. Kim SM, Kim HS. Engineering of extracellular vesicles as drug delivery vehicles. *Stem Cell Investig*. 2017;4:74. doi:10.21037/sci.2017.08.07

52. Jiang L, Jin Y, Marcus RK. Polyethylenimine modified poly(ethylene terephthalate) capillary channeled-polymer fibers for anion exchange chromatography of proteins. *J Chromatogr A*. Sep 2015;1410:200-9. doi:10.1016/j.chroma.2015.07.102

53. Lötvall J, Hill AF, Hochberg F, et al. Minimal experimental requirements for definition of extracellular vesicles and their functions: a position statement from the International Society for Extracellular Vesicles. *J Extracell Vesicles*. 2014;3:26913.

54. Soo CY, Song Y, Zheng Y, et al. Nanoparticle tracking analysis monitors microvesicle and exosome secretion from immune cells. *Immunology*. Jun 2012;136(2):192-7. doi:10.1111/j.1365-2567.2012.03569.x

55. Erdbrugger U, Lannigan J. Analytical Challenges of Extracellular Vesicle Detection: A Comparison of Different Techniques. Review. *Cytometry Part a*. FEB 2016 2016;89A(2):123-134. doi:10.1002/cyto.a.22795

56. Trettner S, Seeliger A, zur Nieden NI. Embryoid body formation: recent advances in automated bioreactor technology. *Methods Mol Biol*. 2011;690:135-49. doi:10.1007/978-1-60761-962-8_9

57. Hu X, Deuse T, Kooremann N, et al. Generation of Hypoimmunogenic Induced Pluripotent Stem Cells for Allogeneic Cell and Tissue Transplantation. Meeting Abstract. *Transplantation*. MAY 2017 2017;101(5):S2-S2. doi:10.1097/01.tp.0000520292.05650.be

58. Geisse S, Henke M. Large-scale transient transfection of mammalian cells: a newly emerging attractive option for recombinant protein production. *J Struct Funct Genomics*. 2005;6(2-3):165-70. doi:10.1007/s10969-005-2826-4

59. Johnsen KB, Gudbergsson JM, Skov MN, Pilgaard L, Moos T, Duroux M. A comprehensive overview of exosomes as drug delivery vehicles - endogenous nanocarriers for targeted cancer therapy. *Biochim Biophys Acta*. Aug 2014;1846(1):75-87. doi:10.1016/j.bbcan.2014.04.005

60. Fuhrmann G, Serio A, Mazo M, Nair R, Stevens MM. Active loading into extracellular vesicles significantly improves the cellular uptake and photodynamic effect of porphyrins. *J Control Release*. May 2015;205:35-44. doi:10.1016/j.jconrel.2014.11.029

61. Stone KD, Prussin C, Metcalfe DD. IgE, mast cells, basophils, and eosinophils. *J Allergy Clin Immunol*. Feb 2010;125(2 Suppl 2):S73-80. doi:10.1016/j.jaci.2009.11.017

APPENDIX D:
CURRICULUM VITAE

Tyler Jordan Slonecki

I was raised with my sister in Mt Pleasant, South Carolina by my parents Jim and Cathy Slonecki. After attending Bishop England High School, I spent 4 years at Wofford College where I achieved a bachelor's of science in biology with a computational emphasis, a bachelor's of arts in applied mathematics, a minor in computer science, and competed in collegiate Track and Field and Cross Country. Upon graduation I enrolled in the Clemson University graduate school where I gained a Master's degree in bioengineering and now, with this dissertation, a PhD in bioengineering. While at Clemson, I served as a teaching assistant for BioE3100: Engineering Analysis of Physiological Processes for 2 years. Additionally, while at Clemson, I garnered 2 co-authors on peer-reviewed publications and I'm listed as a co-inventor on a worldwide patent.

Outside of academia, I am an avid outdoorsman and sportsperson who enjoys hiking, kayaking, and exercising whenever I get the chance.

APPENDIX E:
LETTER OF PERMISSION

(See attachment below)

JOHN WILEY AND SONS LICENSE
TERMS AND CONDITIONS

Nov 25, 2020

This Agreement between Clemson University -- Tyler Slonecki ("You") and John Wiley and Sons ("John Wiley and Sons") consists of your license details and the terms and conditions provided by John Wiley and Sons and Copyright Clearance Center.

License Number	4952820095368
License date	Nov 19, 2020
Licensed Content Publisher	John Wiley and Sons
Licensed Content Publication	Wiley Books
Licensed Content Date	Dec 31, 1969
Licensed Content Volume	40
Licensed Content Issue	4
Licensed Content Pages	1
Type of use	Dissertation/Thesis
Requestor type	Author of this Wiley article

Format	Electronic
Portion	Full article
Will you be translating?	No
Title	Exosome isolation and purification via hydrophobic interaction chromatography using a polyester, capillary-channeled polymer fiber phase
Institution name	Clemson University
Expected presentation date	Nov 2020
Requestor Location	Clemson University 341 Hook Ln MOUNT PLEASANT, SC 29464 United States Attn: Clemson University
Publisher Tax ID	EU826007151
Total	0.00 USD

Terms and Conditions

TERMS AND CONDITIONS

This copyrighted material is owned by or exclusively licensed to John Wiley & Sons, Inc. or one of its group companies (each a"Wiley Company") or handled on behalf of a society with which a Wiley Company has exclusive publishing rights in relation to a particular work (collectively "WILEY"). By clicking "accept" in connection with completing this licensing transaction, you agree that the following terms and conditions apply to this transaction (along with the billing and payment terms and conditions established by the Copyright Clearance Center Inc., ("CCC's Billing and Payment terms and conditions"), at the time that you opened your RightsLink account (these are available at any time at http://myaccount.copyright.com).

Terms and Conditions

- The materials you have requested permission to reproduce or reuse (the "Wiley Materials") are protected by copyright.

- You are hereby granted a personal, non-exclusive, non-sub licensable (on a stand-alone basis), non-transferable, worldwide, limited license to reproduce the Wiley Materials for the purpose specified in the licensing process. This license, **and any CONTENT (PDF or image file) purchased as part of your order,** is for a one-time use only and limited to any maximum distribution number specified in the license. The first instance of republication or reuse granted by this license must be completed within two years of the date of the grant of this license (although copies prepared before the end date may be distributed thereafter). The Wiley Materials shall not be used in any other manner or for any other purpose, beyond what is granted in the license. Permission is granted subject to an appropriate acknowledgement given to the author, title of the material/book/journal and the publisher. You shall also duplicate the copyright notice that appears in the Wiley publication in your use of the Wiley Material. Permission is also granted on the understanding that nowhere in the text is a previously published source acknowledged for all or part of this Wiley Material. Any third party content is expressly excluded from this permission.

- With respect to the Wiley Materials, all rights are reserved. Except as expressly granted by the terms of the license, no part of the Wiley Materials may be copied, modified, adapted (except for minor reformatting required by the new Publication), translated, reproduced, transferred or distributed, in any form or by any means, and no derivative works may be made based on the Wiley Materials without the prior permission of the respective copyright owner.**For STM Signatory Publishers clearing permission under the terms of the STM Permissions Guidelines only, the terms of the license are extended to include subsequent editions and for editions in other languages, provided such editions are for the work as a whole in situ and does not involve the separate exploitation of the permitted figures or extracts,** You may not alter, remove or suppress in any manner any copyright, trademark or other notices displayed by the Wiley Materials. You may not license, rent, sell, loan, lease, pledge, offer as security, transfer or assign the Wiley Materials on a stand-alone basis, or any of the rights granted to you hereunder to any other person.

- The Wiley Materials and all of the intellectual property rights therein shall at all times remain the exclusive property of John Wiley & Sons Inc, the Wiley Companies, or their respective licensors, and your interest therein is only that of having possession of and the right to reproduce the Wiley Materials pursuant to Section 2 herein during the continuance of this Agreement. You agree that you own no right, title or interest in or to the Wiley Materials or any of the intellectual property rights therein. You shall have no rights hereunder other than the license as provided for above in Section 2. No right, license or interest to any trademark, trade name, service mark or other branding ("Marks") of WILEY or its licensors is granted hereunder, and you agree that you shall not assert any such right, license or interest with respect thereto

- NEITHER WILEY NOR ITS LICENSORS MAKES ANY WARRANTY OR REPRESENTATION OF ANY KIND TO YOU OR ANY THIRD PARTY, EXPRESS, IMPLIED OR STATUTORY, WITH RESPECT TO THE MATERIALS OR THE ACCURACY OF ANY INFORMATION CONTAINED IN THE MATERIALS, INCLUDING, WITHOUT LIMITATION, ANY IMPLIED WARRANTY OF MERCHANTABILITY, ACCURACY, SATISFACTORY

QUALITY, FITNESS FOR A PARTICULAR PURPOSE, USABILITY, INTEGRATION OR NON-INFRINGEMENT AND ALL SUCH WARRANTIES ARE HEREBY EXCLUDED BY WILEY AND ITS LICENSORS AND WAIVED BY YOU.

- WILEY shall have the right to terminate this Agreement immediately upon breach of this Agreement by you.

- You shall indemnify, defend and hold harmless WILEY, its Licensors and their respective directors, officers, agents and employees, from and against any actual or threatened claims, demands, causes of action or proceedings arising from any breach of this Agreement by you.

- IN NO EVENT SHALL WILEY OR ITS LICENSORS BE LIABLE TO YOU OR ANY OTHER PARTY OR ANY OTHER PERSON OR ENTITY FOR ANY SPECIAL, CONSEQUENTIAL, INCIDENTAL, INDIRECT, EXEMPLARY OR PUNITIVE DAMAGES, HOWEVER CAUSED, ARISING OUT OF OR IN CONNECTION WITH THE DOWNLOADING, PROVISIONING, VIEWING OR USE OF THE MATERIALS REGARDLESS OF THE FORM OF ACTION, WHETHER FOR BREACH OF CONTRACT, BREACH OF WARRANTY, TORT, NEGLIGENCE, INFRINGEMENT OR OTHERWISE (INCLUDING, WITHOUT LIMITATION, DAMAGES BASED ON LOSS OF PROFITS, DATA, FILES, USE, BUSINESS OPPORTUNITY OR CLAIMS OF THIRD PARTIES), AND WHETHER OR NOT THE PARTY HAS BEEN ADVISED OF THE POSSIBILITY OF SUCH DAMAGES. THIS LIMITATION SHALL APPLY NOTWITHSTANDING ANY FAILURE OF ESSENTIAL PURPOSE OF ANY LIMITED REMEDY PROVIDED HEREIN.

- Should any provision of this Agreement be held by a court of competent jurisdiction to be illegal, invalid, or unenforceable, that provision shall be deemed amended to achieve as nearly as possible the same economic effect as the original provision, and the legality, validity and enforceability of the remaining provisions of this Agreement shall not be affected or impaired thereby.

- The failure of either party to enforce any term or condition of this Agreement shall not constitute a waiver of either party's right to enforce each and every term and condition of this Agreement. No breach under this agreement shall be deemed waived or excused by either party unless such waiver or consent is in writing signed by the party granting such waiver or consent. The waiver by or consent of a party to a breach of any provision of this Agreement shall not operate or be construed as a waiver of or consent to any other or subsequent breach by such other party.

- This Agreement may not be assigned (including by operation of law or otherwise) by you without WILEY's prior written consent.

- Any fee required for this permission shall be non-refundable after thirty (30) days from receipt by the CCC.

- These terms and conditions together with CCC's Billing and Payment terms and conditions (which are incorporated herein) form the entire agreement between you and WILEY concerning this licensing transaction and (in the absence of fraud) supersedes all prior agreements and representations of the parties, oral or written. This Agreement may not be amended except in writing signed by both parties. This Agreement shall be binding upon and inure to the benefit of the parties' successors, legal representatives,

and authorized assigns.

- In the event of any conflict between your obligations established by these terms and conditions and those established by CCC's Billing and Payment terms and conditions, these terms and conditions shall prevail.
- WILEY expressly reserves all rights not specifically granted in the combination of (i) the license details provided by you and accepted in the course of this licensing transaction, (ii) these terms and conditions and (iii) CCC's Billing and Payment terms and conditions.
- This Agreement will be void if the Type of Use, Format, Circulation, or Requestor Type was misrepresented during the licensing process.
- This Agreement shall be governed by and construed in accordance with the laws of the State of New York, USA, without regards to such state's conflict of law rules. Any legal action, suit or proceeding arising out of or relating to these Terms and Conditions or the breach thereof shall be instituted in a court of competent jurisdiction in New York County in the State of New York in the United States of America and each party hereby consents and submits to the personal jurisdiction of such court, waives any objection to venue in such court and consents to service of process by registered or certified mail, return receipt requested, at the last known address of such party.

WILEY OPEN ACCESS TERMS AND CONDITIONS

Wiley Publishes Open Access Articles in fully Open Access Journals and in Subscription journals offering Online Open. Although most of the fully Open Access journals publish open access articles under the terms of the Creative Commons Attribution (CC BY) License only, the subscription journals and a few of the Open Access Journals offer a choice of Creative Commons Licenses. The license type is clearly identified on the article.

The Creative Commons Attribution License

The Creative Commons Attribution License (CC-BY) allows users to copy, distribute and transmit an article, adapt the article and make commercial use of the article. The CC-BY license permits commercial and non-

Creative Commons Attribution Non-Commercial License

The Creative Commons Attribution Non-Commercial (CC-BY-NC)License permits use, distribution and reproduction in any medium, provided the original work is properly cited and is not used for commercial purposes.(see below)

Creative Commons Attribution-Non-Commercial-NoDerivs License

The Creative Commons Attribution Non-Commercial-NoDerivs License (CC-BY-NC-ND) permits use, distribution and reproduction in any medium, provided the original work is properly cited, is not used for commercial purposes and no modifications or adaptations are made. (see below)

Use by commercial "for-profit" organizations

Use of Wiley Open Access articles for commercial, promotional, or marketing purposes requires further explicit permission from Wiley and will be subject to a fee.

Further details can be found on Wiley Online Library
http://olabout.wiley.com/WileyCDA/Section/id-410895.html

Other Terms and Conditions:

v1.10 Last updated September 2015

Questions? customercare@copyright.com or +1-855-239-3415 (toll free in the US) or +1-978-646-2777.